Anti-angiogenic therapy in treating outer barrier dysfunction in diabetic retinopathy

Nikita Ved

2016

A thesis submitted for the degree of doctor of philosophy (PhD)

Department of Genetics
Institute of Ophthalmology
UCL

Declaration

I, Nikita Kirit Ved confirm that the work presented in this thesis is my own. Where information has been derived from other sources, I confirm that this has been indicated in the thesis.

…….. ……

Miss Nikita Ved B.Sc. Date

Abstract

Diabetic retinopathy (DR) is one of the leading causes of blindness in the developed world. Characteristic features of DR are retinal neurodegeneration, pathological angiogenesis and breakdown of both the inner and outer retinal barriers of the retinal vasculature and RPE-choroid respectively. Vascular endothelial growth factor-A (VEGF), a key regulator of angiogenesis and permeability, is the target of most pharmacological interventions of DR. VEGF can be alternatively spliced at exon 8 to form 2 families of isoforms, pro- and anti-angiogenic. $VEGF_{165}$ is the most abundant pro-angiogenic isoform, is pro-inflammatory and a potent inducer of permeability. $VEGF_{165}b$ is anti-angiogenic, anti-inflammatory, cytoprotective and neuroprotective. In the diabetic eye, pro-angiogenic VEGF isoforms are up-regulated such that they overpower $VEGF_{165}b$. I hypothesised this imbalance contributed to increased breakdown of the retinal barriers and by redressing this imbalance, the pathological angiogenesis, fluid extravasation and retinal neurodegeneration could be ameliorated.

$VEGF_{165}b$ prevented $VEGF_{165}$ and hyperglycaemia-induced tight junction breakdown and subsequent increase in solute flux in retinal pigmented epithelial (RPE) cells. In streptozotocin-induced diabetes, there was an increase in Evans' blue extravasation after both 1 and 8 weeks of diabetes, which was reduced upon intravitreal and systemic delivery of $rhVEGF_{165}b$. 8-weeks diabetic rats also showed an increase in retinal vessel density, which was prevented by $VEGF_{165}b$. To try to ensure sustained delivery of $VEGF_{165}b$ in the diabetic eye an adeno-associated virus, $AAV.VEGF_{165}b$ was developed and delivered subretinally. Although injection of $AAV.VEGF_{165}b$ resulted in effective expression of $VEGF_{165}b$ in the eye, this caused a detrimental effect on retinal function.

These results show $rhVEGF_{165}b$ reduce DR-associated BRB dysfunction and angiogenesis. Although the neuroprotective effects of $VEGF_{165}b$ in DR are unclear, evidence from other retinopathies, neuropathy and data presented in this thesis suggest that, if the delivery systems can be optimised, $VEGF_{165}b$ may be a suitable therapeutic in treating DR.

Acknowledgements

Firstly, I would like to thank my supervisors, Professor David Bates and Professor James Bainbridge for giving me this opportunity and making me the scientist I am today. Dave – thank you so much for your emotional and academic support. Jim – thank you so much for pushing me and teaching me the importance of perseverance.

I was fortunate enough to work with brilliant people across 3 different labs, and would like to thank all of them for their contribution. Whilst there are too many people to thank individually, there are people I would like to mention. I would like to thank Professor Andrew Dick and Dr. Lucy Donaldson for their invaluable academic contribution. Selina Azam was kind enough to take me under her wing and taught me the very basics when I first started at UCL. Finally, I would like to thank Dr. Richard Hulse. Thank you for helping to shape my research over the last 4 years and teaching me everything I know. I will always be grateful for your input and encouragement and I consider myself very lucky to have had you as a mentor and friend.

To my loyal friends, your support and solidarity kept my spirits up more than you know. You helped keep my sanity even in times when that seemed a tall order, and for that, I am indebted to you.

Most importantly, I would like to thank my family for their immeasurable support. They know how much they mean to me and these words do little to portray my gratitude. To my parents, Soni and Kirit, and my sister, Natasha, thank you for your patience and encouragement – I could not have done it without you.

List of Contents

List of Figures

List of Tables

Chapter 1: Introduction

1.1 Diabetes

Diabetes mellitus is a metabolic disorder that is characterised by hyperglycaemia as a result of poor insulin secretion, detection, actions or a combination of these actions (National Diabetes Data Group 1979). Currently it is estimated that 387 million people are diagnosed with diabetes and it is predicted that this number will rise to 592 million by the year 2035 (Key findings 2014 | International Diabetes Federation). Diabetes mellitus can be divided into type 1 and type 2 diabetes. Type 1 diabetes is typically an immune or autoimmune-mediated disorder (Atkinson et al. 2014) resulting from an autoimmune T cell-mediated destruction of pancreatic β-cells and the remaining β-cells are incapable of regeneration, resulting in a rapid decline in insulin production (Devendra et al. 2004) and persistent hyperglycaemia. Type 2 diabetes, typically associated with obesity and ageing, is a result of both a lack of insulin secretion and diminished insulin sensitivity (Donath & Shoelson 2011). A β-cell compensatory mechanism involves enhancement of β-cell mass and increased insulin secretion, eventually this mechanism is no longer adequate resulting in a long-term decrease in insulin-mediated glucose uptake and persistent hyperglycaemia (Rydén et al. 2007; Donath & Shoelson 2011). As both types of diabetes progress, patients show a high incidence of macro- and microvascular complications associated with diabetes including atherosclerosis, stroke, neuropathy, nephropathy and retinopathy (Stratton 2000). Type 1 diabetes is treated with insulin supplementation therapy (Atkinson et al. 2014) and type 2 diabetes has multiple treatment strategies aimed at either increasing insulin sensitivity, stimulating insulin secretion or limiting glucose uptake or a combination of the 3, some of which are shown in table 1.1.

Drug	**Mechanism of action**	**Reference**
Metformin	• Increases insulin sensitisation of the liver and decreases hepatic glucose production through AMPK activation • Encourages glucose uptake in skeletal myocytes	• (Dardano et al. 2014) • (Zhou et al. 2001)
Thiazolidinediones	• Peroxisome proliferation activated receptor-gamma (PPARγ) agonist • Improves peripheral insulin sensitivity	• (Yki-Järvinen 2004)

	• Reduces hepatic gluconeogenesis	
Incretins	• Dipeptidyl peptidase-4 inhibitors (DPP4-I). • Stimulate insulin secretion • Suppress glucagon secretion	• (Dardano et al. 2014) • (Ahrén 2003) • (Baggio & Drucker 2007)

Patients with long-term elevated HbA_{1C}, glycated haemoglobin – a marker for average plasma glucose concentration, are more at risk of developing diabetic microvascular complications than diabetics with good glycaemic control (Stratton 2000). Of the many microvascular complications associated with diabetes, the most common are nephropathy, neuropathy and retinopathy.

Diabetic nephropathy is one of the leading cause of kidney disease in the working population of the western world (Gross et al. 2004) and clinically manifests as increased proteinuria, high blood pressure and a decrease in glomerular filtration rate and can eventually lead to end stage renal failure (Fioretto & Mauer 2007). These outcomes are caused by structural changes in the kidney that are initially characterised by mesangial expansion, due to an increase in extra cellular matrix deposition, potentially contributing to the reduced glomerular filtration rate (Mauer et al. 1984). Glomerular endothelial cells, part of the glomerular filtration barrier, show a reduced endothelial glycocalyx in glomerular endothelial cells and in retinal arteries of diabetic patients (Nieuwdorp et al. 2006), contributing to increased albumin clearance (Jeansson & Haraldsson 2006). Albuminuria also correlates with podocyte loss in glomeruli of diabetic patients (Fioretto & Mauer 2007). Eventually these, and other events progress, resulting in gradual decline in kidney function.

Diabetic peripheral neuropathy involves peripheral nerve dysfunction and its occurrence is proportional to magnitude and length of hyperglycaemia (Fowler 2008). Symptoms include tingling, increased allodynia, hyerpalgesia and eventually numbness (Dobretsov et al. 2007). As neurones have a persistently high glucose uptake, hyperglycaemia encourages further, up to fourfold, glucose uptake (Tomlinson & Gardiner 2008b). Prolonged excessive glucose uptake results in glucose neurotoxicity, affecting: sensory afferents, myelinated and unmyelinated nerve fibres (Tomlinson & Gardiner 2008a; Hulse et al. 2015). Nociceptors are more susceptible to activation,

particularly by non-painful stimuli, due to inadequate vascular perfusion, neuronal interference or a combination of both (Hulse et al. 2015). Diabetic rodents also show increased demyelination centrally and peripherally, further leaving the neurones vulnerable to degeneration (Hulse et al. 2015).

1.2 Diabetic retinopathy

1.2.1. Clinical manifestations

Diabetic retinopathy (DR), a condition culminating in a gradual decline in vision, affects both type 1 and type 2 diabetic patients (Klein 1984) and is the leading cause of blindness in the working population of the western world. DR is the most common microvascular complication associated with diabetes (Hammes 2013). As with other complications, prevalence of DR increases with increasing duration of diabetes. Diabetic macular oedema (DME) and proliferative diabetic retinopathy (PDR) are the main causes of vision loss. The risk of developing PDR is greater in type 1 diabetics than type 2, with the converse true for DME (Nentwich & Ulbig 2015).

Presence and grading of DR are initially assessed by fundus examinations, as shown by figure 1.1. Diagnosis and grading of DR can be divided according to PDR and DME. DR is initially characterised by the appearance of microaneurysms and intraretinal haemorrhage (figure 1.1A). As the disease progresses to PDR there is an increase in the number of microvessels in the retina that are prone to rupture and leakage (figure 1.1B). As the vessels continue to grow, PDR can result in retinal detachment (figure 1.1C) As these vessels are compromised, fluid and plasma proteins leak from the microvasculature and accumulate in the macula, resulting in DME (figure 1.1D). DME is often characterised by the appearance of hard exudates, are protein deposits that have accumulated due to increased vessel permeability, and “cotton wool spots”, regions of nerve fibre layer (NFL) infarct (Antonetti et al. 2012). If left untreated, the nascent blood vessels can grow into the vitreous, haemorrhage and result in vision loss. Of these clinical features, macular oedema is most closely correlated with the degree of vision loss (Moss et al., 1988).

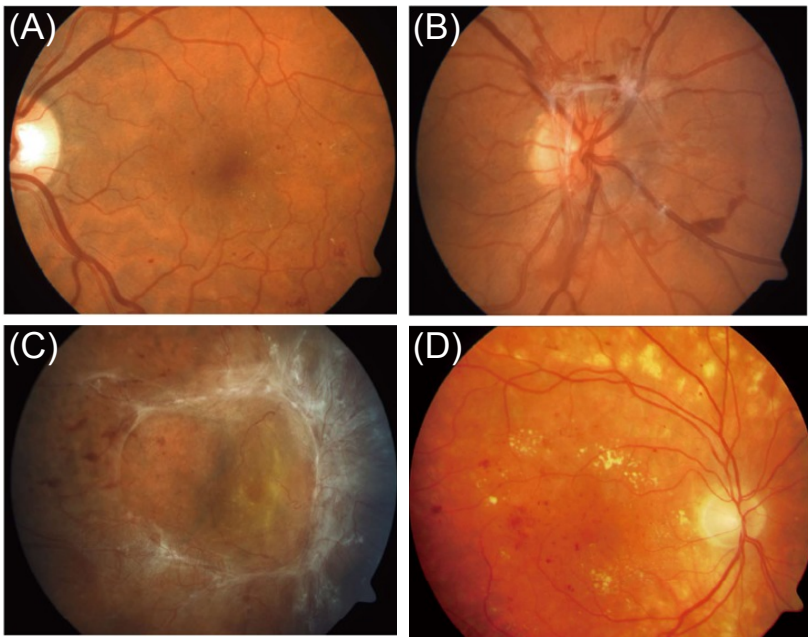

Figure 1.1. Stages of diabetic retinopathy by fundus examination (Adapted from Nentwich & Ulbig 2015).

There are two main types of DR, a non-proliferative stage and a proliferative stage. For diagnostic purposes, the non-proliferative stage can be further sub-divided into mild/background, moderate and severe. Mild/background non-proliferative retinopathy shows presence of microaneurysms in the retinal microvasculature (A). As the retina become progressively ischaemic, there is increased angiogenesis in the retina resulting in PDR (B). leaving them prone to rupture and leakage. As well as leaking blood, these vessels also leak plasma proteins that aggregate to form hard exudates. With this increase in blood vessel growth, also increases the rate at which hard exudates are formed and microaneurysms occur, resulting in tractional retinal detachment (C). The fluid that has leaked from these vessels then accumulates in the macula, resulting in its thickening, which eventually results in DME (D).

1.2.2. Proliferative diabetic retinopathy

PDR, like many other retinal neovascular retinopathies, occurs as a result of an ischaemic retina. Persistent hyperglycaemia in diabetic patients causes structural, functional and haemodynamic changes in the retinal vasculature (Nentwich & Ulbig 2015; McGahon et al. 2007) . Changes in blood flow can occur early on in diabetes before any noticeable signs of retinopathy, potentially contributing to the ischaemic retina typically observed in DR (Bursell et al. 1996). This is likely due to improper activity of large-conductance calcium (Ca^{2+})-activated ion channels, located on vascular smooth muscle cells (VSMCs) that enable contraction of retinal arterioles. In the early stages of

DR, rather than eliciting arteriolar vasodilatation, an influx of intracellular Ca^{2+} results in vasoconstriction (McGahon et al. 2007). The earliest detectable sign of diabetes-induced structural changes is loss of pericytes (Cai & Boulton 2002), also contributing to retinal ischaemia. Pericytes, located within the basement membrane of vessels, are associated with maintaining appropriate vessel contractility (Rucker et al. 2000) and with angiogenesis (Hammes et al. 2002). They remain in close contact with endothelial cells, and are highly expressed in the CNS and the retina, in a 1:1 ratio, and it is hypothesised that it is this close relationship that ensures the "tightness" of the BBB and the BRB (Bergers & Song 2005).

Hyperglycaemia induces significant pericyte loss (Hammes et al. 1995), however the mechanisms behind diabetic pericyte dropout are not fully understood. It is hypothesised that this is likely due to an accumulation of hyperglycaemia-induced waste products, such as advanced glycacation end-products (AGEs) that trigger apoptosis within the pericyte (Stitt et al. 1997). It is also suggested that pericyte dropout is an active diabetes-induced angiopoietin-2 mediated process (Hammes et al. 2004). The relationship between pericytes and endothelial cells is so tightly coupled that a loss in pericytes results in a loss of endothelial cells, resulting in acellular capillaries that are inadequately perfused (Kohner & Henkind 1970). These non-perfused regions of the retina result in focal ischaemia and a consequent increase in vascular endothelial growth factor (VEGF-A) expression, amongst other pro-angiogenic factors, in an attempt to redress the hypoxia by triggering angiogenesis (Aiello 1994). This is usually in the form of sprouting angiogenesis, forming from proliferating endothelial cells where there is pericyte loss (Hirschi & D'Amore 1996). As there is persistent hyperglycaemia, the region of non-perfused areas may increase over time, resulting in increased pathological angiogenesis in the retina and into the vitreous. As these newly formed vessels rarely recruit pericytes, they lack vessel integrity and therefore are prone to rupture, as detectable by presence of microaneurysms and haemorrhage.

Whilst the best treatment for PDR is tight glucose control, it merely halts the progression of the condition, but does not necessarily stop it. In the early stages of PDR, pan-retinal laser photocoagulation (PRP) is used to halt progression of PDR and prevent vision loss (Grunwald et al. 1986). Typically, an argon laser is used to create multiple burns approximately 200μm in diameter (Frank 2004). This method aims to ablate the ischaemic retina, therefore reducing the metabolic demand of the outer retina. This results in a reduced oxygen consumption and VEGF production of the RPE layer and

photoreceptors (Wolbarsht & Landers 1980). By burning the outer BRB, more oxygen from the choroidal circulation can be can be made available to the inner retina. This method therefore attempts to halt the progression of DR by preventing angiogenesis and reducing hypoxia. The Diabetic Retinopathy study showed that PRP reduced the risk of blindness by at least 50%. (The Diabetic Retinopathy Research Group, 1981). However PRP is associated with side effects such difficulty with light-dark adapatation, decreased visual acuity and loss of peripheral vision (Cheung et al. 2010) In the later stages of PDR, where there is excessive neovascularisation into the vitreous and/or tractional retinal detachment, surgical interventions are necessary. A pars-plana vitrectomy aims to remove the opacities formed by microaneuryms, from the vitreous (Flynn et al. 1992).

1.2.3. Diabetic macular oedema

DME is a major cause of sight loss in diabetic patients and can occur in patients with non-proliferative DR as well as those with PDR (Wilkinson et al. 2003). DME occurs due to the accumulation of fluid from microaneurysms and haemorrhages and accumulation of plasma proteins that have escaped from leaky blood vessels, within 2 disc diameters of the macula, with vision loss occurring when the macula is involed (Cheung et al. 2010). Clinically significant macular oedema (CSME) is diagnosed when there is thickening 500μm from the macula or thickening of the macula itself (Early Treatment Diabetic Retinopathy Research Group 1985). It is also characterised when there is exudate formation within 500μm of the macula plus adjacent retinal thickening or when there is any retinal thickening within one disc diameter of the macula (Early Treatment Diabetic Retinopathy Research Group 1985). DME can be further subdivided into mild, moderate and severe according to proximity of exudate formation and retinal thickening to the macula (Ciulla et al. 2003). Fluid accumulation in the diabetic retina, monitored using optical coherence tomography (OCT), can occur as a result of vessel rupture from regions where there is pericyte dropout, and from BRB breakdown. Both of these factors worsen with persistent hyperglycaemia and retinal ischaemia-mediated VEGF upregulation.

Treatments for DME can involve both surgical and pharmacological intervention. Again, the best way to assist the prevention of DME is by tight control of HbA_{1C} as well as blood pressure. In patients with CSME without foveal involvement, focal laser

photocoagulation is performed using laser burns 50-100μm in diameter targeting microaneurysms and areas of leakage with the aim of reducing the risk of vision loss by 50% (Early Treatment Diabetic Retinopathy Research Group 1985). Like PRP, focal laser photocoagulation aims to increase the amount of oxygen that diffuses from the choroid and into the retina (Nentwich & Ulbig 2015). It is also hypothesised that focal laser treatment is restorative to the inner and outer BRB by thermally stimulating the RPE and retinal endothelial cell (RECs) respectively as regions of fluid leakage appear to be reduced (Bhagat et al. 2009). Grid laser photocoagulation is prescribed when there is diffuse DME and foveal involvement (Bhagat et al. 2009). However, this method has varying prognoses, usually poor, and so it has since been replaced with the advent of anti-VEGF drugs or carried out in conjunction with anti-VEGF therapy (Nentwich & Ulbig 2015).

1.2.4. Retinal neurodegeneration

Largely associated with disorders of the central nervous system, neurodegeneration is also observed in the retina in conditions such as glaucoma (Kerrigan 1997), retinitis pigmentosa (Baumgartner 2000) and mitochondrial retinopathies (La Morgia et al. 2010). Retinal neurodegeneration is also a key feature of DR and is involved in vision loss.

The changes that typically occur in the diabetic neural retina include neural apoptosis, increased glial fibrillary acidic protein (GFAP) in glial cells and microglia activation (Barber, 2003). These changes are similarly seen in many neurodegenerative disorders of the CNS including Alzheimer's and Parkinson's disease (Cordeiro et al. 2004), further illuminating that DR is also a neurodegenerative disorder. Functional changes that represent some neurodegeneration can often be seen before the characteristic vascular pathology develops, indicating that the neuronal dysfunction may in fact be a primary effect of the diabetes rather than as a result of BRB break down and macular dysfunction (Barber, 2003; Lieth et al., 2000). Whilst clinical diagnosis of DR requires detection of vascular pathology, functional changes in vision can be detected using the electroretinogram (ERG) and contrast sensitivity, indicating that the pathway that allows vision acquisition or processing is compromised (Kern & Barber, 2008).

ERG has been used in the clinic to establish changes in oscillatory potentials in diabetic patients, and in patients diagnosed with diabetes for 7 years or less, it was noticed that the amplitude and latency of oscillatory potentials were reduced before any noticeable changes in vasculature had developed (Frost-Larsen et al., 1990; Juen & Keiselbach, 1990). Whilst the exact origin of the functional changes seen in DR are widely debated, it seems the most likely candidate cells that are compromised are amacrine neurones, bipolar or retinal ganglion cells. In animal models of diabetes, changes in ERG are also used to assess progression of DR. It has been reported that diabetic rats show prolonged peak latencies and a reduced B–wave, indicating dysfunction in bipolar cells, (Segawa et al. 1988; Robinson et al. 2012a). It has been observed that diabetic Lewis and Sprague-Dawley rats showed a reduced scotopic B-wave latency (Kern et al. 2010), a feature similarly seen in the clinic.

DR is often termed as a "neurovascular" disorder, and it is believed that diabetic retinal dysfunction is due to a change in the "neurovascular unit". The neurovascular unit refers to the close physiological and biochemical relationship between the retinal vasculature and retinal neurones. The neurovascular unit in healthy retinae involves close relationship between glial cells, neurones and the pericyte-endothelial cell complex (Antonetti et al. 2012). In diabetic retinae the number of ganglion and bipolar cells decrease, as do the number of pericytes. The numbers of synapses formed between the neurones are decreased as the numbers of dendritic and axonal processes decrease, contributing to the diminished the neural activity in the diabetic retina. There is also decreased interaction between the vascular retina and the neural retina (Lieth et al. 2000; Antonetti et al. 2012).

The relationship between the neurones, glia and microvasculature ensures appropriate energy homeostasis and neurotransmitter regulation. Pericytes surrounding capillaries in particular are essential in this region, as the pericyte – glial – neuronal axis promotes formulation of the blood – retina – barrier (BRB) (Antonetti et al. 2012), which tightly controls the movement of fluids and metabolites. The coupling between these types of cells is so tight that dysfunction in one cell type may affect the whole unit. Conditional VEGF deletion in Müller cells in the diabetic retina showed a marked reduction in leukostasis, tight junction breakdown and vascular leakage compared to untreated diabetic retinae (Wang et al., 2010); again underlying the pivotal role VEGF plays in DR.

Whilst many cell types are implicated in DR, retinal neural dysfunction is likely to be due to loss of retinal ganglion cells (RGC) in the ganglion cell layer (GCL) of the retina. Histological analysis of the human retina and scanning laser polarimetry indicated a thinning of the NFL in diabetic patients (Kerrigan 1997; Takahashi et al. 2006), indicating a loss of RGCs and their axons. Histological analysis indicates that RGCs show an increased expression of apoptotic markers such as: Bax, caspase-3 and caspase-8 in diabetes (Oshitari et al. 2008). Other studies have shown that these cells become TUNEL positive or caspase-3 positive (Kern & Barber, 2008), however this does not correlate with number of cells dying, which could indicate that neurodegeneration, while it may precede neovascularisation, is a slow process.

In the hypoxic retina, there is overproduction of TNF-α from the RPE (Chen et al. 2011). Hyperglycaemia results in less PEDF secretion *in vitro* (Ablonczy et al. 2009), which may translate to reduced neuroprotection *in vivo.* Furthermore, hyperglycaemia results in increased AGE accumulation in the RPE resulting in overproduction of VEGF (Simó et al. 2010), TJ breakdown in the RPE and neurodegeneration. A compromised RPE layer not only means a compromised outer BRB, but also impinges upon its other functions in the retina. Most treatments, pharmacological and surgical, are not targeted towards treating retinal neural dysfunction, likely due to patients seeing an improvement in vision after anti-VEGF treatment. However, considering DR is a neurovascular disorder, and changes in the retinal neurones occurs early on in diabetes, it is important to consider the neural architecture when developing new treatment strategies.

1.3. The blood-retina barrier

The blood-retina barrier (BRB) describes the selectively permeable region formed by TJs on RECs (Shakib & Cunha-Vaz 1966) and RPE (Cunha-Vaz 1976), which form the inner and outer BRB respectively, as shown by figure 1.3. The BRB protects the neural retina from contents of the retinal and choroidal circulation. The BRB also has a vital role in homeostatic maintenance of the neural retina. Much like the blood-brain barrier (BBB), the BRB controls fluid and molecular flux between cells.

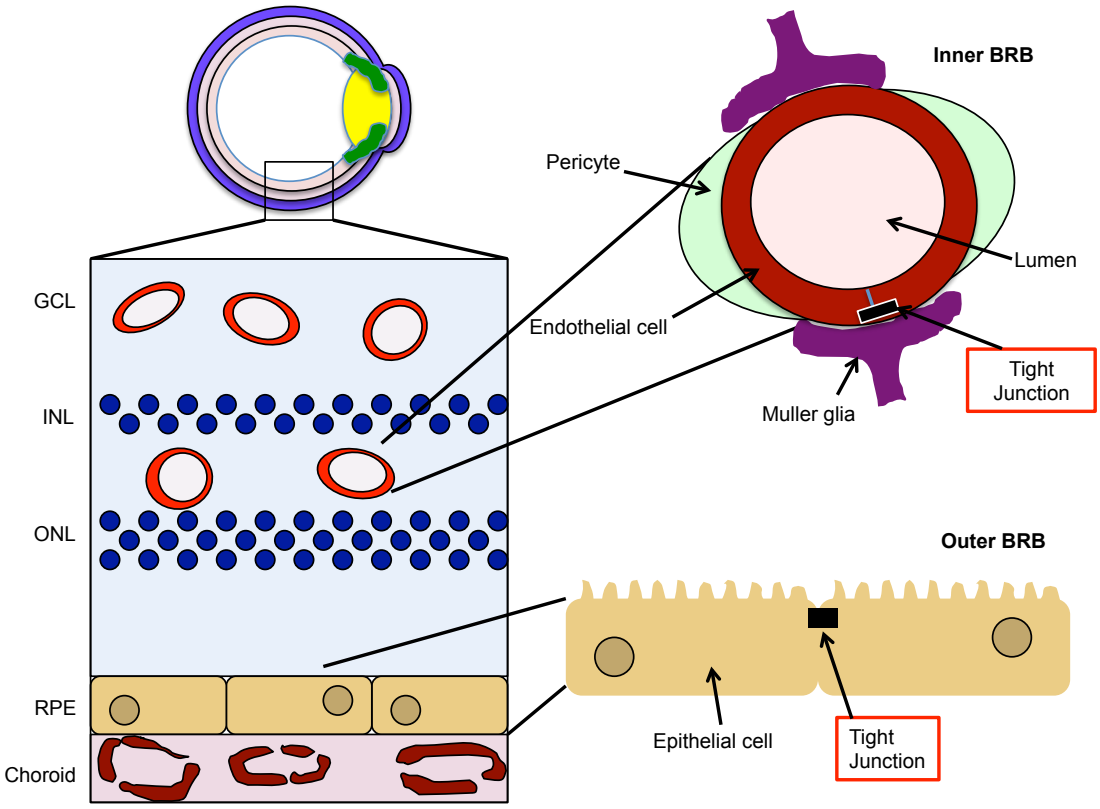

Figure 1.2. Schematic diagram of a cross section of the eye

The neural retina is comprised of many layers the ganglion cell layer (GCL), the inner nuclear layer (INL), the outer nuclear layer (ONL), and is separated from the choroid by the retinal pigment epithelium (RPE). The retina has two regions of blood-retina barrier (BRB); an inner BRB and an outer BRB to protect the neural retina from the retinal and choroidal circulation respectively.

1.3.1. The inner BRB

There are two plexuses of retinal vasculature, an inner plexus located near the GCL and an outer plexus near the OPL, as shown by figure 1.3 (Kaur et al. 2008), the endothelial cells that line form these vessels are the inner BRB. The TJs between these RECs are located on the basal lamina, and provides a selectively permeable barrier to the capillaries. These barrier properties are enhanced by the neurovascular unit that RECs are so closely associated with. Pericytes contribute to TJ integrity by inducing occludin and ZO1 mRNA and protein expression in the REC that they are associated with under normoxic conditions. Furthermore, pericytes partially prevent loss of TJs under hypoxic conditions (Wang et al. 2007). Müller glia are also closely associated with the inner BRB and are involved in nutrient uptake and removal of metabolites (Kaur et al. 2008). Under normal conditions, Müller glia have been shown to secrete pigment epithelium derived

growth factor (PEDF), an anti-angiogenic growth factor (Yafai et al. 2004) perhaps as part of maintenance of the inner BRB. Under diabetic conditions, Müller glia secrete VEGF, which induces retinal vascular leakage and inflammation (Wang et al. 2010).

1.3.2. The outer BRB

The outer BRB is formed by TJs between the RPE cells separates the choroidal circulation from the inner retina (Cunha-Vaz 1976). The apical surface of the RPE contain villi-like structures that are in close contact with rod and cone outer segments for the phagocytosis of photoreceptor outer segment discs (Steinberg et al. 1977), and for vitamin A transport (Kaur et al. 2008). The RPE layer is highly involved in the visual cycle, as mutations of the RPE65, a protein responsible for isomerisation of trans-retinaldehyde to 11-cis-retinaldehyde, results development of Leber congenital amaurosis and severe vision loss (Acland et al. 2001).

Unlike the retinal vasculature, the choroidal plexus is fenestrated, to allow diffusion of nutrients such as glucose and fatty acids from the systemic circulation to the RPE, which in turn transports them to the outer retina. This transcellular movement is also utilised to transport outer retinal waste products back to the choroidal circulation (Weinberger et al. 1995). Due to its close proximity to and association with the chorioidal circulation, TJ integrity of the RPE layer is important. Moreover, the fenestrae of the choroidal plexus may allow macromolecular leakage from the choroid that may otherwise be deleterious in the retina, further reiterating the importance of outer BRB integrity.

As well as providing a barrier function and a transporter of nutrients and waste, the RPE layer also provides a protective mechanism. There is high generation of ROS in the retina, due to its vast oxygen consumption. The RPE contains large amounts of superoxide dismutase, and anti-oxidant to protect the retina against oxidative stress (Simó et al. 2010). In addition to this the RPE protects against oxidative stress using pigments such as lipofuscin and melanin, to filter out light at different wavelengths and contribute to anti-oxidant defence.

As part of maintaining outer retinal and choroidal homeostasis, the RPE produce and secrete many growth factors. The RPE basolaterally secretes VEGF to maintain the choroidal endothelium and to stabilise choroidal fenestrae (Saint-Geniez et al. 2009a). The RPE also secretes PEDF, an anti-angiogenic and neuroprotective growth factor, from

the apical side (Ablonczy et al. 2009). PEDF is also involved in the maintenance of the choroid as well as the retinal vasculature, perhaps by curtailing VEGF-mediated endothelial proliferation.

1.4. Mechanisms associated with DR

Diabetes is a complex metabolic disease and as a result complications associated with diabetes involve multiple pathways. Pathological pathways associated with hyperglycaemia-induced damage specific to this thesis are further discussed below.

1.4.1. Oxidative stress

Generation of reactive oxygen species (ROS) such as superoxide and hydrogen peroxide, is a common by product of the electron transport chain, as well as from NADPH oxidases and nitric oxide synthases (Dröge 2002). Under normal physiological conditions, ROS are produced to support basic cell function, and are then cleared. Overproduction of ROS can result in oxidative stress can be deleterious and result in damage of DNA, proteins, lipids and other cellular mechanisms (Giugliano et al. 1996).

As the retina is one of the most metabolically active tissues in the body, it has a high oxygen and glucose uptake, making it vulnerable to hyperglycaemia-induced oxidative stress (Anderson et al. 1984). Cells in the retina are unable to adequately adapt glucose transport rates when the extracellular environment is hyperglycaemic, resulting in an increased intracellular glucose (Kaiser et al. 1993). Increased intracellular glucose results in increased glucose metabolism through the tricarboxylic acid (TCA) cycle and increased electron transport chain activation, resulting in a ROS production greater than can be scavenged (Giugliano et al. 1996). Not only does elevated ROS result in intracellular damage and apoptosis, that it triggers many other pathogenic pathways involved with diabetes and complications associated with diabetes (Brownlee 2001).

1.4.2. Polyol pathway

Elevated intracellular glucose in the diabetic eye results in increased activation of the polyol pathway. Aldose-reductase, reduces excess glucose to sorbitol, and as it does so converts NADPH to NADP+ (Brownlee 2001). Sorbitol is then oxidised to fructose by sorbitol dehydrogenase, resulting in NADH production. This process results in decreased intracellular NADPH, which is detrimental to the retina as NADPH is involved in the production of glutathione, a ROS scavenger (Kowluru & Chan 2007). This means that there will be a build-up of ROS production as it is unable to be cleared appropriately, triggering further oxidative stress. Furthermore, NADPH is involved in nitric oxide (NO) production (Kowluru & Chan 2007). NO is critically involved in vasomotor tone, therefore a reduction in NADPH results in decreased NO. Any reduction in NO production could result in alterations in vascular perfusion in the already inadequately perfused diabetic retina (Ho et al. 2012). This may further exacerbate tortuosity of the microvasculature. Increased intracellular NADH/NAD+ also results in glyceraldehyde 3-phosphate dehydrogenase (GAPDH) inhibition, resulting in activation of the AGE and PKC pathways (Brownlee 2001).

1.4.3. Advanced glycation end-products (AGEs)

AGEs are formed by reducing sugars, such as glucose, reacting non-enzymatically with amino groups found in proteins, nucleic acids and lipids, which become glycated or glycoxidated (Singh et al. 2001). AGE accumulation takes many weeks, and as it does so it causes the dysfunction of many long-lived proteins and targets regions such as the basement membrane of blood vessels and can cause tubulin dysfunction, both of which are involved in BRB breakdown. AGE also interacts with collagen, and initiates cross-links across these fibres, which can affect vasomotor tone and haemodynamics in the diabetic retina (Brownlee 2001).

AGE formation occurs with increasing age, and forms at an accelerated rate in diabetes and correlates with the progression of retinopathy (Stitt et al. 1997). AGEs bind to their cognate receptors with high affinity, with the most well characterised receptor

being the receptor for AGE (RAGE). They activate inflammatory mediators such as NFKB and TNFα (Brownlee 2001), and elevates ROS, causing further retinal degeneration. RAGE is found in various cells in the retina including pericytes, RPE and RECs and its activation is associated with increased retinal vascular permeability (Hammes 2005). RAGE activation also upregulates cytokines such as VEGF, a key factor involved in diabetic retinal pathology (Hammes et al. 1999). Interestingly, RAGE-induced VEGF upregulation has been found in the RPE and the RGC layer (Hammes et al. 1999) and may participate in outer BRB breakdown and retinal neurodegeneration respectively. Exogeneously applied AGE induces BRB breakdown in normoglycaemic retinae (Stitt et al. 2000) and RAGE inhibition results in a prevention of diabetes-induced vascular leakage (Wautier et al. 1996).

1.4.4. Protein kinase C (PKC) activation

PKC consists of a family of 11 isoforms, divided into typical (α, β_I, β_{II} and γ) activated by diacyglycerol (DAG) and Ca^{2+}, novel (δ, ε, η and θ) activated by DAG and atypical isoforms (ζ and λ) activated by neither DAG nor Ca^{2+} (Parekh et al. 2000) . PKC phosphorylate intracellular proteins using kinases, this is a critical factor in enzyme activation, receptor pathways and gene expression (Donnelly et al. 2004) and can be deleterious if over-activated. Elevated intracellular glucose results in increased DAG expression in the retina (Koya & King 1998), hypothesised to be formed *de novo* (Brownlee 2001). Increased hyperglycaemia-induced ROS production results in increased triose phosphate expression, a precursor to DAG (Inoguchi et al. 2000). This will stimulate the production of DAG upon hyperglycaemia, and increase typical and novel PKC activation. Furthermore, increased PKC activation further increases ROS production and oxidative stress through increased NADPH oxidase activity (Inoguchi et al. 2000). PKC upregulation has been shown to reduce endothelial nitric oxide synthase and NO production, which would impair an already compromised vasomotor tone in the retinal microvessels (Wu et al. 2014). PKC activation triggers activation of many other pathways including increasing expression of transforming growth factor β (TGFβ), which in turn increases collagen and fibronectin activity (Brownlee 2001). This is particularly detrimental in the diabetic eye, as it will help further compromise blood flow, and result in a greater onset of capillary occlusion. PKC activation also increases NFKB expression,

resulting in increased transcription of pro-inflammatory genes and cytokines (Tang & Kern 2011).

PKC phosphorylates intracellular proteins at the serine or threonine residue, which can be pathological if this occurs too frequently, for example in the diabetic retina. Serine and threonine residues are also phosphorylated in the BRB by PKC on tight junction proteins, resulting in barrier dysfunction and permeability in the retina (Harhaj et al. 2006) as well as pericyte dropout (Pomero et al. 2003). The role of PKC β_I and β_{II} have been the most extensively characterised in DR as it is hypothesised that they are the most activated isoforms in response to hyperglycaemia (Donnelly et al. 2004). Hyperglycaemia-mediated VEGF upregulation also increases PKC activation (α, β and δ), however VEGF-induced mitogenic activity appears to be mediated largely by PKCβ, making PKCβ an attractive therapeutic target in treating DR. Interestingly, PKC also increases hyperglycaemia-mediated VEGF expression in the RPE (Poulaki et al. 2002). VEGF-mediated endothelial cell activation (Xia et al. 1996) and retinal permeability (Aiello 2002) were both reduced upon treatment with a PKCβ inhibitor, LY33531 or ruboxistaurin. Ruboxistaurin treatment in diabetic patients has shown a gain in vision and a prevention in DME progression, however it is still awaiting FDA approval (Javey et al. 2012).

Hyperglycaemia also upregulates PKCδ in the retina and induces ROS and NFKB-mediated pericyte apoptosis and formation of acellular capillaries (Geraldes et al. 2009), possibly resulting in VEGF upregulation and PKCβ activation. In hypoxic RPE *in vitro*, VEGF secretion appeared to be PKCδ mediated (Young et al. 2005). PKCζ, an atypical PKC isoform, has been shown to be necessary in hyperglycaemia-mediated VEGF expression (Young et al. 2005). However, when inhibited, PKCζ showed no effect on VEGF secretion, indicating that different PKCs are involved in the expression and secretion of VEGF upon different hyperglycaemic and/or hypoxic stimuli (Young et al. 2005).

1.5. Vascular endothelial growth factor

VEGF-A, or VEGF, is a gene that is a mitogenic factor (Leung et al. 1989), potent inducer of permeability (Adamis et al. 1993) and a neuroprotective agent (Foxton et al. 2013). VEGF exists as multiple isoforms of varying amino acid length, (e.g. $VEGF_{121}$, $VEGF_{145}$, $VEGF_{165}$, $VEGF_{189}$ are examples of human VEGF isoforms and murine isoforms contain one amino acid less). The most widely studied, understood and the most predominant VEGF isoform is $VEGF_{165}$ / $VEGF_{164}$. The biological effects of VEGF are mediated by their cognate receptors, VEGFR1 (Flt-1) and the more biologically active, VEGFR2 (KDR or Flk-1) (Ferrara 2004). Furthermore, neuropilin-1 also binds $VEGF_{165}$ and is crucial in endothelial cell migration (Soker et al. 1998). VEGFR1 and VEGFR2 are expressed by multiple cell types including endothelial cells (Shibuya et al. 1999) and epithelial cells (I Kim et al. 1999), and is ubiquitously expressed in the eye.

1.5.1. Angiogenesis

Angiogenesis is the formation of new blood vessels from pre-existing vasculature and is critical in embryonic development (Carmeliet et al. 1996), wound healing (Nissen et al. 1998) and fertility (Ferrara et al. 1998). There are many angiogenic factors including placental growth factor (PlGF; Maglione et al. 1993) and angiopoeitin-1 (Koblizek et al. 1998). However, VEGF is deemed to be the key regulator of physiological and pathological angiogenesis.

VEGF-mediated angiogenesis in the eye is often driven by hypoxia (Shima et al. 1995). HIF-1α is stabilised and translocated to the nucleus in hypoxic conditions. This interacts with hypoxia response element (HRE) to activate transcription of VEGF (Pe'er et al. 1995). In diseased states where there is persistent hypoxia, oxidative stress or inflammatory response such as DR, there is overexpression of VEGF, VEGR2 and subsequent angiogenesis (Aiello 1994). Blocking VEGF activity results in a reduction of pathological retinal neovascularisation (Aiello 1995).

1.5.2. Vascular leakage

Vascular leakage refers to the movement of fluid or solutes across a capillary wall and is increased upon VEGF stimulation and inflammatory mediators. Vascular leakage is a broad term that includes transcellular leakage and paracellular leakage, the latter being the most deleterious aspect of DR. Paracellular leakage in DME is hypothesised to occur when junctional proteins located on endothelial cells, such as occludin, zonula occludens 1 (ZO1) and VE-cadherin, amongst others, are disrupted (Wallow & Engerman 1977). This disruption allows the contents of the microvasculature, such as plasma proteins, to leak through between the cells, and becomes pathological when this fluid build up exceeds fluid clearance, and accumulates.

Addition of $VEGF_{165}$ to bovine retinal endothelial cells reduced their occludin expression and increased extraction of occludin (Antonetti 1999a). Furthermore, intravitreal addition of VEGF increases vascular permeability (Xu et al. 2001), which reflects what is observed in models of diabetic retinopathy *in vivo* (Qaum et al. 2001). VEGF-mediated PKC activation phosphorylates occludin and ZO1 at the serine and/or threonine residue, resulting in ubiquitination, endocytosis and subsequent degradation of TJs in endothelial cells(Murakami et al. 2009). Interestingly, in the RPE, the actin cytoskeleton anchors TJs, and undergoes a conformational change due to increased PKC activation, resulting in disassembly of TJs and their internalisation in a soluble pool, where they are recycled back to the membrane (Harhaj & Antonetti 2004) . Both of these instances result in increases in paracellular flux, and fluid accumulation.

1.5.3. Anti-VEGF therapy and DR

Since the discovery of VEGF in the pathogenesis of DR (Aiello 1994), the use of anti-VEGF therapy in treating DR has been a widely investigated area of research. The main anti-VEGF treatment strategies are administered intravitreally and mainly targeted at the inner BRB. This aims to neutralise VEGF through soluble VEGF dimer neutralisation or inhibition of VEGFR1 and VEGFR2 dimerization. Anti-VEGF therapy has limited effectiveness in treating DR, with approximately 50% of patients responding to therapy (Stitt et al. 2015). Conversely, anti-VEGF therapy in treating wet AMD is

much more effective with 87% of patients responding positively (Falavarjani & Nguyen 2013).

Ranibizumab (Lucentis, Genentech, San Francisco), a pan-VEGF-A 40kDa fragment antibody, reduces VEGF-A expression by preventing $VEGF_{110}$, $VEGF_{121}$ and $VEGF_{165}$ from interacting with VEGFR1 and VEGFR2 (Ferrara et al. 2006). By doing so, cell proliferation, migration and permeability were reduced. Various multicentre trials have shown that ranibizumab not only prevents vision loss, but also showed a meaningful gain in vision in many patients (Ferrara et al., 2006; da Cruz, 2008). Ranibizumab also shows a reduction in central retinal thickness (CRT) and fluorescein leakage in AMD patients and is now widely used to treat AMD. Data from the READ clinical trial testing the use of ranibizumab in treating DME showed that there was a decrease in oedema and an increase in BCVA, relative to focal or grid laser therapy alone, and is currently being further investigating as a treatment for DME (Nguyen et al. 2010).

Bevacizumab (Avastin, Genentech, San Francisco) a humanised, recombinant monoclonal pan-VEGF-A antibody, binds to the binding domain of all VEGF isoforms, and therefore neutralises the activity of VEGF-A. Bevacizumab has been FDA approved for the treatment of metatstatic colon cancer, metatstatic breast cancer and non-small cell lung cancer. However, it is used off label to treat AMD (Javey et al. 2012). Studies showed that there was a significant improvement in BVCA when compared to laser therapy alone in patients with DME, although further trials are still taking place (Avery et al. 2006).

Whilst ranibizumab and bevacizumab are typically administered intravitreally every 4-6 weeks, aflibercept (Eyelea, Regeneron, NY, USA) is administered every 2 months in AMD patients (Heier et al. 2012). Aflibercept acts as a soluble decoy receptor and inhibits VEGFR1 and VEGFR2 activation, and binds all isoforms of VEGF-A with greater affinity than ranibizumab or bevacizumab and also inhibits VEGFR1 and VEGFR2 more potently than both pan-VEGF-A antibodies *in vitro* (Papadopoulos et al. 2012). Interestingly, aflibercept also possesses a high affinity for $VEGF_{165}$ as well as $VEGF_{121,}$ VEGF-B and PIGF (Heier et al. 2012), and it is these qualities that have now many aflibercept increasingly popular.

Whilst shown to be a promising therapeutic intervention in treating wet AMD, ocular anti-VEGF therapy is still in its infancy. Neutralising or inhibiting an endogenous cytokine like VEGF could prove to be deleterious. Considering diabetic retinae are prone to BRB breakdown, the privileged immunity that the eye obtains is now compromised. As

a result, these anti-VEGF drugs may end up in the systemic circulation, and may prevent the necessary actions of VEGF, systemically. An example would be interfering with wound healing and maintenance and regulation of the systemic vasculature may be harmful, especially in elderly or diabetic patients (Gillies 2006). VEGF is neurogenic and neuroprotective (Jin et al. 2000; Jin et al. 2002). Situations where anti-VEGF agents have leaked into the systemic circulation from compromised BRBs may affect other neurovascular units within the body. Diabetic patients are prone to neurodegeneration, particularly in the peripheral nervous system, to administer anti-VEGF agents and risk its entry into the circulation, may exacerbate the condition further.

Within the eye itself, suppression of VEGF may lead to widespread geographic atrophy (GA). A study looking at the effect of bevacizumab on the development of chorioretinal atrophy (CRA) in patients suffering from CNV, showed that in fact whilst the patients' vision improved, there was often a development and enlargement of CRA as time progressed. CRA has been shown to worsen vision improvement, when compared to patients that did not develop CRA (Oishi et al. 2013). This indicates that either a strategy needs to be put in place to manage this atrophy, or another treatment route needs to be adopted.

Endophthalmitis, inflammation of the intraocular cavities, is usually caused by infection from ocular surgery or intravitreal injections, and can result in permanent vision loss. Whilst its incidence is rare, between 0.019%-1.6% (Falavarjani & Nguyen 2013), it is still one of the greater adverse events associated with intravitreal therapy. Although anti-VEGF therapy is successful in managing and treating DME, all treatments require frequent injections. Therefore although the risk of developing endophthalmitis is low, that risk is still there during every injection. Unfortunately, all current anti-VEGF therapies present this risk, again reiterating the importance of an alternative treatment strategy, one that requires fewer intravitreal injections.

1.5.4. Alternative splicing of VEGF-A

As well as having multiple isoforms of varying amino acid length, VEGF pre-mRNA can be alternatively spliced at exon 8 (Bates et al. 2002a) to generate two families of isoforms, as shown by figure 1.3. There are two different splice sites on exon 8, a proximal splice site (PSS) at exon 8a and a distal splice site (DSS) at exon 8b, and

selection of which results in a pro-angiogenic and anti-angiogenic family of isoforms respectively (Bates et al. 2002a). The anti-angiogenic family, $VEGF_{xxx}b$ (x=amino acid number) has a different terminal six amino acid sequence (Ser-Leu-Thr-Arg-Lys-Asp, SLTRKD) to the by pro-angiogenic family, $VEGF_{xxx}$ (Cys-Arg-Lys-Pro-Arg-Arg, CDKPRR) (Woolard et al. 2004). $VEGF_{165}b$ has since been the most characterised of the $VEGF_{xxx}b$ family, and has unique properties that differ to $VEGF_{165}$, its pro-angiogenic sister isoform, due to this difference in C' terminal sequence. $VEGF_{165}b$ binds to VEGFR2, however unlike $VEGF_{165}$, it does not bind neuropilin 1, and only weakly phosphorylates VEGFR2 due to insufficient rotation of the $VEGF_{165}b$-VEGFR2 complex (Kawamura et al. 2008). This reduced autophosphorylation, relative to $VEGF_{165}$, results in a weakened internal receptor phosphorylation and weakened downstream signalling to that elicited by $VEGF_{165}$.

$VEGF_{165}$ and $VEGF_{165}b$ competitively bind to VEGFR2, therefore binding of $VEGF_{165}b$ to VEGFR2 prevents $VEGF_{165}$ interaction with VEGFR2, thereby preventing pro-angiogenic activity and eliciting anti-angiogenic activity (Woolard et al. 2004). It is hypothesised that the prevalence of one isoform over the other can result in pathology. In diseases characterised by pathological angiogenesis, there is increased $VEGF_{xxx}$ expression, predominantly $VEGF_{165}$ (Bates et al. 2002a; Woolard et al. 2004; M. V. R. Gammons et al. 2013), and in systemic sclerosis, a disease characterised by insufficient angiogenesis, there is systemic upregulation $VEGF_{165}b$ (Manetti et al. 2011).

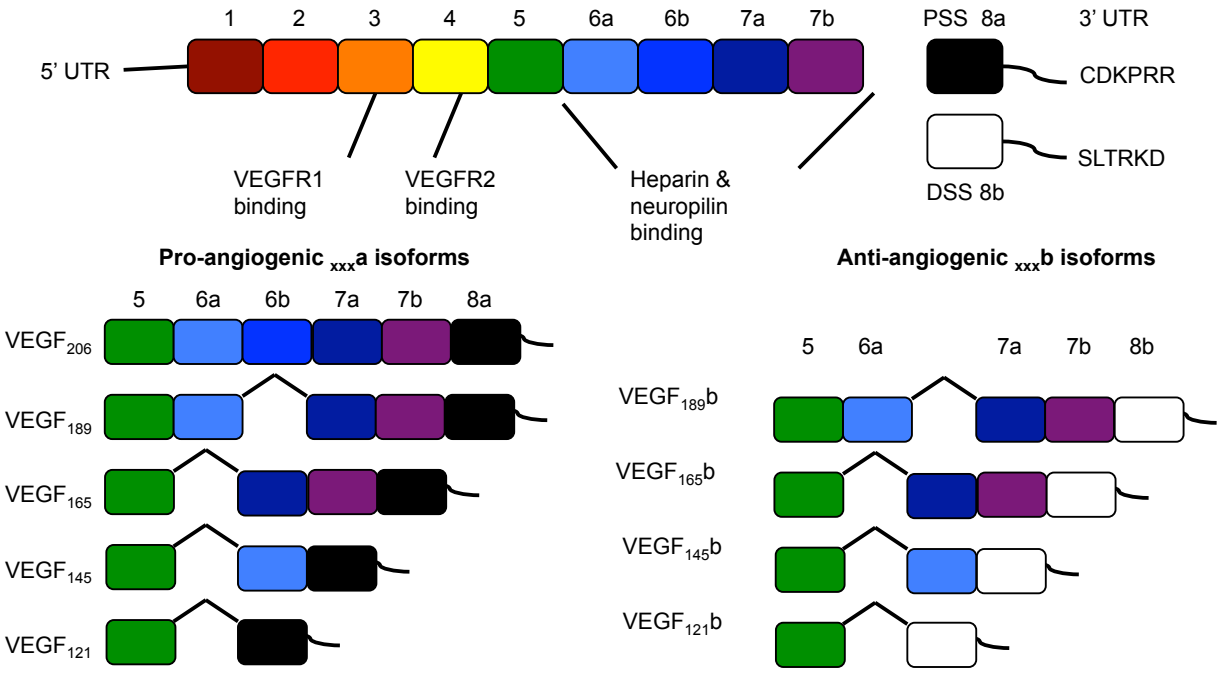

Figure 1.3. Splice variants of the VEGF-A gene

VEGF-A is alternatively spliced at exon 8 to generate two families of isoforms, a pro-angiogenic $VEGF_{xxx}$ family and an anti-angiogenic $VEGF_{xxx}b$ family of isoforms according to proximal or distal splice site selection respectively.

1.5.5. $VEGF_{xxx}b$ in the eye

Since 2002, the expression and use of $VEGF_{xxx}b$ isoforms in various diseases has been studied extensively. It has been identified in many healthy tissues including the kidney (Bevan et al. 2008), the central nervous system (Beazley-Long et al. 2013), the peripheral nervous system (Hulse et al. 2014a) and the eye (Perrin et al. 2005),. $VEGF_{165}b$ has been shown to inhibit endothelial permeability (Bevan et al. 2008), prevent endothelial migration (Woolard et al. 2004) and is neuroprotective (Hulse et al. 2014a).

It is hypothesised that both families of isoforms are required for development and maintenance of tissue, for example foetal eye development requires both families of isoforms (Baba et al. 2012). Over the course of gestation, there are spatial and temporal differences in $VEGF_{165}$ and $VEGF_{165}b$, most notably in the RPE layer and putative NFL, with $VEGF_{165}b$ being most abundant towards the end of the gestation period (Baba et al. 2012). It is well known that pro-angiogenic VEGF is crucial for embryonic development (Carmeliet et al. 1996), however in the very early stages of eye development, $VEGF_{165}b$ is detected at much lower levels than $VEGF_{165}$. It is possible that at this time splicing is in

favour of pro-angiogenic isoforms and switches in favour of $VEGF_{xxx}b$ when necessary later on. It also suggests that the spatial differences in isoform expression are due to their competition in binding to VEGFR2.

$VEGF_{xxx}b$ isoforms are also found in the adult human vitreous, as almost half of the total VEGF expressed in the eye, indicating that both families of isoforms are required for adequate ocular function (Perrin et al. 2005). However, in diabetic patients, this balance shifts in favour of $VEGF_{xxx}$, with the percentage of VEGF in the vitreous that is anti-angiogenic decreasing (12.5±3%) compared to that of normal eyes (65.3±7.2%) (Perrin et al. 2005). This study inferred that DR is governed by a switch in splicing from the anti-angiogenic isoform being the dominant form of VEGF, to the pro-angiogenic isoform in diabetes.

A switch in splicing can also govern the extent of pathological neovascularization in a model of retinopathy of prematurity (ROP). The 50/10 oxygen-induced retinopathy model was subject to new-born rats that received an intravitreal injection of DMSO or SRPIN340, a serine-arginine protein kinase inhibitor that can influence VEGF pre-mRNA splicing (Gammons et al., 2013). OIR causes an increase in $VEGF_{165}$–mediated pre-retinal neovascularization (PRNV) and intravitreal neovascularization (IVNV) in DMSO-treated control eyes. Conversely, eyes treated with SRPIN340, show less PRNV and IVNV. It is likely that this reduction in pathological neovascularization is due to SRPIN340-induced switch in splicing favouring the anti-angiogenic, $VEGF_{165}b$, isoform, therefore inhibiting binding of any excessive $VEGF_{165}$. This strategy as also been used to treat neuropathic pain in diabetic rats. Rats subjected to diabetic peripheral neuropathy show elevated levels of $VEGF_{165}$ and increased mechanical and thermal hyperalgesia (Hulse et al. 2014a). Conversely, rats treated with SRPIN340 show a reduction in pain markers and pain sensitivity and increased levels of $VEGF_{165}b$ (Hulse et al. 2014a).

Direct application of $VEGF_{165}b$ also shows similarly promising results. Intravitreal administration of $VEGF_{165}b$ has shown both a reduction in neovascularization and increased cytoprotection in oxygen-induced retinopathy (Konopatskaya et al. 2006; Magnussen et al. 2010). As well as reducing pathological neovascularization, $VEGF_{165}b$ shows neuroprotectivity. Rats subjected to OIR show a significant reduction in retrograde transport of fluorogold to the RGC layer in untreated retinae relative to $VEGF_{165}b$–treated eyes (Beazley-Long et al. 2013). This indicates that $VEGF_{165}b$ is able to protect RGCs against ischaemic insult, and when compared to control ischaemic eyes and contralateral

eyes, there is a reduction in activated caspase-3 staining suggesting that this neuroprotection is mediated through inhibition of apoptosis in the retina.

It therefore seems likely that $VEGF_{165}b$ can be used to treat the various pathological aspects of PDR, as the diabetic retina is so severely deficient in anti-angiogenic isoforms. The unique neuroprotective, anti–angiogenic and anti-permeability properties that $VEGF_{165}b$ possesses makes it an ideal candidate in targeting the three hallmark pathologies in DR.

1.6. Gene therapy

Retinal gene therapy for the treatment of blindness has shown great progress, particularly with inherited retinal degenerations such as Leber congenital amaurosis (LCA) (Bainbridge et al. 2015) and achromatopsia (Pang et al. 2010). The success of retinal gene therapy, plus the immune privilege nature of the eye have made it an attractive candidate for targeting increased VEGF in AMD and DR for long periods of time. The benefit of a long-lasting treatment strategy such as anti-angiogenic gene therapy removes risks associated with intravitreal injections, such as endophthalmitis, as it reduces the number of injections required relative to standard anti-VEGF therapy.

Adenoviral and AAV-mediated soluble VEGFR1 (sFlt1) gene transfer show a reduction in ischaemia-induced retinal neovascularisation in mice (Bainbridge et al. 2002) and in monkeys (Lai et al. 2005). Endostatin is hypothesised to be anti-angiogenic in the retina (Takahashi et al. 2003). Several groups using endostatin gene therapy have shown a reduction in retinal (Auricchio et al. 2002) and choroidal (Balaggan et al. 2006) neovascularisation. PEDF, also hypothesised to be anti-agiogenic in the eye (Dawson et al. 1999), has shown to cause a reduction in ischaemia-induced neovascularisation (Auricchio et al. 2002) and adenoviral PEDF has been shown to reduce lesion size in patients with AMD (Campochiaro et al. 2006). These are just some examples of the research conducted in anti-angiogenic gene therapy for ocular neovascular diseases, however none are yet to make it past clinical trial stages.

1.7. Hypothesis and Aims

It is clear that VEGF is critical in the progression of DR and that $VEGF_{165}b$ is able to inhibit VEGF-induced pathology. Gene therapy is a potential mechanism for long-term expression. I therefore set out to test the hypothesis that $VEGF_{165}b$ gene therapy would be a novel approach to treating diabetic retinopathy as it targets neovascularisation, oedema and neurodegeneration. Furthermore, it reduces the number of ocular injections required, therefore reducing the incidence of injection-related side effects. I also hypothesised that outer BRB dysfunction is involved in the pathogenesis of DR, and RPE-targeted treatment would be a novel way of treating DR. Specifically, I designed a series of experiments that tested the hypotheses to determine: -

I. Whether $rhVEGF_{165}b$ could prevent $VEGF_{165}$-induced changes in TJ expression and function in 1˚ human RPE *in vitro*, to test the hypothesis that $VEGF_{165}b$ could prevent $VEGF_{165}$-induced pathology in an *in vitro* model of the outer retinal barrier.

II. Whether an *in vitro* model of diabetic retinopathy, specifically diabetic outer BRB dysfunction, could be created, and whether $rhVEGF_{165}b$ could prevent any potential changes in TJ function and expression. This tested the hypothesis to see whether $VEGF_{165}b$ would be suitable in treating hyperglycaemia-induced outer BRB breakdown.

III. Whether intravitreal administration of $rhVEGF_{165}b$ can prevent a diabetes-induced increase in fluid extravasation in acute, type 1 diabetic rats *in vivo*. This tested the hypothesis that locally administered $VEGF_{165}b$ would prevent BRB breakdown in the diabetic retina.

IV. Whether 8-week diabetic rats showed an increase in retinal fluid extravasation, and if so, could this be prevented by systemic administration of $VEGF_{165}b$; to test the hypothesis that $VEGF_{165}b$ could be tolerated long-term and prevent diabetes induced-BRB breakdown *in vivo.*

V. If 8-week diabetic rats showed changes in barrier properties, they may also show a difference in vascular density, which may be ameliorated by systemic rhVEGF$_{165}$b treatment. This tested the hypothesis that VEGF$_{165}$b would be able to prevent neovascularization in a potential model of PDR, *in vivo*.

VI. Whether long-term diabetes could induce a decrease in A- and B-wave ERG amplitude and a change in retinal thickness, which may be prevented upon subretinal delivery of AAV.VEGF$_{165}$b, to test the hypothesis that VEGF$_{165}$b gene therapy can prevent diabetes-induced retinal neurodegeneration and thinning of the rat retina.

Chapter 2: Materials and Methods

2.1. Cell culture

2.1.1. Isolation and culture of primary human RPE cells.

All cell extractions were carried out under cell culture hoods in class II facilities using sterile and autoclaved instruments and solutions, approved by the HTA ethics guidelines. Primary human RPE were extracted from human donor globes obtained within 24 hours post-mortem (Bristol Eye bank, Bristol Eye Hospital). Retinae were excised with choroid-RPE sheets intact, finely chopped and digested in a petri dish with 5ml Dulbecco's Modified Eagle Medium (DMEM):F12 (1:1) + GlutaMAX (Invitrogen) with added collagenase (0.3mg/ml) for 15 minutes at 37˚C. Following digestion, 30ml DMEM:F12+GlutaMAX was added to the choroid:RPE sheets, supplemented with 10% foetal bovine serum (FBS, Invitrogen), 0.5% penicillin / streptomycin (Invitrogen). The samples were spun at 1500 rotations per minute (rpm) for 10 minutes at room temperature to pellet cells. The supernatant was discarded and the pellet resuspended in 4ml DMEM:F12+GlutaMAX supplemented with 25% FBS and transferred to a T25 flask (Greiner). Upon reaching 80% confluence, cells were split and either transferred to a T75 flask (Greiner) or used for experimental purposes. RPE were used until passage 8 and cultured in DMEM:F12 + GlutaMAX supplemented with 10% FBS and 1% penicillin / streptomycin.

2.1.2. HEK293T cells

Cells were maintained in in DMEM (Invitrogen) + 10% foetal calf serum (FCS, Invitrogen). Media was supplemented with 1% penicillin G and streptomycin and 0.25µg/ml amphotericin B (all Invitrogen). This medium will henceforth be referred to as "D10". Cells were cultured on 150cm^2 plates (Nunclon Surface, Nunc) and split when reaching 80% confluence and were transfected with plasmids between passages 10 and 24.

2.2. Treatments with growth factors

2.2.1. Vascular endothelial growth factor (VEGF-A).

RPE were treated with both isoforms of VEGF-A, proangiogenic $VEGF_{165}$ and anti-angiogenic $VEGF_{165}b$, both at varying doses (0nM, 0.1nM, 0.2nM, 0.5nM, 1.0nM, 2.5nM, 5.0nM), to assess the effects of both isoforms on tight junction integrity. 24 hours prior to treatment, cells were subject to serum starvation by replacing culture medium with serum–free medium. 24 hours following treatment, cells were stained for tight–junctions, and protein lysate was extracted for further analysis or immediately post-treatment cells were subject to trans-epthelial electrode resistance (TEER, section 2.3).

2.2.2. Glucose

RPE were treated with D-glucose (Sigma) at 5mM and 35mM to test the effect of normoglycaemia and hyperglycaemia on tight-junctions respectively. RPE were simultaneously treated with mannitol (30mM mannitol + 5mM glucose, Sigma), as an osmotic control for 35mM glucose. Cells were also subject to co-treatment of glucose with 2.5nM $VEGF_{165,}$ 2.5nM $VEGF_{165}b$ and 1µM anti-$VEGF_{165}b$ (56/8) 24 hours prior to treatment, cells were subject to serum starvation by replacing culture medium with serum – free medium. 24 hours following treatment, cells were stained for tight – junctions, and protein lysate and conditioned media was also extracted for further analysis; or immediately post-treatment cells were subject to trans-epthelial electrode resistance (TEER, section 2.3).

2.3. Trans–epithelial electrode resistance

Trans-epithelial electrode resistance (TEER) was measured using electric cell-substrate impedance sensing (ECIS, Applied Biophysics, Troy, NY, USA) using a 1600R ECIS model. Human primary RPE cells were plated on 8 well plates (8W10E+ plates, Applied Biophysics). Wells were pretreated with 10mM L-cysteine (Sigma) for 30 minutes at 37˚ to neutralise the electrodes and enable to cells to adhere to the wells. After the 30-minute period the L-cysteine was aspirated, and the wells were washed with

distiller water at room temperature. Following this wash, the wells were filled with 400ul medium (DMEM: F12+GlutaMAX, Gibco) and the electrodes were stabilised on the machine.

The wells were plated with 60,000 cells per well in 400ul medium. Cells are deemed confluent when the resistance is greater than 1000Ω. Measurements were collected at multiple frequencies (125Hz, 250Hz, 500Hz, 1000Hz, 2000Hz, 4000Hz, 8000Hz and 16000Hz) for one hour, to establish baseline data. Once baseline was established, the programme was paused and plates were taken to a laminar flow hood, and growth factor treatment (see section 2.2) was prepared in 50µl medium. 50µl of medium was carefully aspirated from each well of the plate and replaced with 50µl of growth factor treatment, and was allowed to equilibrate for 30 minutes before reattaching the plates to the ECIS and recommencing TEER evaluation, so as to prevent any convection–induced detachment of cells from a change in solutions. Plates were then assayed for changes in TEER for at least 15 hours. Data was analysed at 500Hz to give an indication of tight-junction integrity and paracellular flux.

2.4. Protein work

2.4.1. Protein extraction

Protein was collected from freshly excised retinae or choroids by homogenising them in 200µl ice-cold radioimmunoprecipitation buffer (RIPA, Sigma) containing protease inhibitor (Sigma) on ice. Protein lysate was extracted from cells when cells reached 80% confluence in 6–well (Greiner). Cells were washed twice in ice-cold 1xPBS, followed by 50µl RIPA buffer plus cocktail inhibitor. Cells were incubated on ice for 5 minutes, scraped from the wells and transferred to a 0.5ml eppendorf. All samples were kept on ice for a further 15 minutes, followed by sonication for 15 minutes and centrifugation at 10,000 x g at 4˚C for 15 minutes. Supernatants were collected in fresh eppendorfs and stored at -20˚C.

2.4.2. Protein quantification

Total protein was quantified using the Bradford method with protein assay dye reagent (BioRad). The dye was diluted 1:5 in distilled water, and 200µl added to 10µl of each sample in triplicate on a 96-well plate. Protein samples were assayed against protein standards made from BSA serial dilutions. Colorimetric analysis was performed on a microplate reader at 595nm (OpsysMR; Dynex Technology).

2.4.3. Immunoblotting

50µg protein was denatured for 5 minutes at 95˚C in sodium dodecyl sulphate polyacrylamide (SDS) loading buffer (100mM Tris-HCl, 4% SDS, 20% glycerol, 0.2% (w/v) bromophenol blue, 5% 2-mercaptoethanol, pH 6.8, all from Sigma). Samples were separated using SDS poly-acrylamide gel electrophoresis (SDS PAGE), either in homemade gels or pre-cast gels (4-20%, BioRad) for homemade gel percentages, see table 2.1. Homemade gels were run at 90V in ice-cold running buffer (25mM Tris-HCl, 250mM glycine, 0.1% SDS, pH8.3) for 90 minutes. Precast gels were run at 150V for 40 minutes. All gels were then wet – transferred onto a polyvinylidene fluoride (PVDF) membrane (BioRad) in cold transfer buffer (50mM Tris-HCl, 38mM glycine, 20% methanol, pH8.3) for 2 hours at 90V. For high MW proteins such as VEGFR2 and pVEGFR2, membranes were transferred at 4˚C for 15 hours at 0.15A.

Resolving Gel	**10%**	**12%**	**Stacking Gel**	**4% (for 2 gels)**
MilliQ water		3.3ml	MilliQ water	7.3ml
30% Acryl/Bis		4ml	30% Acryl/Bis	1.3ml
1.5M Tris HCl pH8.8		2.5ml	1M Tris HCl pH6.8	1.25ml
20% SDS		50µl	20% SDS	50µl
10% AMPS		50µl	10% AMPS	50µl
TEMED		5µl	TEMED	10µl

Table 2.1. Homemade stacking and resolving gel recipes.

Membranes were blocked using 3% bovine serum albumin (BSA, Sigma) for an hour at room temperature with agitation, and then washed in solution of PBS and 0.01% TWEEN®20 (Sigma), PBS-T, 3 times for 5-minute intervals. This was followed by incubation with a primary antibody, also diluted in 3% BSA, at 4˚C overnight, with gentle agitation, dilutions of primary antibodies used are shown in table 2.2. The primary antibody is then poured off, and is followed by 3 consecutive 5-minute washes in PBS-T. The horseradish peroxidase (HRP) conjugated secondary antibody is either diluted in 3% BSA, and is added to the membrane and allowed to incubate at room temperature for 1 hour. Following this incubation period, the antibody is again poured off, and washed 3 times in PBS-T. Protein bands are then detected using Amersham ECL Prime Western Blotting Detection Reagent (GE Life sciences, USA), and chemiluminescence is detected using a Fujifilm LAS-1000. Western blots were also detected using fluorescent-labelled secondary antibodies (1:7000, Licor Odyssey) and incubated at room temperature for 1 hour, followed by detection using Licor software.

Antibody	**Dilution**	**Supplier**
Rabbit anti-pan VEGF (A20)	1:500	Santa Cruz
Rabbit anti-ZO1	1:500	Invitrogen
Mouse anti-occludin	1:500	Invitrogen
Mouse anti – VE cadherin	1:500	BD Biosciences
Mouse anti – HIF-1α	1:250	BD Bioscience
Mouse anti – ERK	1:1000	Cell Signalling
Mouse anti – pERK	1:1000	Cell Signalling
Rabbit anti – VEGFR2 (Ty1175)	1:500	Cell Signalling
Rabbit anti – pVEGFR2 (Ty1175)	1:500	Cell Signalling
Rabbit anti – cleaved caspase	1:500	Cell Signalling
Mouse anti- α tubulin	1:1000	Santa Cruz
Goat anti – β actin	1:200	Santa Cruz
Goat anti-rabbit HRP conjugated secondary	1:10000	Pierce Biotech

Goat anti-mouse HRP conjugated secondary	1:10000	Pierce Biotech
Donkey–anti mouse IRdye 2˚ anti-body	1:7000	Licor
Donkey–anti rabbit IRdye 2˚ anti-body	1:7000	Licor

Table 2.2. List of antibodies and concentrations at which they were used for immunoblotting

2.4.4. Enzyme-Linked Immunosorbent Assay (ELISA)

96 well cell culture plates (Fischer), were coated with the capture antibody (Pan VEGF AF293, and $VEGF_{165}b$, MAB3405 R&D Systems) and we left overnight at room temperature with gentle agitation. The antibody was then discarded, and washed with 0.05% PBS-T, three times. The pan VEGF plate and the $VEGF_{xxx}b$ plate was blocked with 1% BSA and 5% BSA respectively, for a maximum of two hours at room temperature, with gentle agitation. Following this period, the blocking solution was discarded from both plates, and then each plate was washed 3 times in PBS-T. A minimum volume of 50µl of whole eye, retinal or cellular protein was added to the plates in duplicate, as well as pan VEGF and $VEGF_{xxx}b$ standards (4000pg/ml, 2000pg/ml, 1000pg/ml, 500pg/ml, 250pg/ml 125pg/ml, 62.5pg/ml, 31.25pg/ml and 15.625pg/ml). Samples were left to incubate at 37˚C for 1 hour, and discarded and the wells were washed with PBS-T three times. Following this wash, 100µl of detection antibody was added to each well(Pan VEGF, 840163, $VEGF_{165}b$, BAF293, R&D systems), and allowed to incubate at room temperature for an hour, followed by 3 washes with PBS-T. 100µl Streptavidin-HRP (1:200) was added to each well, and the plates were wrapped in foil and allowed to incubate at room temperature for 20 minutes followed by the wash steps. Substrate solutions A and B were added (1:1, 100µl) to each well, and allowed to incubate for 20 minutes, wrapped in foil. To stop the reaction, 50µl Stop solution was added to each well and gently tapped to enable thorough mixing and the optical density was measured immediately at 450nm.

2.5. Immunfluorescence

2.5.1. Cell Immunofluorence

Cells grown on glass coverslips (13mm, Fischer Scientific), were treated with either $VEGF_{165}$, $VEGF_{165}$b or glucose and then 24 hours post–treatment, media was aspirated off and cells washed with PBS, 3 times. They were fixed at room temperature with 4% paraformaldehyde, permeabalised in 0.05% Triton-X (Sigma) in PBS and then blocked in 5% normal goat serum (Sigma) in PBS, all for 30 minutes at room temperature respectively. All cells were incubated in primary antibody in PBS, at 4˚C overnight (Mouse anti – occludin and rabbit – anti ZO1, both at 4µg/ml and both Invitrogen). Coverslips were then incubated with Alexa-Fluor 488 conjugated secondary antibody (1:500 Invitrogen) in PBS, for 45 minutes at room temperature. Cells were then incubated with Hoescht (1:5000, Sigma), for ten minutes at room temperature. Coverslips were then mounted on glass slides (Fischer) and mounted with Vectasheild (Fischer).

2.5.2. Retina flat mount immunofluorescence

Rats were culled using a lethal dose of Euthatal (Merial Animal Health). Upon confirmation of death, eyes were enucleated using curved forceps and curved tip scissors (World Precision Instruments, WPI) and pierced using a 35g needle, and placed in cold 4% PFA for 1 hour. Eyes were then placed in a petri dish with approximately 100µl PBS, and connective tissue surrounding the eye was carefully dissected away. An incision was made anterior to the ora serrate (figure 2.1A) and microdissection vannas scissors (WPI) were used to cut around the circumference of the eye. The iris, lens and cornea were discarded. One blade of a fine pair of forceps (WPI) was placed between the retina and the sclera (figure 2.1B) and slid gently around the eye cup, to separate the retina from the sclera, followed by 4 incisions being made at 90˚ to each other, vertically approximately 2/3 down the eye. The sample was then turned over and sclera was carefully peeled back to expose the retina in a cross shape (figure 2.1C). Retinae are then transferred to a 24 – well plate and blocked in blocking solution (5% NGS, 3% Triton-X100 and 1%BSA) for 2 hours. Blocking solution was then discarded and replaced with IB4 containing blocking solution (1:200). This was left to incubate at 4˚C overnight, followed by 3 PBS washes at 5-minute intervals and then incubation with Alexa-fluor 488 (1:500, diluted in blocking

solution) at room temperature for 2 hours. After this incubation period, the fluid was carefully aspirated off and discarded, followed by 3 PBS washes at 5-minute intervals. After the last wash, samples were carefully flatmounted onto a microscope slide (VWR) and mounted with Vectashield containing DAPI.

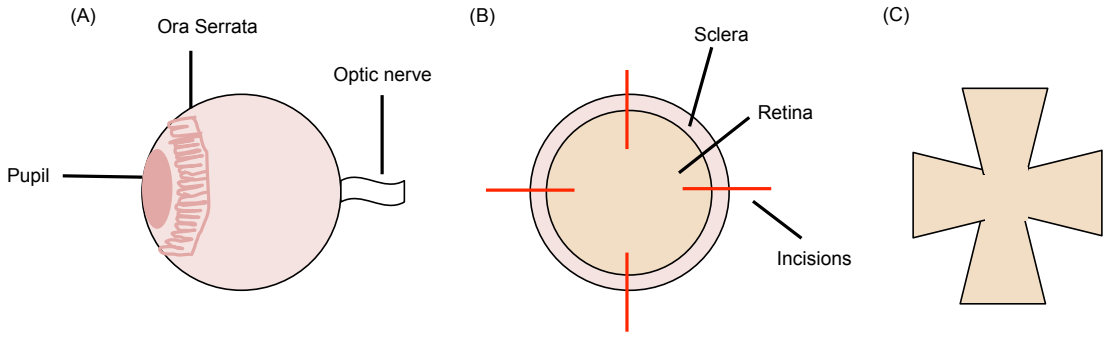

Figure 2.1. Schematic diagrams depicting where incisions are made to flat-mount retinae.

2.5.3. Cryosectioning and immunofluorescence

Animals were sacrificed and eyes were enuculeated and fixed in 4% PFA for 1 hour. Eyes were dissected to eye cups are shown in figure 2.1B, and embedded in O.C.T medium (R.A Lamb), carefully ensuring no air bubbles were trapped in the eye cup. Samples were gently frozen in isopentane (Sigma), which was solidified upon contact with liquid nitrogen. Once the O.C.T had solidified, samples were stored at -20˚C. Samples were then sectioned using a Bright cryostat; 18µm thick sections were then placed onto Superfrost slides (Fischer Scientific), and also stored at – 20˚C.

When staining, slides were air dried at room temperature for 10 minutes, and the perimeter around sections was drawn around using a hydrophobic pen. Samples were washed with 1xPBS for 5 minutes, 3 times. This is followed by blocking for 2 hours at room temperature in block solution containing: 1% BSA, 2% normal goat serum (NGS) and 3% Triton X100. Following this 2-hour period, block solution was carefully discarded from slides and primary antibody, diluted in block solution at the appropriate concentration, was added to the slides and allowed to incubate at 4˚C overnight. Primary antibodies were then discarded from the slides gently, and washed in 1xPBS for 5 minutes, 3 times. This was followed by addition of secondary antibodies (Alexa Fluor

488 and 555 secondary antibodies, Invitrogen) diluted in block solution 1:500 for 2 hours at room temperature. Samples were then mounted in Vectashield containing DAPI and imaged on a confocal microscope at x40 or x63 maginification (Leica SPE).

Antibody	Working concentration	Supplier
Isolectin B4 (biotin conjugated) from *Bandeiraea simplicifolia*	5µg/ml	Sigma Aldrich
Mouse anti-Neun	2µg/ml	Millipore
Mouse anti-occludin	4µg/ml	Invitrogen
Rat anti-ZO1	4µg/ml	Invitrogen
Rabbit anti – CD45	2µg/ml	Abcam
Rabbit anti GFAP	1µg/ml	Abcam

Table 2.3. Primary antibody concentrations used for immunofluorescence staining

2.6. Image analysis

2.6.1. Analysis of cell immunofluorescence

Images were analysed using a custom made macro on Image J that creates a binary image of the picture and a mask overlay that subtracts the nucleus from each image, therefore excluding any nuclear staining. Staining intensity was then calculated relative to control cells.

2.6.2. Image analysis of IB4 stained retinae

Samples were imaged within 24 hours of staining using either an epifluorescence microscope (Nikon Eclipse E400) or a confocal microscope (Leica SPE). Retinae were imaged at 40x magnification and 5 images were taken per retina and analysed using Image J and Imaris software. Further details are described below.

2.6.2.1. Manual vessel count

Vessels were manually counted per field of view using Image J and then an average of each eye was calculated based on the 5 fields of view taken per sample.

2.6.2.2. Integrated density

All images were converted to 8 bit images and integrated density was measured using Image J. Average integrated density was calculated upon the 5 fields of view taken per sample.

2.6.2.3. Analysis using Imaris software

The "surfaces" tool on Imaris software was used to calculate area and volume occupied by vasculature. Minimum vessel diameter was set to 3µm and areas highlighted that were deselected. The "surfaces" tool also calculated vessel straightness (tortuosity) and branch points and endpoints were manually positioned and vessel straightness was measured according to the following formula: height / length of vessel, as shown by figure 2.3.

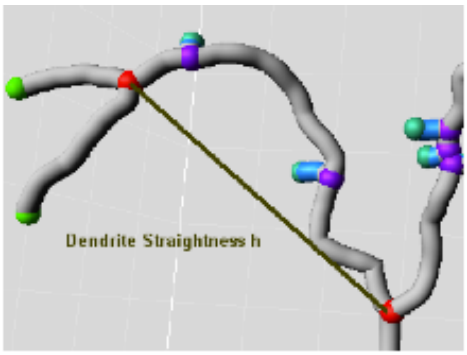

Figure 2.3. Calculation of vessel tortuoisity using Imaris software (www.bitplane.com).

2.6.3. Analysis of immunfluorescent retinae sections

Immunofluorescent cells of interest were either manually counted or total fluorescence per field of view was calculated using integrated density, as previously described.

2.4. DNA work

2.4.1. Transformation of bacteria and amplification of plasmid DNA

Chemically "competent" DH5−α cells (α-Select, Bioline) were aliquoted at 50µl, and were incubated with 5 -10 µl of DNA for 30 minutes on ice. Samples then underwent "heat shock" at 42˚C for 1 minute, followed by a further 5-minute incubation on ice. After this incubation period, 1ml of SOC medium (Invitrogen) was added to each sample, followed by another incubation period at 37˚C for 60 minutes. This would ensure that plasmids containing antibiotic resistance genes would be sufficiently expression, and therefore can be successfully used as a selection marker of all appropriately transformed bacteria. Samples were then carefully smeared, using a sterile spatula, on lysogeny both (LB) / agar plates (10cm^2, Greiner) with the appropriate antibiotics. Plates were incubated at 37˚C overnight, following bacterial colony selection using a sterile, autoclaved pipette tip. DNA from these colonies were amplified using mini – prep kits (GenElute, Sigma). Clones that expressed the appropriate DNA were mixed with glycerol and frozen at -80˚C, ensuring multiple stocks and long term storage. For a larger scale amplification, a sterile pipette tip was used to scrape a fragment of a desired plasmid glycerol stock, and was expelled into a flask containing autoclaved 25% (w/v) LB medium, Flasks were incubated overnight at 37˚C with vigorous agitation of flasks. DNA from flasks was amplfied using a mega-prep kit (EndoFree Plasmid Megaprep Kit, Qiagen).

2.4.2. Cloning

Vectors were usually cloned by using restriction enzymes (New England Biolabs) to remove the insert fragment at the backbone vector to ensure "sticky end" ligation. Alternatively, digestion products were blunted using the Klenow polymerase digestion method, to adjust for the 5' overhangs. Quality assurance of vectors were verified by restriction enzyme digest and sequencing. DNA was quantified using a NanoDrop ND1000 Spectrophotometer (LabTech Int.) using photospectroscopy at 260nm.

2.4.3. Restriction enzyme digests

To verify plasmids or generate fragements for further study, vectors were cut in specific regions using restriction enzymes (New England Biolabs). The reaction mix consisted of: 1µg DNA, 0.5µl per restriction enzyme, 1.6µl 10x buffer 1, 2, 3 or 4 (New England Biolabs) and 1.6µl BSA (New England Biolabs). The mixture was topped up with sterile, deionised water create a total of 16µl in volume. The mixture was incubated at 2hours at 37˚C.

2.4.4. Ligation of DNA

Follwing enzyme digest, purified DNA was inserted into vector backbones at a 1:10 molar ratio of backbone : insert. To ensure correct, site-specific ligation, any residual "sticky ends" were melted at 45˚C for 5 minutes, followed by immediate cooling on ice. Ligation mixes contained : 4µl of DNA, 5µl of ligation buffer (2x LigaFast, Promega) and 1µl of T4 DNA Ligase (LigaFast, Promega). The mixture incuabted at 4˚C overnight, followed by heat inactivation of the ligase at 65˚C for 10 minutes.

2.4.5. Electrophoresis and gel extraction

A 3% (w/v) agarose gel was prepapred using 1xTBE buffer containing ethidium bromide (Sigma, 1:50 dilution). The samples generated from restriction enzyme digest were mixed with 6x loading dye (Blue/Orange loading dye, Promega) and loaded into the wells, with the final well used for a DNA ladder (1kb, Promega). DNA fragments were separated at 190V for a minimum of 30 minutes or until all bands are separated. Gels were imaged using ultraviolet transillumination (Geldoc EZ, BioRad).

Bands of interest were extracted using an ultraviolet light box (and appropriate protection) and a scalpel blade. DNA was was extracted from these isolated bands using a QIAquick Gel Extraction Kit (Qiagen)., and further quantified using a NanoDrop.

2.5. Production of Adeno-associated viruses (AAVs)

2.5.1. Plasmid transfection

A 3-plasmid transfection system was adopted in the production of all viruses. The plasmids used were:

- viral genomic plasmid, expressing the gene of interest. This plasmid is based on a pd10 backbone and will be inserted between the capsid and the ITR. All maps are located in appendices.
- A pHGTI helper plasmid containing various parts of the adenovirus 4 genome, and supplies the AAV with the necessary genes required for A AAV package and assembly.
- An AAV2/8 packaging plasmid, containing the Rep78 gene and the viral capsid gene.

The plasmids in a ratio of 1:3:1 respectively were combined with a polyethylenimine (PEI) and OptiMEM (Invitrogen, UK) transfection reagent to a total volume of 50ml, and allowed to equilibrate for 10 minutes at room temperature. PEI was used in the ratio of 2.25:1 PEI: µg DNA. Following the incubation period, the transfection mix was divided amongst 20x 15cm cell culture plates of confluent HEK293t cells grown in DMEM (Invitrogen, UK), leaving 2.5ml per plate. The mixture was carefully added; drop wise, to ensure minimal disruption to the cell monolayer. The cells were placed back in the incubator and were allowed to grow as normal (37˚C and 5% CO_2) until 2-days post-transfection, when cells would be harvested.

2.5.2. Virus Purification

Cells were scraped off the plate using cell scrapers and re-suspended in total of 15ml TD buffer (140mM NaCl, 5mM KCl, 0.7nM K_2HPO_4, 25 mM Tris HCl (pH 7.4)). The lysate was then subjected to 4 freeze (-80˚C, 20 minutes) /thaw (37˚C, 20 minutes)/vortex cycles to liberate the vector. A further volume of TD buffer was added to the lysate, to increase the volume to approximate 45ml, at which point 50U/ml benzonase (Sigma, UK) was added to the lysate and allowed to incubate at 37˚C for 1 hour, with

intermittent inversion of the falcon tube to allow sufficient mixing of the reaction mixture. This was to ensure that any non–packaged DNA in the lysate would be destroyed.

The lysate is then centrifuged for 30 minutes (2000g) and the supernatant is then filtered through a 0.4µM PVDF filter (Millipore, UK). Upon confirmation that the lysate is endotoxin-free, filtered lysate was purified using a 2-step AKTA prime fast protein liquid chromatography (FLPC) ion-exchange system (GE Healthcare, USA), whereby the virus was purified according to its binding affinity to a resin, chosen according to its binding affinity with the virus. After the lysate has been prepared, fractionating tubes containing purified virus were chosen according to the peak they produced during the elution stage, and pooled together, and topped up with an equal volume of PBS-MK. The mixture was then divided between two Vivaspin 4 (GE healthcare) columns (10kDa) and centrifuged (5000g) for 15-minute intervals until the total volume of virus is approximately 100µl. The virus is then pooled into a tube and topped with an equal volume of PBS-MK, and then distributed into 30µl aliquots and stored at -80˚C.

2.5.3. Quantifying Viral Genome Copy Numbers

Viral genome copy numbers were determined by dot blot hybridisation and also by qPCR.

2.5.3.1. Titering of AAV using qPCR

To establish virus titre by qPCR, a PD10 plasmid was linearised using HindIII (New England Biosciences, USA) and diluted in a series of 6-fold dilution steps (10^5 – 10^{11} molecules), to establish a standard curve. Each virus sample was diluted in a series of 4 10-fold serial dilution steps, in triplicate. The amplification reaction mix contained: 5µl AAV2/8 sample or standard, 12.5µl Master Mix (Sigma-Aldrich, USA), 1µl ITR forward primer diluted to 100nM, 3.4µl ITR reverse primer diluted to 340nM, 1µl probe diluted to (Sigma-Aldrich, USA), 2.1µl ddH_2O, resulting in a final volume of 25µl per well. A 7900HT Fast Real-Time PCR system (Applied Biosystems, USA) was used to run the reactions (50˚C for 2 minutes, 95˚C for 10 minutes, 95˚C for 15 seconds and 60˚C for 1 minute, 40 cycles). The Sequence Detection Systems programme (SDS 2.2.2, Applied Biosystems, USA) plotted a graph of cycle number against fluorescence intensity, where

the thresholds were determined on the most linear part of the graph. The value obtained at this point of the graph, the cycle number at threshold (Ct) value was plotted against number of molecules, equation of the best-fit line (y=mx+c) was then used to calculate the titre of the virus.

2.5.3.2. Titering of AAV using dot blot hybridisation

Viral genome copy number was also established by dot blot hybridization. Aliquots of 5µl and 1µl of each virus was used to establish viral titre. To each sample, 95µl or 99µl of ddH_2O respectively was added, followed by 100µl proteinase k buffer (2x, Sigma) and 1µl proteinase k and the reaction mixture was incubated at 56˚C for 30 minutes. Following this incubation, 20µg glycogen (Sigma), 21µl sodium acetate (3M NaOAc) and 500µl ethanol absolute (Sigma) was added to the mixture, which was followed by another 30-minute incubation, at -20˚C. The samples were centrifuged for 10 minutes at 14000 rpm, followed by pellet wash with 70% ethanol (sigma) and an additional 2 minute spin. The pellet was then dissolved in 200µl sodium hydroxide (Sigma) and 10mM Ethylenediaminetetraacetic acid (EDTA, Sigma). A dilution series of plasmid DNA was used to calculate the viral genome copy number. When calculating the titre of the AAV.$VEGF_{165}$b, a probe was used against the CMV promoter, however AAV.Null does not have a CMV promoter, and so an alternative biotinylated probe was made. The desired fragment was excised from a 1% agarose gel using a gel-extraction kit (Invitrogen). The fragment was resuspended in 65µl ddH_2O, and a 34µl aliquot was denatured at 95˚C for 2 minutes, followed by a 2-minute incubation on ice. To the reaction mix, the following was added in this order: 10µl 5x labeling mix (containing random octomers), 5µl dNTP mix, 1µl Klenow fragment (New England Biosciences) and left to incubate at 37˚C for a minimum of 1 hour. The biotinylation reaction was terminated by adding 5µl 0.2M EDTA, pH 8. The probe was then precipitated by adding 5µl 3M NaOAc, 150µl 100% ethanol and incubating at -20˚C for 20 minutes. The mixture was then centrifuged at 14000 rpm for 10 minutes at 4˚C. The probe was resuspended in 20µl TE buffer (Invitrogen). 5µl of the probe was added to 0.4M NaOH and 10mM EDTA in a total of 180µl, and denatured for 95˚C for 2 minutes, and then transferred to ice.

Following preparation of samples and probe, a nylon membrane (GE Healthcare, USA) was attached to a dot blot manifold (Bio-Rad, USA). The wells to be used were

filled with 200µl ddH_2O, vacuumed, and then filled with 200µl of each sample and diluted plasmid DNA, vacuumed and then filled with 200µl 0.4M NaOH 10mM EDTA, and vacuumed a final time. The membrane was dried for 2 hours at 95˚C. Meanwhile, the Church's hybridization buffer (500ml $NaHPO_4$, 10g BSA, 2ml 0.5M EDTA, 70g SDS, in 1L ddH_2O) was heated to 65˚C, and the membrane was placed in the warmed solution, and allowed to rotate for a minimum of 30 minutes. 5µl of the denatured biotinlyated probe was added to the mix, and allowed to hybridize overnight. Following this incubation, the Church's mix is discarded, and the membrane is washed in 40ml 33mM NaPi for 5 minutes. This process is repeated a further three times, upon which the membrane is placed in a tray and submerged in block solution (5% SDS, 125nM NaCl, 25nM $NaPO_4$), for 5 minutes at room temperature, and then repeated for another 5 minutes but with streptavidin diluted 1:1000 (New England Biosciences, USA). This is followed by two 5-minute washes in wash solution I (diluted block solution 1:10). The solution is then drained off and then replaced with 1:1000 biotinylated alkaline phosphatase (New England Biosciences, USA), diluted in block solution, for 5 minutes, followed by a 5 minute incubation in block solution alone and two 5-minute washes in wash solution II (50mM Tris-HCl, 1mM $MgCl_2$, 1mM NaCl, pH 9.5). The membrane was removed, and placed on acetated and CDP-Star reagent mix (New England Biosciences, USA) was added to the blot for 5 minutes. The solution was drained and imaged on a Fujifilm LAS-500 at 470nm.

2.5.4 Assessment of Virus purity

To establish the purity of the virus, proteins in the AAV2/8 virus were separated electrophoretically on a 10% polyacrylamide gel. Then 5µl and 1µl of each virus were tested with 5µl 2x Laemmli buffer (4% SDS, 20% glycerol, 10% 2-mercaptoethanol, 0.004% bromphenol blue and 0.125 M Tris HCl, pH6.8.), 0µl and 4µl of PBS-MK respectively, giving a total of a 10µl reaction mixture for each sample. The samples were incubated at 95˚C for a maximum time of 10 minutes, and then loaded onto the gel. The samples were allowed to run until the blue dye ran to the bottom of the gel. The gel was then placed in 100ml fix solution (50% methanol, 7% acetic acid in dH_2O) and was placed on a shaker at 55rpm for 30 minutes at room temperature. The solution was then poured off, and 100ml SYPRO® Ruby gel stain was added to the gel, and allowed to incubate overnight at room temperature at 55rpm, surrounded in foil to prevent entry of

light. Following this incubation period, the solution is poured off, and replaced with wash solution (10% methanol, 7% acetic acid in dH_2O), for 30 minutes followed by another 30-minute wash. After the second wash, the gel is washed in ddH_2O for a minimum of 2 minutes, and then imaged (GelDoc, Syngene), bands were expected at 80kDa, 65kDa and 59kDa representing the presence of the VP1, VP2 and VP3 proteins within the AAV2 capsid.

***In vivo* work**

Mice and rats were maintained in the animal facility at University College London, University of Bristol and the University of Nottingham. Experiments were conducted in accordance with the Policies on the Use of Animals and Humans in Neuroscience Research, revised and approved by the ARVO statement for the Use of Animals in Ophthalmic and Vision Research.

2.6. Intraocular Injections

Two types of intraocular injections were performed during the course of this study: intravitreal and subretinal. Intravitreal injections were used to deliver drugs to the eye for short–term evaluation of PBS and $rhVEGF_{165}b$. Sub–retinal injections were used to deliever AAVs to the retina, and ensure long – term expression of our vector of interest.

2.6.1. Intravitreal injections

Intravitreal injections were performed under a dissection microscope in anaesthetised rats. Rats were anaesthetised with a single 10mg/ml intra-peritoneal (i.p) injection of Dormitor (medetomine hydrochloride, Pfizer, UK) and Ketaset (ketamine hydrochloride, Zoetis, USA). Pressure was applied either side of the eye using fine, curved forceps (World Precision Instruments), allowing the eye to become more exposed. The eye was then grasped at the conjunctiva and a 1.5cm 34-gauge hypodermic needle (Hamilton, Switzerland) attached to a 5µl syringe (World Precision Instruments) was inserted into the posterior chamber of the eye at a 45˚ angle. 5µl of either sterile PBS or

50ng rhVEGF$_{165}$b was injected into the vitreous. Animals were then recovered and monitored for approximately 2 hours and returned to their cages with wet mash.

2.6.2. Subretinal injections

Subretinal injections were carried out under general anaesthesia using an operating microscope (Zeiss). Rats were anaesthetised as described above, and pupils were dilated using 1% w/v tropicamide (Bausch and Lomb). A 5mm coverslip (Fischer) was attached to the eye using Viscotears ® (Novartis Pharmaceuticals), to minimise corneal refraction of light. Fine forceps (World Precision Instruments) were placed either side of the eye with slight pressure, to expose the eye further. Whilst holding the eye at the conjunctiva, a 1.5cm, 34 gauge needle in a 5µl syringe (both Hamilton, World Precision Instruments). The needle was placed under the coverslip and pierced the sclera under the ora serrata and into the subretinal space. Contents of the syringe were then expelled into the subretinal space to form a retinal detachment or "bleb". Animals usually had two subretinal injections, one in the superior region of the retina and one inferior. The needle was carefully removed to prevent backflow of injected material from the vitreous, and 1% w/v chloramphenicol (FDC International) was applied to the eye to prevent infection and the anaesthesia was reversed. Mice had 2 x 2µl injections and rats were subject to 2 x 4µl, 5µl or 6µl injections.

2.7. Streptozotocin–induced diabetes

2.7.1 Induction of 8–weeks diabetes

Female Sprague-Dawley rats (200-300g, Harlan and Charles River in University of Bristol and University of Nottingham respectively, n = 45) were weighed and fasted overnight, prior to diabetes induction. The following morning, rats were given a single intraperitoneal (i.p) injection of streptozotocin (STZ, 50mg/kg, Sigma) freshly made in ice cold saline and a foil covered bijou, control rats were injected with 300µl saline i.p. Rats were then given 30% sucrose (Fischer Scientific drinking water and normal food *ad libitum.* On the same day, a third of an insulin capsule (LinShin) was implanted subcutaneously using a 15g trocar under isofluorane anaesthesia (3-5%), to maintain body

weight over the following 8 weeks. On day 4 post–induction of STZ, blood glucose was tested from a bolus of blood extracted from the tail vein and assayed using an AccuChek monitor. Rats with blood glucose of 15mmol/l and above were deemed diabetic. If any STZ–injected rats did not become hyperglycaemic on day 4, they were re-fasted overnight and then re-injected with STZ the following morning. Diabetic rats were treated with 20ng/g rhVEGF$_{165}$b (i.p, R&D Systems) biweekly for the experimental period or saline (n = 15 for both). Control groups remained untreated for the duration of the experiment. Drinking water supplemented with 30% sucrose was replaced with normal drinking water 3–days post induction of diabetes. Oestrus stages were not controlled during the experiment. Rats were weighed biweekly for the duration of the experiment.

2.7.2 Induction of 1-week diabetes

Female Sprague dawley rats (200- 250g, Harlan) were weighed and fasted overnight prior to induction of diabetes. The following morning, rats were injected with freshly prepared STZ in PBS (50mg/kg) as mentioned previously. On day 6 post-induction, blood glucose was assessed using an Accuchek monitor, and those with a blood glucose ≤15mmol/l were sacrificed. Those that had higher blood glucose were subject to an intravitreal injection of vehicle (5µl PBS) in one eye and VEGF$_{165}$b (50ng) in the contralateral eye. Control animals had vehicle in one eye and no injection in the contralateral eye. On day 7, rats were terminally anaesthetised and subject the Evans' blue dye perfusion technique.

2.8. Evans' blue dye perfusion

An Evans' blue dye perfusion experiment was conducted to assess BRB breakdown. Evans Blue has been shown to quantitatively measure vascular leakage in the retina (Xu *et al.,* 2001), therefore a similar protocol has been adopted with minor changes.

Evans' blue dye (Sigma) was prepared by dissolving it in normal saline (45mg/kg) and filtered were anaesthetised with 10mg/ml Vetalar (ketamine hydrochloride, Boehringer Ingelheim, Germany) and Dormitor (medetomine hydrochloride, Pfizer, UK) with additional anaesthesia provided as needed. The left jugular vein and femoral artery

were cannulated with with 33 gauge tubes filled with saline and heparinised saline (400UI/ml) respectively. Evans' blue was injected via the left jugular vein over 10 seconds, followed by 100µl saline. Two minutes post-infusion, 200µl blood was removed from the femoral artery, to establish the initial Evans' blue concentration. Fifteen minutes post-infusion, 100µl blood was removed, and this volume was withdrawn every 15 minutes for two hours, which would determine the time-averaged Evans blue-plasma concentration. Eyes were kept moist using Viscotears (Novartis Pharmaceuticals). Two hours post-infusion, the chest cavity was opened and 200µl blood was withdrawn from the left ventricle, to determine the final plasma Evans blue concentration. Following this, the rats were perfused with 50ml saline through the left ventricle at a physiological pressure of 120 mm Hg, to flush out Evans' blue from the circulation.

Immediately after perfusion, both eyes were enucleated and bisected at the equator. The retinas were dissected and weighed (wet weight) and then dried at 70˚C overnight, and weighed again (dry weight). 120µl formamide was added to each sample and was kept at 70˚C overnight, to extract the Evans blue from the samples. Following the dye extraction, the samples were centrifuged at 12000 rpm at 4˚C for 45 minutes. The supernatant was used to determine the Evans blue concentration, and was diluted 1:1 in formamide.

The blood samples were kept on ice through the experiment and then centrifuged at 4˚C at 12000 rpm for 45 minutes and diluted 1/100 in formamide (Sigma). The absorbance of all samples was then measured at 620nm, and the concentration of Evans' blue dye in formamide was calculated using a standard curve of Evans' blue in formamide. Formulae for solute flux and permeability – surface area product (PA) are in the appendix.

2.9. Imaging of the eye *in vivo*

To assess changes in vasculature, thickness and overall atrophy *in vivo*, animals were imaged using the Spectralis ® (Heidelberg Engineering, Germany). All *in vivo* imaging was carried out under general anaesthesia, followed by dilation of the pupil using tropicamide. Following imaging, animals were then recovered or sacrificed according to experimental end point. All imaging was quantified using Image J by calibrating the scale appropriately, circling a region of interest and measuring the area of that region.

2.9.1. Scanning Laser Ophthalmoscopy

Scanning Laser Ophthalmoscopy (SLO) was used to assess changes in geographic atrophy in the retina using the Spectralis HRA with a 55˚ lens (Heidelberg engineering). Anaesthetised animals were positioned in front of the lens such that the whole eye was in focus, with the pupil in the centre. This was facilitated using the infrared setting (790nm) on the machine (figure 2.XA). Once the optimal position was acquired, settings were changed to the 488nm laser at a power setting of 95% and images were taken, and an average was taken over 30 individual frames. One image was captured focused on the retina and a second image was taken focused as much on the choroid as the camera would allow (figure 2.4A).

This was then repeated for the contralateral eye.

The same protocol was adopted when assessing fluorescein leakage in the choroid, with the addition of a single ip injection of 200µl of 2% fluorescein (Sigma) in sterile water. Fluorescein was injected immediately before dilation of pupils, and images were taken over a 90 second period, as decribed above.

2.9.2. Optical Coherence Tomography

Retinal thickness was measured using spectral domain optical coherence tomography (SD-OCT) with minor modifications to accommodate the rat eye. To ensure that differences in refraction power, eyeball length, focal length and maximal pupil dilation between humans and rats could be adjusted for (Guo et al. 2010), a customised, achromatic 30˚, ±25 – diopter doublet lens was attached to the machine. A single B–scan (figure 2.4) was taken at 8 different points in the retina, as shown by figure 2.4C.

OCT images were usually carried out immediately after capturing SLO images under the same anaesthesia, with additional maintenance of anaesthesia as required. Eyes were kept moist using 0.3% w/v hypromellose drops (Martindale Pharma) and were carefully removed using cotton swabs. Already – dilated eyes were focused on, with particular emphasis on the radial lines formed by the nerve fibre layer on the infrared setting. When a satisfactory position was acquired, OCT mode was selected and cursor was placed according where the desired B – scan would take place, and a 30 frame image was captured, as well as the location at which the B – scan was taken. This ensured that at

subsequent monthly time points, the software would recognise where the image was taken and re-capture a B-scan at that same place.

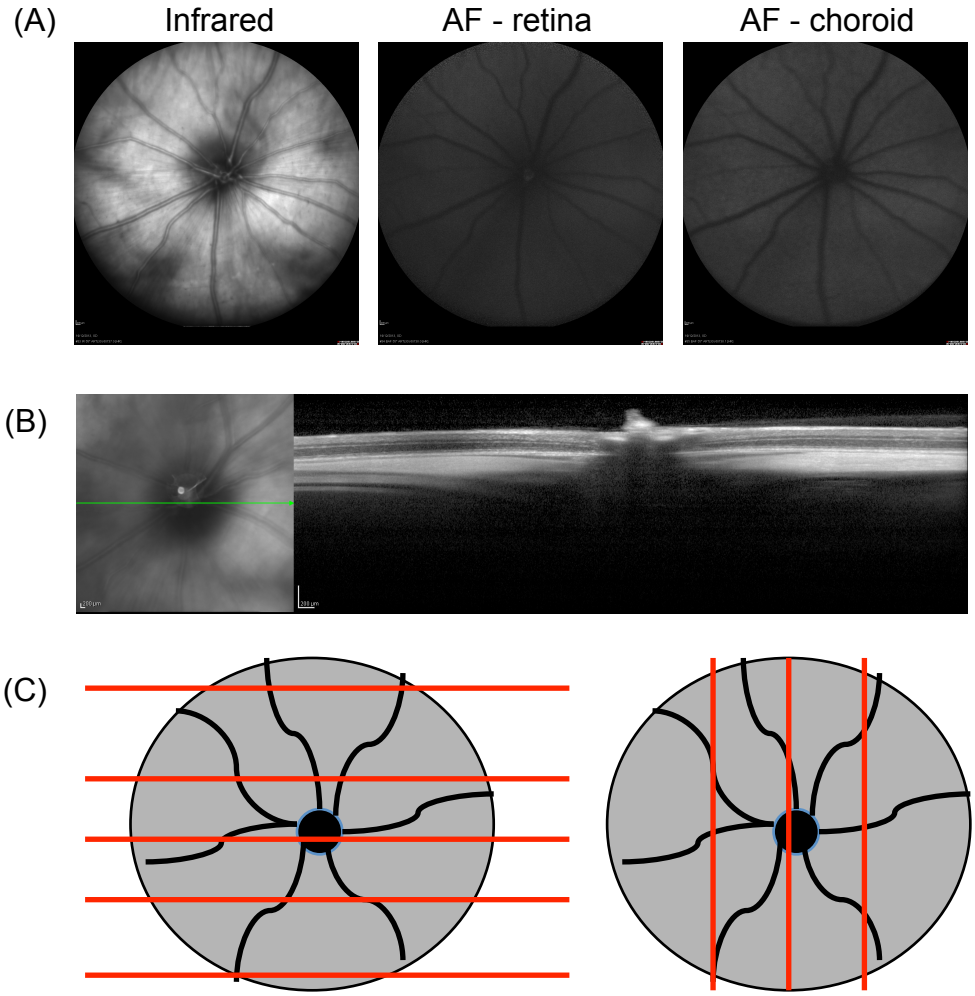

Figure.2.4. *in vivo* imaging using the Spectralis ® HRA + OCT.

Anaesthetised animals were imaged using a 55˚ lens under infrared settings (A) to establish a central optic disc. The setting was then switched to a confocal SLO 488nm laser to assess autofluorescence (AF) of the retina and choroid. OCT images (B) were also taken under the same anaesthesia to determine thickness of the retina. Individual B–scans (C) were captured at 8 different points within the retina, and repeated at these same points, monthly.

2.10. Electroretinograms

Changes in retinal neural architechture were assesed *in vivo* by measuring the electroretinogram (ERG) once a month (Espion 6, Diagnosys UK) in dark adapted

(minimum 5 hours) diabetic and non-diabetic Lewis rats. Lewis rats were anaesthetised using Dormitor and Ketaset as described above. Pupils were dilated using tropicamide and phenylephrine (1% w/v, Bausch & Lomb, UK). Anaesthetised rats were then connected to four electrodes, 2 on each cornea, 1 under the tongue and 1 in the tail to ensure a complete circuit with minimal external electrical activity interfering with the readings. Corneal electrodes were placed on eyes with Viscotears ® (Novartis) on the eyes to ensure good connectivity and low impedence within the circuit. Following an additional 5 minute dark adaptation, an 11-step scotopic program with light intensities ranging from 0.0001 (S)cd.s/m^2 to 75.28(S)cd.s/m^2 was started. After the scotopic programme, a 6-step photopic programme was started following a 5-minute light adaptation, with intensities from 0.1(S)cd.s/m^2 to 75.28 (S)cd.s/m^2.

2.11. Laser–induced choroidal neovascularization

To assess the anti-angiogenic properties of vectors, mice were subject to laser induced CNV 2 - weeks post – subretinal virus administration. Mice were anaesthetised and 3 laser burns were delivered to retina of each eye using a slit – lamp – mounted diode 680 nm laser (Keeler, UK). The laser burns were at 210mM for 100ms with a 100µm spot diameter (Balaggan et al. 2006). A successful breach of Bruch's membrane was noted down when a small gas bubble was evident, subretinally. Burns where there was no "successful" subretinal bubble were excluded from further analysis. This was repeated in the contralateral eye. Mice were then subject to fluorescein angiography at 3, 7 and 14 days post – laser, using the Spectralis ® (Heidelberg Engineering), as described previously. On day 14, mice were sacrificed after imaging and choroids were flatmounted and stained for IB4. Flatmounts were imaged using a Leica SPE confocal microscope Analysis of *in vivo* and *ex vivo* images were carried out using Image J and any burns that had merged were also excluded from analysis.

2.12. Statistical Analyses

Unless otherwise stated, all data are shown as mean ± SEM. All data, graphs and statistical analyses were calculated with Microsoft Excel (Microsoft Office Software), GraphPad Prism (GraphPad Software Inc.), Image J and Imaris (Bitplane). Parametric

and non-parametric statistical tests were chosen upon the results of the D'Agostino-Pearson normality test in Graphpad Prism (GraphPad Software Inc.). All results were considered statistically significant at $p<0.05$ (*), $p<0.01$ (**) and $p<0.001$ (***).

Chapter 3: Assessing RPE barrier properties *in vitro*

3.1. Introduction

The retina is the most metabolically active tissue in mammals (Xu et al. 2011) and therefore requires a rich blood supply. The inner retina, including retinal ganglion cells (RGCs), Müller glia and amacrine cells, is supplied by the central retinal artery, which branches into a complex retinal microvascular network. The outer retina, including RPE and photoreceptors, is supplied by the choriocapillaris, a dense area of fenestrated capillaries in the choroid (Xu et al. 2011). The BRB is similarly subdivided. The inner BRB is formed by retinal microvascular endothelial cells and the outer BRB, formed by the RPE, both of which exert a protective role over the inner and outer retina respectively from cytokines and inflammatory factors of the systemic circulation (Omri et al. 2011). Traditionally, PDR and DME are thought to be diseases of inner BRB dysfunction, as most exudate formation occurs as a result of lipid leakage, protein leakage and cyst formations from microvascular endothelial cells with compromised TJs. As a result, less emphasis has been placed on dysfunction of the RPE and the outer BRB in the pathogenesis of DR.

The RPE is a monolayer of epithelial cells and provides a selectively permeable barrier to ions, lipids and fluid between the outer retina and the choriocapillaris. Paracellular flux is highly regulated by tight-junctions (TJs) in the cell membrane that allow the RPE layer its barrier function, including the family of claudins, occludin and the zonula occludens (ZO) family (Xu et al. 2011). RPE are polarised cells and express VEGF receptors (Ivana Kim et al. 1999) and GLUT receptors (Takata 1996) and also supply VEGF and glucose to the choriocapillaris and neural retina to maintain synchrony with the high metabolic demand of the rest of the eye and maintain fenestrations of the choroidal endothelium respectively (Simó et al. 2010). When the extracellular environment stresses RPE, for example during hypoxic conditions where there are high levels of VEGF, TJs such as occludin and the claudins are compromised and undergo phosphorylation and ubiquitination, causing their internalisation (Murakami et al. 2009). Upon internalisation, TJs are either degraded or recycled back to the cell membrane (Harhaj & Antonetti 2004). It is this internalisation of TJs that allows increased paracellular transport of fluid, which can then accumulate in the subretinal space. If left unimpeded, this can result in oedema and retinal detachment.

Pigment epithelium derived growth factor (PEDF) and VEGF are two of the principal growth factors secreted by the RPE, and exert opposing actions. PEDF is proposed to have anti-angiogenic properties (Dawson 1999) and VEGF is well known for its potent angiogenic activity (Leung et al. 1989). Whilst it is well-documented that up-regulated VEGF results in TJ breakdown (Antonetti 1999), reductions in anti-angiogenic PEDF also elicit a similar effect (Dawson 1999), and by increasing PEDF, VEGF-induced increases in RPE permeability are inhibited (Simó et al. 2010).

Relative to RECs, the importance of RPE and their involvement in the pathogenesis of DME has only recently been established. Changes in the RPE proteome occur early on in patients with DR in a "pre-retinopathic" phase, whereby markers of increased metabolism and oxidative stress are up-reglated (Decanini et al. 2008). Patients also showed increased fluorescein leakage from the RPE in the peri-macular region, independent of cystic changes, a characteristic of inner BRB breakdown (Weinberger et al. 1995; Xu et al. 2011). In experimental models of diabetes, studies have shown an impaired C-wave amplitude (Pautler & Ennis 1980), leakage of fluorescein in the outer retina (Xu & Le 2011) and morphological changes in RPE (Aizu et al. 2002), all indicative of RPE dysfunction.

There is mounting evidence to suggest that dysfunction of the RPE layer has a significant role in the progression of DME. I wanted to investigate this notion with the hypothesis VEGF-induced dysfunction of the ORB may be prevented using anti-angiogenic therapy. To address this hypothesis further, this study looked at cultured primary human RPE (primary hRPE) and established if VEGF and hyperglycaemia induced changes in barrier properties such as reduced TJ expression and increased paracellular flux, as published in the literature, could be prevented using $VEGF_{165}b$. Furthermore, I wanted to establish an *in vitro* model of DME using cultured RPE and culturing them in high-glucose environments to observe changes in TJ integrity, and if so, to reverse them with $VEGF_{165}b$ treatment.

3.2. Methodology

Human primary RPE (1˚RPE) were extracted from donor eyes (Bristol Eye Hospital and Institute of Ophthalmology) and were cultured for use *in vitro*. RPE were assayed for tight junction (TJ) immunofluorescence and protein expression with and without VEGF intervention. Furthermore, RPE were assayed for changes in paracellular flux by assessing trans-epithelial electrode resistance (TEER) upon VEGF treatment. Hyperglycaemia assays were also carried out on RPE cells, and assayed for TJ integrity through occludin immunofluorescence and protein expression and TEER, with and without VEGF co-treatment. 5mM and 35mM glucose were added to media already supplemented with glucose (17mM). These concentrations were chosen because RPE cultured in media without supplemented glucose were difficult to maintain. Conditioned media from these treatments were assayed for VEGF expression (ELISA). Unless otherwise stated, all replicates are technical replicates. All methods are described in detail in Chapter 2.

3.3 Results

3.3.1. Effect of $VEGF_{165}$ on 1°RPE cells and tight junction integrity

To assess the effect of $VEGF_{165}$ on the outer BRB *in vitro,* RPE cells were subject to a $rhVEGF_{165}$ dose-escalation experiment. Staining was quantified using ImageJ (see chapter 2 "Materials and Methods"). As the dose of $VEGF_{165}$ increased, occludin fluorescence intensity decreased (figure 3.1A). There was a significant reduction upon 1.0nM $VEGF_{165}$ treatment (0.75±0.03, figure 3.1B) when compared with untreated cells. This is further noticeable when the dose increases to 2.5nM (0.592±0.0346) and 5.0nM (0.461±0.0628), when compared with untreated controls.

(A)

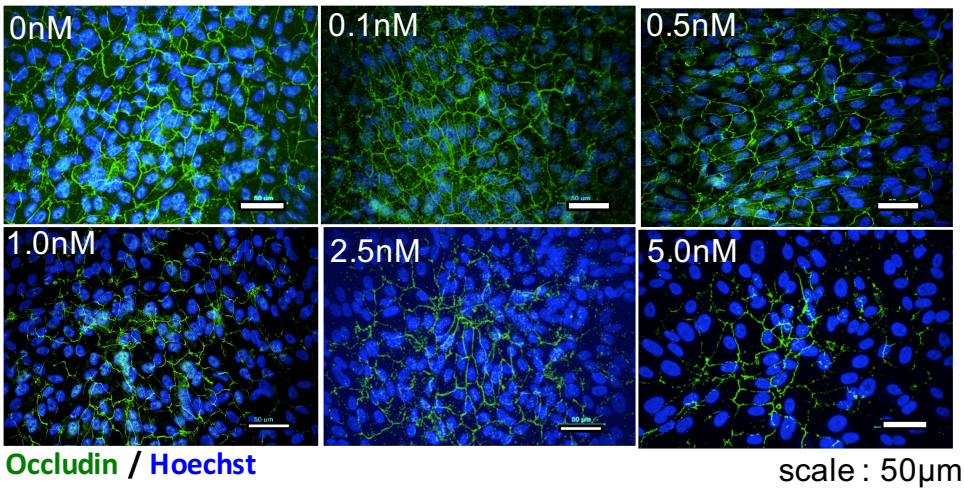

(B)

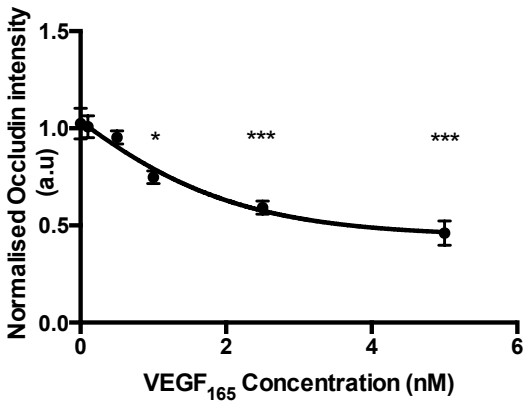

Figure.3.1. $VEGF_{165}$ dose dependently reduces TJ expression in RPE cells.

RPE cells were treated with increasing doses of $rhVEGF_{165}$ for 24 hours (n=3). Cells were fixed and (A) stained for TJ marker, occludin (green) and nuclei co-stained with Hoechst (blue). Normalised data (B) showed that as the dose of $VEGF_{165}$ increases, occludin expression decreases at the cell membrane achieving significance at 1.0nM ($p<0.05$), 2.5nM ($p<0.001$) and 5.0nM ($p<0.001$) (One-way ANOVA, Dunnett's post-hoc, *$p<0.05$, ***$p<0.001$).

Although a loss in TJs is indicative of increased barrier permeability *in vivo*, to confirm that TJ loss results in increased barrier permeability *in vitro*, RPE cells were plated on 8-well ECIS plates, and TEER was measured upon $VEGF_{165}$ treatment (0, 0.1, 0.5, 1.0, 2.5 and 5.0nM). As time progressed, permeability increased in all groups treated with $VEGF_{165}$, however, it became significant upon 2.5nM and 5nM treatment (figure 3.2A). Interestingly, 1nM treatment showed no significant change in paracellular flux, however, when calculating the area under the curve (figure 3.2B), there was a clear trend showing that as $VEGF_{165}$ concentration increased, so too did the area under the curve, indicating a trend in increased paracellular flux. These data were normalised and (figure 3.2C) and then log transformed (figure 3.2D) showing an EC50 of 0.97nM, further details are in chapter 2 "Materials and Methods".

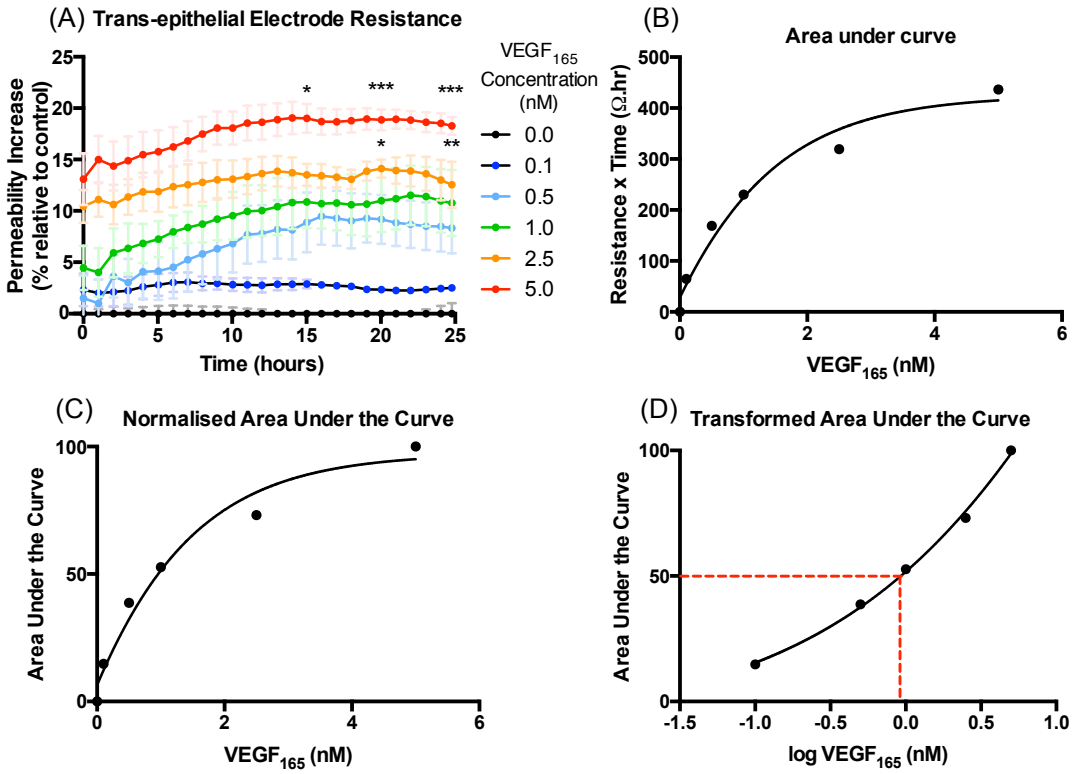

Figure 3.2 $VEGF_{165}$ dose-dependently increase paracellular flux in RPE cells.

RPE cells were plated on ECIS plates (n=3, mean+SEM) and subject to a range of $VEGF_{165}$ concentrations (0 – 5.0nM). Impedance was measured every hour for 24 hours and permeability was calculated as 1-resistance. As concentration increased, so did permeability (A) achieving significance at 15 hours post treatment at 5.0nM and 20 hours post treatment at 2.5nM (2-way ANOVA with Bonferroni post-hoc, significance shown at 5-hour intervals). This was reflective in the area under the curve (B). When normalised (C) and then transformed (D) and constrained between 0 and 100%, the EC50 could be calculated (red line) as 0.97nM (*$p<0.05$, **$p<0.01$, ***$p<0.001$).

The RPE layer has been proposed to be the primary source of VEGF in the outer retina *in vivo*, and that VEGFR1 and VEGFR2 are preferentially expressed on the basolateral aspect of the cell (nearest to the choriocapillaris) (Saint-Geniez et al. 2009a). Decreased VEGFR2 expression in endothelial cells is associated with a reduction in permeability (Whittles et al. 2002), and so I hypothesised that an increase in VEGFR2 expression in RPE cells would correlate with a decrease in TJ expression. To test this hypothesis, RPE cells were treated with $VEGF_{165}$ of varying doses for 24 hours, and protein lysate was assayed by western blot for occludin expression and VEGFR2 expression.

As the concentration of $VEGF_{165}$ increased, occludin expression decreased (figure 3.2A) as it did in figure 3.1A. Again, much like figure 3.1A, the change in expression was significant upon 1.0nM $VEGF_{165}$ treatment (0.724±0.0302, figure 3.2B) and a greater decrease was seen at 2.5nM $VEGF_{165}$ (0.558±0.153) and 5.0nM (0.424±0.0506), with an IC50 of 1.11nM (figure 3.2C, red line). VEGFR2 expression increased, upon an increase in $VEGF_{165}$ concentration (figure 3.2B), again being significant at 1.0nM (0.929±0.0417) and further increasing with 2.5nM (0.996±0.0100) and 5nM (0.998±0.0142) with an EC50 of 0.62nM (figure 3.2C, blue line).

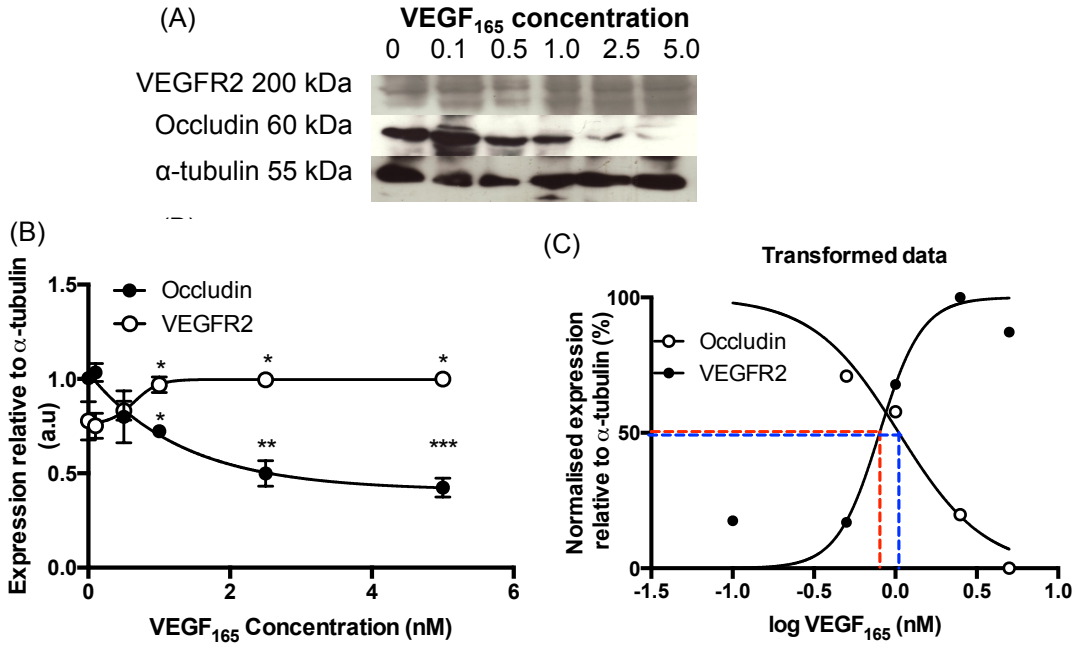

Figure 3.3. $VEGF_{165}$-induced occludin degradation is mediated through VEGFR2 in RPE cells.

RPE cells (n=2, mean+SD) were subject to $VEGF_{165}$ treatment of varying doses for 24 hours (0nM – 5.0nM). Protein lysate was then extracted and immunoblotted for occludin and VEGFR2 expression. Membranes were stripped and reprobed for α-tubulin expression to confirm equal loading of protein (A). $VEGF_{165}$ significantly reduced occludin expression at 1.0nM, 2.5nM and 5nM (B). VEGFR2 expression conversely increased upon $VEGF_{165}$ treatment, also significantly at 1.0nM, 2.5nM and 5nM (B). These data were normalised, log transformed and constrained to 0% and 100% to calculate IC50 (red line) and EC50 (blue line) of occludin (1.11nM) and VEGFR2 (0.62nM) respectively (C). (One way ANOVA with Dunnett's post hoc test, *$p<0.05$, **$p<0.01$, ***$p<0.001$)

3.3.2 Effect of $VEGF_{165}$b on primary human RPE tight junction integrity

It has been hypothesised that diabetes induces a switch in splicing in the human eye that favours pro-angiogenic isoforms relative to anti-angiogenic isoforms (Perrin et al. 2005), and that this imbalance of both isoforms attributes to DR. $VEGF_{165}$b is anti-angiogenic in the eye as shown by a reduction in neovascular area in rodents with laser-induced CNV, a model for AMD (Konopatskaya et al. 2006). It is possible that if the imbalance of both isoforms is redressed, $VEGF_{165}$b may also elicit an anti-angiogenic response in the diabetic eye and therefore may be a potential target in treating PDR. To test the feasibility of using $VEGF_{165}$b, RPE cells were subject to a dose-escalation

experiment using $VEGF_{165}b$ at 0, 0.1, 1.0, 2.5 and 5.0nM, to keep consistent with figure 3.2. Cells were then assayed for changes in TEER over 24 hours.

There was a slight increase in paracellular flux upon $VEGF_{165}b$ treatment, which was not dose dependent and not significantly different when compared to 0nM when assessing changes in permeability (figure 3.4A). Interestingly, when measuring area under the curve, it indicated that as the $VEGF_{165}b$ concentration decreased, paracellular flux increased with an IC50 of 0.7nM.

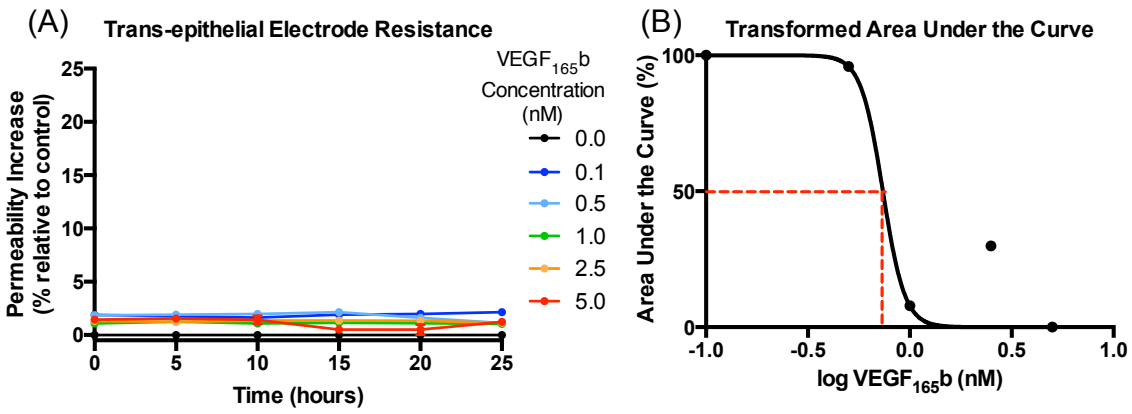

Figure 3.4 Increasing doses of $VEGF_{165}b$ has minimal effect on paracellular flux

RPE cells were plated on ECIS plates (n=3, mean+SEM) and treated with varying concentrations of $VEGF_{165}b$ (0nM – 5.0nM) and impedance was measured over 24 hours (A). There was no significant difference between any concentration at any time point over 24 hours (2-way ANOVA with Bonferonni's post hoc). When measuring area under the curve, data were normalised and log transformed to show an IC50 of 0.7nM.

I wanted to assess the ability of $VEGF_{165}b$ to abrogate $VEGF_{165}$ induced changes in TJ expression and permeability, however we needed to establish at what proportions of each drug to co-treat with and how this may affect solute flux. To assess this, I treated RPE cells with a single concentration of $VEGF_{165}$ and increasing $VEGF_{165}b$, thereby changing the proportion of $VEGF_{165}$: $VEGF_{165}b$. I chose 1nM $VEGF_{165}$ as my constant as the IC50 (figures 3.1 and 3.3) or EC50 (figure 3.2) of $VEGF_{165}$ was approximately 1nM when assessing TJ dysfunction and it was also the minimum concentration required to induce any change in TEER. Once treated, TEER was assayed for 24 hours. When compared with untreated wells (figure 3.5A), the minimum concentration required to prevent $VEGF_{165}$–induced changes in solute flux was 0.2nM $VEGF_{165}b$ at 24 hours

(0.972±0.105). When assessing area under the curve (figure 3.5B), the IC50 was calculated as 1.07nM $VEGF_{165}b$.

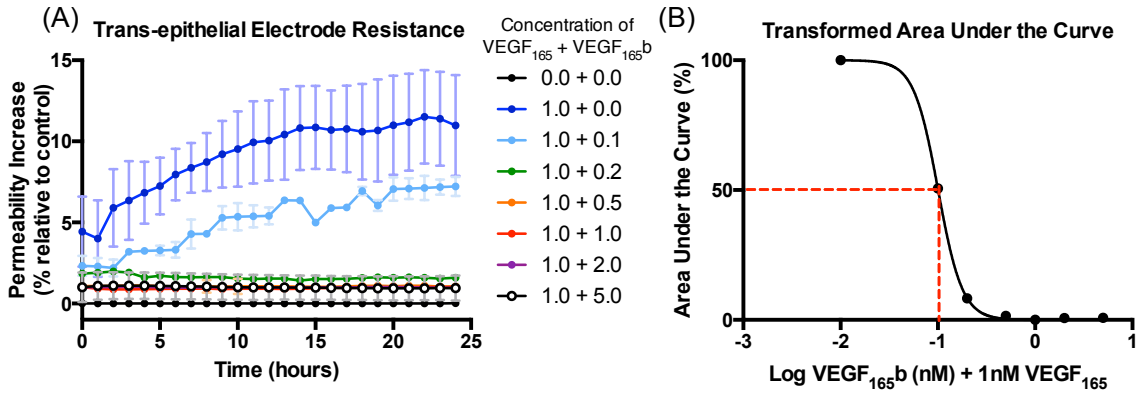

Figure 3.5. $VEGF_{165}$ co-treatment with a dose escalation of $VEGF_{165}b$ reduced paracellular flux.

RPE cells were treated with different proportions of $VEGF_{165}b$: $VEGF_{165}$ and TEER was measured over 24 hours (n=3, mean+SEM). (A) At 24 hours, there was a significant difference between 1.0nM $VEGF_{165}$ + 0.0nM $VEGF_{165}b$ and untreated wells and 1.0nM $VEGF_{165}$ + 0.1nM $VEGF_{165}b$ (***$p<0.001$, two-way ANOVA with Bonferroni's post hoc). When the area under the curve was assessed, normalised and log transformed (B), the IC50, 1.07nM $VEGF_{165}b$, could be determined.

It has been published that 2.5nM $VEGF_{165}b$ co-treatment with 2.5nM $VEGF_{165}$ prevented HUVEC migration (Bates et al. 2002b). Given that $VEGF_{165}$ and $VEGF_{165}b$ bind to VEGFR2 with equal affinity (Woolard et al. 2004), I hypothesised that 2.5nM $VEGF_{165}b$ would be sufficient to prevent $VEGF_{165}$-induced changes in permeability by at least 50%. RPE were treated with 2.5nM $VEGF_{165}$, 2.5nM $VEGF_{165}b$ and 2.5nM $VEGF_{165}$ co-treated with 2.5nM $VEGF_{165}b$ for 24 hours. Cells were then fixed and stained for ZO1, an alternative TJ marker, and fluorescence intensity was measured using ImageJ.

Figure 3.6 shows that $VEGF_{165}b$ by itself had no significant effect on ZO1 expression or location (86.3%±25.0). $VEGF_{165}$ significantly reduced ZO1 expression (43.7%±5.6), similar to when 2.5nM $VEGF_{165}$ reduced occludin expression in figure 3.1. Co-treatment of $VEGF_{165}$ and $VEGF_{165}b$ ("both") showed no significant change in ZO1 expression (84.3%±5.6), compared to untreated, but showed a significant difference relative to $VEGF_{165}$ treated wells.

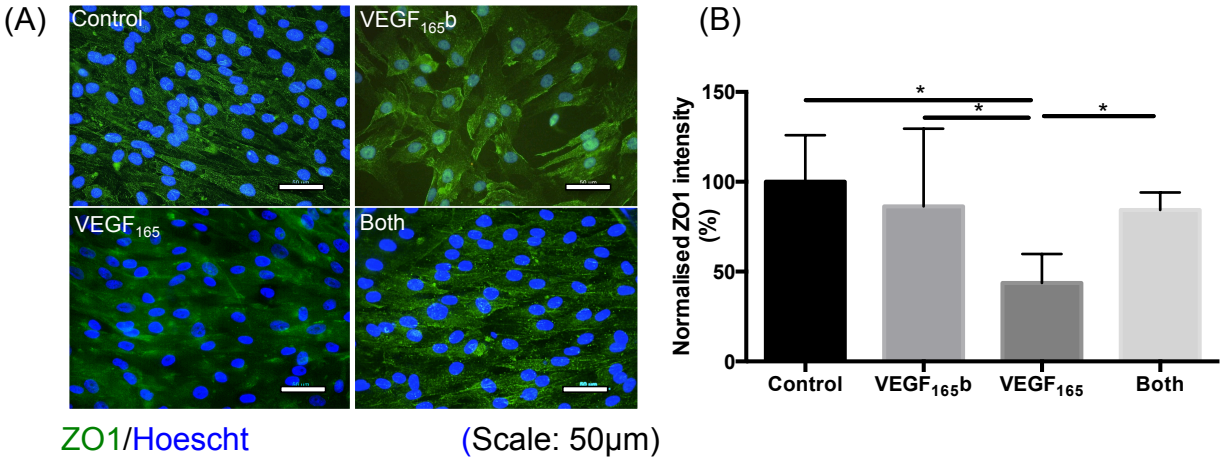

Figure 3.6 $VEGF_{165}b$ can restore $VEGF_{165}$-induced changes in ZO1 expression.

RPE cells (n=3, mean+SEM) were treated with 2.5nM $VEGF_{165}b$, 2.5nM $VEGF_{165}$ and 2.5nM of both $VEGF_{165}$ and $VEGF_{165}b$ for 24 hours. (A) Cells were stained for ZO1 (green) and fluorescence intensity was calculated. $VEGF_{165}b$ had no effect on ZO1 staining intensity (B). $VEGF_{165}$ treatment reduced ZO1 intensity significantly, which was restored upon 2.5nM $VEGF_{165}$ co-treatment. (One-way ANOVA, Tukey post-hoc test, *$p<0.05$).

To confirm the results of figure 3.6, RPE cells were again treated with 2.5nM $VEGF_{165}$, 2.5nM $VEGF_{165}b$ and 2.5nM $VEGF_{165}$ co-treated with 2.5nM $VEGF_{165}b$ for 24 hours. Protein lysate was extracted and assayed for ZO1 and occludin expression (figure 3.7). Similarly to figure 3.6, $VEGF_{165}b$ has no detrimental effect on ZO1 and occludin expression. $VEGF_{165}$ reduces ZO1 and occludin expression (0.126±0.09 and 0.227±0.15 respectively). $VEGF_{165}$ and $VEGF_{165}b$ co-treatment shows no significant TJ loss, as there was no significant difference when compared with untreated control wells.

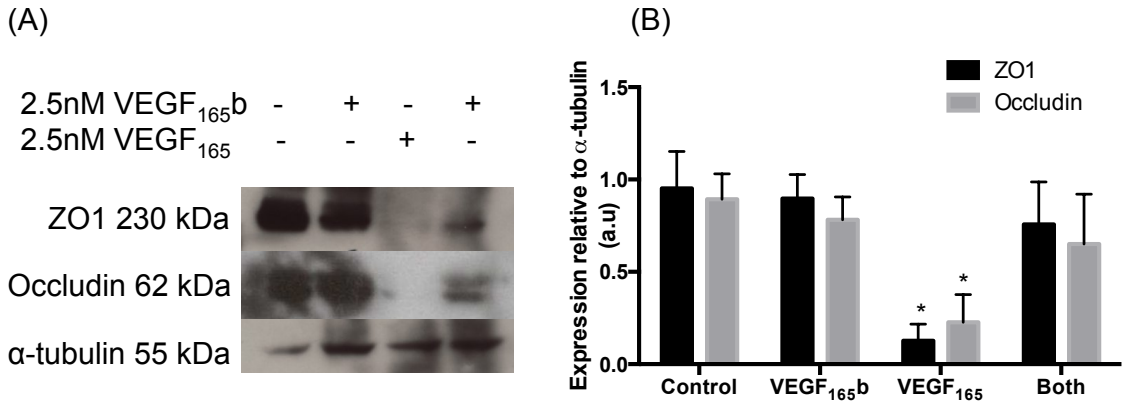

Figure 3.7 $VEGF_{165}b$ ameliorates $VEGF_{165}$-induced TJ degradation.

RPE cells treated with 2.5nM $VEGF_{165}$, 2.5nM $VEGF_{165}b$ and 2.5nM $VEGF_{165}$ co-treated with 2.5nM $VEGF_{165}b$ for 24 hours (n=3, mean+SEM). Protein lysate was immunoblotted for ZO1 and occludin expression. Membranes were stripped and reprobed for α-tubulin expression. There was no significant difference between $VEGF_{165}b$ treated cells in both TJ markers. 2.5nM $VEGF_{165}$ significantly reduced occludin and ZO1 expression, which was restored upon co-treatment with 2.5nM $VEGF_{165}b$. (one-way ANOVA, Tukey post-hoc test, *$p<0.05$).

I have shown that $VEGF_{165}b$ can ameliorate $VEGF_{165}$–induced TJ reorganisation, but I wanted to see if this would translate, functionally. I hypothesised that $VEGF_{165}b$ co-treatment would prevent $VEGF_{165}$–induced changes in permeability, as it did with TJ immunofluorescence and protein expression (figures 3.6 and 3.) To assess this, I performed the same experiment as above (figures 3.6 and 3.7) and measured TEER.

As predicted, 2.5nM $VEGF_{165}$ treatment caused a significant increase in permeability over time compared to untreated wells (10%±1.30 at 15 hours). RPE treated with 2.5nM $VEGF_{165}b$ alone showed no significant difference at any time point when compared to untreated wells (figure 3.8A). There was however a significant difference between $VEGF_{165}b$-treated wells and $VEGF_{165}$-treated wells across all time points ($p<0.001$ at every time point). There was no significant difference between wells treated with both $VEGF_{165}$ and $VEGF_{165}b$ and untreated wells, however there was a consistently significant difference between $VEGF_{165}$ treated wells and wells treated with both isoforms ($p<0.001$ at every time point).

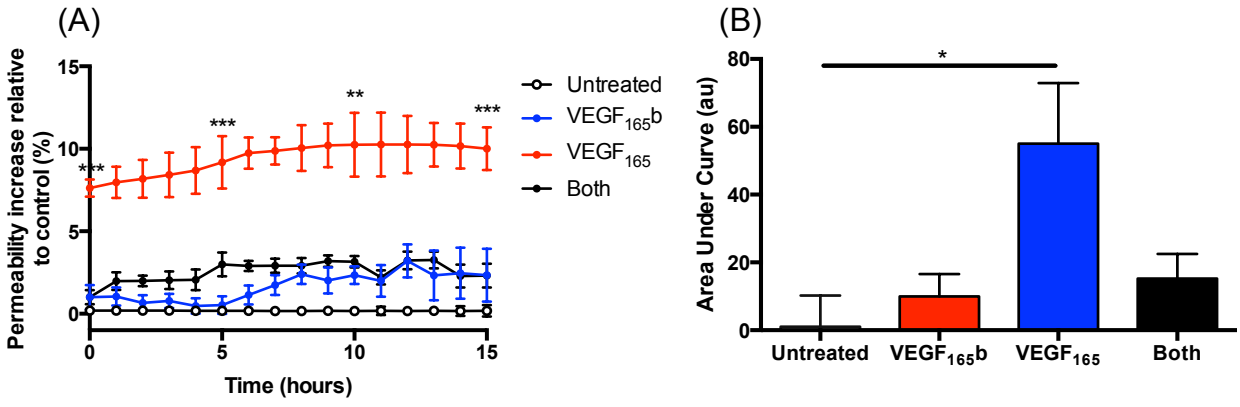

Figure 3.8 Co-treatment of both isoforms restores $VEGF_{165}$ – induced changes in permeability.

RPE cells treated with 2.5nM $VEGF_{165}$, 2.5nM $VEGF_{165}b$ and co-treatment of 2.5nM of both isoforms (A) showed that $VEGF_{165}$ significantly increased permeability relative to untreated wells and that this was abrogated by co-treatment of $VEGF_{165}b$ (2-way

ANOVA with Dunnett's post hoc, **p<0.01, ***p<0.001). Area under the curve analysis showed that this was only reflected when comparing $VEGF_{165}$ and untreated wells (n=4, mean+SEM, 1-way ANOVA, Tukey's post-hoc test, *p<0.05).

3.3.3 Effect of VEGF and hyperglycaemia on 1˚RPE cells

It is well established that hyperglycaemia-induced increased activity of PKCβ and PKCδ, NFKB and p38 MAPK result in pericyte death and retinal microvascular dysfunction and subsequent hypoxia/ischaemia (Aiello 2002; Geraldes et al. 2009). As a result, $VEGF_{165}$ is up-regulated in the diabetic retina causing excessive VEGFR1 and VEGFR2 stimulation and TJ reorganisation (Antonetti 1999a). As there is an increase in pro-angiogenic isoforms relative to anti-angiogenic $VEGF_{xxx}b$ isoforms in the diabetic eye (Perrin et al. 2005), we wanted to see if we could induce an *in vitro* model of hyperglycaemia-induced outer BRB dysfunction in 1˚RPE, and if any pathology could be reversed with $VEGF_{165}b$.

To test the hypothesis that hyperglycaemia could induce TJ reorganisation in RPE cells, RPE were cultured in difference concentrations of glucose: none (0mM), low glucose (5mM) to represent normal glycaemic levels, high glucose (35mM) to represent diabetic blood glucose levels and mannitol (5mM glucose + 30mM mannitol) as an osmotic control. Many groups have identified changes in RPE barrier properties between 20mM glucose and 40mM glucose treatment (Gillies et al. 1997; Qin et al. 2013). However, as there has been conflicting evidence using 20mM treatment, whereby some groups see changes in barrier properties and others do not (Villarroel et al. 2009), therefore I chose 35mM to represent diabetic conditions as a compromise.

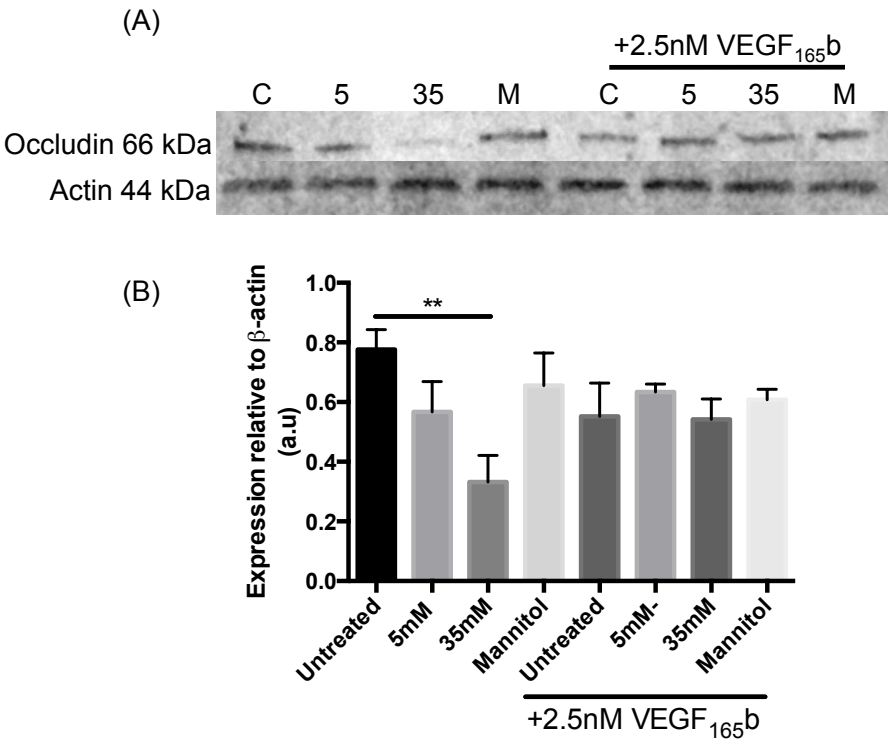

Figure 3.9. $VEGF_{165}b$ prevents hyperglycaemia – induced TJ degradation in RPE cells. RPE cells were cultured in 5mM glucose ± 2.5nM $VEGF_{165}b$, 35mM glucose ± 2.5nM $VEGF_{165}b$ and mannitol ± 2.5nM $VEGF_{165}b$ for 24 hours and immunoblotted against occludin. Blots were then stripped and reprobed for β-actin (A). There was a significant decrease in occludin expression (B) upon 35mM glucose treatment, which was reversed upon 2.5nM $VEGF_{165}b$ co-treatment (n=2, mean+SD, 1-way ANOVA, Tukey's post-hoc test, **$p<0.01$).

After 24 hours, protein lysate was extracted and immunoblotted against occludin and actin (figure 3.9). I hypothesised that high glucose treatment will reduce TJ expression and that this may be reversed with $VEGF_{165}b$ co-treatment.

Cells cultured in 35mM glucose expressed significantly less occludin (0.332±0.066) than untreated cells (0.776±0.0660). There was no significant difference in occludin expression upon 5mM glucose (0.567±0.101) or mannitol (0.655±0.109) treatment. Co-treatment of 35mM glucose and 2.5nM $VEGF_{165}b$ restored occludin expression (0.542±0.0684) relative to 35mM glucose alone. Although there was no significant difference between 35mM and 35mM + 2.5nM $VEGF_{165}b$, there was a trend that indicates $VEGF_{165}b$ is able to reduce TJ degradation. There was no significant difference between any $VEGF_{165}b$-treated group and untreated groups.

As it is well established that VEGF is secreted from RPE, particularly when stressed (Shima et al. 1995), I assessed the conditioned media from the above assay

(figure 3.9) for total VEGF isoforms by ELISA. I observed that upon treatment with 35mM glucose, there was a significant increase in VEGF secretion by RPE (9.05±1.03) relative to untreated wells (4.78±0.160). There was no significant difference between mannitol treated wells and untreated wells. There was a significant difference between the amount of VEGF secreted by 5mM treated RPE (2.41±1.61). There was no significant difference in VEGF secretion in wells treated with $VEGF_{165}b$, compared to conditions without $VEGF_{165}b$ co-treatment.

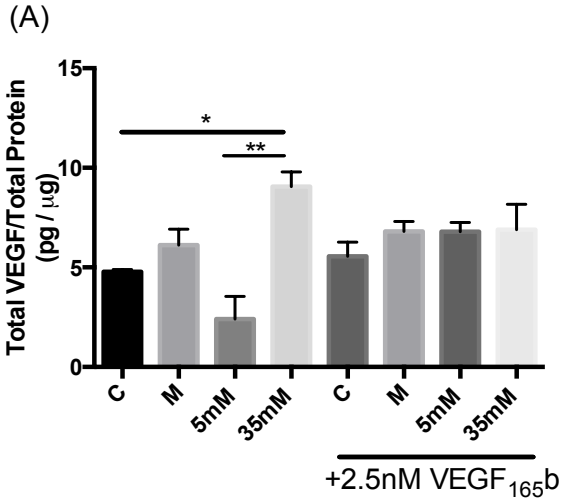

Figure 3.10. RPE cells cultured in high glucose conditions secrete increased VEGF compared to control treated cells.

RPE cells were treated with 5mM glucose ± 2.5nM $VEGF_{165}b$, 35mM glucose ± 2.5nM $VEGF_{165}b$ and mannitol ± 2.5nM $VEGF_{165}b$ for 24 hours. Conditioned media was then assayed for VEGF expression. There was a significant increase in VEGF secretion upon 35mM glucose treatment relative to control wells. There was no significant difference between $VEGF_{165}b$ co-treated wells when compared to untreated wells and when compared to all other treatments (1-way ANOVA with Sidak's post hoc test, *$p<0.05$, **$p<0.01$).

To corroborate these findings, I wanted to see if this was reflected in occludin immunofluorescence. As the osmotic control showed no significant difference in occludin expression or VEGF secretion, I omitted them from further experiments. I hypothesised that occludin immunofluorescence would reflect protein expression (figure 3.9). To assess this I treated RPE cells with 5mM glucose, 5mM glucose + 2.5nM $VEGF_{165}$ to see if pro-angiogenic VEGF would exacerbate occludin degradation, 5mM glucose + 1µM

56/8 to neutralise $VEGF_{165}b$ also to see if occludin degradation increased. The high glucose (35mM) remained the same as figures 3.9 and 3.10, 35mM ± 2.5nM $VEGF_{165}b$.

Cells cultured in low glucose conditions alone (0.952±0.052) showed no difference in occludin expression relative to untreated wells (0.893±0.0390). Co-treatment of 5mM glucose and 2.5nM $VEGF_{165}$ induced no significant difference in occludin staining (0.772±0.127). Co-treatment of low glucose cultured RPE with 1µM 56/8, a $VEGF_{165}b$ monoclonal antibody, also showed no signicant difference in occludin expression (0.803±0.052). When cultured in 35mM glucose, RPE cells express significantly less occludin (0.295±0.026) when compared with untreated cells and compared with 5mM glucose. When co-treated with 2.5nM $VEGF_{165}b$, there was a no significant change in occludin expression (0.362±0.096).

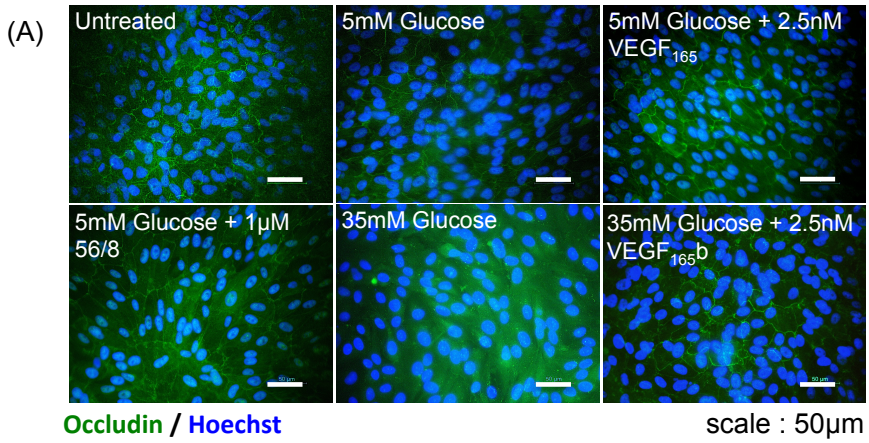

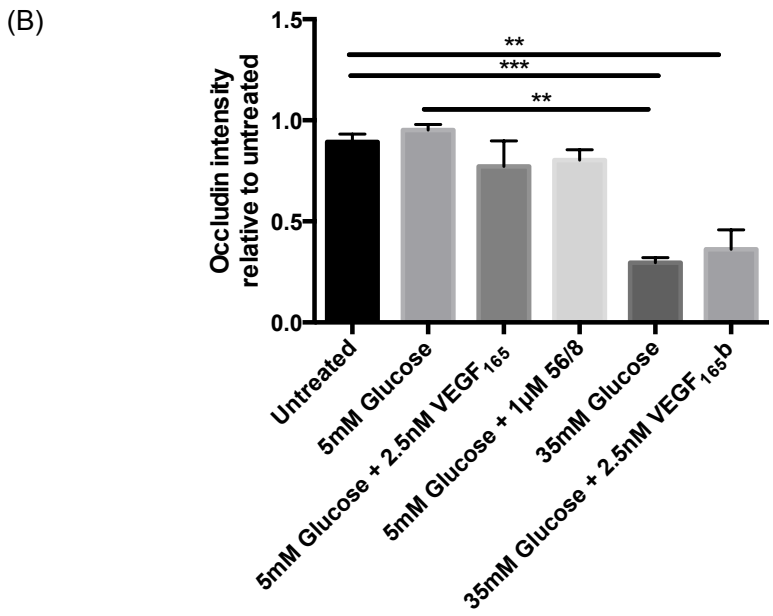

Figure 3.11. Occludin expression is reduced in RPE cells cultured in high glucose media. RPE (n=3) were cultured in 5mM glucose, 5mM glucose + 2.5nM $VEGF_{165}$, 5mM glucose + 1µM 56/8, 35mM glucose and 35mM glucose + 2.5nM $VEGF_{165}b$ for 24 hours (A) and stained for occludin (green) and nuclei were stained for Hoechst (blue). There was a significant reduction in occuldin expression (B) upon 35mM treatment compared to untreated wells and 5mM treated wells. There was also a significant difference between 35mM glucose + 2.5nM $VEGF_{165}b$ treated cells and untreated cells. (2-way ANOVA with Tukey's post-hoc, **$p<0.01$, ***$p<0.001$).

It appears that upon 35mM glucose treatment, occludin was no longer localised to the cell membrane, but rather transported to the cytoplasm. This fits with previous studies that suggest that TJs internalise when compromised. However, unlike protein expression (figure 3.9), 2.5nM $VEGF_{165}b$ co-treatment was unable to restore occludin immunofluorescence. To assess whether we have functionally induced a change in paracellular flux, I assessed the same conditions as above (3.11) using TEER.

Interestingly, the TEER more closely reflects the immunofluorescence data as opposed to the protein expression (figures 3.11 and 3.9 respectively). There was increased permeability at 24 hours (22.5%±4.70) relative to control treated cells (0.144%±0.143). $VEGF_{165}b$ co-treatment reduced permeability at 24 hours (17.0%±4.73), but it was not a significant difference when compared to 35mM glucose alone. There was no significant difference between all other groups when compared to untreated cells. This is reflected when measuring area under the curve, there was a significant difference between untreated wells (4.33±1.12) and 35mM treated wells (250±57.6) and untreated and 35mM + $VEGF_{165}b$ (183±29.3). Whilst there was no change in permeability upon 35mM + $VEGF_{165}b$ relative to 35mM glucose alone. However, power calculations showed that whilst not showing a significant difference, the actual power of these data is 0.95 and would show significance if I increased my sample size from n=3 to n=5. The area under the curve indicates that whilst not significant, 5mM glucose causes a slight increase in permeability at 24 hours, which may be increased with $VEGF_{165}$ co-treatment.

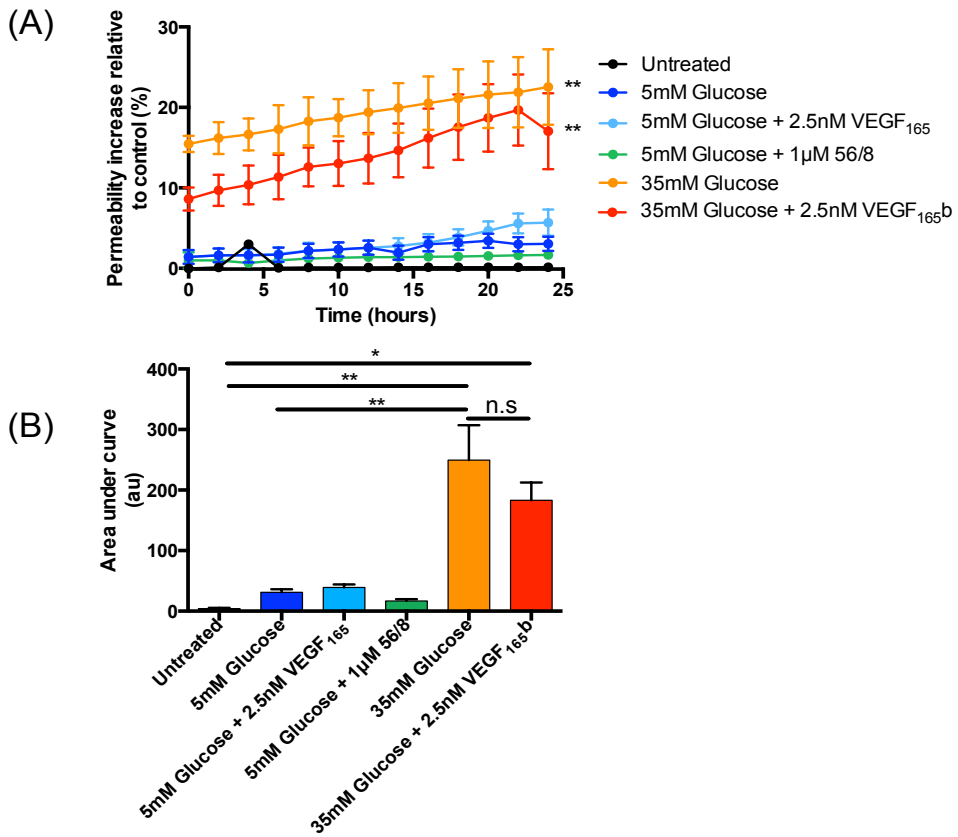

Figure 3.12. Hyperglycaemic conditions induce increased permeability in RPE cells. TEER was assayed in RPE (A) cultured in 5mM glucose, 5mM glucose + 2.5nM $VEGF_{165}$, 5mM glucose + 1µM 56/8, 35mM glucose and 35mM glucose + 2.5nM

$VEGF_{165}b$ for 24 hours. There was an increased in permeability upon 35mM glucose treatment after 24 hours, which was not significantly reduced upon 2.5nM $VEGF_{165}b$ co-treatment (n=3, 1-way ANOVA with Tukey's post-hoc test, **$p<0.01$).

It is apparent that 2.5nM $VEGF_{165}b$ may not be sufficient to restore hyperglycaemia (35mM glucose)–induced changes in RPE cells, despite appearing to restore occludin protein expression (figure 3.9).

3.4. Discussion

3.4.1 $VEGF_{165}$ induces tight junction disassembly in RPE.

It is widely accepted that VEGF is up-regulated in diabetic retinopathy (Aiello 1994). It is also well established that $VEGF_{165}$ is a potent permeability factor and is implicated in increasing vascular permeability in many conditions including tumour progression, blood-brain barrier disruption and diabetic retinopathy, the mechanisms are still yet to be fully understood.

Studies looking at the inner BRB, specifically RECs, have shown that increasing levels of VEGF both *in vitro* and *in vivo* induce "rapid phosphorylation" of occludin and ZO1 resulting in increased barrier permeability (Antonetti 1999b). In this chapter I showed that $VEGF_{165}$ could dose-dependently reduce occludin expression (figures 3.1 and 3.3) in RPE cells, by almost 50%. I also saw that this decrease in occludin expression coincided with an increase in paracellular conductance (figure 3.2), confirming that occludin expression is tightly linked with paracellular flux. As $VEGF_{165}$ concentration increased from 0nM to 5nM, occludin protein expression decreased by almost half (figure 3.3) and this was indirectly proportional to VEGFR2 expression. As one would expect, an increase in $VEGF_{165}$ concentration would likely induce an increase in VEGFR2 expression in RPE. An increase in VEGFR2 stimulation results in increased VEGFR2 phosphorylation and increased activity of PKC (Harhaj et al. 2006). Increased PKC activity is hypothesised to induce changes in the actin cytoskeleton, which would in turn induce changes in the ZO1 – occludin complex. This conformational change is hypothesised to result in a separation of the ZO1-occludin complex, resulting in occludin internalisation into a soluble cytoplasmic pool that will be recycled at a later time, or degraded (Antonetti 1999b; Wang et al. 2001). It also hypothesised that VEGF induces phosphorylation of occludin at the serine/threonine region and tyrosine phosphorylation of ZO1 (Wang et al. 2001; Harhaj & Antonetti 2004), resulting in endocytosis of occludin and ZO1 and again either recycled or degraded. This pathway, although well understood in RECs, is assumed to have similar characteristics in RPE. I have shown that $VEGF_{165}$ elicits a very similar effect on RPE as published in RECs, and this therefore may play a role in DME.

3.4.2. $VEGF_{165}b$ prevents $VEGF_{165}$–mediated changes in barrier properties.

$VEGF_{165}b$, whilst it binds to VEGFR2 with equal affinity as $VEGF_{165}$, does not activate the receptor completely. When it binds, it only partially phosphorylates VEGFR2, and therefore elicits a different downstream effect of reducing permeability, promoting cell survival and reducing angiogenesis (Harper & Bates 2008).
It has previously been acknowledged that there is a switch in isoform splicing in the diabetic eye in favour of pro-angiogenic isoforms such that $VEGF_{165}$ levels overwhelm $VEGF_{165}b$ levels (Perrin et al. 2005). This means that competitive binding of both isoforms to VEGFR2 will also be in favour of $VEGF_{165}$, resulting in increased angiogenesis and increased permeability. I showed that unlike $VEGF_{165}$ (figure 3.2), $VEGF_{165}b$ alone does not elicit an increased paracellular flux in RPE (figure 3.4) when treated at the same concentrations, lending confidence to the notion that $VEGF_{165}b$ does not impair TJ integrity. Figures 3.6 and 3.7 show that 2.5nM $VEGF_{165}b$ treatment alone has no significant effect on location of ZO1 or on ZO1 and occludin expression. Nevertheless, translocation of TJs are synonymous with increased paracellular flux (Wang et al. 2001), and we did not see any changes in permeability upon dose escalation of $VEGF_{165}b$, we can infer that it was unlikely that there was any change in location or distribution of TJs in RPE membranes.

Although I showed that concentrations as little as 0.2nM $VEGF_{165}b$ can prevent 1nM $VEGF_{165}$ induced increase in permeability (figure 3.5), I chose to use published values of 2.5nM $VEGF_{165}$ and $VEGF_{165}b$ in future *in vitro* studies (Woolard et al. 2004). I saw that $VEGF_{165}$ alone, as predicted, reduced occludin and ZO1 expression (figures 3.6 and 3.7), and this was reflected functionally when we saw increased permeability in RPE (figure 3.8). Other models have shown similar results using brain microvascular endothelial cells (BMECs) and bovine retinal endothelial cells (BRECs), as models for the BBB and BRB respectively (Antonetti 1999a; Wang et al. 2001). By co-treating $VEGF_{165}$ with $VEGF_{165}b$, we saw a restoration in TJ expression and a reduction in permeability to baseline (figures 3.6, 3.7 and 3.8). Similar but less robust effects have also been shown using typical and atypical PKC inhibitors, whereby VEGF-induced increased TER and occludin phosphorylation was reduced (Harhaj et al. 2006; Titchenell et al. 2012). As mentioned earlier, $VEGF_{165}b$ binding to VEGFR2 results in incomplete autophosphorylation of the receptor in endothelial cells. As a result, downstream signalling events such as activation of PKC is reduced (Harper & Bates 2008). This

points to a potential mechanism by which $VEGF_{165}b$ protects barrier integrity by reducing PKC activation, in an environment where both isoforms are balanced, although the mechanisms of VEGFR2 activation or inhibition in RPE cells remain to be elucidated.

This is encouraging as it supports my hypothesis that anti-angiogenic therapy using $VEGF_{165}b$ may be a potential treatment in DME.

3.5. Hyperglycaemia induces changes in barrier properties *in vitro*.

The characteristic hyperglycaemia observed in diabetes is directly linked to disruptions in the TJ complex, in the BBB and the BRB, as when patients observe "good glycaemic control" the progression of DR slows down. I wanted to see if I could induce a model of hyperglycaemia-induced TJ dysfunction *in vitro*.

I observed that upon additional 5mM glucose treatment, after 24 hours there was no significant difference in TJ expression (figures 3.9 and 3.11), nor any difference in paracellular flux (3.12). Mannitol treatment also showed no effect on protein expression (figure 3.9). Both 5mM (low glucose) and mannitol treatment were tested to illustrate that the effects seen upon high glucose treatment (35mM glucose), were in fact due to a hyperglycaemic environment and not as a result of osmotic shock to the cell. These data are consistent with published data (Gillies et al. 1997)

I then wanted to see if I could mimic the effects of hyperglycaemic insult by co-treating 5mM glucose with 2.5nM $VEGF_{165}$. This concentration proved to be sufficient to induce a change in TJ expression and permeability, and so I deemed it appropriate to co-treat with. However there was no difference in TJ expression or paracellular flux. This unexpected result could be explained by the levels of VEGF secreted by RPE upon glucose treatment (figure 3.10), 5mM glucose treatment reduces VEGF secretion into media, compared to both untreated and mannitol treated media. Low glucose treatment may be beneficial to RPE, which is why they secrete less VEGF and why co-treatment of $VEGF_{165}$ elicits no significant effect on TJ expression or function. However, to confirm this 5mM glucose would need to be co-treated with a $VEGF_{165}$ dose-escalation and assayed for TJ integrity.

By co-treating 5mM glucose with 56/8, I attempted to neutralise any $VEGF_{165}b$ that may be in the cell or media, and assess how this would influence RPE barrier integrity. There was no significant difference in occludin expression or TEER (figures

3.11 ad 3.12 respectively), however this could again be resolved under the hypothesis that 5mM glucose is a closer representation to normal physiological conditions, and therefore metabolic processes that normally occur in untreated media, are occurring at a slightly enhanced rate upon 5mM treatment, and therefore 2.5nM $VEGF_{165}$ will not elicit the same effect in this environment. In a model of oxidative stress in *ex vivo* rat lenses, co-treatment with 2mM glucose prevented superoxide-induced damage (Kletzky et al. 1986), upon which they concluded that low levels of glucose may exert a protective mechanism when subject to stress.

Upon high glucose treatment (additional 35mM), there was a significant reduction in occludin protein expression (figure 3.9), which was restored upon $VEGF_{165}b$ co-treatment. However this result was not reflected when looking at occludin immunofluorescence data (figure 3.11). $VEGF_{165}b$ co-treatment did not significantly reverse hyperglycaemia-induced occludin breakdown. However, it appears that upon 35mM glucose treatment alone, occludin staining appeared to be cytoplasmic rather than at the membrane. It is possible that this particular anti-occludin antibody (Invitrogen), may detect only membrane-bound occludin in protein lysate. This also seems like a reasonable explanation when considering TEER data. Upon high glucose treatment, paracellular flux increases by 20% relative to untreated RPE (figure 3.12A), which is not reversed upon 2.5nM $VEGF_{165}b$ co-treatment. There is a trend that would suggest the a slight reduction in permeability and slight increase in occludin fluorescence upon $VEGF_{165}b$ co-treatment, however they are both not significant and indicate that, although promising, the dose of $VEGF_{165}b$ is not sufficient to reverse the functional effects of high-glucose exposure. Few studies show a reversal in hyperglycaemia-induced insult using TEER. One group using taurine extracted from goji berries showed that taurine reversed high-glucose mediated increase in paracellular permeability in ARPE19 cells, an immortalised RPE cell line, through VEGF inhibition (Pavan et al. 2014).

These data indicate a potential *in vitro* model of outer BRB dysfunction in DME whereby high glucose concentrations result in an increase in AGE production and superoxide production, both of which increase levels of VEGF secreted by the cell. This increased extracellular VEGF results in increased VEGFR2 activation, and as a result increased activation of typical PKC isoforms, resulting in TJ phosphorylation and internalisation, resulting in reduced TEER. Increased glucose also results in increased atypical PKC isoform activation, which can also directly affect TJ integrity. This

hypothesis would be confirmed upon culturing RPE in 35mM glucose ± PKC inhibitors and characterising changes in barrier integrity.

3.5. Concluding Remarks

RPE cells, when subject to hyperglycaemia, secrete increased levels of $VEGF_{165,}$ which contributes to TJ dysfunction and an increased in cellular permeability, which is not reversed by $VEGF_{165}b$ *in vitro*. $VEGF_{165}$ treatment alone also reduces TJ expression and increases parcellular permeability, however this is reversed by $VEGF_{165}b$ co-treatment.

As $VEGF_{165}b$ treatment alone has no significant effect on TJ expression or function (TEER) on RPE, we hypothesise that it is safe to use on the outer-retinal barrier *in vivo*. I also hypothesise that $VEGF_{165}b$ may have therapeutic potential in preventing VEGF–induced BRB breakdown in a model of diabetes *in vivo.*

Chapter 4: rhVEGF$_{165}$b in Diabetic Retinopathy

4.1. Introduction

DR affects both type 1 and type 2 diabetics, and as the population of patients diagnosed with diabetes rises, so will the number of patients diagnosed with DR (http://www.who.int/blindness/causes/priority). Hyperglycaemia triggers a multitude of events that result in an increase in hypoxia (Pe'er et al. 1995), pro-inflammatory cytokines (Joussen et al. 2004) and an increase in ROS (Al-Shabrawey et al. 2008), amongst others. Much like wet AMD, there is a hypoxia and inflammation-mediated upregulation of VEGF production (Hoeben et al. 2004; Tang & Kern 2011) in the diabetic eye, and therefore much research is focused on anti-VEGF therapy in treating DR.

In the UK, the current treatment for the earlier, proliferative stage of DR is pan retinal laser photocoagulation (PRP), as recommended by the Royal College of Ophthalmologists (https://www.rcophth.ac.uk/standards-publications-research/clinical-guidelines). PRP alleviates retinal hypoxia bye RPE-focused laser treatment. However, despite the restoration of oxygen levels, the success of this procedure is limited by the fact that patients subject to laser therapy show variable improvements in vision. Regions of the retina will be lost to laser therapy and as well as loss of photoreceptors due to their outer retinal location, resulting in poor vision. Moreover, PDR is the major cause of vision loss, but rather DME is; and therefore laser treatment is often used as a precursor to or an adjunct with anti-VEGF treatment.

The consensus in treating wet AMD appears to be in favour of anti-VEGF therapy, with the main candidate drugs being: bevacizumab (Avastin, Genentech Inc., San Francisco), a monoclonal VEGF-A antibody (Ferrara et al. 2004), ranibizumab (Lucentis, Genentech Inc., San Francisco) a pan VEGF fragment antibody (Ferrara et al. 2006) and aflibercept (Eyelea Regeneron Pharmaceuticals Inc., New York) a soluble decoy receptor for extracellular VEGF and a VEGFR1 and VEGFR2 inhibitor (Holash et al. 2002). However, there are concerns over anti-VEGF therapy, considering that the outer BRB is also compromised in DME, IVT anti-VEGF therapy can enter the systemic circulation. This may be a disadvantage to diabetic patients as this may prevent wound healing, induce hypertension and result in increased cardiac events (Simó & Hernández 2008).

Part of the discovery of new anti-angiogenic agents in the treatment of DR is using reproducible and representative models. There are several models of both type 1

and type 2 diabetes, with the most commonly used being the streptozotocin (STZ)-induced model of both insulin and non-insulin dependent diabetes. STZ, synthesised from *Streptomycetes achromogenes* (Szkudelski 2001). STZ is transported into pancreatic β-cells via GLUT2 transporters and induces β-cell necrosis through DNA fragmentation and alkylation-mediated toxicity (Szkudelski 2001; Lenzen 2008). STZ is also a NO donor and generates ROS within β-cells, also contributing to DNA damage (Szkudelski 2001). STZ inhibits the Krebs cycle and subsequently, drastically reduces ATP production within β-cells resulting in poly ADP-ribosylation (PARP) activation as a way to rectify the damage (Szkudelski 2001; Lenzen 2008). However this only further depletes ATP reserves and further induces β-cell necrosis and subsequent ablation of insulin secretion (Lenzen 2008). Eventually, more β-cells die resulting in hyperglycaemia and subsequent retinal ischaemia.

Unfortunately, there is no single model of DR that encompasses all 3 arms of the condition, but rather animal strains and models of diabetes are chosen to assess particular aspects of the condition. To investigate outer BRB dysfunction in the diabetic retina, STZ-induced diabetes in Sprague-Dawley rats (Kern et al. 2010) is the preferred method. PDR can be assayed by counting immunostained vessels in the presence and absence of diabetes. DME involves changes in solute flux across the BRB, and so the Evans' blue dye perfusion technique has been used to assess changes in retinal "permeability" *in vivo* (Xu et al. 2001; Qaum et al. 2001; Abcouwer et al. 2010). Evans' blue (EB) is low molecular weight dye (961Da) that binds to albumin and wherever there is albumin leakage, for example from vasculature with compromised TJs, there will also be EB leakage. This will eventually accumulate into the surrounding tissue, which when analysed for EB absorbance at 620nm will give an indication of how "leaky" that particular tissue is.

The purpose of this study was to assess whether 8 weeks of STZ-induced diabetes would be a satisfactory method of modelling PDR and DME, and whether $VEGF_{165}b$ would be able to reverse hyperglycaemia-induced retinal pathology.

4.2. Methodology

Sprague-Dawley (SD) female rats (Harlan and Charles River in Bristol and Nottingham respectively), aged 6-8 weeks and weighing between 200-250g were used in models of DR. SD rats have been successfully used to document changes in retinal vasculature upon induction of diabetes (Kern et al. 2010; Robinson et al. 2012). Diabetes was induced using streptozotocin (STZ) as it is a well-established model of diabetes and is regularly used to study complications associated with diabetes including diabetic nephropathy and diabetic neuropathy, as well as DR (Brownlee 2001; Kern et al. 2010).

Animals were fasted overnight prior to induction of diabetes, and injected with STZ (50mg/kg) the next day. Rats used for 8 weeks diabetes also had an implantation of 1/3 of a slow release insulin pellet implanted into the neck scruff under isofluorane anaesthesia on the same day as STZ injection. Rats were either studied for 1 or 8 weeks. Diabetic cohorts studied for 8 weeks were injected i.p biweekly for 8 weeks with saline or $VEGF_{165}b$. Cohorts studied for 1 week were subject to IVT injections under recovery anaesthesia, 6 days after injection of STZ.

Cohorts studied for 1 week were subject to the Evans' blue dye (EB) perfusion technique to assess diabetes-induced changes in BRB properties, as described by Xu and colleagues (Xu et al. 2001). 3 cohorts were studied for 8 weeks, 1 cohort was subject to EB perfusion and 2 cohorts were sacrificed at 8 weeks and retinae were excised and either unfixed for protein lysate extraction and western blotting, and contralateral retinae were fixed, stained and flat-mounted for Isolectin B4, a vessel marker, and neuronal nuclear antigen (NeuN), a marker of retinal ganglion cells. Immunofluorescence was quantified using ImageJ and Imaris software. All methods are described in detail in Chapter 2.

4.3. Results

4.3.1. Systemic $VEGF_{165}b$ treatment reduces diabetes-induced changes in vascular remodelling.

There are multiple models of diabetes in rodents, however most physiological changes in rat retinae typically occur 6-8 weeks after onset of diabetes (Robinson et al. 2012b). To assess whether systemic administration of $VEGF_{165}b$ can prevent diabetes-induced changes across the BRB, 7 SD rats (200-250g, figure 4.1A) were induced with diabetes using STZ and supplemented with insulin, with two groups: STZ + vehicle (saline i.p, biweekly) and STZ + $VEGF_{165}b$ (20ng/g i.p, biweekly), and a third untreated, non-diabetic group injected with saline at week 0 (n=3). Rats with blood glucose ≥15mmol/l were deemed diabetic (figure 4.1B). All animals were culled at 7-8 weeks post-confirmation of hyperglycaemia, and retinae excised, fixed and stained for isolectin B4, a vessel marker. Vessels were manually counted per field of view on Image J and then confirmed using integrated density on Image J.

All of the control group (no STZ) retinae were badly damaged by an accident during processing, and I could not image them. There were significantly fewer vessels per field of view (figure 3.1A) in the $VEGF_{165}b$ treated animals (274.8 ± 8.878, n=4) than in the vehicle treated animals (302.3 ± 8.738, n=3). This was corroborated when measuring fluorescence using integrated density (figure 4.1B), with the notion that the greater the number of vessels, the greater the total fluorescence which would translate to a greater integrated density. Retinae of $VEGF_{165}b$ treated diabetic rats showed lower integrated density (50.23 ± 2.181, n=4) compared to vehicle treated rats (77.34 ± 9.039, n=3).

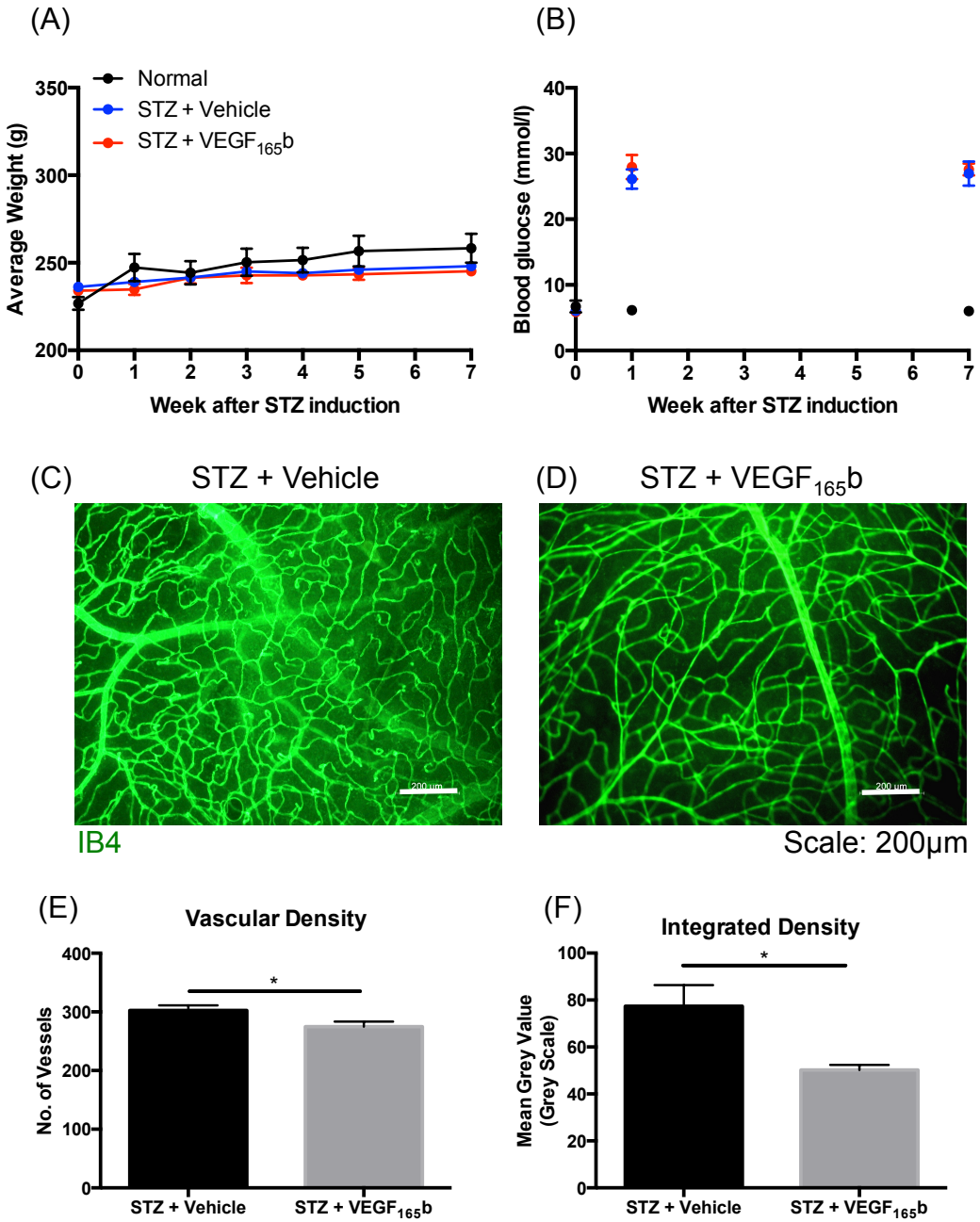

Figure 4.1. $VEGF_{165}b$ can significantly alter retinal vessel density in diabetic rats.

Sprague-Dawley rats induced with diabetes were treated with vehicle (PBS) or $VEGF_{165}b$ (20ng/g) biweekly (i.p) for 7 weeks after onset of hyperglycaemia. Animals were weighed weekly (A) and blood glucose measured 1 day before (week 0), 1 week after and 7 weeks after STZ induction (B). At week 7 retinae were excised and stained for IB4 (green). Diabetic rats treated with $VEGF_{165}b$ (C) showed a lower vascular density (E) and integrated density (F) than vehicle treated diabetic rats (C) (unpaired, 2-tailed Student's t-test, *$p<0.05$).

To assess whether the diabetic retinae had a reduced TJ expression and increased VEGF expression typically associated with diabetes (Antonetti 1999b), contralateral eyes from the above cohort were subject to protein extraction, and lysate was immunoblotted against VEGF-A, occludin and ZO1. I hypothesised that diabetic rats would express greater VEGF-A and reduced TJs relative to control rats, based on data in chapter 3 and published data. Protein extraction from the diabetic rats treated with $VEGF_{165}b$ was unsuccessful due to an accident in processing.

There was a small, yet significant increase in VEGF-A in diabetic retinae (0.81±0.03) relative to control animals (0.709±0.0212) (figure 4.2A). The same retinae showed a significant reduction in TJ expression in diabetic rats (0.681±0.0246) relative to control retinae (0.843±0.0428). There was a similar trend observed with occludin expression, whereby diabetes reduced occludin expression (0.460±0.0176) relative to control animals (0.521±0.0203), however this did not achieve significance (figure 4.2B).

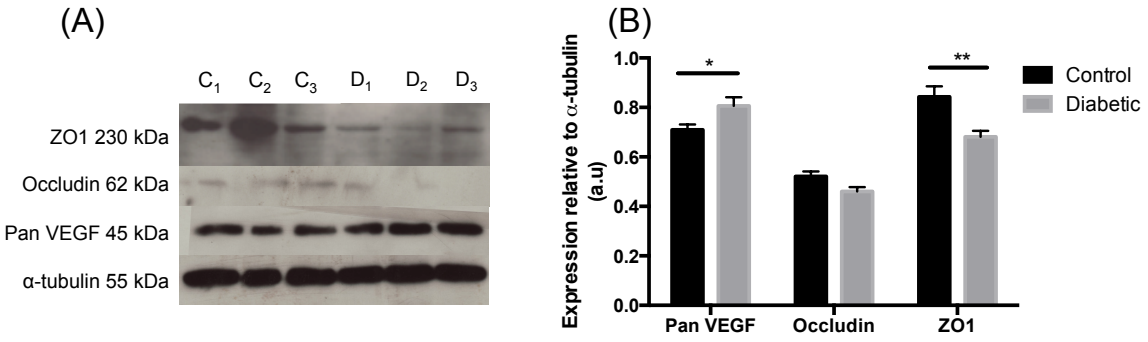

Figure 4.2. Diabetes causes an increase in VEGF in diabetic Sprague-Dawley retinae and a decrease in TJ expression.

Control and STZ + vehicle (C_x and D_x respectively) Sprague-Dawley rats were culled after 7 weeks of onset of hyperglycaemia and protein lysate extracted from retinae was immunoblotted against ZO1, occludin and VEGF-A. Blots were then stripped and reprobed for α-tubulin (A). Densitometry analysis (B) showed there was a significant increase in VEGF expression, and a significant decrease in ZO1 expression, however there was no change in occludin expression (unpaired, 2-tailed T test, *$p<0.5$, **$p<0.01$).

Although these data were encouraging and show $VEGF_{165}b$ could reduce vessel density in the diabetic eye (figure 4.1), as I did not have untreated, non-diabetic animals, I could not infer whether the vessels seen in STZ + vehicle groups were a result of neovascularisation or if the reduction induced by $VEGF_{165}b$ was a subnormal value and potentially pathological. To readdress this, I repeated the above pilot experiment (figures 4.1 and 4.2)

with the addition of an untreated, control group of rats (figure A). This would also give me a complete data set from which I could also extract protein lysate from contralateral eyes not used for immunofluorescence. Following fixation, retinae were hemisected and stained for different markers to maximise the data obtained from one study in order to reduce the numbers of animals used, whilst still achieving statistical power.

All images were taken under standardised settings on a confocal microscope (488 laser power = 30%, offset = 15%, gain = 800), all on the same imaging session in order to reduce variability between images. To increase the reliability and accuracy of analysis, rather than manually counting vessels in IB4 stained retinae (figure 4.3B), which can be vulnerable to error, I calculated volume occupied by vasculature using Imaris software (figure 4.3C). Vessel density was inferred from area and volume occupied by vasculature. I hypothesised that diabetic rats treated with vehicle would express a greater volume of vasculature in their retinae, relative to untreated retinae, and that this could be reversed upon treatment with $VEGF_{165}b$. There was a significantly increased vascular area in the diabetic retinae (figure 4.3D) when compared with control retinae (1.15± 0.08 mm^2 and 0.85±0.007 mm^2respectively). $VEGF_{165}b$ treated diabetic retinae showed a reduction in vascular area compared to both control retinae and diabetic + vehicle treated retinae. As would be expected, these data were mirrored in the volume occupied by vasculature. Diabetic + vehicle treated retinae expressed a greater vascular volume (figure 4.3E) relative to control retinae ($5.6x10^6 \mu m^3 \pm 4.8x10^5$ and $3.8x10^6$ $\mu m^3 \pm 3.8x10^5$ respectively). $VEGF_{165}b$ treatment prevented diabetes-induced vascular remodelling ($2.3x10^6 \mu m^3 \pm 2.9x10^5$), but also showed a significant difference relative to control retinae. I also analysed the integrated density of these data (figure 4.3F) to assess whether they showed a similar trend to figure 4.1. There was an increase in integrated density in the diabetic + vehicle retinae (48.2±2.63) relative to control retinae (34.4±0.615). This increase was significantly prevented upon $VEGF_{165}b$ intervention (40.1±0.490). The diabetic data from figure 4.3 mirrors 4.1, indicating that this model is also reproducible.

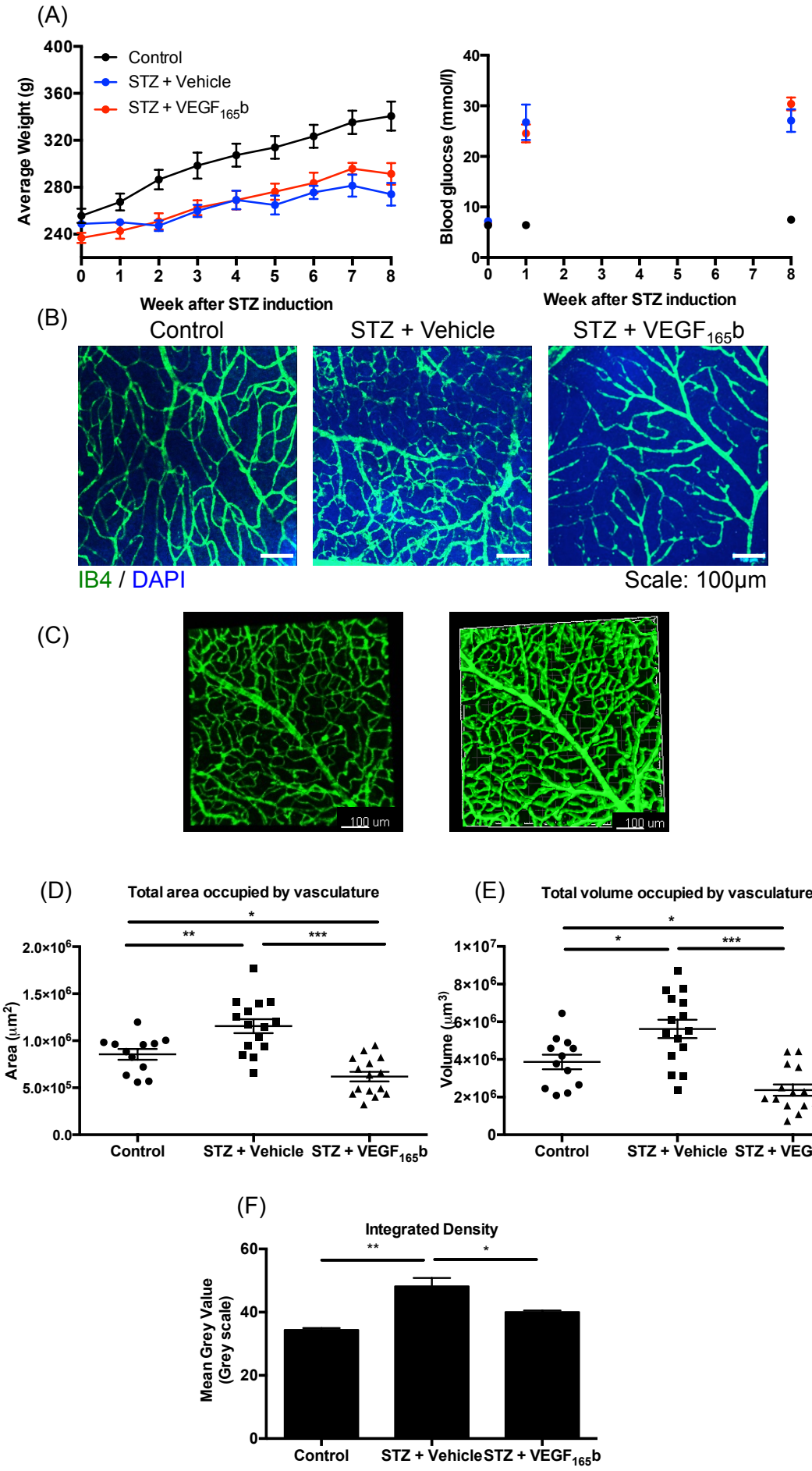
(A)
Control
STZ + Vehicle
STZ + VEGF165b
Average Weight (g)
Week after STZ induction
Blood gluocse (mmol/l)
Week after STZ induction
(B)
Control
STZ + Vehicle
STZ + VEGF165b
IB4 / DAPI
Scale: 100μm
(C)
100 um
100 um
(D)
Total area occupied by vasculature
Area (μm2)
Control
STZ + Vehicle
STZ + VEGF165b
(E)
Total volume occupied by vasculature
Volume (μm3)
Control
STZ + Vehicle
STZ + VEGF165b
(F)
Integrated Density
Mean Grey Value (Grey scale)
Control
STZ + Vehicle
STZ + VEGF165b

Figure 4.3. Systemic administration of $VEGF_{165}b$ prevents diabetes-induced neovascularisation *in vivo.*

STZ (50mg/kg, i.p) was used to induce diabetes in Sprague-Dawley rats (n=10). Saline was injected in vehicle controls (i.p, n=4). Diabetic rats were either treated with $VEGF_{165}b$ (20ng/g, biweekly i.p, n=5) or saline (biweekly i.p, n=5). All groups were weighed weekly and rats with a blood glucose ≥15mmol/l were deemed diabetic (A). Rats were sacrificed at 8 weeks and retinae were stained for blood vessels (B) using isolectin B4 (IB4) and DAPI. Vascular density was calculated using Imaris software (C). There was an increase in the area occupied by vessels per field of view (D) in diabetic + vehicle treated rats, relative to untreated controls, which was reversed by $VEGF_{165}b$ treatment. There was also an increase in the volume occupied by the vasculature per 3D stack (E) in the diabetic + vehicle treated animals, relative to control rats. This was also reversed upon $VEGF_{165}b$ treatment. Integrated density was calculated using Image J (F) and showed that there was increased fluorescence of our fluorescent marker in STZ + vehicle retinae relative to controls, and that this was prevented upon $VEGF_{165}b$ treatment (1-way ANOVA, Tukey's post hoc test, *p<0.05, **p<0.01, ***p<0.001).

The data from figure 4.3 shows that diabetes causes an increase in vascular area, volume and fluorescence, per field of view, indicative of increased vascularisation relative to untreated controls, corroborating what is observed in clinical settings. $VEGF_{165}$ shows a reduced vascular area and IB4-fluorescence per field of view, when compared to vehicle-treated diabetic rats. Vessel tortuosity is a another pathological feature of PDR (Gardner et al. 2002; Miller et al. 2013) where vessels dilate in response to ischaemia and become more curved. This aspect usually precedes neovascularisation (Hart et al. 1999) and is often used as an indicator of severity of disease in other ocular diseases as well as DR. I predicted that since I observed changes in vessel density at 8 weeks, I might also see a change in vessel tortuosity in diabetic retinae relative to control retinae. To assess this, I used Imaris software to measure "vessel straightness" on IB4 stained retinae from figure 4.3. I used this value to calculate the change in vessel straightness (figure 4.4) and observed that there was a trend in diabetic + vehicle animals where individual rats showed an increase in tortuosity (figure 4.4A) relative to control rats and diabetic + $VEGF_{165}b$ treated rats. Although there was a non-statistically significant difference between diabetic + vehicle retinae (0.087±0.003) when compared with control retinae (0.074±0.003), power calculations show had we increased the sample size from n=4 to n=6, we would achieve statistical significance with a power of 0.95. Systemic $VEGF_{165}b$ intervention showed a statistically significant reduction in average vessel tortuosity (0.074±0.004). There was no difference between untreated and $VEGF_{165}b$ treated groups.

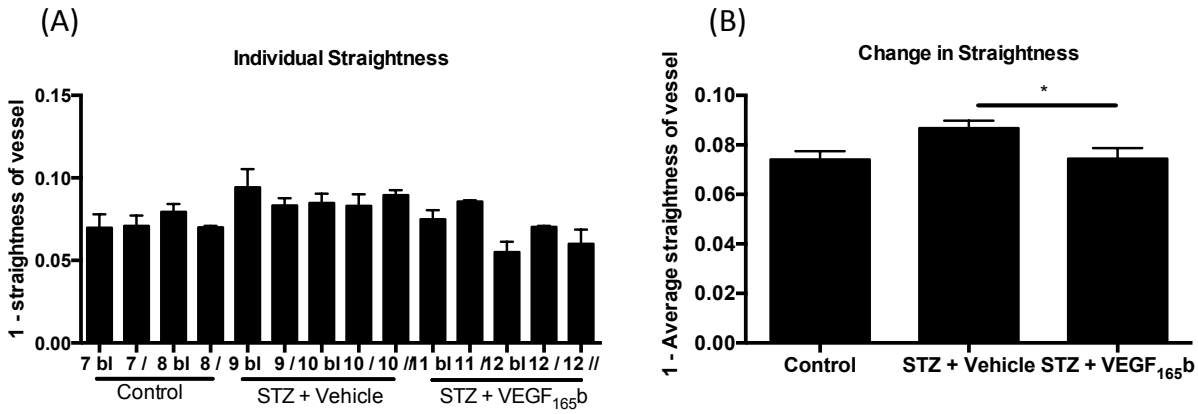

Figure 4.4. Systemic administration of $VEGF_{165}b$ prevents diabetes-induced vessel tortuosity.

IB4 stained retinae from control, STZ + vehicle and STZ + $VEGF_{165}b$ injected rats were assessed for vessel straightness using Imaris software. STZ + vehicle treated retinae showed a trend whereby there was increased change in straightness, therefore increased tortuosity (A) relative to control retinae. However this was not statistically significant development (B). There was a statistically significant reduction in tortuosity upon $VEGF_{165}b$ treatment, compared to STZ + vehicle retinae (1-way ANOVA, Tukey's post-hoc test, *$p<0.05$).

With the remaining, contralateral, retinae I extracted protein lysate to immunoblot against various markers of angiogenesis. I hypothesised that the pathology observed from this model was hypoxia-mediated, thus causing an upregulation of VEGF, resulting in subsequent angiogenesis. To assess this, I immunoblotted against HIF-1α and pan VEGF (figure 4.5A), and observed that there was no change in HIF-1α expression (figure 4.5B) in diabetic retinae (1.56±0.643) relative to control retinae (0.996±0.712) despite it appearing that there is increased HIF expression in the diabetic retinae. $VEGF_{165}b$-treated rats only saw a slight reduction in HIF-1α expression, however this was not significant. VEGF expression increased significantly in diabetic retinae (1.72±0.451) relative to control retinae (0.988±0.265). This elevated VEGF level remained unchanged upon $VEGF_{165}b$ treatment (1.63±0.351), however this may be due to the VEGF antibody detecting elevated $VEGF_{165}b$ isoforms present in treated retinae. Unfortunately I was unable to obtain a successful $VEGF_{165}b$ western blot to confirm this. Power calculations show that to achieve statistical significance with 0.95 power, between control and STZ + vehicle groups, the sample size would have to be n=4, considering the sample size in this

study was n=3, this only 1 extra animal would be needed to achieve statistical significance therefore we can infer that this is a reliable trend.

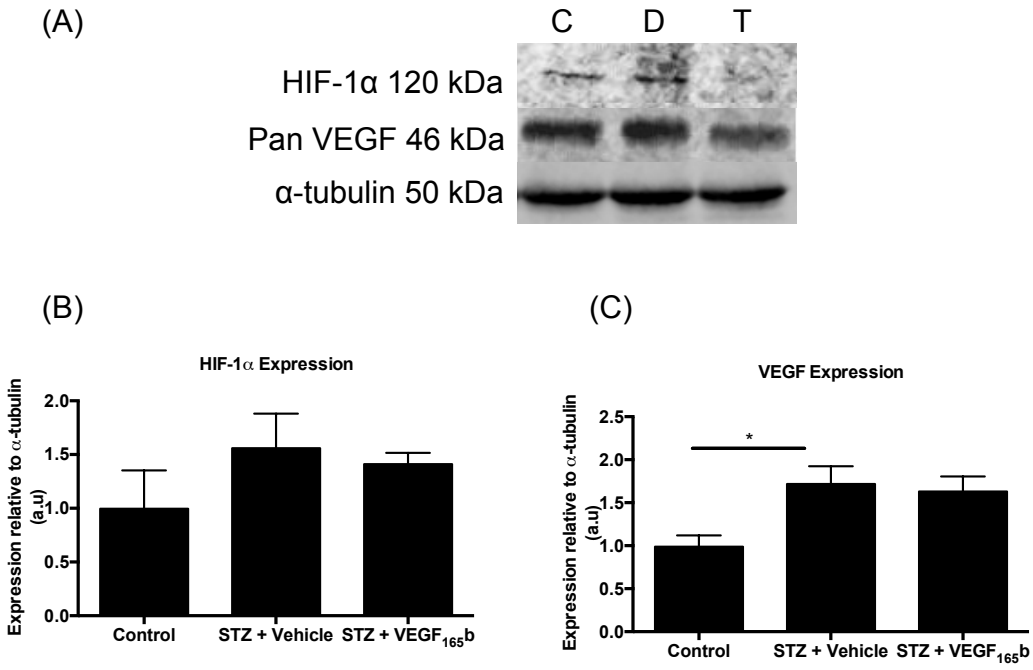

Figure 4.5. STZ-induced diabetic neovascularisation in SD rats is VEGF mediated. Protein lysate from control retinae (n=3), STZ-induced (50mg/kg) diabetic retinae (n=3) and diabetic retinae + $VEGF_{165}b$ (20ng/g, biweekly i.p) was collected 8 weeks after onset of diabetes. Lysate was immunoblotted (A) against HIF-1α and VEGF-A; western blots were then stripped and reprobed for α-tubulin (C, D, T = Control, STZ + vehicle, STZ + $VEGF_{165}b$ respectively). Densitometry analysis (B) showed that there was an increase in HIF-1α and VEGF expression (C) in diabetic retinae, relative to controls, however there was no significant difference in $VEGF_{165}b$ treated groups (1-way ANOVA with Tukey's post hoc test, *$p<0.05$).

To further investigate whether the pathology is indeed VEGF-mediated, I immunoblotted protein lysate from the same cohort against VEGFR2 (figure 4.6B) and phosphorylated VEGFR2 (pVEGFR2, figure 4.6C), with the hypothesis that both expression and activation of VEGFR2 would increase in diabetic retinae, resulting in proliferation, and that this could be reduced with $VEGF_{165}b$ intervention (figure 4.6A). When pVEGFR2 expression was analysed relative to VEGFR2 expression (figure 4.6D), there appeared to be no difference between the treatment groups. However, this is likely due both proteins changing expression in the same direction. Looking at VEGFR2 expression alone (figure 4.6B), although there appears to be an increase in VEGFR2

expression in diabetic retinae (1.30±0.224) relative to control retinae (0.904±0.230), it was not significant. Similarly, there was no change in expression in $VEGF_{165}b$-treated groups (1.048±0.126) relative to diabetic groups, despite appearing to decrease. This trend was mirrored in pVEGFR2 expression (figure 4.6C), where there was no change in expression although appearing as though as there was an increase in expression in diabetic retinae (1.18±0.200) relative to control retinae (0.842±0.060), and this slightly reduced with $VEGF_{165}b$ intervention (1.05±0.234).

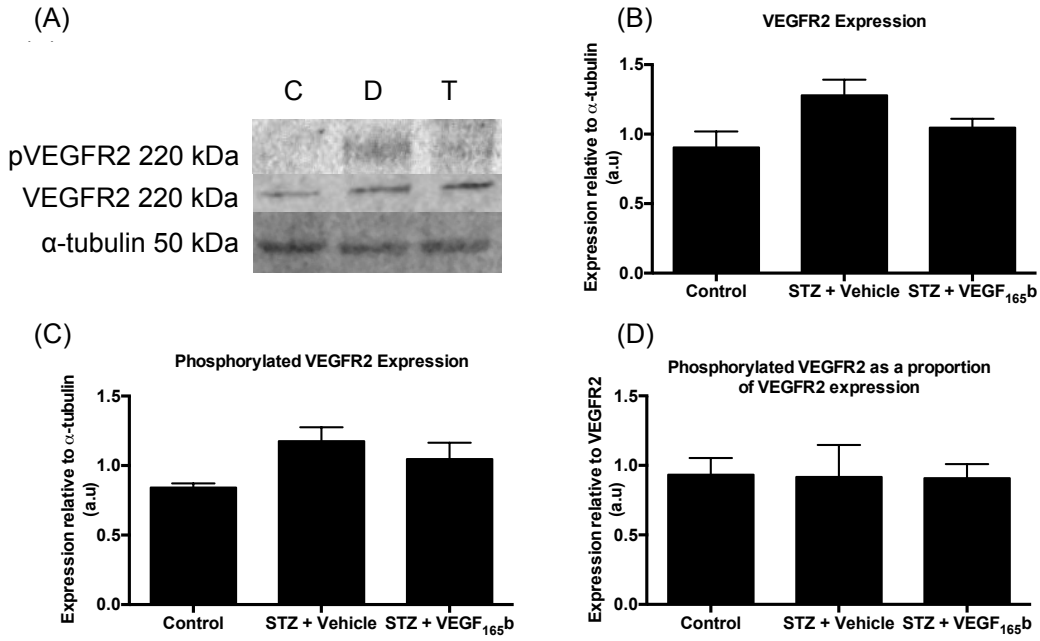

Figure 4.6. STZ-induced diabetes causes increased expression and phosphorylation of VEGFR2 in the retina.

Protein lysate from control retinae (n=3), STZ-induced (50mg/kg) diabetic retinae (n=3) and diabetic retinae + $VEGF_{165}b$ (20ng/g, biweekly i.p) was collected 8 weeks after onset of diabetes. Lysate was immunoblotted (A) against VEGFR2 and pVEGFR2; western blots were then stripped and reprobed for α-tubulin (C, D, T = Control, STZ + vehicle, STZ + $VEGF_{165}b$ respectively). There was no change in VEGFR2 expression (B) in diabetic retinae, relative to controls, and a non-significant difference in $VEGF_{165}b$ treated groups relative to diabetic groups. PVEGFR2 expression (C) also showed no change in diabetic retinae, compared to both control and $VEGF_{165}b$-treated groups Densitometry analysis (D) showed that there was no change in pVEGFR2 expression relative to VEGFR2 expression in all conditions. (1-way ANOVA with Tukey's post hoc test).

Although the densitometry appeared to show a change in VEGFR2 activation, this did not achieve statistical significance with the n numbers and sensitivity of the assay, I wanted to see if a more robust difference could be elucidated in the differences of

intracellular pathways involved in angiogenesis and diabetes. To test this hypothesis, I tested the protein lysate for ERK, phosphorylated ERK (pERK) and cleaved-caspase 3 with the hypothesis that increased angiogenesis will result in increased ERK phosphorylation and apoptosis in diabetic retinae, and that this may be reduced upon $VEGF_{165}b$ treatment, (figure 4.7A). ERK expression relative to α-tubulin (figure 4.7B) appears to be unchanged across all groups, however pERK expression relative to α-tubulin (figure 4.7C) appears to increase in diabetic retinae (1.11±0.198) relative to control retinae (0.885±0.235), although not statistically significant. $VEGF_{165}b$ treatment shows a minute reduction relative to diabetes alone (1.05±0.226), however the difference is so minimal; it is unlikely that it is indicative of a reduction in ERK phosphorylation. There was an increase in pERK expression relative to ERK in diabetic retinae (1.39±0.215) compared to control retinae (1.06±0.15) (figure 4.7D), which showed a reduction upon $VEGF_{165}b$ treatment (1.21±0.122), although both trends did not achieve significance. Unexpectedly, there was a decrease in cleaved caspase-3 expression (figure 4.7E) in diabetic retinae (0.877±0.170) compared to control (1.01±0.293) and $VEGF_{165}$-treated retinae (1.05±0.215).

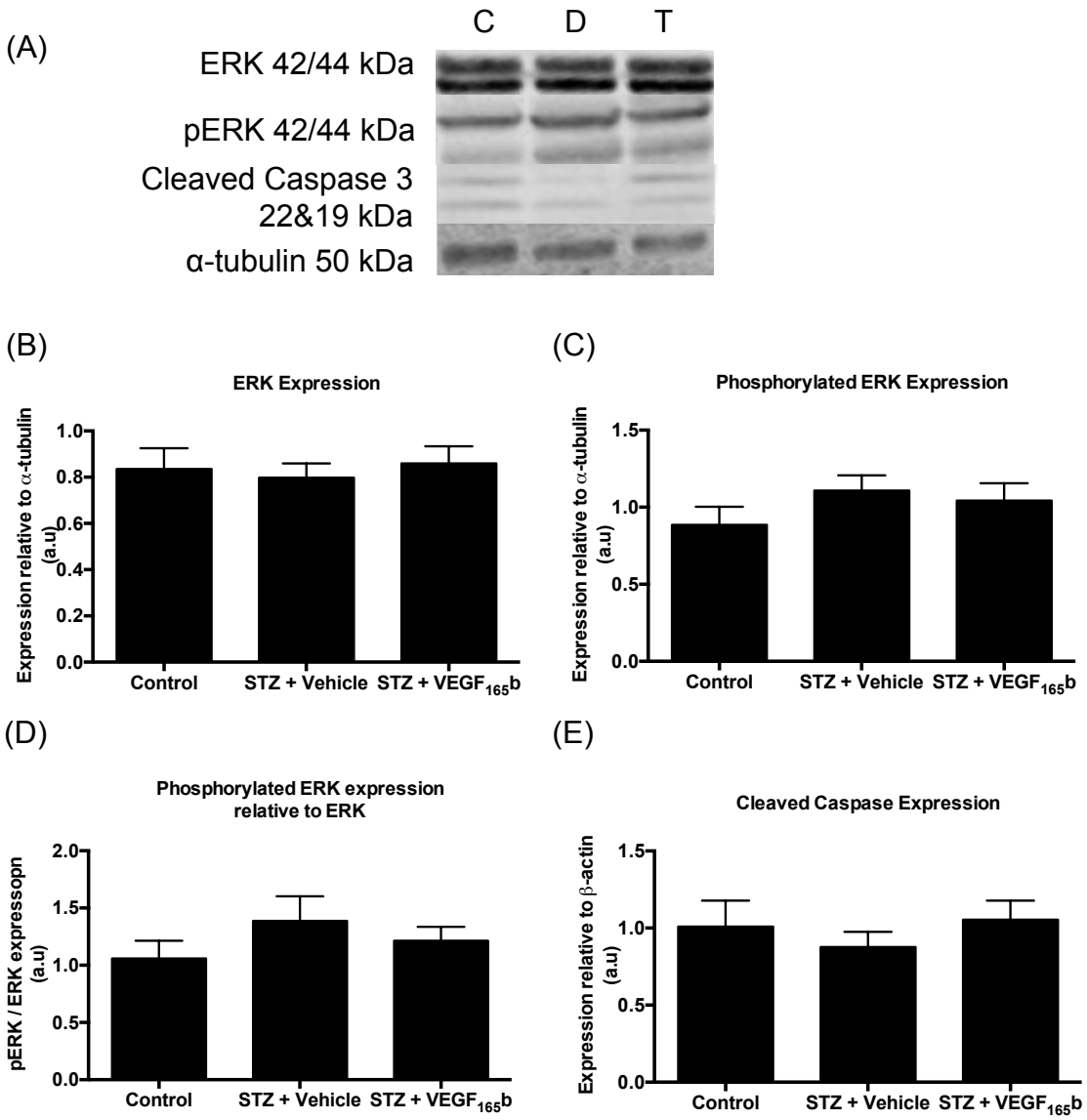

Figure 4.7. STZ-induced diabetes results in increased ERK phosphorylation, which is not reversed in $VEGF_{165}b$ treated groups

Protein lysate from control retinae (n=3), STZ-induced (50mg/kg) diabetic retinae (n=3) and diabetic retinae + $VEGF_{165}b$ (20ng/g, biweekly i.p) was collected 8 weeks after onset of diabetes. Lysate was immunoblotted (A) against ERK, pERK and cleaved caspase-3 expression; western blots were then stripped and reprobed for α-tubulin (C, D, T = Control, STZ + vehicle, STZ + $VEGF_{165}b$ respectively). Densitometry analysis (B) showed that there was a slight increase in pERK expression relative to ERK expression in in diabetic retinae relative to control and $VEGF_{165}b$-treated diabetic retinae. There was no change in ERK expression (C) across all groups. pERK expression (D) also showed a no change in diabetic retinae, compared to both control and $VEGF_{165}b$-treated groups. There was no change in cleaved caspase-3 expression (E) in diabetic retinae relative to control and $VEGF_{165}b$ (1-way ANOVA with Tukey's post hoc test).

Having seen changes in vascular density, I wanted to see if this model would also induce changes in barrier properties, as observed in figure 4.2. To assess this, I used protein lysate from the same cohort as above and I immunoblotted against VE-cadherin,

an endothelial cell-specific TJ marker and occludin, which is expressed in RPE as well as RECs.

Both TJ markers showed a reduction in expression in diabetic conditions (figure 4.8A). This was significant for VE-cadherin expression (figure 4.8B) in diabetic retinae (0.685±0.125) relative to control retinae (1.06±0.123). There was a slight increase in VE-cadherin expression in $VEGF_{165}b$ treated rats (0.904±0.115), however this was not statistically significant. This was also reflected in occludin expression (figure 4.8C), diabetes resulted in a non-significant decrease in occludin expression in diabetic retinae (1.02±0.426) relative to control, non-diabetic retinae (1.50±0.124). $VEGF_{165}b$ treatment appeared to have an increase in occludin expression, however this was not significant (1.57±0.329).

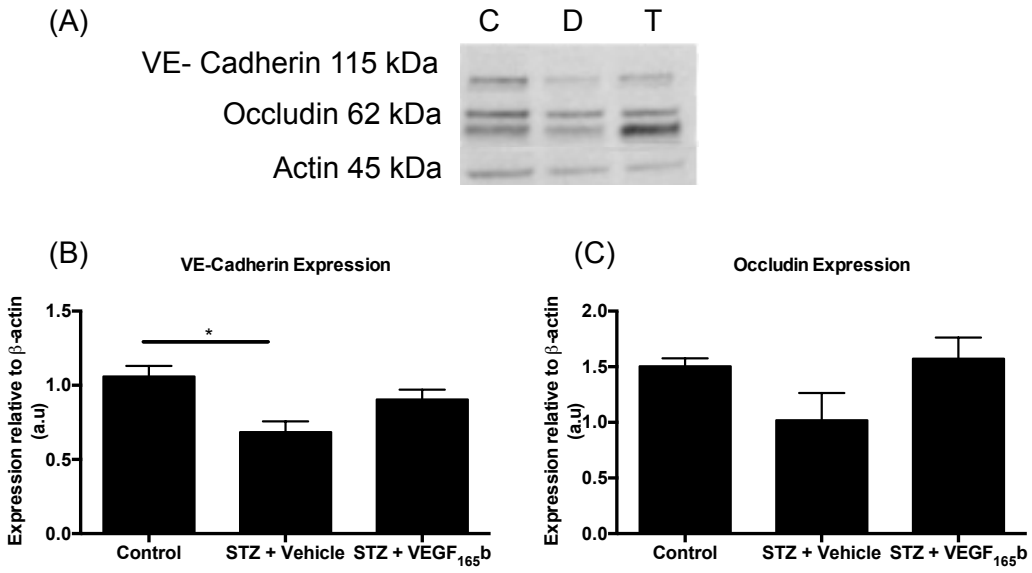

Figure 4.8. $VEGF_{165}b$ potentially prevents diabetes-induced TJ dysfunction.

Protein lysate from control retinae (n=3), STZ-induced (50mg/kg) diabetic retinae (n=3) and diabetic retinae + $VEGF_{165}b$ (20ng/g, biweekly i.p) was collected 8 weeks after onset of diabetes. Lysate was immunoblotted (A) against VE- cadherin and occludin; western blots were then stripped and reprobed for β-actin (C, D, T = Control, STZ + vehicle, STZ + $VEGF_{165}b$ respectively). Densitometry analysis (B) showed VE-cadherin expression decreased in diabetic retinae relative to control and $VEGF_{165}b$-treated retinae. This trend was reflected in occludin expression (C) however this was not statistically significant (1-way ANOVA with Tukey's post hoc test, *$p<0.05$).

4.3.2. $VEGF_{165}b$ prevents diabetes-induced increase in solute flux.

Given that figure 4.8 indicated that TJ expression decreased in diabetic retinae, and there may be a potential rescue with $VEGF_{165}b$, we wanted to see if we could see functional changes in barrier properties, as observed in DME. To investigate this further, a third cohort of SD rats were induced with diabetes using STZ (figure 4.9A), and repeated as cohort 2. Diabetes was confirmed 4 days post-induction and rats with blood glucose ≥15mmol/l were deemed diabetic (figure 4.9B). Diabetic rats were either injected with vehicle (saline, biweekly i.p, n=5) or $VEGF_{165}b$ (20ng/g, biweekly i.p, n=5). Non-diabetic rats were injected with saline (i.p) as opposed to STZ on day 0 (n=5). After 8 weeks, rats were injected subject to the EB technique.

Plasma was collected every 15 minutes for two hours (figure 4.9D), followed by cardiac perfusion of saline at 120mmHg, to remove EB-albumin from the vascular volume, followed by tissue extraction (figure 4.9C). EB solute flux and permeability-surface area product (PA) were calculated to give an indication of EB tissue accumulation and EB extravasation relative to plasma EB absorbance respectively (Further details described in chapter 2, "Materials and Methods").

I hypothesised that based on figure 4.8, there will be an increase in EB solute flux and PA in diabetic retinae relative to control retinae, and that this could be prevented in the $VEGF_{165}b$-treated groups. Upon excision of retinae I observed that STZ + vehicle treated retinae, were noticeably more blue (figure 4.9C) than both control and STZ + $VEGF_{165}b$-treated retinae. EB solute flux (figure 4.9E) significantly increased in diabetic retinae (0.148±0.047µg/min/g) relative to control retinae (0.012±0.028 µg/min/g). $VEGF_{165}b$-treated retinae had a significantly reduced EB solute flux (0.0002±0.021 µg/min/g) relative to diabetic + vehicle retinae. There was no statistically significant difference between control and diabetic + $VEGF_{165}b$ treated retinae. This trend was also observed in EB PA (figure 4.9F), there was a significantly increased EB PA in diabetic retinae (0.007±0.002µl/g/hr) relative to control retinae ($1.12x10^{-5}$ ±$4.08x10^{-4}$ µl/g/hr). There was a significant decrease in EB PA in $VEGF_{165}b$ treated groups ($6.63x10^{-5}$ ±$8.96x10^{-4}$ µl/g/hr), relative to diabetic + vehicle treated groups. There was no significant difference between control and $VEGF_{165}b$ treated groups.

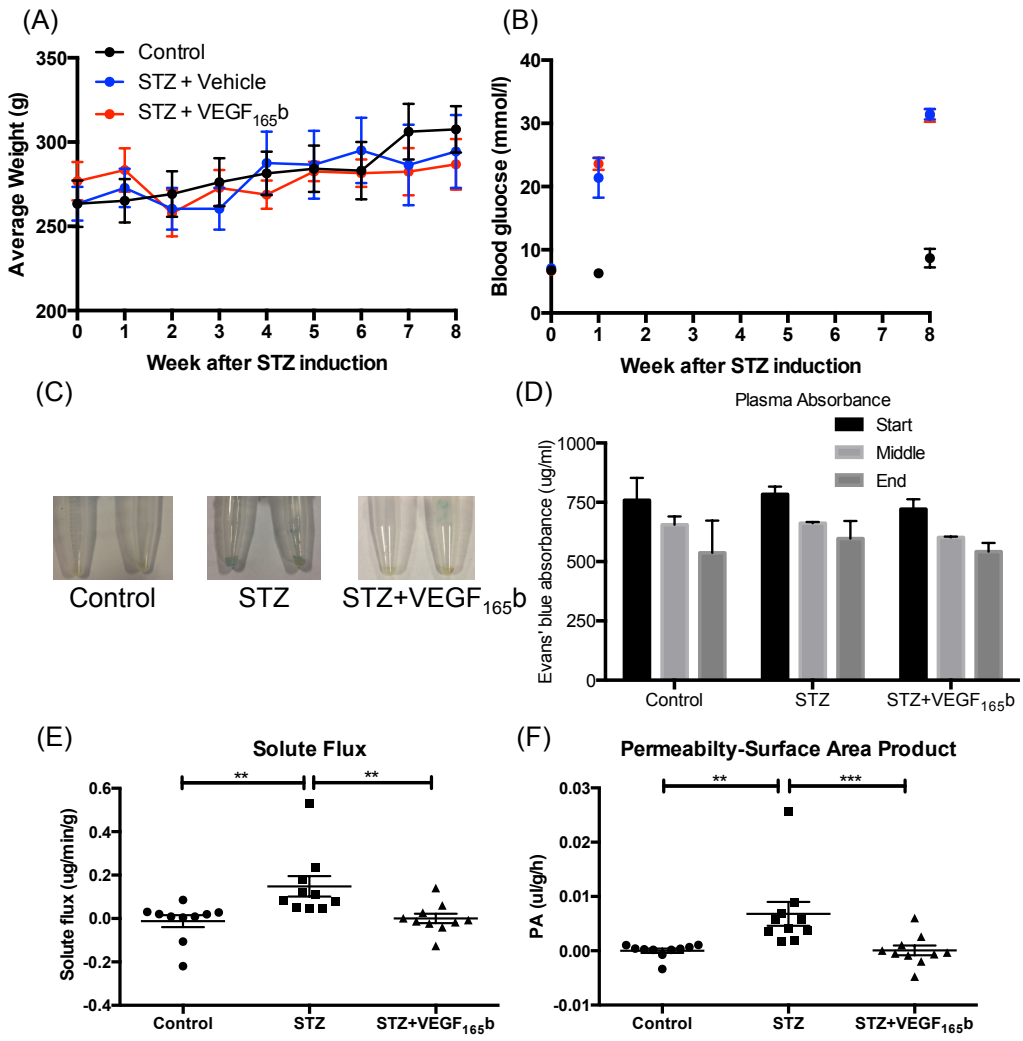

Figure 4.9. Systemic $VEGF_{165}b$ administration prevents diabetes-induced Evans' blue extravasation.

Sprague-Dawley female rats were induced with diabetes using STZ (50mg/kg i.p, n=10) and control rats (n=5) were injected with saline (i.p) on day 0 and weighed weekly (A). After 4 days, blood glucose was tested and blood glucose ≥ 15mmol/l were deemed diabetic (B). Diabetic rats were treated with either vehicle (saline, biweekly i.p, n=5) or $VEGF_{165}b$ (20ng/g, biweekly i.p, n=5). At 8 weeks post-STZ induction, Evans' blue (EB, 45mg/kg) was injected i.v into terminally anaesthetised rats. Plasma was collected every 15 minutes for 2 hours, after which, animals were sacrificed and retinae excised (C). Retinae were weighed and EB was extracted using formamide. EB solute flux (E) was calculated from the amount of EB per wet weight of tissue per hour. EB solute flux significantly increased in the diabetic retinae relative to control retinae and $VEGF_{165}b$-treated retinae. Permeability-surface area product (F) calculated from solute flux relative to the mean plasma Evans blue level during the 2-hour circulation. This also increased in diabetic retinae relative to control and $VEGF_{165}b$ treated animals (Kruskall-Wallis test with Dunn's post-hoc test, **p<0.01, ***p<0.001).

These data indicate that we can model diabetes-induced BRB dysfunction, and that $VEGF_{165}b$ when administered systemically can prevent TJ reorganisation *in vivo*. However, most treatments for DR and AMD are administered locally, either intravitreally (IVT) or subretinally, as most drugs are hypothesised to not cross the BRB effectively. I wanted to see whether local administration of $VEGF_{165}b$ in STZ-induced diabetic rats would also prevent diabetes-mediated TJ dysfunction. However, given the short half life of $VEGF_{165}b$ (Rennel et al. 2008), the 8 week STZ model would be unsuitable as the rat would require several intraocular injections a week, which would require the animal to be anaesthetised and subject to a procedure that has a 1% risk of endophthalmitis, multiple times per week. To address this problem, I shortened the length of diabetes to 1-week, as many studies have shown that microvascular complications associated with diabetes can occur after 1 week-post STZ injection (Qaum et al. 2001; Xu et al. 2001). As the duration of diabetes was significantly shorter, I did not supplement with insulin.

To establish whether IVT $VEGF_{165}b$ could prevent EB extravasation in diabetic retinae, I based a 7-day protocol on Xu et al., 2001. SD rats were induced with diabetes using STZ, and on day-6 post-induction, diabetic rats were anaesthetised and subject to IVT injection $VEGF_{165}b$ (50ng) in one eye and vehicle (saline) in the contralateral eye, followed by recovery. Control rats were injected with saline on day 0, and vehicle injection in one eye and the contralateral eye serving as an untreated control. On day 7 rats were terminally anaesthetised and subject to the Evans' blue (EB) dye perfusion technique as described earlier in this chapter and in chapter 2. I hypothesised that based on EB data acquired earlier (figure 4.9), that local administration of $VEGF_{165}b$ would prevent diabetes-mediated EB leakage into the retina. I observed that upon excision of retinae, diabetic + vehicle treated retinae were considerably more blue than contralateral, $VEGF_{165}b$ injected eyes (figure 4.10A). Plasma EB absorbance (4.10B) decreased in both treatment groups over time, as expected as the volume of circulating plasma also decreases every 15 minutes. EB solute flux was calculated as described earlier in this chapter, and showed a significant increase in EB tissue accumulation (figure 4.10C) in diabetic retinae (0.244 ±0.05µg/min/g) relative to control + vehicle injected retinae (0.089 ± 0.024 µg/min/g) $VEGF_{165}b$ treatment induced no change in EB solute flux (0.131 ± 0.038µg/min/g). Interestingly, there was no significant difference between vehicle injected control retinae and untreated retinae (0.067 ± 0.016µg/min/g) indicating that the IVT injection did not exert a significant, inflammatory effect. When measuring EB PA (figure 4.10D), diabetes alone caused a significant increase in EB extravasation (0.012 ±

0.004 µl/g/hr) relative to vehicle treated and untreated controls (0.002 ± 0.008 µl/g/hr and 0.002 ± $4.0x10^{-4}$ µl/g/hr respectively). $VEGF_{165}b$ treatment significantly reduced EB extravasation (0.005± 0.001 µl/g/hr) relative to contralateral diabetic retinae. There was no significant difference between STZ + $VEGF_{165}b$-treated, control + vehicle and untreated groups. When we normalised these data to data obtained earlier at 8 weeks (figure 4.9), we saw that relative solute flux (figure 4.10E) increased robustly between 1 and 8 weeks in diabetic animals (3.63±0.744 µg/min/g and 46.1±14.6 µg/min/g respectively), whereas relative solute flux in $VEGF_{165}b$ injected animals remained relatively unchanged between 1 and 8 weeks of treatment (1.95±0.568 µg/min/g and 1.03±6.81 µg/min/g respectively). The difference between STZ + vehicle-treated solute flux and STZ + $VEGF_{165}b$-treated solute flux at 1 and 8 weeks is significantly different at both time points. This trend is similar in relative PA (4.10F). Relative PA is greater at 8 weeks than 1 week in diabetic + vehicle retinae (11.0±3.54 µl/g/hr and 6.47±2.35 µl/g/hr), however the opposite trend is observed in $VEGF_{165}b$-treated retinae, where there is a reduction in PA at 8 weeks relative to 1 week (0.107±1.44 µl/g/hr and 2.61±0.544 µl/g/hr respectively).

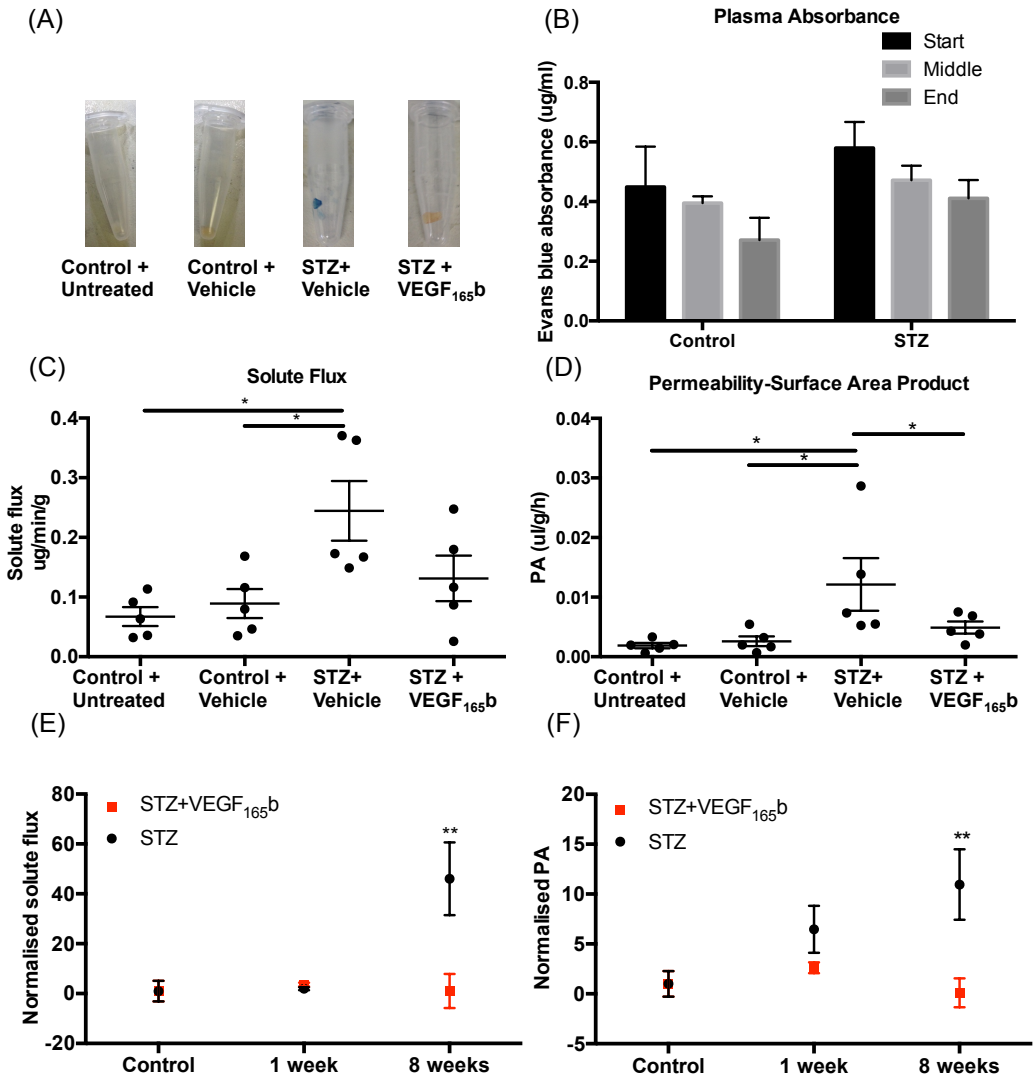

Figure 4.10. Intravitreal $VEGF_{165}b$ administration can prevent diabetes-induced Evans' blue extravasation in 1-week diabetic rats.

Sprague-Dawley rats were induced with diabetes using streptozotocin (STZ, 50mg/kg). After 6 days, 5µl saline was injected into one eye of each diabetic rat, and 5µl 10ng/µl rh$VEGF_{165}b$ injected into the contralateral eye (n=5). Control rats had no injection in one eye, and 5µl saline in the contralateral eye (n=5). On day 7, Evans blue (EB, 45mg/kg) was injected into anaesthetised rats (iv) Plasma was collected every 15 minutes for 2 hours (B), after which, animals were sacrificed and retinae excised (A). Evans blue solute flux (C) was calculated from total EB absorbance after 2 hours and permeability-surface area product (PA) was calculated (F) using solute flux as a measure of plasma EB absorbance. Solute flux and relative solute flux increased after 1 week in STZ + vehicle treated retinae (C) and at 8 weeks (E) relative to $VEGF_{165}b$ treatment. PA increased in diabetic retinae at 1 week (D) and 8 weeks post STZ induction (F) relative to vehicle treated and $VEGF_{165}b$-treated retinae (B and C = 1-way ANOVA with Bonferonni's post-hoc test, E and F = 2-way ANOVA with Tukey's post-hoc test, *$p<0.05$, **$p<0.01$)

These data suggest that TJ dysfunction associated with diabetes occur as early as 1 week post STZ, and that 24 hours treatment of rhVEGF$_{165}$b is sufficient to prevent onset. These data also suggest that the model is more robust at 8 weeks and that 8 weeks of systemic STZ administration is sufficient to reverse it to the extent that there is no significant difference between controls or between 1-week STZ + VEGF$_{165}$b.

EB extravasation in the CNS was also assessed, as the BRB and BBB share similar properties, to investigate whether STZ-induced diabetes could reflect a similar result as in figure 4.9. To assess this, spinal cords and brains were dissected from the same animals as figure 4.9 and EB solute flux and PA was calculated as described previously.

I observed that there was slight increase in brain EB solute flux (figure 4.11A) in diabetic brains (0.009±0.005 µg/min/g) relative to control brains (0.005±0.003 µg/min/g), however this was not significant. VEGF$_{165}$b-treated retinae had a noticeable reduction in EB solute flux (0.001±0.001 µg/min/g) relative to control brains, however this did not achieve statistical significance. Brain PA (figure 4.11B) showed a large variance, and therefore there was no significant difference between control and diabetic retinae ($2.15x10^{-4}$ ±$8.28x10^{-5}$ µl/g/hr and $3.02x10^{-4}$ ±$1.59x10^{-5}$ µl/g/hr respectively). There was a more noticeable difference in VEGF$_{165}$b-treated groups ($4.77x10^{-5}$ ± $2.48x10^{-5}$ µl/g/hr) relative to diabetic brains, although this did not achieve significance. I saw a trend in the opposite direction in the spinal cord. EB solute flux in diabetic spinal cords (figure 4.11C) decreased relative to control spinal cords (0.162±0.025 µg/min/g and 0.350±0.079 µg/min/g). VEGF$_{165}$b-treated rats showed an increased EB solute flux relative to diabetic spinal cords (0.633±0.246 µg/min/g), however this was not significant. Spinal cord PA followed a similar trend (figure 4.11D); diabetic spinal cords showed a decreased EB PA (0.007±0.0009 µl/g/hr) compared to control spinal cords (0.011 ± 0.00092 µl/g/hr). VEGF$_{165}$b treated animals showed an increased EB PA in the spinal cord (0.0157±0.005 µl/g/hr) relative to diabetic spinal cords, however both changes were not significant.

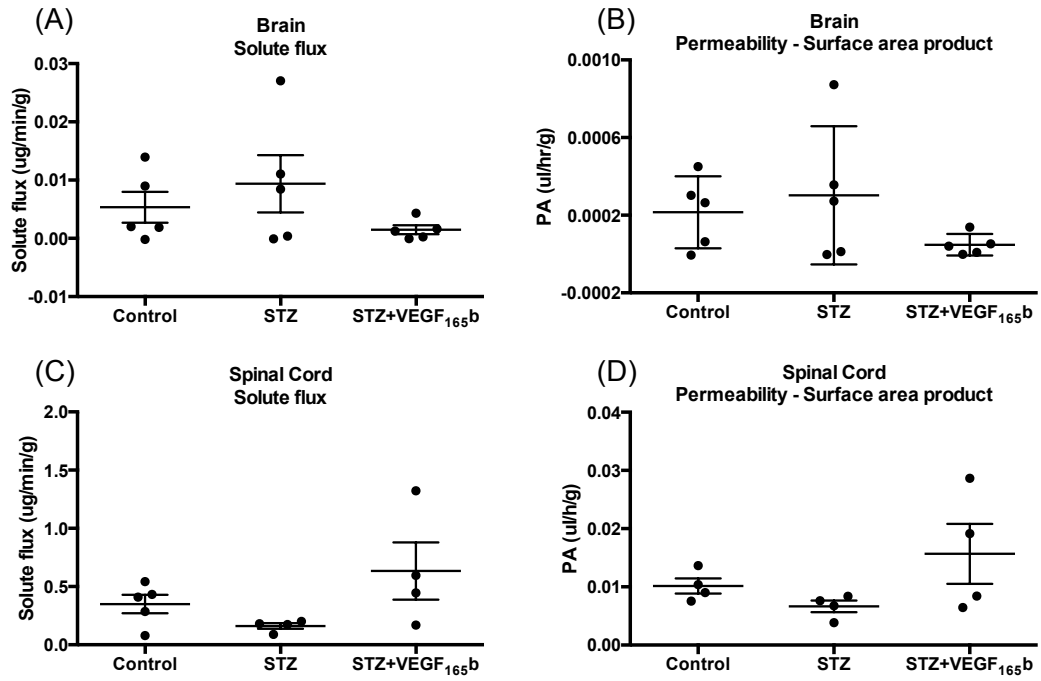

Figure 4.11. STZ-induced diabetes has no significant effect on Evans' blue extravasation. (*In collaboration with Dr. Richard Hulse)*

Sprague-Dawley female rats were induced with diabetes using STZ (50mg/kg i.p, n=10) and control rats (n=5) were injected with saline (i.p) on day 0 and weighed weekly Diabetic rats were treated with either vehicle (saline, biweekly i.p, n=5) or $VEGF_{165}b$ (20ng/g, biweekly i.p, n=5). At 8 weeks post-STZ induction, Evans' blue (EB, 45mg/kg) was injected i.v into terminally anaesthetised rats. Plasma was collected every 15 minutes for 2 hours, after which, animals were sacrificed and brains and spinal cords were collected. Brain solute flux (A) was calculated relative to hours of EB circulation and showed there was no change in diabetic brains relative to control and $VEGF_{165}b$ treated animals. Brain PA (C) was calculated relative to EB plasma absorbance and showed a similar trend, where STZ alone increased EB PA relative to control and $VEGF_{165}b$ treated animals. The opposite trend was observed in spinal cord solute flux (C) and PA (D) (Kruskall-Wallis test with Dunn's post-hoc test).

DR and diabetic neuropathy are both neurovascular disorders that occur in both type 1 and type 2 diabetics, and have similar pathogeneses (Bloomgarden 2005). Sufferers of diabetic neuropathy experience vascular dysfunction in the peripheral nervous system, particularly in tissue involved in nociception. Previous data from our group has shown that 8 weeks of STZ-induced diabetes results in increased mechanical allodynia and thermal hyperalgesia, indicative of increased pain sensitivity. This was reversed upon 20ng/g biweekly $VEGF_{165}b$ treatment (Hulse et al, unpublished). I hypothesised that there would there would be a change in EB extravasation in the diabetic nervous tissue (figure 4.12) relative to control tissue, which would be translated to the

hind paw plantar skin, where the nociceptors would be hyper-sensitised. I also hypothesised that any changes seen in diabetic animals could be reduced in $VEGF_{165}b$ treated diabetic animals.

I observed that there was a significant increase in both EB solute flux and PA in diabetic dorsal root ganglia (DRG, R3, R4, R5), relative to control DRGs (figures 4.12A and 4.12B respectively). This was reduced in $VEGF_{165}b$ treated diabetic rats, however this was not significant. Similarly there was an increase in saphenous nerve solute flux (figure 4.12C) and PA (figure 4.12D) in diabetic rats relative to control rats, and this was significantly reversed upon $VEGF_{165}b$ treatment. However, in the sciatic nerves, this trend wasn't fully observed. Diabetic sciatic nerves showed more EB solute flux (figure 4.12E) and a greater PA (figure 4.12F) relative to control tissue, however this was not statistically significant. There was no significant or discernable difference between diabetic + vehicle treated groups, and diabetic + $VEGF_{165}b$ treated groups for both solute flux and PA. However, there was a statistically significant difference between control and $VEGF_{165}b$ treated sciatic nerves. Perhaps indicating that dysfunction of the sciatic nerve cannot be reversed with our current treatment strategy. EB solute flux (figure 4.12G) and PA (figure 4.12H) increased in diabetic plantar skin relative to control skin, however this was not statistically significant in both assays. This result was prevented in $VEGF_{165}b$ treated groups, achieving significance in both assays.

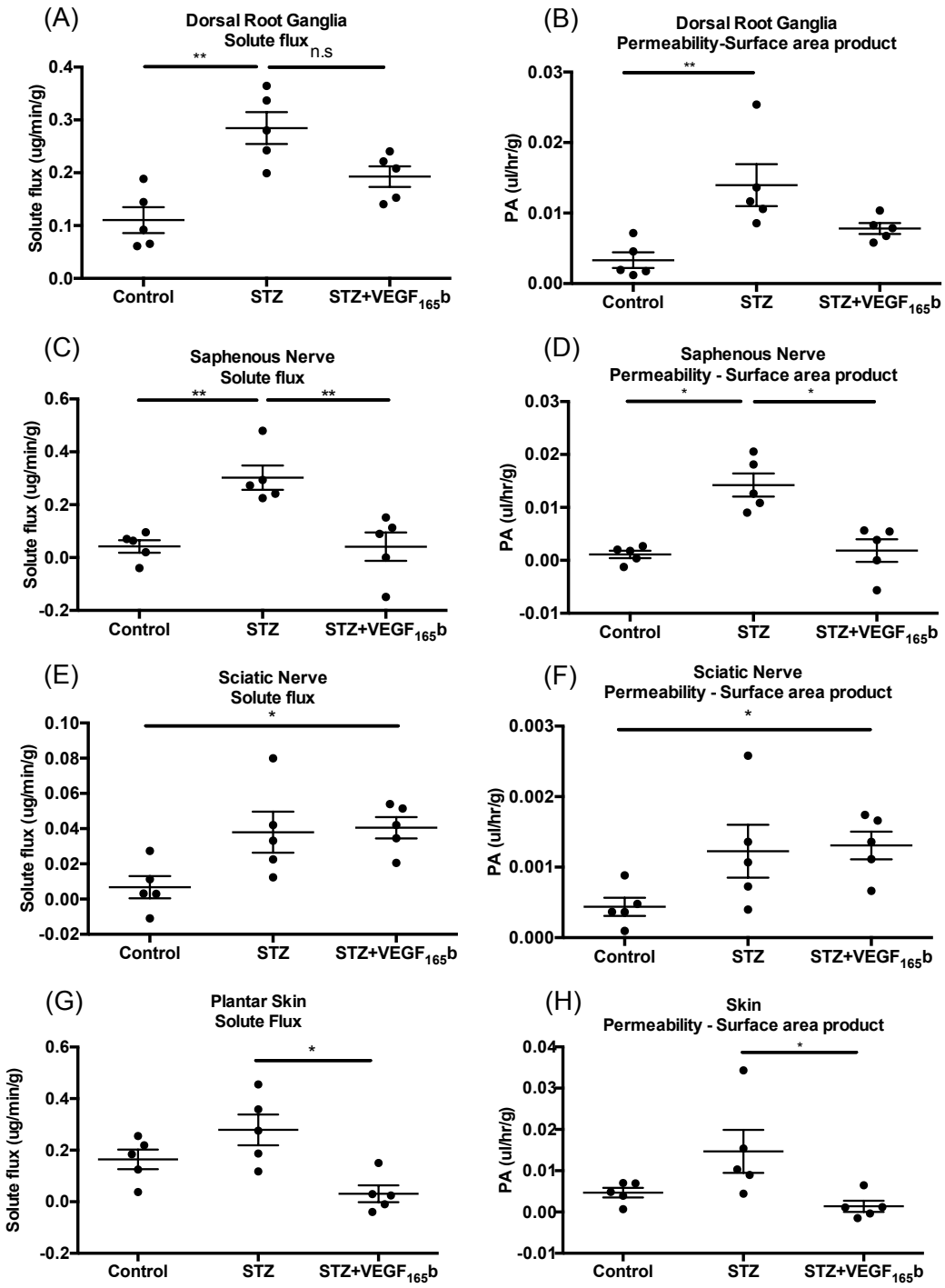

Figure 4.12. Diabetes induced changes in peripheral neurovascular function can be prevented by $VEGF_{165}b$ treatment.

Sprague-Dawley female rats were induced with diabetes using STZ (50mg/kg i.p, n=10) and control rats (n=5) were injected with saline (i.p) on day 0 and weighed weekly Diabetic rats were treated with either vehicle (saline, biweekly i.p, n=5) or $VEGF_{165}b$ (20ng/g, biweekly i.p, n=5). At 8 weeks post-STZ induction, Evans' blue (EB, 45mg/kg) was injected i.v into terminally anaesthetised rats. Plasma was collected every 15 minutes for 2 hours, after which, animals were sacrificed and dorsal root ganglia (DRGs R3, 4, 5), saphenous nerves, sciatic nerves and plantar skin were collected. EB solute flux increased in diabetic DRGs (A), saphenous nerves (C), sciatic nerves (E) and skin samples (G)

relative to respective controls. VEGF165b reduced this in all groups except in sciatic nerves. The same trend was observed when assessing permeability-surface area product (PA), which increased in diabetic DRGs (B), saphenous nerves (D), sciatic nerves (F) and skin samples. Similarly, this increase was prevented in all $VEGF_{165}b$-treated groups except for sciatic nerves (Kruskall-Wallis test with Dunn's post-hoc test, *$p<0.05$, **$p<0.01$).

These data indicate that diabetes causes vascular dysfunction in the retina, indicated by increased EB extravasation into the tissue. This suggests that there is indeed BRB dysfunction in this model and as blood vessels leak albumin-bound EB into the retina. This dysfunction is ameliorated in $VEGF_{165}b$ treated groups, suggesting that $VEGF_{165}b$ may be a useful therapeutic target in treating DME. As well as DME, these data suggest that other complications associated with diabetes, such as diabetic neuropathy, show promising results upon $VEGF_{165}b$ intervention.

4.3.3. Assessing the effect of $VEGF_{165}b$ on diabetes-induced retinal neurodegeneration

Data presented in this chapter indicate that $VEGF_{165}b$ can prevent characteristic vascular features of DR. Retinal neurodegeneration, another canonical feature of DR, precedes vascular dysfunction in DR. Loss of the retinal ganglion cell layer (RGC) is a prominent feature of DR and attributes to the poor visual acuity that sufferers of DR experience (Barber et al. 1998; Alistair J. Barber 2003). It has previously been shown that loss of RGC occurs in SD rats with STZ-induced diabetes (Barber et al. 1998). I wanted to assess if retinal neurodegeneration would occur in this model, to mimic the neuronal dysfunction observed in diabetic patients, and whether any changes could be reversed with $VEGF_{165}b$. To investigate this hypothesis, I used the remaining hemisected retinae from figure 4.3 and stained RGCs (figure 4.13A) using neuronal nuclear antigen (NeuN). Both cell count and cell body area were assessed using Image J. I observed that there was no change in number of RGCs (figure 4.13B) expressed in diabetic + vehicle retinae (67±15.8) relative to control retinae (94±9.07). There was a slight increase in RGC number in $VEGF_{165}b$ treated diabetic retinae (76.9±2.97), however this was not significant. When assessing RGC body area (figure 4.13C), a similar trend was observed. Diabetes alone showed no change in average cell body area (87.5μm^2±19.5) compared with control retinae (113μm^2±8.53). There was no change in cell body area upon

$VEGF_{165}b$ treatment (127.9µm^2±9.35) relative to diabetes alone. When this information was further analysed and separated according to size profile (4.13D), it was evident that there was indeed a difference in RGC body area amongst treatment groups. Diabetic RGC bodies were smaller than control cell bodies, with most RGCs being 0 -39µm^2 and 80-19µm^2 respectively. Diabetic rats treated with $VEGF_{165}b$ also had peak expression within 80-119µm^2. Interestingly, at 0-30µm^2, there was significantly more RGC bodies within that range in diabetic retinae (4.19±0.908) relative to both control (0.583±0.583) and diabetic + $VEGF_{165}b$ (0.021±0.917).

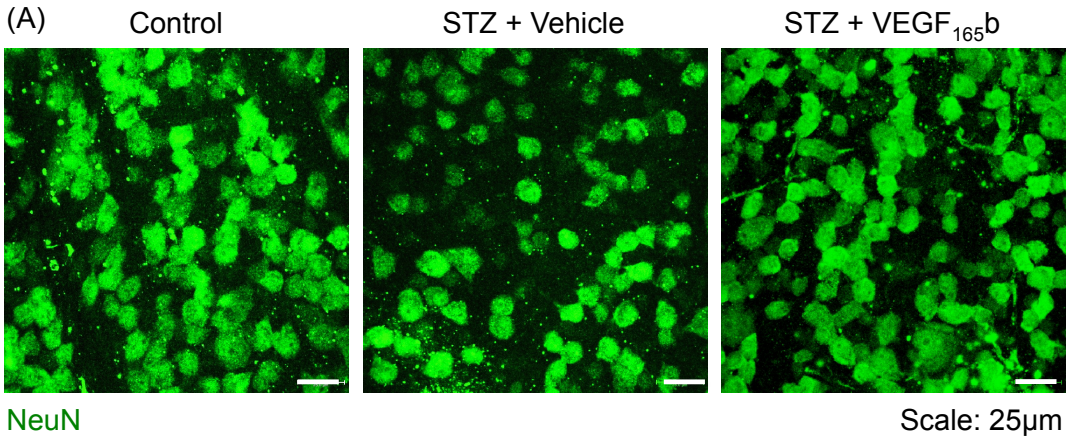

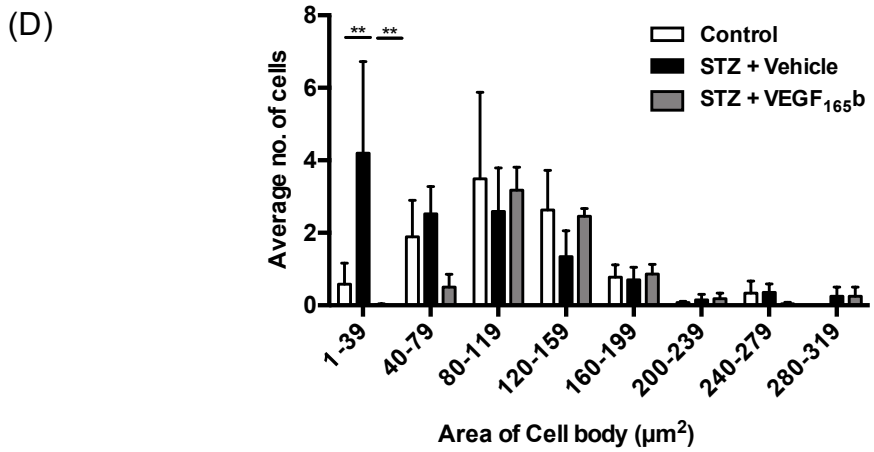

Figure 4.13. $VEGF_{165}$ prevents diabetes-induced RGC body shrinkage.

Sprague-Dawley rats induced with diabetes were treated with vehicle (saline i.p, n=4) or $VEGF_{165}b$ (20ng/g i.p, n=4) biweekly for 8 weeks. Animals were then sacrificed and retinae excised and stained (A) for retinal ganglion cell marker (RGC) NeuN. There was non-significant decrease in RGC population (B) in diabetic groups relative to control (n=3) and $VEGF_{165}b$-treated groups. There was a non-significant increase RGC shrinkage in the diabetic retinae (C), relative to control retinae with most RGCs being $\leq 39\mu m^2$ and $\leq 119\mu m^2$ respectively (D). This was also significant compared to diabetic + $VEGF_{165}b$ treated retinae. This leftward shift in average RGC area was restored upon $VEGF_{165}b$ treatment (2-way ANOVA with Tukey's post hoc test, **$p<0.01$).

These data indicate a general trend that diabetes induces a cell shrinkage, which may precede a potential cell death, and that this could be prevented in $VEGF_{165}b$ treated groups. However as figures 4.13A and 4.13B did not achieve significance, possibly due to a low n number or due to deficiencies in the model, conclusions need to be drawn with care.

4.4. Discussion

4.4.1. STZ-induced diabetes as model for PDR and testing rhVEGF$_{165}$b prevention of vascular remodelling

The use of STZ-induced hyperglycaemia is a widely used and accepted model of type 1 diabetes due to its rapid, reliable and robust phenotypic onset. STZ, combined with the addition of long-term insulin enables a more accurate model of type-1 diabetes. It has been hypothesised that PDR is the predominant "sight-threatening lesion" in type 1 diabetic patients (Simó et al. 2010), however, comorbidities associated with diabetes typically take many years of poor glycaemic control to develop. To compensate for this, the experimental protocol duration was set at 7-8 weeks. This time frame has been shown to produce reproducible features of diabetic neuropathy (Hulse et al. 2015), and as diabetic neuropathy and retinopathy occur over a similar time frame, we hypothesised that this would also be a suitable model of PDR.

We wanted to assess the how addition of VEGF$_{165}$b systemically would influence diabetes-mediated pathology in the eye, by measuring IB4-positive retinal vessel density in untreated, diabetic + vehicle and diabetic + VEGF$_{165}$b treated groups. However we were unable to stain control retinae with IB4 (figure 4.1), therefore hindering any conclusions as whether the model we are using works and also whether our systemic VEGF$_{165}$b treatment is having any effect. However, there was a small but significant decrease in retinal vessel density and fluorescence per field of view in the VEGF$_{165}$b-injected diabetic animals relative to vehicle treated diabetic animals (figure 4.1B). This was promising as it indicated that systemically administered VEGF$_{165}$b was affecting the retina, that the duration of the experiment was suitable enough to see differences in treatment and that the n numbers we chose were sufficient enough that the experiment had a suitable statistical power.

There was a difference in VEGF expression in the first cohort of rats (figure 4.2). All VEGF isoforms were up-regulated, however it is widely accepted within the literature that in the retina, hypoxia-mediated VEGF upregulation is principally the predominant pro-angiogenic VEGF$_{165}$ isoform (Shima et al. 1995; Shima et al. 1996). It is also well established that the characteristic hyperglycaemia observed in diabetes results in hypoxia-mediated elevated VEGF expression in the eye (Brownlee 2001), resulting in many of the

pathologies seen in DR. Therefore, it is probable that the elevated VEGF expression observed in the STZ + vehicle treated eyes is driving the concurrent reduction in occludin and ZO1 expression (figure 4.2). Reduction in TJ expression is a hallmark feature of DR, particularly DME, which often follows from PDR. Again, these data combined with the results of figure 4.1 indicate that the model may be working and that systemic $VEGF_{165}b$ administration is sufficient enough to induce a change in retinal vascular density.

The experiment was then repeated, building on the pilot data and changing the method of analysis from manual vessel counts to using Imaris software to semi-automate it. By calculating both area and volume, potential counting error was reduced, and takes into account changes in vascular depth. Manual vessel counts are a 2D representation of what occurs in these retinae, however calculating the volume gives a 3D view of how diabetes may affect retinal vasculature. It was evident that there was indeed an increase in retinal vascular density in diabetic retinae compared to untreated, after 8 weeks of diabetes. Increased area and volume occupied by vasculature both increased in vehicle treated, diabetic retinae (figures 4.3D and E). This change was prevented in the diabetic rats treated with $VEGF_{165}b$ and a similar trend was also observed when assessing integrated density (figure 4.3F). Similarly, there was an increase in change in vessel straightness (figure 4.4), or increased vessel tortuosity in diabetic retinae, relative to untreated and $VEGF_{165}b$-treated diabetic retinae. The increase in vessel density in the diabetic eye is consistent with what is traditionally observed in patients with PDR, however it cannot be described as neovascularisation without confirmation of proliferation using Ki67 staining.

Changes in protein expression for markers of angiogenesis (figures 4.5-4.7) have not been robust despite the changes observed in vascular remodelling. Whilst I expected to see a marked upregulation of VEGFR2 and pVEGFR2, as well as increased perk, I saw increases that were not statistically significant, and therefore firm conclusions cannot be made. However, this is not surprising as hypoxia-mediated changes in angiogenic markers occur in hypoxic microenvironments and are likely to be transient once new vessels have formed in response to the hypoxic stimuli. The whole diabetic retina is unlikely to be globally hypoxic at any given time, and therefore changes in markers such as VEGFR2 may be subtle and difficult to detect. A potential experiment to test this hypothesis would be staining retinal flat-mounts for the above markers and observing whether these changes are indeed global or local. However, due to limited retinae I was unable to pursue this experiment.

4.4.2. $VEGF_{165}b$ prevents diabetes-induced vascular remodelling: a potential mechanism

The microvascular phenotypes observed in the diabetic retinae was likely due to hyperglycaemia-induced hypoxia (figure 4.5). Hypoxia results in increased VEGF expression and VEGFR2 activation (figure 4.6). This causes increased endothelial nitric oxide synthase expression (eNOS), resulting in a change in NO production thus affecting vasomotor tone (Ho et al. 2012) in the retina. Vessel tortuosity typically precedes angiogenesis and is indicative of a hypoxic environment. Instances where there are changes in NO expression in the retina, will also result in changes in vasodilatation both longitudinally and radially, both occurring at different rates and therefore resulting in a meandering structure (Hart et al. 1999), as observed in the diabetic + vehicle-treated rat retinae (figure 4.4). Interestingly, in $VEGF_{165}b$-treated groups there was less vessel tortuosity, reflected in a trend to a reduction in HIF and VEGF protein expression (figure 4.5). This may indicate that $VEGF_{165}b$, when applied systemically, can cross the BRB and potentially interferes with eNOS signalling by preventing HIF transcription or by interfering with NO production. This would prevent the need for the vessels to constantly dilate and reperfuse, as the vasculature may not be occluded at all. This demonstrates the importance in maintaining the correct balance between both VEGF isoforms. To investigate this hypothesis further, one could potentially assess the effect of $VEGF_{165}b$ on eNOS production in models of OIR. Assaying levels of eNOS, NO and HIF-1α mRNA in $VEGF_{165}b$ treated hypoxic retinae would test my hypothesis sufficiently, however as this goes beyond the scope of my project, it was not pursued.

Despite the reperfusion efforts, HIF levels stay elevated, resulting in increased pro-angiogenic VEGF expression in diabetic retinae (figure 4.5). This lead to increased expression and phosphorylation of VEGFR2 in diabetic retinae (figure 4.6). Increased VEGFR2 phosphorylation results in increased ERK-mediated endothelial cell proliferation and migration, key factors of angiogenesis (Brownlee 2001; Geraldes et al. 2009). We observed a no change in both VEGFR2 and ERK phosphorylation (figure 4.7), despite appearing to increase in expression. It is likely that the proliferation seen in these retinae are likely due to this pathway. This increased proliferation is potentially why there is reduced cleaved caspase expression in the diabetic retinae, relative to control and $VEGF_{165}b$-treated retinae (figure 4.7E). The elevated angiogenesis observed in figure 4.3 is likely to be mediated by delta-like ligand 4 (DLL4). In hypoxic microenvironments

where there is increased VEGF expression and VEGFR2 activation, endothelial cells in these regions may express more DLL4. This results in tip cell formation of those DLL4-expressing cells, DLL4 then binds to its cognate Notch receptor in neighbouring cells, thus inhibiting further DLL4 expression, turning neighbouring cells into stalk cells. This results in tubule formation and, eventually, widespread angiogenesis (Hellström et al. 2007; Suchting et al. 2007). In models of CNV and choroidal hypoxia, angiogenesis has been linked with increased VEGF-induced DLL4 expression (Dong et al. 2011). This has been consistently shown to be the key aspect of retinal angiogenesis (Suchting et al. 2007), however without protein expression showing elevated DLL4 in these diabetic retinae, we are unable to conclude this.

$VEGF_{165}b$-treated retinae show a reduced vascular density (Figure 4.3) relative to diabetic retinae. In a model of *in vitro* haemangioma, $VEGF_{165}b$ treatment does not induce DLL4 expression and furthermore, $VEGF_{165}b$ prevents $VEGF_{165}$-induced DLL4 expression in haemangioma endothelial cells (*Dr. Ye, manuscript submitted*). This, combined with the data obtained in this chapter, indicates that in the diabetic + $VEGF_{165}b$ treated retinae there was competitive binding of both isoforms to VEGFR2 preventing excessive $VEGF_{165}$-induced VEGFR2 activation. As a result, more $VEGF_{165}b$ binding to VEGFR2 and a resultant weakened activation of the receptor, as observed in figure 4.6C. This results in a diminished downstream pathway activation, including weakened ERK signalling (figure 4.7), which has been shown to directly mediate DLL4 expression (Estrach et al. 2011). A reduction in ERK phosphorylation would likely result in a reduced DLL4 expression, and therefore reduced angiogenesis, as observed in figure 4.3. Future studies may involve electron microscopy analysis of these retinae, to assess whether $VEGF_{165}b$ can prevent-diabetes mediated basement membrane thickening and pericyte dropout.

We do not have DLL4 expression data. Nevertheless, this pathway is a highly established pathway involved in sprouting angiogenesis, and therefore the assumption that it is DLL4-mediated is not unreasonable. However, there are other key factors involved in angiogenesis, for example increased NO production in the diabetic retinae could trigger angiogenesis as well was increased VEGF-induced NFκB expression. Multiple pathways have been implicated in retinal angiogenesis and it is likely that they are all involved.

Figure 4.3 shows that $VEGF_{165}b$ treatment reduces vessel density in the diabetic retina significantly, relative to control, healthy rat retinae. However it is not apparent whether this difference is detrimental to the eye. If $VEGF_{165}b$ reduces the vasculature in the eye, the retina may become hypoxic and trigger the very cascade of events it aims to block. In this case, if the retina does become hypoxic and increases pro-angiogenic VEGF expression, as long as $VEGF_{165}b$ is continuously administered, as in this model, then $VEGF_{165}b$ will prevent VEGF-induced pathological neovascularisation. A future experiment to investigate this further could involve performing electroretinograms (ERG) on all groups, particularly at week 8. If no change was observed in A- and B-wave amplitudes of the $VEGF_{165}$ b-treated diabetic retinae, this would indicate that long-term $VEGF_{165}b$ treatment, if it crosses the BRB, would not cause a detrimental effect on visual function. As changes in the neural architecture often precede changes in vasculature in the diabetic retina, it would be possible to determine whether $VEGF_{165}b$ negatively impacts upon the visual pathway. However, this was not part of the experimental aim, SD rats were chosen for this study for their ability to develop a vascular pathology within 6 weeks. Diabetic SD rats supplemented with insulin have been reported to not develop any neuro-retinal phenotype during this time (Kern et al. 2010), and therefore ERGs were not included in this experiment.

4.4.3. STZ-induced diabetes as a model of DME and the effect of rhVEGF$_{165}$b on diabetic hyperpermeability

DME has been linked with sufferers of type 2 diabetes (Simó et al. 2010), however many type 1 diabetic patients initially present with PDR, that eventually escalates to DME. For this reason, and with support from published data (Xu et al. 2001; Qaum et al. 2001), we used the STZ model of diabetes to assess changes in retina solute flux. A study showed that in a rat model of insulin-supplemented diabetes, there was an insulin-induced increase in VEGF expression in the RPE (Poulaki et al. 2002), indicating that this model may be suitable for assessing changes in the outer BRB.

To assess how retina solute flux and PA is affected by SD rats, I modelled an experiment pioneered by Xu and colleagues in 2001, whereby Evans' blue was injected intravenously in diabetic and non diabetic animals ± intravitreal VEGF administration (Xu et al. 2001). With minor modifications, I implemented this semi-quantitative

technique to investigate my hypothesis that $VEGF_{165}b$ could prevent diabetes-induced increase in PA in the retina. Despite being a model of type 1 diabetes, it is evident that there is indeed a change in EB solute flux and PA in the diabetic retina after 8 weeks of diabetes, and even after as little as 1 week post induction (figures 4.9 and 4.10 respectively).

There was an increase in EB solute flux and PA after 8 weeks of diabetes (figure 4.9), in the vehicle treated diabetic retinae relative to healthy rat retinae. This, combined with the reduction in ZO1, occludin and VE-cadherin expression (figures 4.2 and 4.8) indicate that there is a disruption of the BRB upon diabetes, however despite appearing to be a marked change, decreases in occludin expression never reach statistical significance. VE-cadherin is an endothelial specific TJ, and therefore we can support already established hypotheses that DME involves the inner BRB. However, there is growing evidence in the literature that support the importance of the outer BRB. Previous *in vivo* permeability assays have shown low and high MW FITC-dextran accumulation at the outer BRB in models of diabetes, OIR and endotoxin-induced uveitis (Xu et al. 2011), thus reiterating the importance of the outer BRB in DME. However, as there is no RPE-specific TJ, we are unable to confirm this hypothesis in this particular model.

$VEGF_{165}b$-treated diabetic rats show a statistically significant reduction in EB extravasation into the retina, relative to vehicle-treated diabetic rats, indicating an inhibition of hyperglycaemia-induced insult on TJs. This is further supported by significant increases in VE-cadherin expression (figure 4.8). A similar result was observed after 1-week of non-insulin supplemented diabetes (figure 4.10). There was an increase in EB extravasation in the diabetic vehicle-injected retinae relative to control, vehicle-injected retinae and untreated retinae. This supports previously published findings that 7 days of diabetes is sufficient to induce changes in retinal "permeability". Intravitreal administration of $VEGF_{165}b$ for 24 hours was sufficient to reduce changes in EB extravasation, indicating that once it is definitely across the outer BRB, $VEGF_{165}b$ has a very robust effect. These data also suggest that the 8 weeks diabetes cohorts from figures 4.1, 4.3 and 4.9, were not treated with $VEGF_{165}b$ prophylactically, but rather upon onset of retinal pathology. Diabetic rats were first treated with vehicle or $VEGF_{165}b$ 1-week post confirmation of hyperglycaemia, and as I, and others have shown, 1-week is all that is required to see changes in "permeability"(Xu et al. 2001; Qaum et al. 2001). As an increase in solute flux and accumulation of fluid is the major sight-threatening aspect of DME, it is fair to hypothesise that this both the 1-week and 8-weeks model of diabetes

can be regarded as models of DME, and the $VEGF_{165}b$, whether administered IP or IVT, is able to prevent fluid accumulation in the retina, induced by diabetes.

Figures 4.10E and 4.10F show the differences between both models, and it appears that 8 weeks of diabetes provides a more robust phenotype, relative to 1-week diabetes as there is an increase in both EB solute flux and PA in the 8 week model relative to the 1 week model. This could be due to excessive insulin-induced VEGF expression in the RPE resulting in a more compromised outer BRB than perhaps would be seen without insulin treatment. It also shows that there is no significant difference between 24 hours of IVT $VEGF_{165}b$ treatment versus 8 weeks systemic $VEGF_{165}b$ treatment, indicating the robust nature of IVT treatment.

With regards to the BBB (figure 4.11), this model may not be robust enough to induce changes in permeability in other regions of CNS, despite seeing significant decrease in spinal cord permeability after 1 week of diabetes and seeing changes in the retina at both time points. However there were marked increases in both EB solute flux and PA in the DRGs, sciatic nerves, saphenous nerves and plantar skin in the diabetic + vehicle treated rats, relative to control animal tissue (figure 4.12). These regions are all associated with neuropathic pain and the same rats were more sensitive to mechanical and thermal stimuli, indicating peripheral neuropathy (Hulse et al. 2015). $VEGF_{165}b$ treatment reduced EB extravasation in these tissues, which correlated with a reduction in pain sensitivity. This indicates that the 8-weeks model of insulin-supplemented type 1 diabetes is a good model to assess complications associated with diabetes and that the EB technique is a robust method at detecting neurovascular dysfunction.

The Evans' blue dye perfusion technique has limitations whereby as it is only semi-quantitative, we cannot categorically claim changes in permeability. When vessels are perfused with EB, it is difficult to tell how much EB is unbound. Previous studies have shown that approximately 50% of EB does not bind to albumin and circulates as free dye (Levick & Michel 1973). Considering EB is only 961 Da, if left unbound it could pass through pores in the vasculature, smaller than those created by loss of TJs or induced by pathology, and may give a false positive result. Another caveat to this experiment does not account for changes in blood pressure. Whilst diabetic patients have a high incidence of hypertension (The National High Blood Pressure Education Program Working Group 1994), there are conflicting data whether STZ diabetic rats are hypertensive (Kusaka et al. 1987). The EB technique requires constant removal of blood from the femoral artery that

will reduce blood pressure throughout the experiment. Changes in blood pressure will affect flow of EB across capillary walls (Levick & Michel 1973), and therefore EB accumulation in the tissue could, in part, be also due to fluctuating blood pressure. Whilst we cannot definitively say that the diabetic eyes were more "permeable" than the non-diabetic eyes, changes in solute flux and PA are often regarded as markers of permeability,

4.4.4. $VEGF_{165}b$ prevents diabetes-induced permeability: a potential mechanism

There are many pathways by which fluid extravasation occurs in this model, many experts within the field suggest that is likely to be PKC mediated-TJ phosphorylation. This relies on the assumption that the increased solute flux is due to diabetes, and not due to other changes in vasoactivity. Similar models using the EB technique are in agreement that diabetes increases EB leakage and is likely mediated by PKC (Aiello 2002; Harhaj et al. 2006; Titchenell et al. 2012). There are two families of PKC isoforms, typical and atypical, and both families of isoforms have been implicated in the pathogenesis of DME. In the diabetic retina, there is an increase in extracellular glucose, which upon binding to cells, triggers *de novo* synthesis of DAG, which in turn upregulates typical PKC isoforms, including -α, -β, -δ and -γ (Brownlee 2001). These PKC isoforms have been linked directly to occludin phosphorylation *in vitro* and *in vivo* predominantly at the serine and threonine residues, and potentially these residues on ZO1 (Harhaj et al. 2006; Titchenell et al. 2012), resulting in their internalisation to an intracellular pool. However the Food and Drug Administration (FDA) did not approve a PKCβ inhibitor, ruboxistaurin, for the treatment of DME until another phase III clinical trial is completed (Javey et al. 2012). Furthermore, typical PKC inhibition only partially prevented hyperglycaemia-induced increase in permeability in RECs (Harhaj et al. 2006). Indicating that perhaps the RPE / outer BRB are involved more than previously thought and that also perhaps other PKC isoforms may be involved. Inhibition of atypical PKC isoforms, such as PKCζ, have shown promising results with regard to VEGF-induced but not diabetes-induced permeability *in vivo* (Titchenell et al. 2012). Activation of PKCζ is not calcium or DAG dependent like the typical PKCs, furthermore, inhibition of PKCζ also results in a reduction in tumour necrosis-α (TNF-α), a potent inflammatory factor. In a model of type-2 diabetes, Goto Kakizaki rats showed an increase in PKCζ activation in the RPE

layer resulting in inflammatory cell trafficking between the choroid and the RPE. There was a resultant increase in microglia and macrophage accumulation in the subretinal space (Omri et al. 2011), further confirming that the importance of the outer BRB in DR.

Activation of DAG and PKC results in an upregulation of $VEGF_{165}$ (or the mouse equivalent, $VEGF_{164}$) and NFKB, both of which are pro-inflammatory and upregulate expression of intracellular adhesion molecule (ICAM-1) and TNF-α. It has been suggested that an increase in these pro-inflammatory cytokines result in increased retinal permeability (Ishida 2003; Joussen et al. 2004; Tang & Kern 2011). $VEGF_{165}b$ has been shown to reduce TNF-α mediated ICAM activation in RPE cells, and therefore is potentially anti-inflammatory (Thichanpiang et al. 2014). Furthermore, $VEGF_{165}$ has shown to activate PKC (Hulse et al. 2014b), whereas $VEGF_{165}b$ blocks PKC activation *in vitro* (*S. Bestall, unpublished data*).

However, both types PKC of treatment show partial prevention in permeability, whereas data in this chapter shows almost a complete reversal of pathology. A potential mechanism by which $VEGF_{165}b$ prevents permeability could be by targeting both families of isoforms. $VEGF_{165}b$ competitively binds to VEGFR2, and therefore only partially activates DAG and therefore partially activates typical PKC isoforms; therefore there is little or no phosphorylation of TJs. $VEGF_{165}b$ also reduces TNF-α expression in the outer BRB, perhaps by blocking atypical PKC activation in the RPE, also preventing TJ phosphorylation and subsequent hyperpermeability. This again further underlines the importance of maintaining both pro- and anti-angiogenic VEGF isoforms. However, to test this hypothesis, the above experiments would need to be repeated with and without inhibitors of each PKC family ± $VEGF_{165}b$ co-treatment.

4.4.5. STZ-induced 8 –weeks diabetes is not a robust enough model to induce retinal ganglion cell death

RGC loss is a prominent feature of the neurodegenerative arm of DR and is significantly part of vision loss. To assess if this change would be observed in STZ-induced diabetes, retinae 8-week diabetic rats ± $VEGF_{165}b$ and control retinae were stained for NeuN, a marker of RGCs (figure 4.13A). When counting the NeuN-positive cells, there was a non-significant decrease in these cells in diabetic + vehicle treated eyes relative to control eyes, and there was a slight increase in $VEGF_{165}b$ treated groups

(figure 4.13B). These findings have been supported in previous work that shows SD rats develop a non-significant reduction in RGCs even after 4 months of insulin-supplemented diabetes (Kern et al. 2010). This conflicts with what is seen in diabetic patients as RGC layer thinning occurs before the onset of any vasculopathy (Kern & Barber 2008), indicating that STZ-induced diabetes in SD rats does not produce all aspects of DR.

There was no significant difference in total RGC area (figure 4.13C), however when these findings were dissected further and categorised by size (figure 4.13D), it was evident that diabetic + vehicle treated rats showed RGC shrinkage, relative to control and $VEGF_{165}b$ treated rats. This suggests that whilst the model may not be successful in reducing RGC number, it is causing dysfunction in the RGC layer. It is possible that the thinning of the RGC layer in patients is also due to RGC shrinkage, and that shrinkage precedes RGC death. A future direction for this experiment may be to repeat this experiment, with the addition of assaying ERGs of each eye at the end of the 8-week period.

VEGF is upregulated in the diabetic retina, particularly in insulin-treated diabetes in SD rats (Poulaki et al. 2002) and is possibly exerting a neuroprotective role on the RGC layer as it does in other models of eye disease (Jin et al. 2000; Shima et al. 2004; Foxton et al. 2013). Furthermore, insulin has been hypothesised to prevent RGC apoptosis in rat models of DR (Kern & Barber 2008), again conflicting with what is observed in patients whereby insulin therapy in fact causes a transient worsening of retinopathy (Dahl-Jorgensen et al. 1985; Anon 1993; Chantelau & Kohner 1997). VEGF and insulin may be protecting the RGC layer from the vascular dysfunction in the earlier stages of DR. It is possible that over time, once the vascular dysfunction develops and there is an increase pro-inflammatory markers, RGCs are no longer sufficiently protected by VEGF and insulin and start to shrink. If we extend this model to a significantly longer time point there may be RGC dysfunction. An additional caveat to this experiment is that some NeuN antibodies have been known to also stain cholinergic amacrine cells that have been displaced to the GCL. However this is usually only 15-20% of cells stained by NeuN, and it is therefore likely that the majority of these results are from RGCs (Schlamp et al. 2013). Nevertheless, $VEGF_{165}b$ does appear to protect against RGC shrinkage and perhaps amacrine cell shrinkage, both cell types associated with visual dysfunction in DR. At the time of writing this study, is the only treatment that appears to treat neovascularisation, oedema and neuronal dysfunction in the diabetic eye.

4.5. Concluding Remarks

The current gold-standard treatments for DR involve a combination of PRP laser therapy and anti-VEGF therapy in treating both PDR and DME. Systemic $VEGF_{165}b$ administration appears to be less invasive than laser therapy, as no anaesthesia or analgesia is required in systemic application of this drug. Furthermore, laser therapy is only a temporary measure and often results in neural retina damage and further sight loss. Laser-treated patients will usually require further laser treatment or a combination of laser treatment and anti-VEGF therapy (Hammes 2013).

A major concern associated with using anti-VEGF therapy is the risk of anti-VEGF agents entering the choroidal and then systemic circulation, resulting in adverse events in diabetic patients. As $VEGF_{165}b$ is already an endogenous cytokine, if it enters the systemic circulation, it is perhaps less likely to cause an adverse event than other treatments. When investigating peripheral tissue and kidney and heart tissue (data not shown) it appears that systemic $VEGF_{165}b$ had no adverse effect on vessel integrity in these regions. Also, having observed no difference between IVT and IP administration of $VEGF_{165}b$ on EB extravasation, $VEGF_{165}b$ could be administered whichever way would associate with less risk of possible adverse events. It is therefore plausible that $VEGF_{165}b$ could be a potential therapeutic agent in treating DME.

With regards to the vascular complications of DR, a future step may be to test the effect of $VEGF_{165}b$ in experimental DR in higher mammals and assessing if a similar result is observed as well as treatment associated toxicity. A more suitable method of BRB leakage may be to do fluorescein angiography, if using non-albino animals. An immediate future direction would be to reassess this model, and select a strain of rats more suitable for assessing neuronal dysfunction in the retina and investigating the whether $VEGF_{165}b$ improves visual function in the diabetic eye.

Chapter 5: AAV.VEGF$_{165}$b and diabetic retinopathy

5.1. Introduction

Anti-VEGF therapy for diabetic retinopathy has recently become widely used both experimentally and clinically, due to its ability to curb both PDR and DME (Ferrara et al. 2006; Stewart 2014). Although this has shown positive results in reducing NV, macular thickness and in some cases gaining of letters (Wells et al. 2015), anti-VEGF agents are not suitable for the early stages of DR. Retinal neurodegeneration precedes ischaemia-induced changes in retinal vasculature (Lieth et al. 2000; Alistair J. Barber 2003), furthermore, VEGF is neuroprotective in the retina (Foxton et al. 2013). Therefore by administering anti-VEGF therapy as an early treatment would likely prove to be detrimental. Nevertheless, early or even preventative treatment for DR directed towards neuroprotection may be a beneficial therapeutic strategy as there is an hypothesis that suggests that it is retinal neurodegeneration can contributes to the vascular pathology seen later on (Lieth et al. 2000). Also, most current therapies target the vascular component of DR, leaving the neurodegeneration as a secondary aspect.

Gene therapy as a potential treatment for preventing retinal neurodegeneration is a widely investigated field showing promising results. Leber congenital amaurosis (LCA), a condition resulting in infant blindness can result from a defect in the *RPE65* gene. Dogs that are deficient in this gene suffer from severe vision loss, and when treated with the rAAV-*RPE65* vector showed a significant improvement in vision (Acland et al. 2001) and recent clinical trial data shows that there is also an improvement in retinal function in patients with LCA (Bainbridge et al. 2015). In a model of recessive retinitis pigmentosa, the retinal degeneration slow mouse (RDS) is unable to produce peripherin 2, due to a mutation in the gene that encodes it (*Prph2*; Chang et al. 1993). This membrane glycoprotein is essential for photoreceptor disc formation therefore RDS mice are unable to form proper outer segments and photoreceptor discs, and as a result show poor phototransduction. Eventually, photoreceptors undergo apoptosis starting approximately two weeks post-birth, resulting in gradual blindness (Chang et al. 1993). Introduction of the *Prph2* minigene into these deficient eyes using AAV2 under a rhodopsin promoter resulted in stable outer disc formation and increased ERG A- and B-wave amplitude (Ali et al. 2000).

Gene therapy to treat neovascular complications has also been widely investigated. Vectors expression anti-angiogenic compounds such as sFlt1 (Bainbridge et

al. 2002), PEDF (Auricchio et al. 2002) and endostatin (Balaggan et al. 2006) have all shown to reduce ocular angiogenesis *in vivo*. However few vectors aim to address neuroprotection as well as inhibiting angiogenesis. $VEGF_{165}b$ has shown to be neuroprotective against RGC death upon ischaemic insult (Beazley-Long et al. 2013) and against diabetic insult in the peripheral nervous system (Hulse et al. 2014b). It has also shown to be cytoprotective in culture and in the retina (Magnussen et al. 2010). Considering the progress being made in retinal gene therapy, using this approach may facilitate long-term expression if $VEGF_{165}b$ and also minimise the number of injections needed and therefore also reducing likelihood of possible injection-related side effects. I therefore attempted to test the hypothesis that Lewis rats induced with diabetes would show an increase in retinal neural dysfunction and this would be translated into a reduction in retinal thickness. I also attempted to test the hypothesis that AAV.$VEGF_{165}b$ would prevent diabetes-induced changes in neural dysfunction and retinal thickness.

5.2 Methodology

This study used AAV2/8 due to its previously described low immunogenicity (Anand et al. 2002) and its ability to transduce RPE and photoreceptors efficiently (Buch et al. 2008). Three viruses were prepared: AAV.GFP, AAV.VEGF$_{165}$b and AAV.Null (negative control, see appendices for details). As the primary aim of the experiment was to observe and potentially prevent neurodegeneration of the diabetic retinal architecture, Lewis rats were chosen for this experiment for their previous history of showing RGC loss within 4 months of induction of diabetes (Kern et al. 2010).

Lewis rats (n=33) were divided into two main groups, diabetic and non– diabetic controls. Two weeks prior to induction of diabetes, rats were subretinally injected with two 5µl subretinal injections, superior and inferior, of approximately 1x10^{12} vp/ml of: AAV.VEGF$_{165}$b, AAV.Null or no injection. Viruses were only injected in one eye, with the contralateral eye serving as an untreated control reference eye. The groups were further divided as shown by table 5.1.

Diabetic (n=18)	**Non–diabetic (n=15)**
Untreated (n=5)	Untreated (n=5)
AAV.Null (n=6)	AAV.Null (n=5)
AAV.VEGF$_{165}$b (n=7)	AAV.VEGF$_{165}$b (n=5)

Table 5.1. Treatment groups for long–term diabetes study.

Two weeks following virus injection, the rats listed in table 5.1 were subject to STZ injection (i.p, 50mg/kg). Control rats were given a saline injection i.p. Diabetic rats were then implanted with 1/3 of an insulin capsule (LinShin) in the same afternoon. Three days post–injection, blood glucose was assessed for hyperglycaemia and rats with blood glucose >15mmol/l were deemed diabetic. One-week post confirmation of diabetes, rats were subject to ERG, SLO and OCT analysis under general anaesthesia to assess retinal function, atrophy and thickness respectively. This time point was regarded as month 0 and *in vivo* assessment was repeated monthly for 4 months. At the end of the study, rats were sacrificed and eyes were fixed and frozen in OCT ready for sectioning and staining. For further details, see chapter 2 “Materials and Methods”.

To validate the AAV.VEGF$_{165}$b, I also used in the laser CNV model in C57BL6j mice. Adult female mice (6-8 weeks old) were given two 2µl injections of either AAV.VEGF$_{165}$b or AAV.Null (titre- matched at 1x10^{12} vp/ml). Two weeks post injection, mice were subject to a 3 laser burns on each eye under general anaesthesia. At 3, 7 and 14 days post-laser burn, FFA was carried out on all mice. On day 14, mice were sacrificed and choroids were fixed, flat-mounted and stained for IB4. Burn area was calculated *in vivo* and *ex vivo* using Image J. For further details, please see chapter 2, "Materials and Methods".

To test the neuroprotectivity of AAV.VEGF$_{165}$b in an alternative model, RDS (retina degeneration slow) mice were also injected with either AAV.VEGF$_{165}$b or AAV.Null. However, as mice were injected at P10, only 1 subretinal injection was administered under general anaesthesia (2µl of virus at 1x10^{12} vp/ml). Two weeks post virus administration; mice were subject to monthly ERGs for 2 months. For further details, please see chapter 2, "Materials and Methods".

All viruses, unless otherwise stated, we administered via a subretinal injection under general anaesthesia.

5.3. Results

5.3.1. Optimisation of vector dosage

To determine whether we could transduce the Lewis rat eye appropriately, Lewis rats were injected with 2x5µl of vector at $1x10^{12}$ vp/ml, in one eye, with the contralateral eye serving as an untreated control. Volumes of virus injected were chosen based on relative GFP expression in SLO images (see Appendix 4). Two weeks following injection, rats underwent scanning laser ophthalmoscopy (SLO), and the fluorescence was observed (figure 5.1A). Immediately after imaging, rats were culled and eyes were fixed and imaged using the 488 laser to observe where GFP was transduced (figure 5.1B). The data showed that we were able to transduce the outer retina and most importantly to our hypothesis, the ORB (RPE).

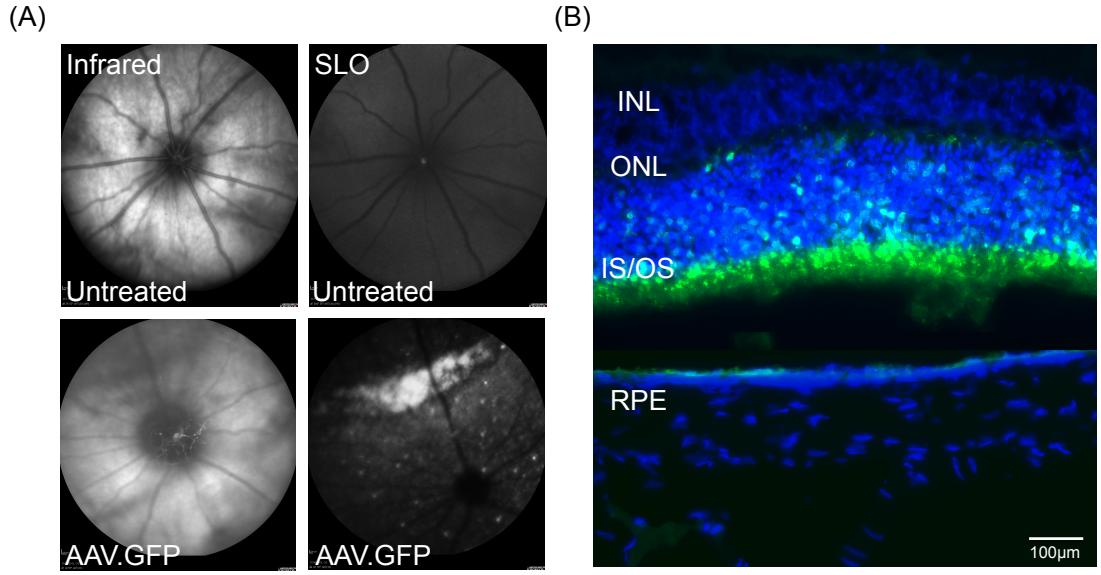

Figure 5.1. Infrared and SLO images of AAV.hrGFP injected Lewis rat eyes

Lewis rats (n = 3) were injected with 2x5µl AAV.hr.GFP ($1x10^{12}$ vp/ml) in the right eye, subretinally. The left eyes, served as an untreated control. Two weeks following injection, rats were subject to infrared and SLO (A) imaging and eyes were enucleated, sectioned and imaged and relative areas of fluorescence were observed (B). AAV.hrGFP is able to successfully transduce the rat eye when given two injections of 5µl AAV.hrGFP at $1x10^{12}$ vp/ml.

To determine the amount of $VEGF_{165}b$ produced by $AAV.VEGF_{165}b$, Lewis rats (n=4) were injected with the same dose and same volume ($1x10^{12}$ and 2x5µl respectively) of $AAV.VEGF_{165}b$ in one eye (n=4), and AAV.Null (n=2) or untreated (n=2) in the contralateral eye. Two weeks post – injection, rats were culled and eyes were enucleated and retinae and choroids were assayed for $VEGF_{165}b$ expression. Retinae were subject to immunoblotting using the 56/8 anti-$VEGF_{165}b$ antibody (figure 5.2A). ELISA assayed both retinae and choroids for $VEGF_{xxx}b$ (figure 5.2C - E). There was a threefold increase in $VEGF_{165}b$ expression in the $AAV.VEGF_{165}b$ injected eyes compared to both negative control groups (figure 5.2B). There was a significant increase in $VEGF_{xxx}b$ expression in the $AAV.VEGF_{165}b$ injected groups, compared to AAV.Null and untreated groups, when calculating expression relative to total VEGF expression, and this trend was observed in both retinae (figure 5.2C) and choroids (figure 5.2E). However, when measuring $VEGF_{xxx}b$ expression relative to total protein expression, $VEGF_{xxx}b$ was only significantly overexpressed when compared with untreated groups in both retinae (figures 5.2D and 5.2F respectively). However, we do observe a 1.5 fold increase in $VEGF_{xxx}b$ expression in $AAV.VEGF_{165}b$ injected groups compared to the other groups, relative to total protein in both retinae and choroid (figures 5.2D and 5.2F)

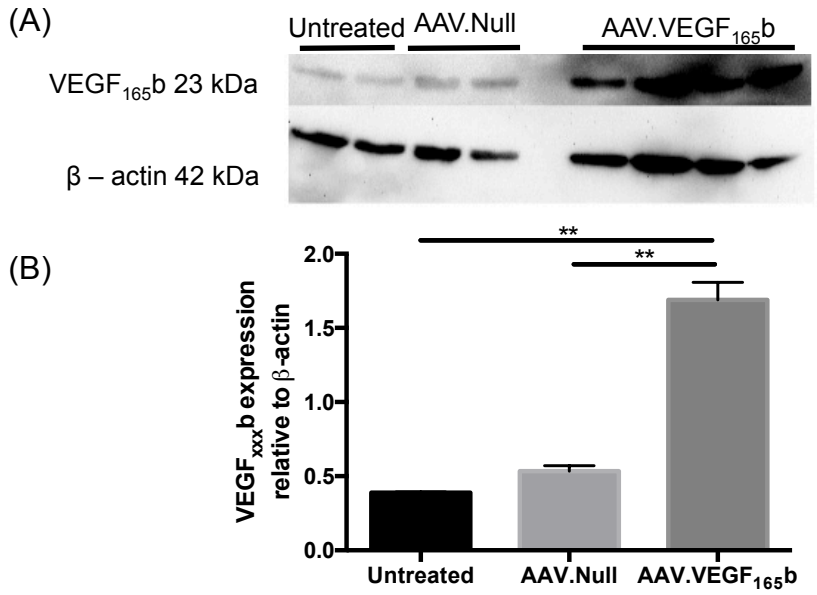

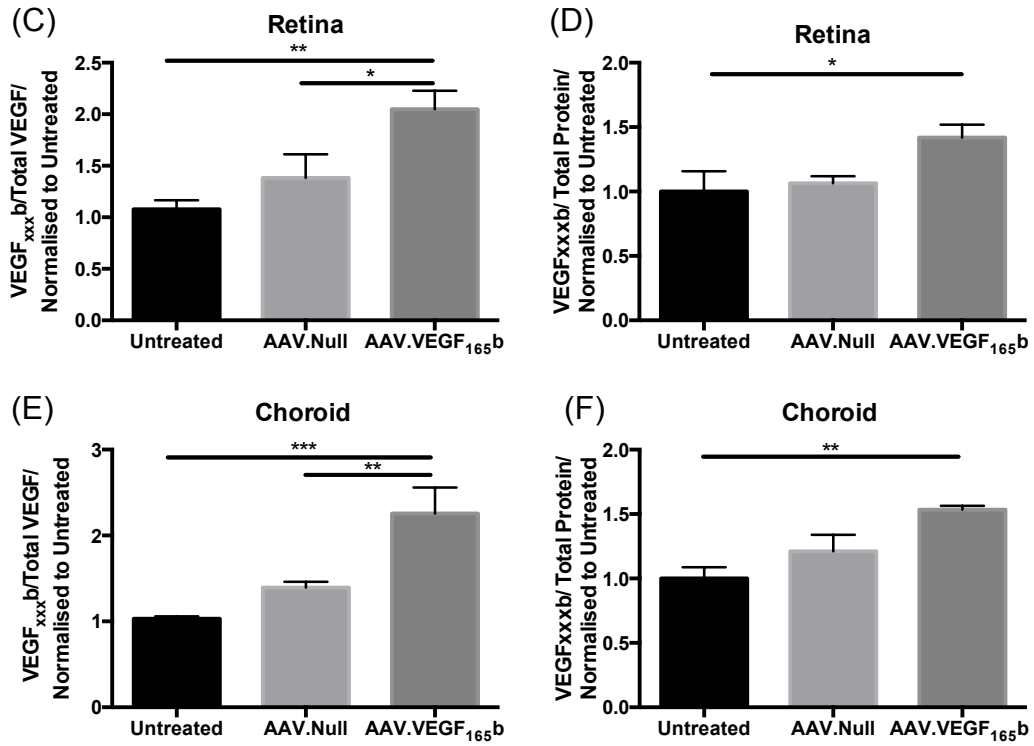

Figure 5.2. AAV.VEGF$_{165}$b was able to successfully induce VEGF$_{165}$b expression in retinae and choroids in Lewis rats.

Lewis rats were injected with AAV.VEGF$_{165}$b, AAV.Null or left untreated and were culled two weeks post – injection, at which point retinae and choroids were assayed for VEGF$_{xxx}$b expression. Retinae were immunoblotted against 56/1, a VEGF$_{165}$b specific antibody (A) and protein expression was quantified relative to β – actin expression (B). There was a significant increase in VEGF$_{165}$b expression in the AAV.VEGF$_{165}$b treated groups, relative to AAV.Null and untreated groups. Retinae and choroids were assayed for VEGF$_{xxx}$b expression by ELISA. Values were either represented relative to total VEGF expression (C and E) where VEGF$_{xxx}$b was significantly overexpressed relative to AAV.Null and untreated groups in retinae and choroids. When calculated as a measure of total protein expression (D and F), retinae and choroids injected with AAV.VEGF$_{165}$b only expressed increased levels of VEGF$_{xxx}$b relative to untreated groups (1-way ANOVA with Tukey's post hoc test, *$p<0.05$, **$p<0.01$).

Figure 5.2 shows that not only did we successfully cause overexpression of VEGF$_{165}$b using AAV.VEGF$_{165}$b but there was also no upregulation of VEGF$_{165}$b upon injection of AAV.Null, confirming we have an adequate negative control. For further assays regarding AAV.Null expression, please see appendices.

5.3.2. STZ – induced diabetes does affect ERG amplitude or retinal thickness in Lewis rats

Having confirmed that AAV.VEGF$_{165}$b did increase VEGF$_{165}$b expression (figure 5.2) and that AAV.Null does not induce VEGF$_{165}$b or expression of the original RK.RPGR construct (appendix 3), the viruses could be used further. To investigate whether VEGF$_{165}$b gene therapy could prevent degeneration of the retinal neural architecture, Lewis rats were injected with saline or STZ (50mg/kg, as described in Chapter 2: "Materials and Methods"). Each animal either received: AAV.VEGF$_{165}$b, AAV.Null or no injection in the right eye, with the left eye serving as a reference eye (see table 5.1). Differences in neural retina were measured *in vivo* by ERG for 4 months as the Kern group have reported differences in ERG B–wave amplitude in insulin-supplemented diabetic Lewis rats after 3–4 months (Engerman & Kern 1995; Kern et al. 2010; Robinson et al. 2012b). As mentioned previously, the hypothesis of this experiment was to see whether we could prevent diabetes – induced degeneration of the neural retina using AAV.VEGF$_{165}$b. To assess whether diabetes induced retinal neural degeneration in this model, I compared control rat ERGs with diabetic rat ERGs, both of which were untreated eyes, at 4 months of diabetes. I hypothesised that after 4 months of diabetes the ERG amplitude for almost all measurements, particularly the B–wave amplitudes, would be reduced relative to control rats. However despite maintaining a steady weight (figure 5.3A) and being consistently hyperglycaemic (figure 5.3B), there was no significant difference between controls and diabetics in the rod mediated (scotopic) A or B wave (figure 5.3 B and C respectively). There was also no difference in A or B–wave amplitude in the cone–mediated (photopic) response between controls and diabetics. However, there did appear to be a small, but non–significant difference in the scotopic B–wave (figure 5.3D) at the higher light intensities.

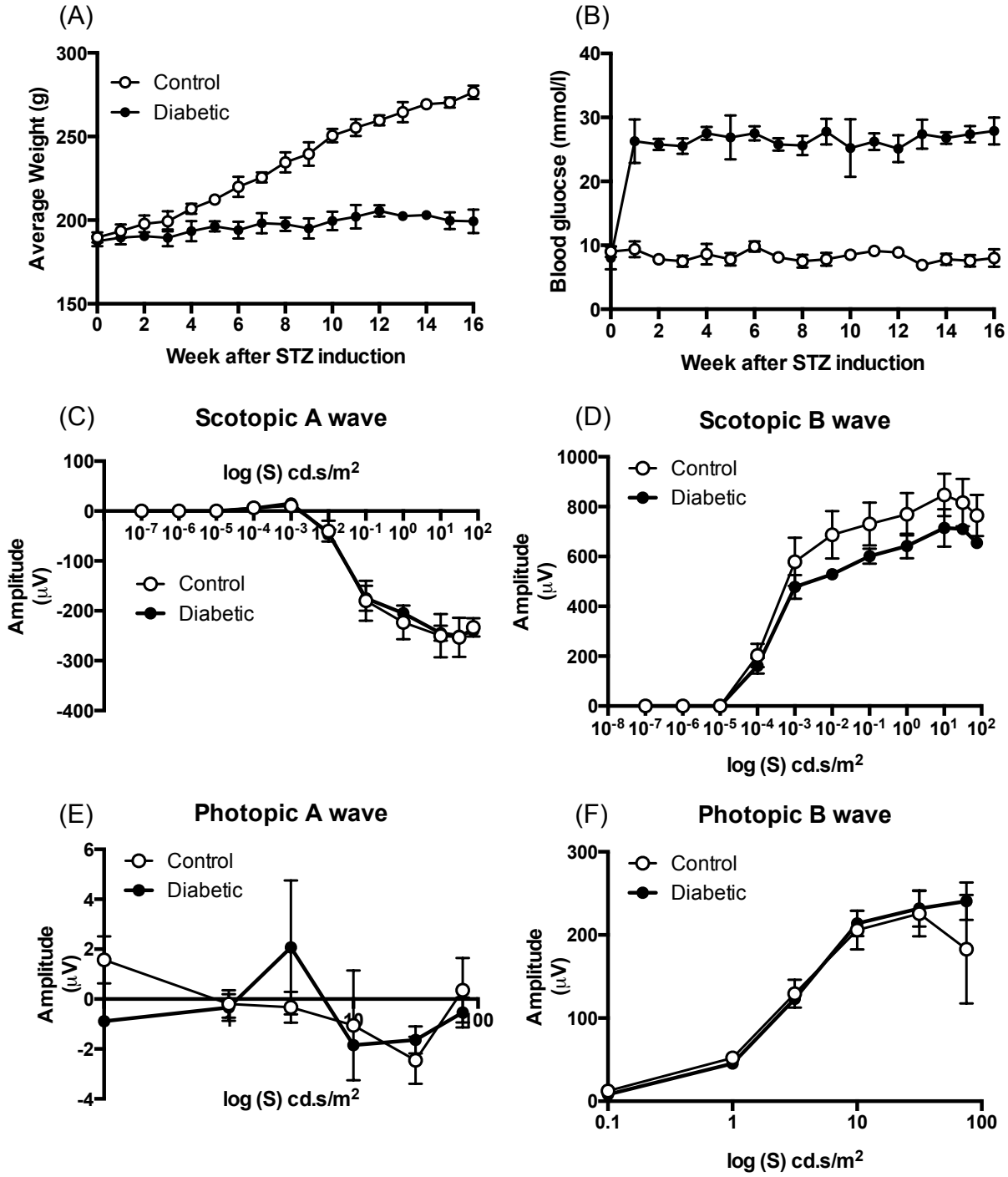

Figure 5.3 STZ–induced diabetes has no effect on relative ERG amplitude in Lewis rats at 4 months

Lewis rats were induced with diabetes (n=5) using STZ (50mg/kg, i.p) and supplemented with insulin (subcutaneous pellet) to prevent weight loss (A). Rats with a blood glucose ≥15mmol/l were deemed diabetic (B) and were subject to monthly ERG assessment for 4 months. Diabetics and saline–injected rats (control, n=5) were dark-adapted overnight prior to assessment to ensure no photo bleaching would skew scotopic measurements. A custom programme was designed to best assess amplitude for both scotopic and photopic responses. Scotopic measurements were assessed over an 11–step intensity protocol

ranging from 0.001(S).cd/s^2 to 75.35(S).cd/s^2. Photopic intensities were measured of a custom-designed 6–step protocol ranging from 0.1 (S).cd/s^2 to 75.38(S).cd/s^2. There was no significant difference between controls and diabetic in their rod–mediated A- or B-wave amplitude (C an D respectively), Similarly there was no difference in cone–mediated A- and B–wave amplitude (E and F respectively).

Although there is no significant difference in ERG amplitude in any of the parameters, it is possible that there they may have been a difference during earlier time points. To assess this hypothesis, I plotted the scotopic A– and B–wave amplitudes obtained at minimal and maximal intensities (0.001 and 75.38 cd.s/m^2 respectively) of control and diabetic ERGs over the 4–month period. As evident from figure 5.3, photopic A– waves were unreliable even in control animals, and have therefore been excluded from further analyses in this chapter, and so only amplitudes obtained at minimal and maximal photopic B wave intensities have been plotted (0.1 and 75.38 cd.s/m^2 respectively). Figure 5.4 shows that there was no significant difference at any time point across any parameter. Interestingly, even the healthy animals show retinal dysfunction over the 4-month period in all B–wave responses (figure 5.4C – 5.4F). Furthermore, in all B–wave responses diabetic seem to have greater amplitude than control B–waves, however these data are not statistically significant.

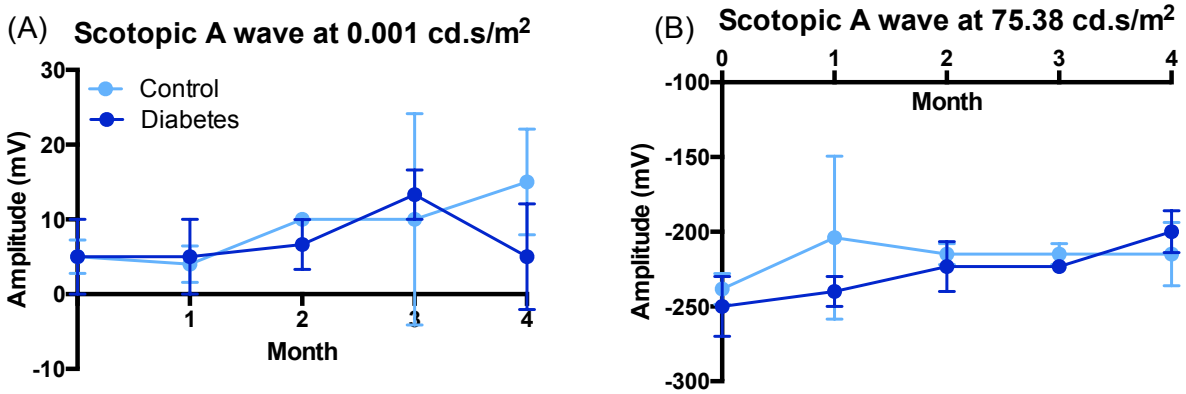

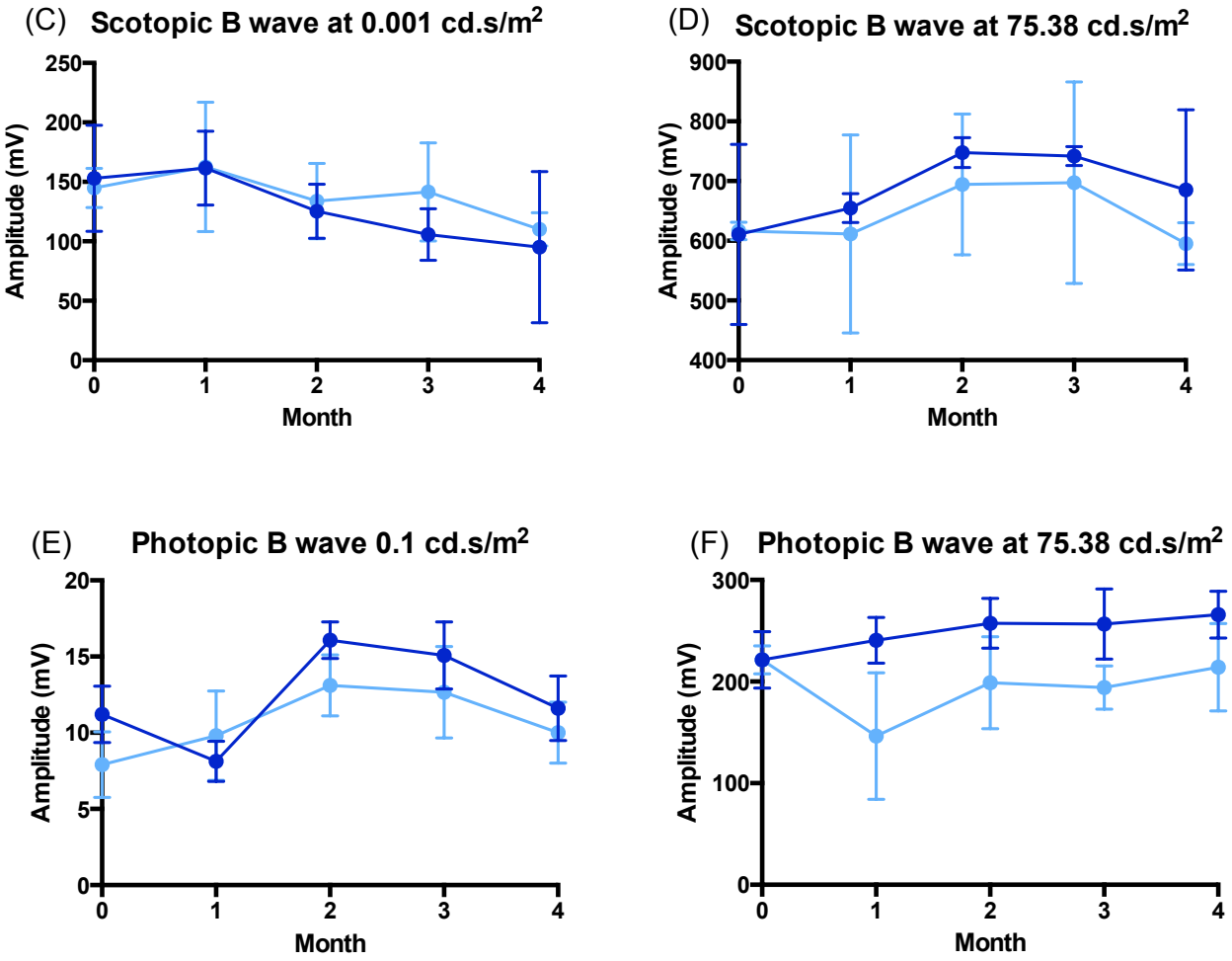

Figure 5.4. STZ–induced diabetes does not affect ERG amplitude in Lewis rats over a 4-month period

Lewis rats were induced with diabetes (n=5) using STZ (50mg/kg, i.p) and supplemented with insulin (subcutaneous pellet) Rats were subject to monthly ERG assessment for 4 months. Diabetic rats and age-matched controls, injected with saline i.p (n=5) were subject to ERG assessment monthly, and minimal and maximal light intensities were plotted. There was no difference in rod mediated A– or B–response both at minimal intensity (A and C) or maximal intensity (B and D). There was also no difference in the cone-mediated response at both ends of the 6–step process (E and F).

To investigate this further, I sectioned and stained these retinae for DAPI and measured GCL thickness by counting DAPI–positive cells within the GCL (figure 5.5A). I observed that there was no significant difference in the number of cells in the GCL between control retinae and diabetic retinae (figure 5.5B).

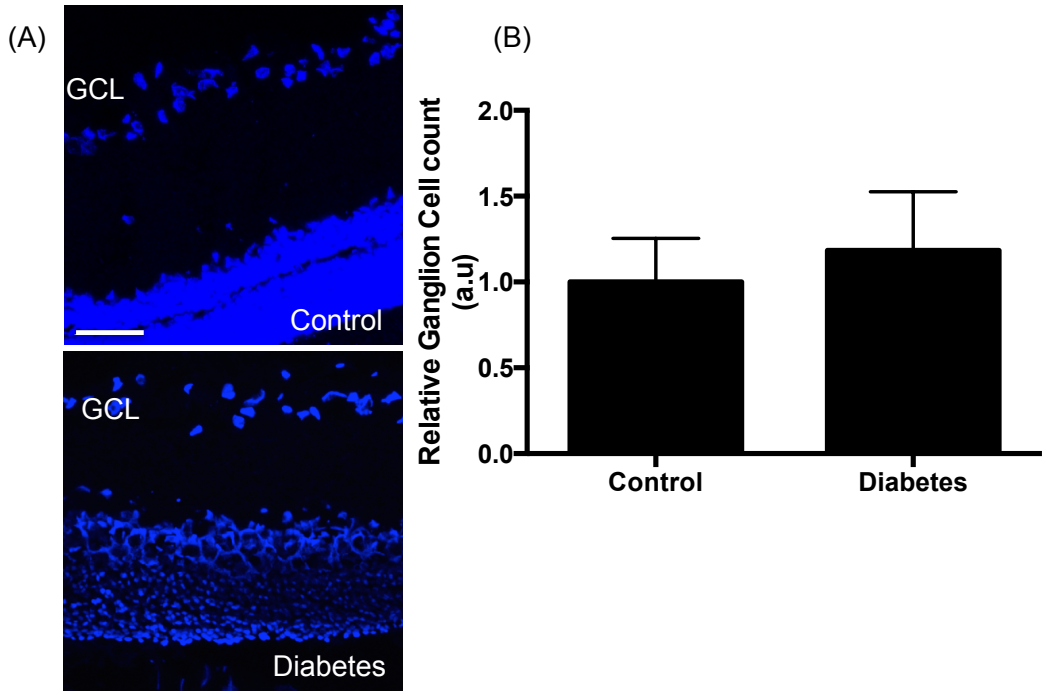

Figure 5.5. 4–months STZ–induced diabetes does not alter number of DAPI–positive cells in the GCL in Lewis rats.

Lewis rats were induced with diabetes (n=5) using STZ (50mg/kg, i.p) and supplemented with insulin (subcutaneous pellet). Four months post–induction, diabetic and age–matched controls (n=5) were culled and retinae were sectioned and stained for DAPI (A). Cells in the GCL were counted using Image J which showed there was no significant difference in DAPI–positive cells in the GCL between control and diabetic retinae (Student's T-test).

Diabetes usually causes thinning of the GCL and thickening of the macula, and although rodents are devoid of maculae, I initially wanted to characterise this model and see how retinal thickness may differ between control and diabetic groups. To investigate this further, on the same day as ERG measurements were undertaken and under the same anaesthetic regimen, I measured retinal thickness in 4 regions of the retina using OCT. I then quantified the retinal thickness by determining an ROI (GCL to RPE) using Image J (for further details please read chapter 2 "Materials and Methods"). I observed that in all regions of the retina, there was no difference in retinal thickness between control and diabetic groups.

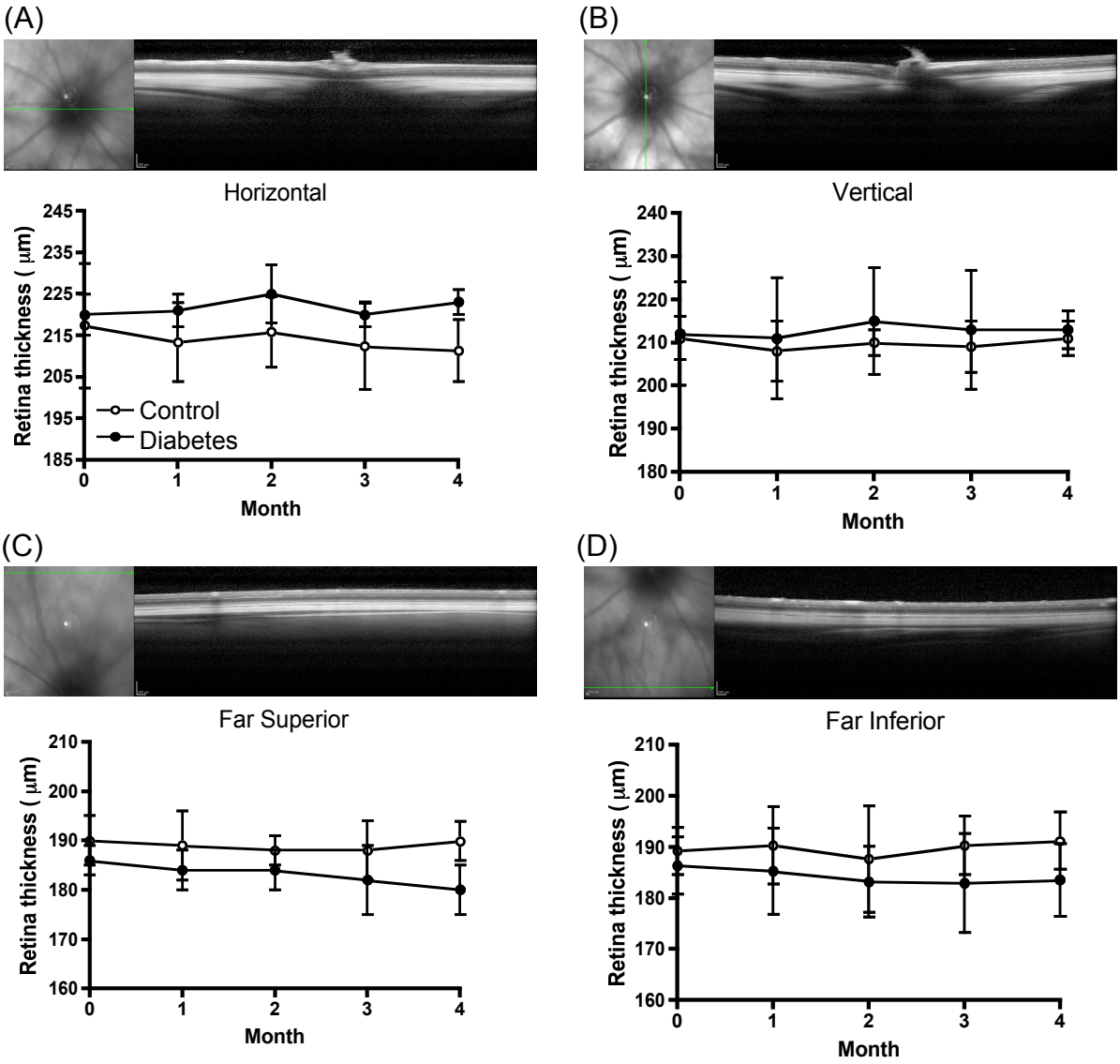

Figure 5.6. 4–months STZ–induced diabetes does not alter total retinal thickness in Lewis rats.

Lewis rats were induced with diabetes (n=5) using STZ (50mg/kg, i.p) and supplemented with insulin (subcutaneous pellet). Retinal thickness in diabetic rats and saline controls (i.p, n=5) were measured using OCT on the same day as ERG. Four main regions were imaged over the 4 month period: a horizontal cross section (A), a vertical cross section (B), a cross section the furthermost superior region of the eye (C) and a cross section through the furthermost inferior region of the eye (D). These same regions repeatedly imaged every month and showed no significant change at any time point over the 4–month period.

5.3.3. Subretinal gene therapy induces retinal neurodegeneration not exacerbated by diabetes.

To investigate the effect that gene therapy had on the development of diabetic retinopathy, Lewis rats were induced with diabetes (as described in 5.3.2.) and subretinally injected with AAV.VEGF$_{165}$b and AAV.Null, in tandem with experiment 5.3.2. Rats were subjected to monthly ERGs to assess the progression of retinal neurodegeneration. I observed that subretinal administration of AAVs induced diminished ERG amplitudes in all measurements. When comparing treatments amongst healthy rats (untreated, AAV.Null and VEGF$_{165}$b) there was a diminished response over the 4-month period in both vector-injected groups (figure 5.7). These data also indicate that AAV.Null injected eyes express a diminished response, particularly 2-months post-injection. This became especially noticeable at the higher light intensities, reaching significance at 2 months post-induction of diabetes in the scotopic A-wave at 75.38cd.s/m^2 (figure 5.7B). Null vector injected eyes showed reduced peak amplitude (8.02±3.74 mV) relative to untreated eyes (10±0.22 mV) at 2 months. There was no significant difference between diabetic AAV.Null injected eyes (5±7.07mV) and untreated eyes or diabetic AAV.Null eyes control AAV.Null eyes. There was a similar trend when observing B-wave amplitudes at 75.38cd.s/m^2 (figure 5.7D) whereby there was decreased amplitude at 2 months in the control + AAV.Null groups (296±100mV), that eventually improved after 3 months, relative to untreated groups (697±168mV) and diabetic AAV.Null groups (645±50mV). There was a significant difference at 2 months and 3 months between untreated groups and control + AAV.Null groups. Paradoxically, in all parameters, the diabetic groups did not show any significant difference relative to untreated groups. Whilst there was also no difference between control AAV.Null and diabetic AAV.Null, it does appear that diabetes prevented the vector-induced degeneration. Furthermore, the curves of both untreated eyes and diabetes + AAV.Null are very similar amongst almost all parameters, further indicating that diabetes prevented vector-induced degeneration.

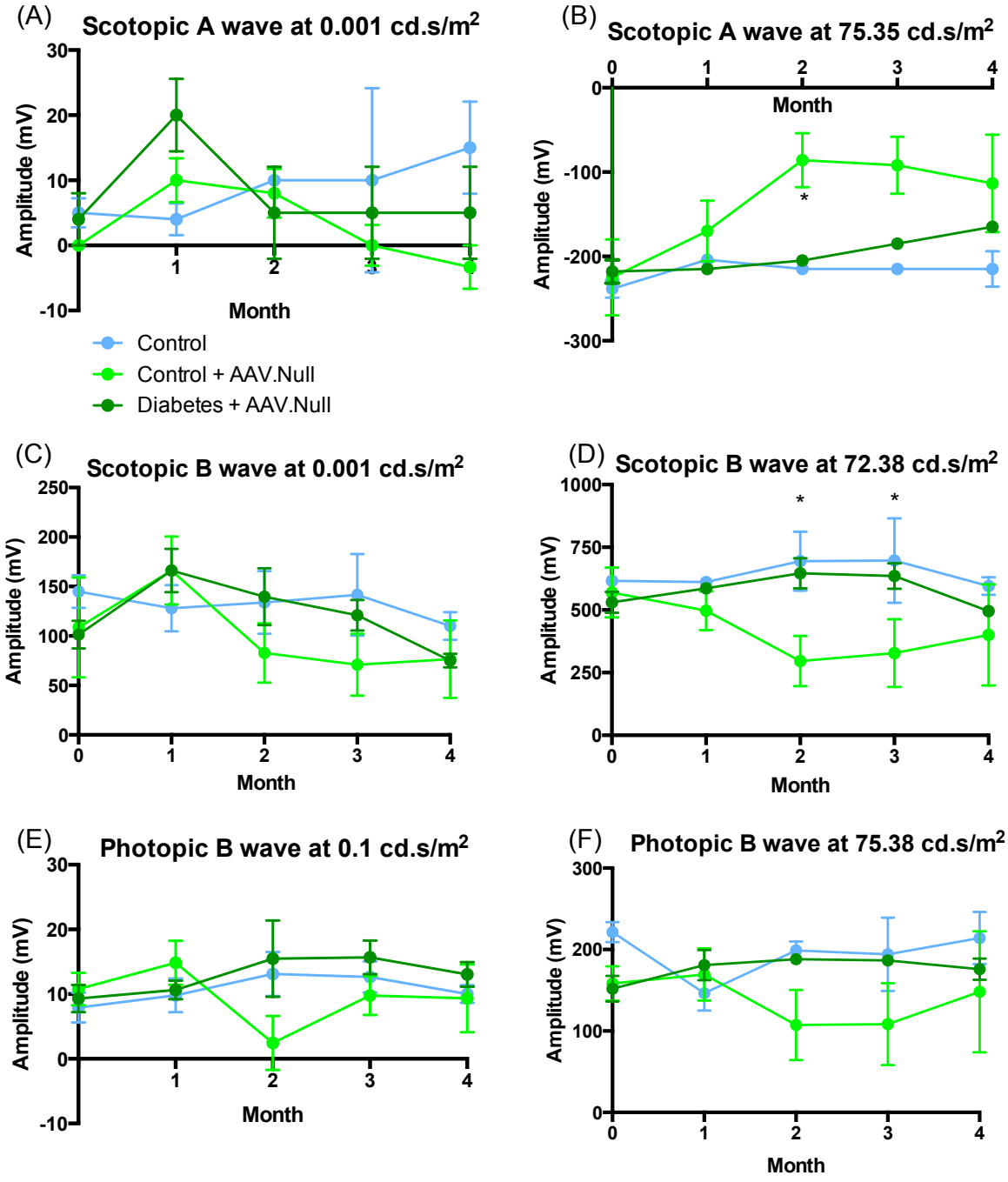

Figure 5.7. Null vector administration worsens ERG amplitude in control rats.

Lewis rats (n=11) were injected subretinally with AAV.Null (2x5µl of vector at $1x10^{12}$ vp/ml). AAV.Null-injected rats were induced with diabetes 2-weeks post-subretinal injection (n=6) using STZ (50mg/kg, i.p) and supplemented with insulin (subcutaneous pellet). The remaining AAV.Null rats (n=5) were injected with saline (i.p). Age-matched control, untreated rats (n=5), diabetic AAV.Null rats and control AAV.Null rats subject to monthly ERG assessment for 4 months and minimal and maximal light intensities were plotted. There was no difference in rod mediated A– or B–response both at minimal intensity (A and C). There was a significant decrease in amplitude at 2 months when assessing maximal scotopic A-wave (B) between control + untreated rats and control + AAV.Null. There was also a significant decrease in maximal scotopic B-wave amplitude at 2 and 3 months post–induction of diabetes (D). There was also no difference in the

cone-mediated response at both ends of the 6–step process (E and F) (Student's 2-tailed t-test, *p<0.05).

It is possible that $VEGF_{165}b$ over expression may prevent the neurodegeneration induced by vector administration. To test this hypothesis, I plotted AAV.Null injected control rats' ERG data with AAV.$VEGF_{165}b$ control ERGs. I observed the opposite to my hypothesis when assessing rod-mediated low light intensity A-wave responses (figure 5.8A). There was a significantly lower amplitude observed at 1 month in AAV.$VEGF_{165}b$ (0±0mV) injected eyes relative to AAV.Null eyes (10±3.5mV). At all other time points and parameters (figure 5.8B-E), there was no significant difference in amplitude between both treatment groups. However, the AAV.$VEGF_{165}h$ groups did appear to have constantly lower amplitude 1 month onwards, despite only being significant in the 0.001cd.s/m^2 scotopic A-wave amplitude.

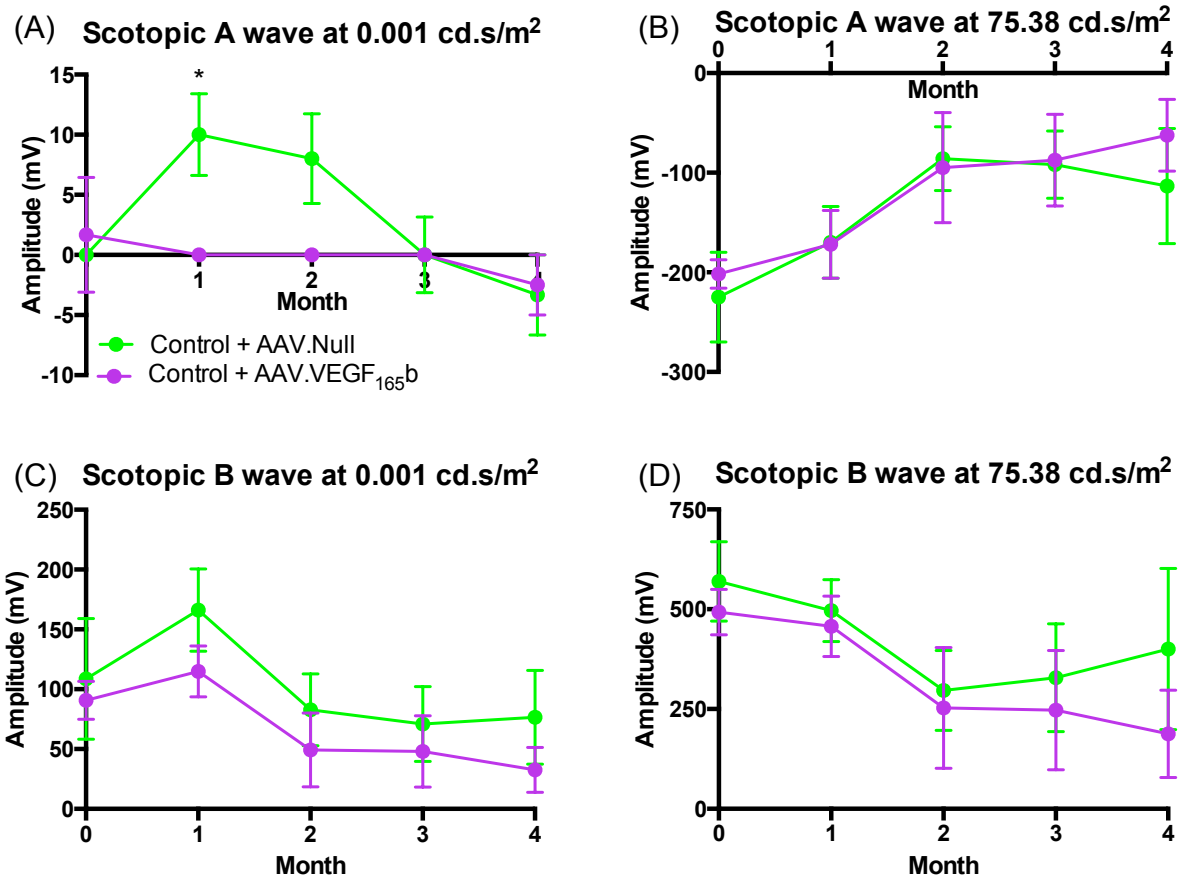

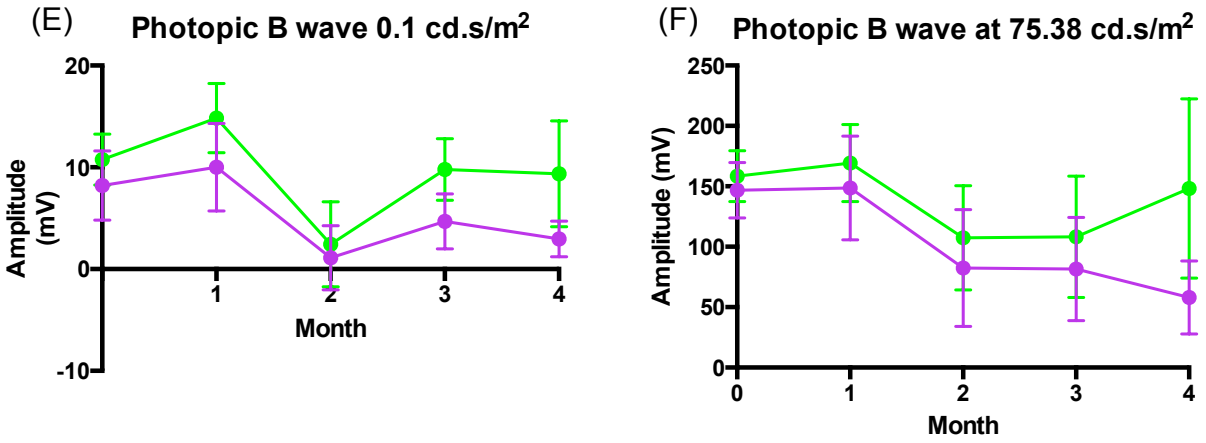

Figure 5.8. AAV.VEGF$_{165}$b does not significantly worsen ERG amplitude relative to AAV.Null in healthy rats.

Lewis rats (n=10) were injected subretinally (2x5µl of vector at 1x10^{12} vp/ml) with AAV.Null (n=5) or AAV.VEGF$_{165}$b (n=5). All rats were injected with saline (i.p) two weeks post subretinal injection and subject to ERG assessment for 4 months 1 week post saline injection, and minimal and maximal light intensities were plotted. There was a significant reduction in A-wave amplitude at 0.001 cd.s/m^2 at 1 month in the AAV.VEGF$_{165}$b group relative to the AAV.Null eyes (A). There was no significant difference in high light intensity scotopic A-wave response (B), nor was there any difference between groups in the scotopic B-wave at low (C) and high (D) light intensities. There was also no significant difference between groups when looking at low light (E) and high light (F) intensities when assessing scotopic B wave amplitude (2-tailed, Student's t-test, *p<0.05).

As diabetes appeared to have no significant effect on ERG amplitude (figures 5.4 and 5.7), I wanted to see how diabetic AAV.Null amplitudes, which show no significant change when compared to untreated rats, compared to diabetic AAV.VEGF$_{165}$b amplitudes. I hypothesised that there would be no significant difference between both treatment groups and I tested this hypothesis by plotting the amplitudes obtained from diabetic AAV.Null groups alongside diabetic AAV.VEGF$_{165}$b groups. When measuring scotopic A-wave at 0.001 cd.s/m^2 at 1 month, there was a significant reduction in ERG amplitude in diabetic AAV.VEGF$_{165}$b injected groups relative to diabetic AAV.Null groups (Figure 5.9A). However, it is possible that this point is an outlier as it so significantly greater than all other points it is tested against, including control, untreated retinae. There was no significant difference between diabetic AAV.VEGF$_{165}$b and diabetic AAV.Null in any parameter (figure 5.9). Despite the great variability in the AAV.VEGF$_{165}$b groups, when just comparing mean values AAV.VEGF$_{165}$b does appear to diminish the ERG amplitudes in all measurements and at all time points.

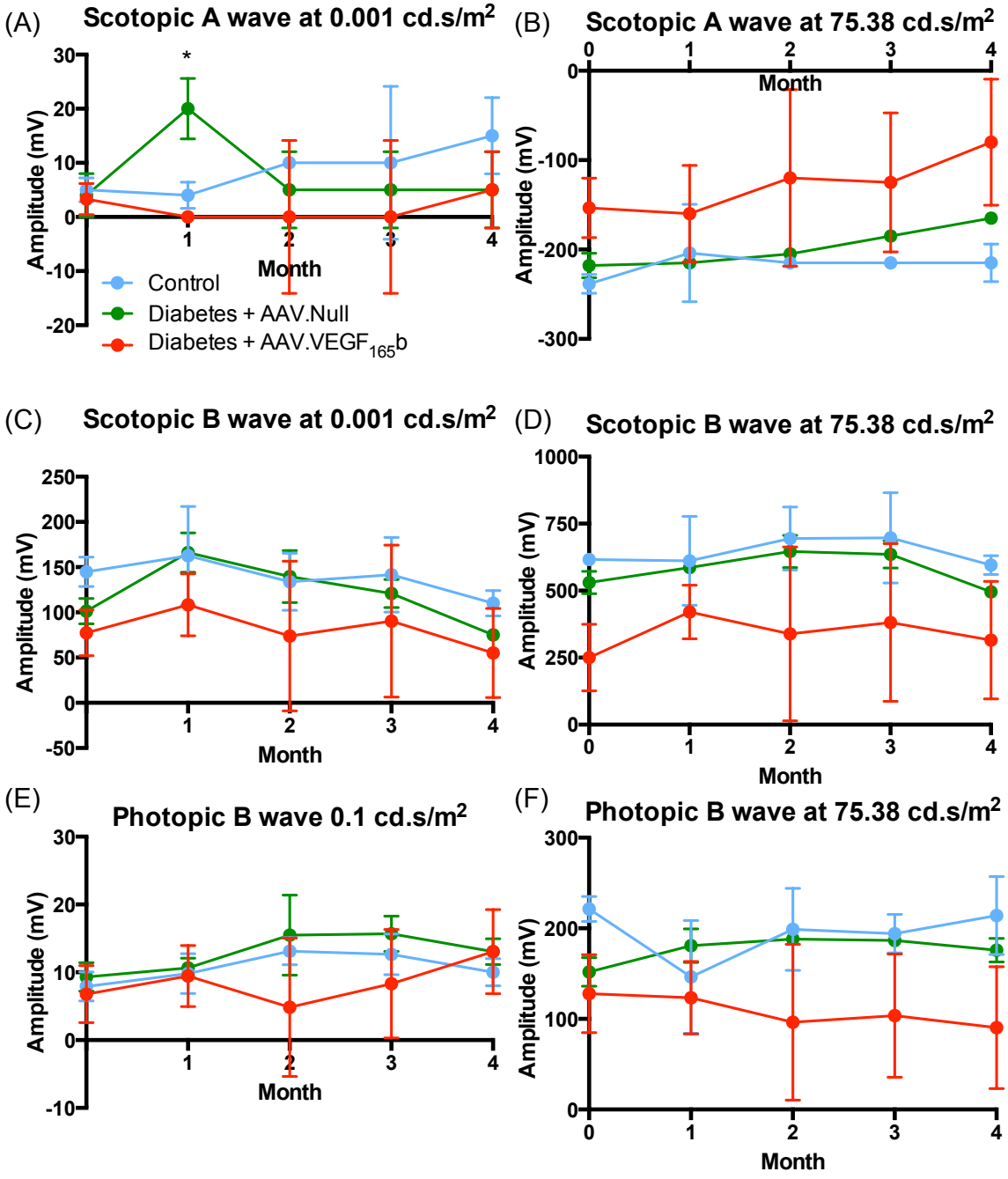

Figure 5.9. Diabetic Lewis rats injected with AAV.VEGF$_{165}$b show no significant difference in ERG amplitude relative to diabetic AAV.Null rats and control rats.

Lewis rats (n=13) were injected subretinally with AAV.Null (n=6) or AAV.VEGF$_{165}$b (n=7) (2x5µl of vector at 1x10^{12} vp/ml) and then induced with diabetes 2-weeks post-subretinal injection using STZ (50mg/kg, i.p) and supplemented with insulin (subcutaneous pellet). Control rats (n=5) were injected with saline (i.p). Control rats, diabetic AAV.Null rats and diabetic AAV.VEGF$_{165}$b rats subject to monthly ERG assessment for 4 months and minimal and maximal light intensities were plotted. There was no difference in rod mediated A– or B–response both at minimal intensity (A and C)

and maximal intensity (B and D). There was also no difference in the cone - mediated response at both ends of the 6–step process (E and F).

Diabetic AAV.VEGF$_{165}$b injected rats showed a reduction in ERG amplitudes in both scotopic and photopic measurements relative to control amplitudes. However, to assess whether this result is diabetes induced or as a result of the vector, I plotted the both saline and diabetic AAV.VEGF$_{165}$b groups on the same graph. I hypothesised that there would be no difference in ERG amplitude between both treatment groups. I observed that there was no significant difference between both control and diabetic AAV.VEGF$_{165}$b injected groups (figure 5.10). Moreover, when comparing both AAV.VEGF$_{165}$b injected groups to control + untreated groups, there was no significant difference between diabetic AAV.VEGF$_{165}$b groups and control groups in all parameters. There were differences in amplitude when comparing control amplitudes against control AAV.VEGF$_{165}$b amplitudes. There was a significant difference in ERG amplitudes at 4 months when comparing control amplitudes (15±7.07mV) with control AAV.VEGF$_{165}$b amplitudes (-2.5±2.5mV) at the minimal scotopic A-wave intensity (figure 5.10A). When assessing peak A-wave amplitude at 75.38cd.s/m^2 (Figure 5.10B), there was a significant difference in amplitude between control and control + AAV.VEGF$_{165}$b amplitudes at 3 months (-215±7.1 and -85.5±46.1mV respectively) and at 4 months (-215.0±21.2mV and -62.5±36.1mV respectively). There was no difference in scotopic B-wave amplitude at the lowest light intensity (figure 5.10C) between control and control + AAV.VEGF$_{165}$b amplitudes. This was not reflected in the scotopic B-wave amplitudes at the highest light intensity (figure 5.10D) where there was a significant difference between control amplitudes and control + AAV.VEGF$_{165}$b amplitudes at 4 months (595±35.4mV and 187.5±109.8mV respectively). The photopic B-wave response showed a difference in amplitude between control and control + AAV.VEGF$_{165}$b at 2 months (13.1±2.4mV and 1.11±3.1mV respectively) and 4 months (10±1.4mV and 2.96±1.74mV respectively) upon 0.1cd.s/m^2 light stimulation (figure 5.10E). This was reflected when stimulating at the highest photopic intensity (figure 5.10F) as there was a significant decrease in ERG amplitude in the control + AAV.VEGF$_{165}$b groups (58.0±30.3mV) and control + untreated groups (214.2±32mV).

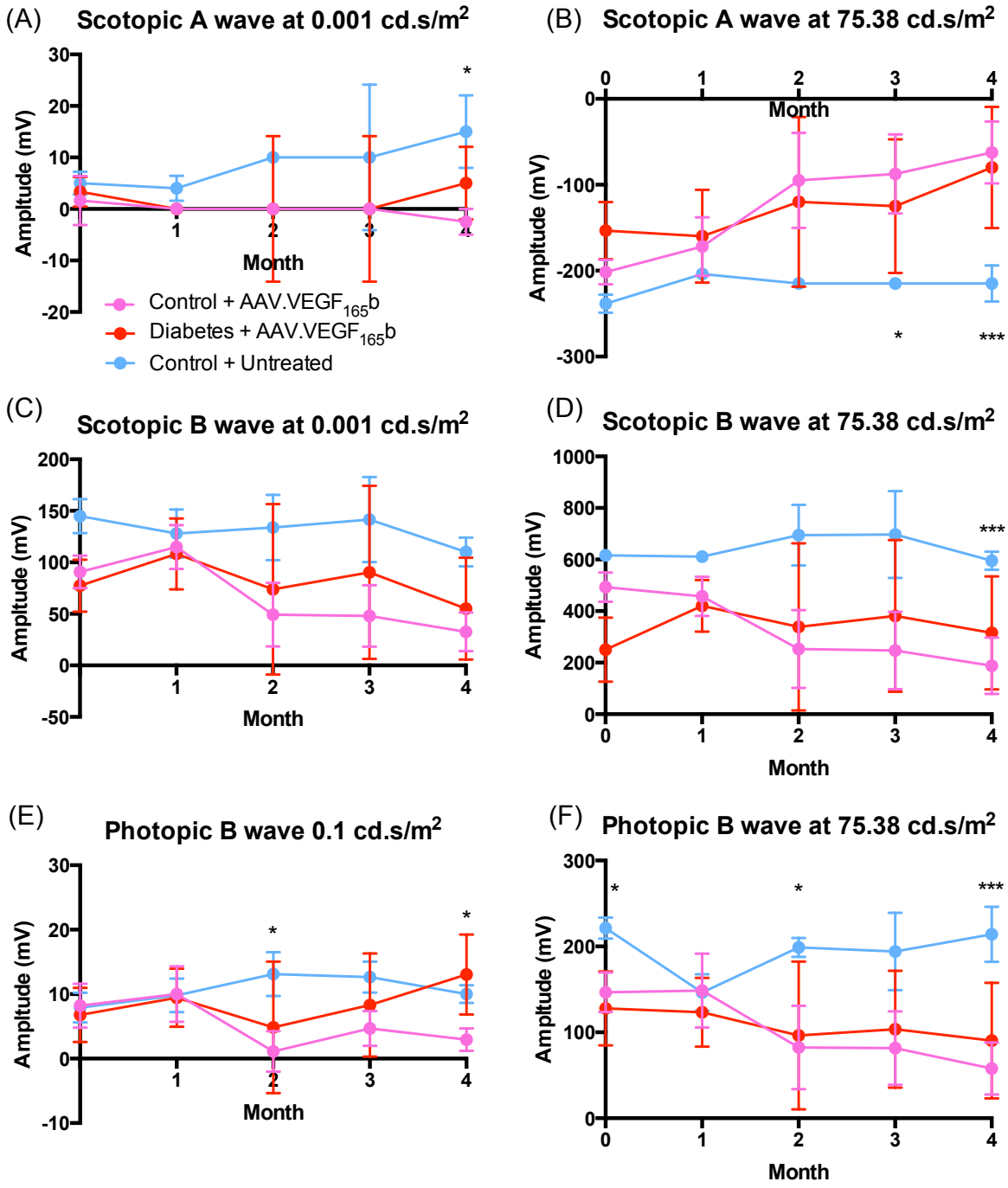

Figure 5.10 Control Lewis rats injected with AAV.VEGF$_{165}$b show no difference in ERG amplitude relative to diabetic Lewis rats injected with AAV.VEGF$_{165}$b but do show a difference relative to control amplitudes.

Lewis rats (n=17) were injected subretinally with AAV.VEGF$_{165}$b (n=12, 2x5µl of vector at 1x10^{12} vp/ml) and then induced with diabetes 2-weeks post-subretinal injection using STZ (n=7, 50mg/kg, i.p) and supplemented with insulin (subcutaneous pellet) or saline (n=5). Control + untreated rats (n=5) were injected with saline (i.p) and no subretinal injection. Rats subject to monthly ERG assessment for 4 months and minimal and maximal light intensities were plotted. There was no difference in rod mediated A– or B–

response both at minimal intensity (A and C) and maximal intensity (B and D) between control + AAV.VEGF$_{165}$b and diabetic + AAV.VEGF$_{165}$b. There was a decrease in ERG amplitude in the control + AAV.VEGF$_{165}$b groups relative to control groups at minimal scotopic A-wave intensities (A) at 4 months and at maximal intensities for scotopic A-wave at both 3 and 4 months (B). There was no difference in ERG amplitude at minimal light intensities when assessing scotopic B-wave responses (C) between control and control + AAV.VEGF$_{165}$b groups. There was a difference between these groups at 4 months, where control + AAV.VEGF$_{165}$b groups had a significantly lower ERG amplitude than control groups. There was no difference in the cone - mediated response at both ends of the 6–step process (E and F) between control + AAV.VEGF$_{165}$b and diabetic + AAV.VEGF$_{165}$b groups, however there was a decrease in control + AAV.VEGF$_{165}$b amplitude relative to control amplitudes at both 2 and 4 months at both 0.1 and 75.38cd.s/m^2 (Students 2-tailed t-test, *$p<0.05$, ***$p<0.01$).

Whilst in all the treatments I have compared, there was no significant difference between most groups (figure 5.4 and figures 5.7-5.10), when comparing all groups together overall there does appear to be a trend that suggests there is a slight difference between groups (figure 5.11). The groups that showed the lowest ERG amplitudes were the AAV.VEGF$_{165}$b injected groups, followed by the AAV.Null groups. The diabetic groups tend to have a greater ERG amplitude relative to their control counterparts, for example diabetic + untreated groups to have a greater ERG amplitude than control + untreated groups when looking at scotopic and photopic B-wave responses at maximal light intensities (figure 5.11D and F respectively). Similarly, diabetic AAV.Null groups show a greater ERG amplitude than control AAV.Null groups when looking at maximal scotopic A- and B-wave responses (figure 5.11B D respectively), although many of these comparisons do not achieve significance. It is easier to observe these differences at the higher light intensities than at the lower intensities, indicating that the degeneration observed is either difficult to detect at lower intensities or that it does not affect the response at lower intensities.

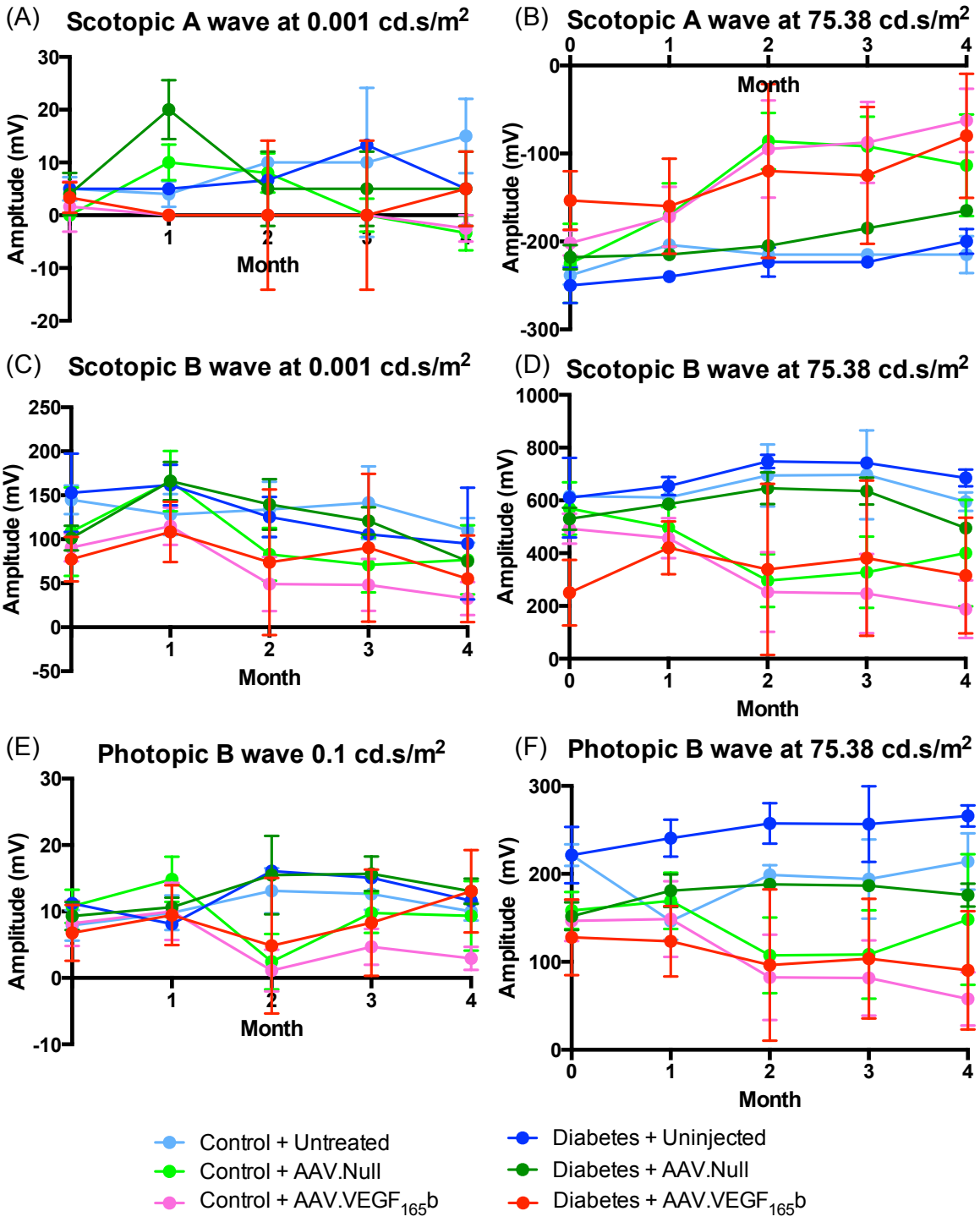

Figure 5.11. ERG responses from control and diabetic rats injected subretinally show reduced ERG amplitude relative to untreated amplitudes.

Lewis rats were injected subretinally with AAV.Null (n=11,2x5µl of vector at $1x10^{12}$ vp/ml) or titre-matched $AAV.VEGF_{165}b$ (n=12) or left untreated (n=10). Two weeks post-subretinal injections, rats were either injected with saline (n=15, i.p) or STZ (n=18, 50mg/kg, i.p). One-week post injections, blood glucose were tested and rats with a blood glucose ≥15mmol/l were deemed diabetic. Rats were then subject to ERG assessment on

a monthly basis measuring scotopic A- wave (A and B) and B-wave (C and D) amplitudes in response to 0.001 cd.s/m^2 and 75.38 cd.s/m^2 light intensities. Photopic responses for B wave amplitudes were also measured at 0.1 and 75.38 cd.s/m^2 (E and F respectively).

5.3.4. Subretinal AAV.VEGF$_{165}$b is detrimental to ocular health

SLO was carried out in parallel with ERG and OCT assessment, and showed that over the 4-month period (figure 5.12A), there was an increase in retinal auto-fluorescence (AF) in the vector-injected groups (figure 5.12). These regions of AF are consistent with previously published findings of fundus geographic atrophy (GA) (Holz et al. 2001). GA usually occurs as a result of lipofuscin accumulation in the RPE and as lipofuscin is a fluorophore, as more accumulates it appears as small white speckles in an SLO image. Lipofuscin deposits in the retina are commonly associated with diseases such as AMD (Holz et al. 2001) and Stargardt disease (Birnbach et al. 1994), and so are indicative of increased retinal pathology. I observe that as time progressed, I was able to image fewer AAV.VEGF$_{165}$b–injected eyes as the eyes became so damaged, there was no reflectivity from the retina, and by month 4 I was only able to image the outside of the eye and not the retina (figure 5.12A). At month 0 (figure 5.12) there was no significant difference in AF between treatment groups. At month 1, there was already an increase in AF in both AAV.VEGF$_{165}$b injected groups although only reaching significance in the diabetic animals (37.0±3.60) relative to both control and diabetic + untreated groups (26.6±1.67 and 26.4±1.18 respectively). At month 2 (figure 5.12D) control + AAV.VEGF$_{165}$b injected animals showed a significantly greater fluorescence (37.9±1.16) than diabetic AAV.Null (28.4±2.11), control AAV.Null (28.8±1.75), diabetic + untreated (28.4±0.98) and control + untreated (27.8±0.92). As only 1 diabetic AAV.VEGF$_{165}$b could be imaged, it could not be compared against the other groups, however it is clearly much greater than other treatment groups (36.9). By month 3 (figure 5.12E), more control + AAV.VEGF$_{165}$b injected animals could not be imaged, meaning they could not be part of the analysis. However it appeared that both AAV.VEGF$_{165}$b injected groups have a higher AF than other groups, although not significant. There was however a significant increase in AF in the diabetic AAV.Null group relative to control untreated groups. There was no change in AF in the control + Null groups, relative to both untreated groups. These data indicate that AAV.Null was also causing a detrimental effect on the ocular health. By month 4 (figure 5.12F) no AAV.VEGF$_{165}$b injected animals could be imaged.

There was also no significant difference between the untreated groups and the AAV.Null groups.

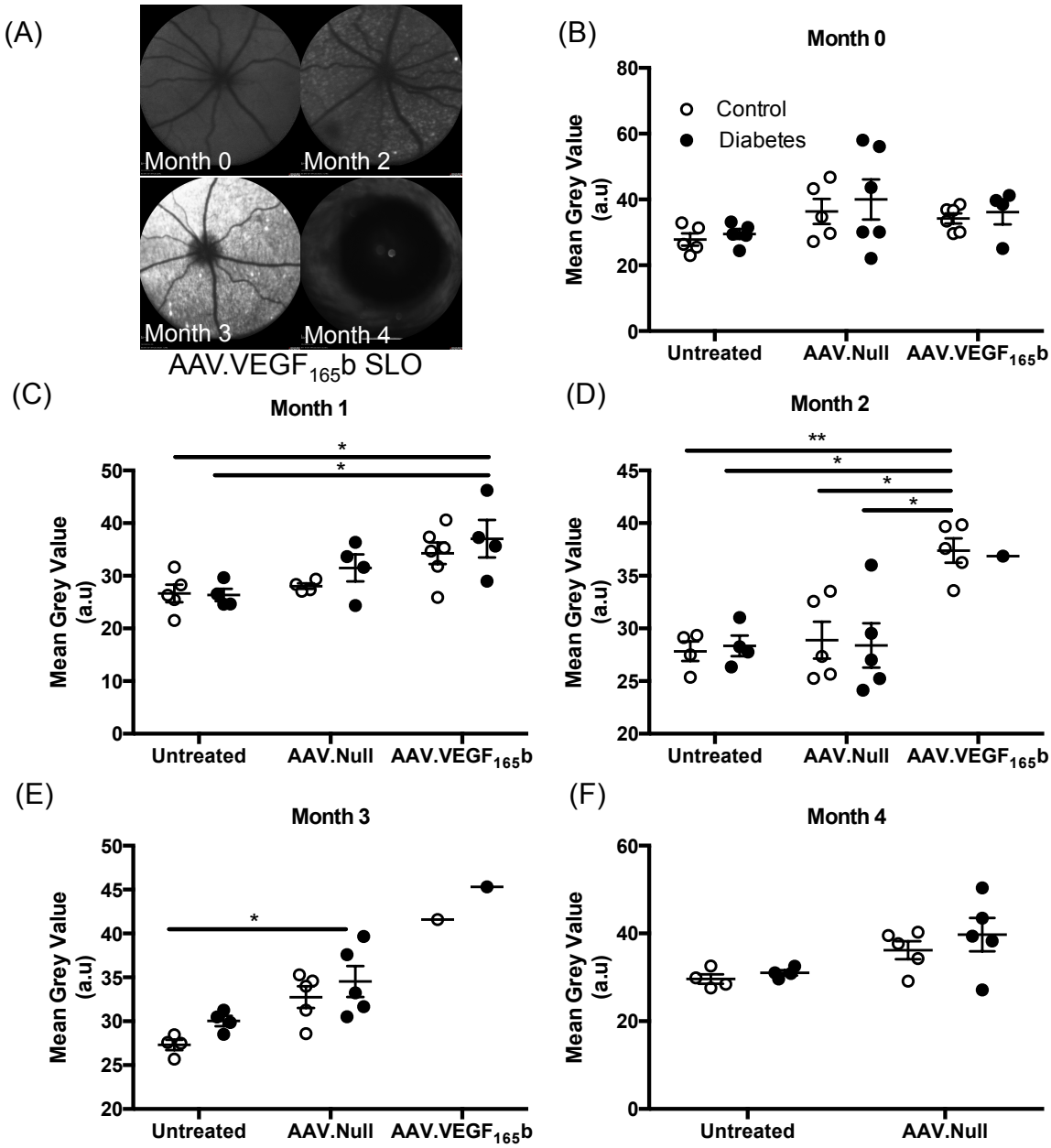

Figure 5.12. Subretinal AAV.VEGF$_{165}$b increases the AF area observed using SLO.

Lewis rats were injected subretinally with AAV.Null (n=11,2x5µl of vector at 1x10^{12} vp/ml) or titre-matched AAV.VEGF$_{165}$b (n=12) or left untreated (n=10). Two weeks post-subretinal injections, rats were either injected with saline (n=15, i.p) or STZ (n=18, 50mg/kg, i.p). One-week post injections, blood glucose were tested and rats with a blood glucose ≥15mmol/l were deemed diabetic. Rats were then subject to month SLO assessments over 4 months, measuring retinal AF (A). At month 0 there is no difference between treatment groups. At month 1, AAV.VEGF$_{165}$b injected groups have a significantly greater area of AF (B). At month 2, only 1 diabetic AAV.VEGF$_{165}$b rat could not be imaged due to significant ocular dysfunction. At month 2, control AAV.VEGF$_{165}$b

eyes were significantly more AF than all other groups (D). At month 3, only 1 control AAV.VEGF$_{165}$b animal could be imaged. Diabetic AAV.Null eyes had a significantly greater AF than control untreated eyes (E). By month 4 no AAV.VEGF$_{165}$b eyes could be imaged. There was no significant difference between untreated groups and AAV.Null groups (2-way ANOVA with Sidak's post hoc test, *$p<0.05$, **$p<0.01$).

At the end of the study, rats were culled and eyes were enucleated, fixed and embedded in OCT. Sections were stained for CD45, a broad inflammatory marker and GFAP, a marker of neurodegeneration and glial stress (figure 5.13). I observed that there were very low levels of CD45 activation in the control (figure 5.13A) and diabetic untreated retinae (figure 5.13D). There is little CD45 activation in most retinae apart from the control and diabetic AAV.VEGF$_{165}$b treated retinae (5.13C and 5.13F respectively. There appears to be a basal level of GFAP activation, as demonstrated in the control, healthy eyes (figure 5.13A). This increases with AAV.Null administration (figure 5.13B) and increases further upon AAV.VEGF$_{165}$b administration. Interestingly the trend observed in ERG traces whereby diabetes appears to have a "protective effect" on ERG amplitude relative to control eyes when injected with virus, was mirrored in the immunofluorescence. The diabetic virus injected retinae express less CD45 and GFAP than the control virus injected retinae (figure 5.13G). However this difference was not significant. There is also a trend within both control and diabetic groups, whereby expression of these markers increases from control, to AAV.Null to AAV.VEGF$_{165}$b. This reiterates that AAV.Null, although expressing nothing, induces retinal pathology. Furthermore, there is increasing evidence that AAV.VEGF$_{165}$b causes retinal degeneration.

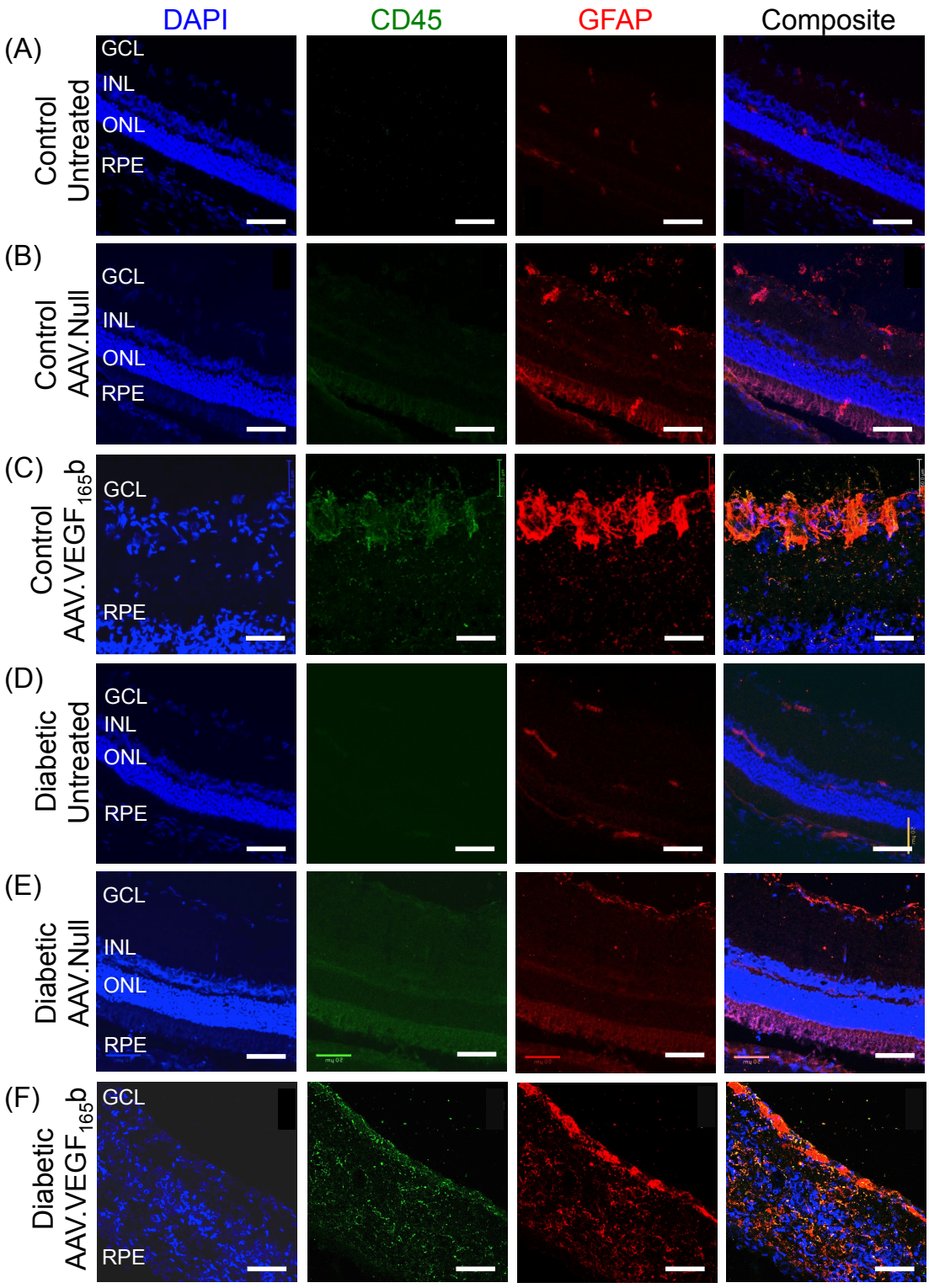
DAPI
CD45
GFAP
Composite
(A)
Control
Untreated
GCL
INL
ONL
RPE
(B)
Control
AAV.Null
GCL
INL
ONL
RPE
(C)
Control
AAV.VEGF165b
GCL
RPE
(D)
Diabetic
Untreated
GCL
INL
ONL
RPE
(E)
Diabetic
AAV.Null
GCL
INL
ONL
RPE
(F)
Diabetic
AAV.VEGF165b
GCL
RPE

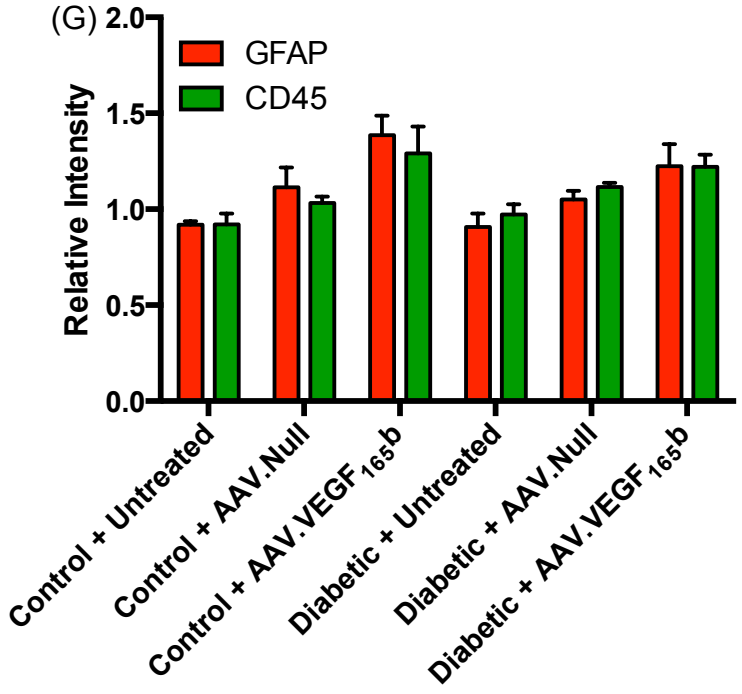

Figure 5.13. Subretinal gene therapy causes an increase in inflammatory and neuronal stress markers

Lewis rats were injected subretinally with AAV.Null (n=11,2x5µl of vector at $1x10^{12}$ vp/ml) or titre-matched AAV.$VEGF_{165}$b (n=12) or left untreated (n=10). Two weeks post-subretinal injections, rats were either injected with saline (n=15, i.p) or STZ (n=18, 50mg/kg, i.p). One-week post injections, blood glucose were tested and rats with a blood glucose ≥15mmol/l were deemed diabetic. Rats were culled after 4 months and eyes were cryo-embedded, sectioned and stained for DAPI (blue), CD45 (green) and GFAP (red, scale: 50µm, x40 magnification). There was little expression of both markers in control untreated and diabetic eyes (A and D). Expression of both markers increased upon AAV.Null injection in control and diabetic eyes (B and E) and was greatest in AAV.$VEGF_{165}$b injected eyes (C and F). This was quantified using Image (G). There was no significant difference in intensity relative to control groups (1-way ANOVA with Bonferroni post test).

The immunofluorescence indicates that AAV.$VEGF_{165}$b is detrimental to ocular health. This is particularly evident when looking at the structure of the retina. The typically stratified organisation, as observed in figure 5.13A, is not apparent in the AAV.$VEGF_{165}$b injected eyes. I observed that there are no definitive layers in these retinae, which is likely to contribute to a reduction in ERG amplitude. During analysis, I also observed many AAV.$VEGF_{165}$b injected retinae had structures growing through the middle of the eyes (figure 5.14A). When stained for the same markers, there was little expression in the new region of growth (figure 5.14B). However, as they appeared to resemble blood vessels, I stained them for occludin (figure 5.14C) and hypothesised that

these structures were likely to be vessels. This was further confirmed with CD31 staining (appendix 4). This region was also positive for HIF1α, particularly in the cells lining the proposed "lumen" of the new vasculature.

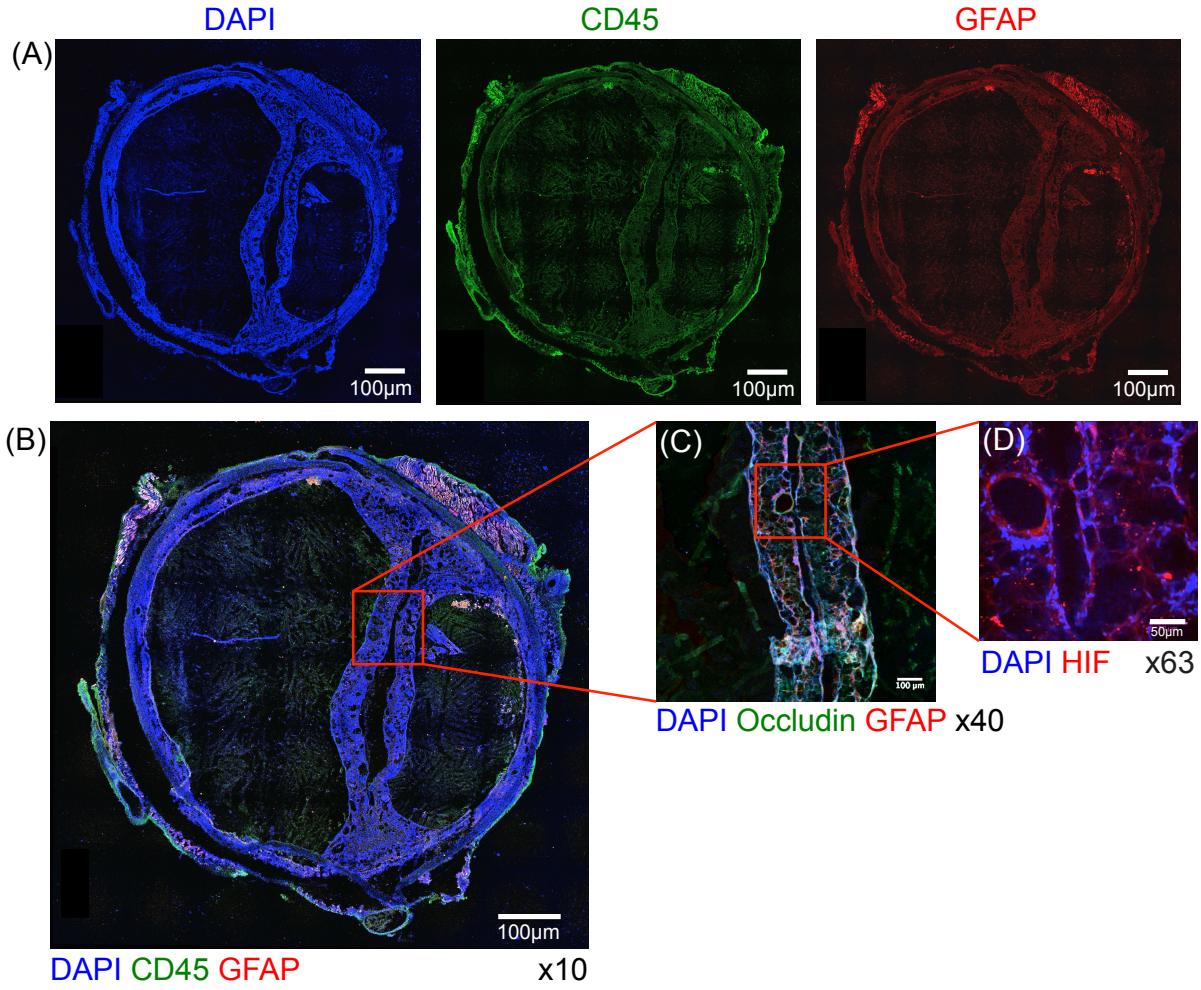

Figure 5.14. Novel vascular structures are apparent in many AAV.VEGF$_{165}$b injected eyes

Lewis rats were injected subretinally with AAV.VEGF$_{165}$b (n=12) and were culled 4 months post-injection. Eyes were enucleated, cryo-embedded, sectioned and stained for (A) DAPI (blue), CD45 (green) and GFAP (red). However as these markers were weakly expressed, particularly in the novel structure across the eye (B), sequential sections were stained (C) for occludin (green) and GFAP (red). These occludin positive regions appeared to be blood vessels that were also (D) HIF positive (red). This indicates that this region is likely to be new blood vessels forming across the eye.

5.3.5. AAV.VEGF$_{165}$b is detrimental to ocular health in other eye diseases.

The primary aim of AAV.VEGF$_{165}$b was to assess its potential neuroprotectivity in diabetes-induced retinal degeneration. As it showed no effect in this model, I tested the virus in the mouse retina degeneration slow (RDS) mouse. This model results in a slow onset of degeneration of photoreceptors and I hypothesised that AAV.VEGF$_{165}$b would prevent photoreceptor degeneration. To test this hypothesis, mice were injected subretinally at P10 with a single injection of 2µl AAV.VEGF$_{165}$b ($1x10^{12}$ vp/ml) in one eye, with the contralateral eye serving as an untreated control. Mice were then subject to monthly ERGs 2-weeks post-injection to assess changes in rate of onset of degeneration for 2 months. As this condition concerns photoreceptor degeneration, I only assessed changes in amplitude in response to photopic light stimuli. For the duration of the experiment I observed that for both A- and B-wave responses, AAV.VEGF$_{165}$b injected eyes had consistently lower ERG amplitudes relative to control eyes. There was no significant difference in ERG A-wave amplitude between untreated eyes and AAV.VEGF$_{165}$b injected eyes across all light intensities tested at month 0 (Figure 5.15A). When assessing the photopic B-wave amplitudes at month 0 (Figure 5.XB), there was a significant difference between both groups. At 0.1 cd.s/m^2, AAV.VEGF$_{165}$b injected eyes had a significantly lower amplitude (15.7±2.32µV) than control eyes (30.5±1.97µV). At month 1 there is no difference between both treatment groups when measuring A-wave amplitudes (figure 5.15C) as both group seems to express a decrease ERG amplitude relative to month 0. This is also true of B-wave responses at month 1 (figure 5.15D). However at month 2, there is a difference in A-wave response (figure 5.15E). At 0.1 cd.s/m^2 AAV.VEGF$_{165}$b injected groups have a significantly lower ERG amplitude (0±0µV) relative to control eyes (1.68±0.24µV). This is also observed when stimulated with 31.6 cd.s/m^2 light, AAV.VEGF$_{165}$b injected groups have a significantly lower A-wave amplitude (0±0.47µV) relative to control eyes (-2.4±0.45µV). B-wave responses at month 2 (figure 5.15F) were also less in the AAV.VEGF$_{165}$b injected groups relative to control groups, but only reaching significance at 0.1 cd.s/m^2 (0±0µV and 7.27±1.16µV respectively).

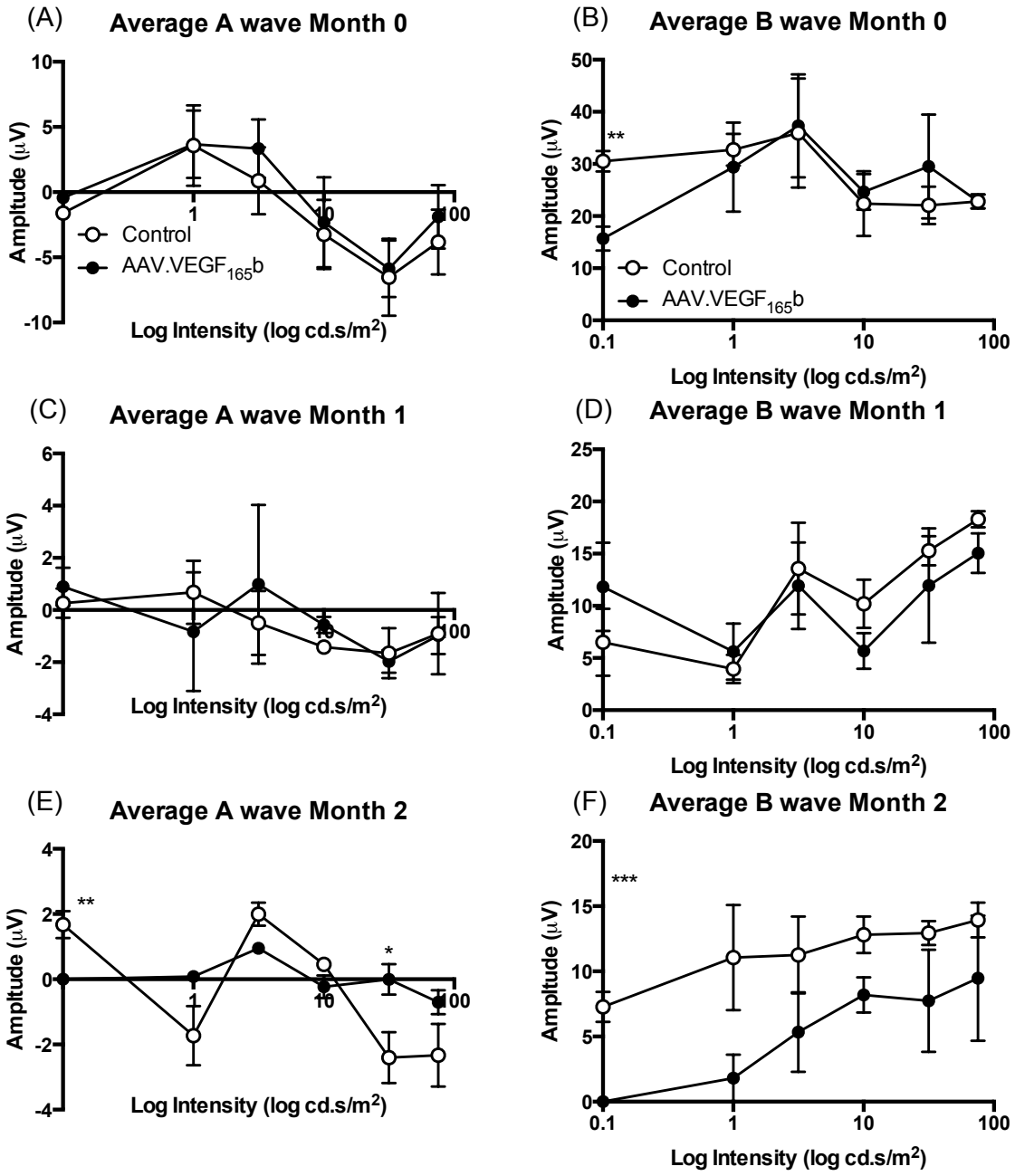

Figure. 5.15. Subretinal AAV.VEGF$_{165}$b worsens photopic ERG amplitudes in RDS mice.

RDS mice (n=5) were injected with subretinally with 2µl AAV.VEGF$_{165}$b ($1x10^{12}$ vp/ml) at P10, with the contralateral serving as an untreated control group. Two weeks post injection, mice were subject to month ERGs, measuring only photopic A- and B-wave responses evoked upon 6 different light stimuli (0.1, 1.0, 3.16, 10, 31.6 and 75.38 cd.s/m^2). At month 0, there was no difference between both groups' A-wave responses across all intensities tested (A), however there was a significant difference at 0.1cd.s/m^2 evoked B-wave response (B). At month 1, there was no difference in ERG amplitude between both groups when assessing A- and B-wave response (C and D respectively). At month 2, AAV.VEGF$_{165}$b groups had a significantly lower A-wave amplitude at 0.1 and 31.6 cd.s/m^2 (E) and had a significantly lower B-wave amplitude at 0.1 cd.s/m^2 (F) (Student's t-test, *p<0.05, **p<0.01, ***p<0.001).

Data from chapter 2 indicates that $VEGF_{165}b$ may be anti-angiogenic and so I hypothesised that AAV.$VEGF_{165}b$ may also be anti-angiogenic. I tested this hypothesis by injecting C57bl6j mice with either 2x2µl of AAV.$VEGF_{165}b$ or AAV.Null (subretinal, $1x10^{12}$ vp/ml) and comparing neovascular area upon laser-induced rupture of Bruch's membrane, relative to untreated eyes (see Chapter 2: "Materials and Methods" for further details). I hypothesised that AAV.$VEGF_{165}b$ injected eyes would have a lower area of CNV relative to both AAV.Null and control groups. Two-weeks post subretinal injection, mice were subjected to lasering, followed by FFA using an SLO 3, 7 and 14-days post-laser and lesion sizes were calculated using Image J, with n=number of burns. Any lesions that had merged, as shown in figure 5.16C, were discounted from analysis. Day 3 post-laser (Figure 5.16A) showed that there was no change in relative lesion size in AAV.$VEGF_{165}b$ injected groups (figure 5.16B). On Day 7 (Figure 5.16B), there was no significant difference between treatment groups (Figure 5.16C), despite the apparent decrease in lesion size. On day 14 (figure 5.16E) there was a significant increase in relative lesion size in the AAV.Null injected groups (1.74±0.46) relative to control lesions (1±0.18). It appears that AAV.$VEGF_{165}b$ injected group had a lower lesion size (0.29±0), however this data is from 1 lesion only and therefore may be skewing the data. I observed that as time progressed, AAV.$VEGF_{165}b$ injected eyes appeared more swollen and increasingly difficult to image (figure 5.16G), as I had observed in Lewis rats (figure 5.12), as a result the number of burns imaged decreased from 8 to 1 by day 14.

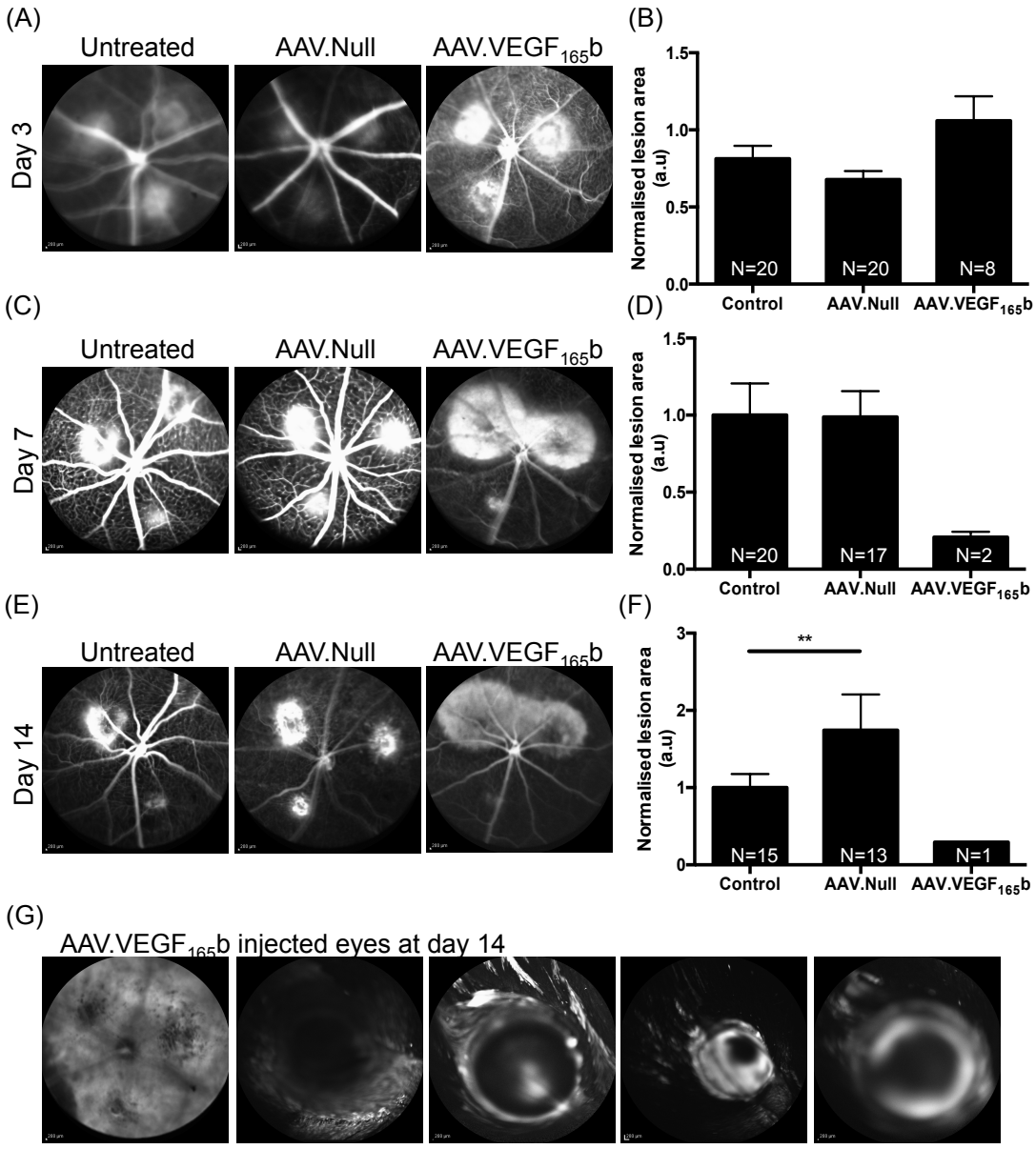

Figure 5.16. Subretinal AAV.VEGF$_{165}$b does not significantly reduce lesion size in mice with CNV.

Female C57bl6j mice (n=14) were injected subretinally with 2x2µl AAV.VEGF$_{165}$b or AAV.Null (1x10^{12} vp/ml) or were left untreated. Two weeks post-injection, mice were subject to 3 laser burns using a 680nm laser to breach Bruch's membrane. Mice were subject to FFA on day 3, 7 and 14-post laser. On day 3 (A) there was no significant difference in normalised lesion size (B) between groups (n=number of lesions). On day 7 (C), there was no difference in normalised lesion size (D) between control and AAV.Null eyes. Only 2 lesions could be analysed in AAV.VEGF$_{165}$b eyes, however there is a non-significant reduction in lesion size relative to both control and AAV.Null eyes. On day 14 (E), there was a significant increase in normalised lesion size (F) in AAV.Null injected eyes relative to control lesions. Only 1 lesion could be measure in AAV.VEGF$_{165}$b eyes due to inability to image from poor ocular health and potential inflammation (G) (1-way ANOVA with Tukey's post-test, **$p<0.01$).

As I was unable to measure lesion sizes in all the groups using FFA and SLO, choroids were dissected, flat-mounted and stained for IB4 (figure 5.17A) and lesion size was calculated using Image J. However, many of the AAV.VEGF$_{165}$b eyes were in such poor condition that many of the choroids were lost upon dissection. Having been unable to image using SLO and seeing the condition of the eyes, I hypothesised that the AAV.VEGF$_{165}$b injected eyes would have a greater lesion size than both AAV.Null groups and control groups. I observed that there was no significant difference in normalised lesion size between treatment groups (figure 5.17B). There does appear to be a trend that indicates virus injection may exacerbate CNV. AAV.Null eyes have no change in normalised lesion size (1.69±0.26) relative to control eyes (1.0±0.42). AAV.VEGF$_{165}$b injected eyes have an even greater normalised average lesion area (3.0±0.34) relative to AAV.Null eyes and control eyes.

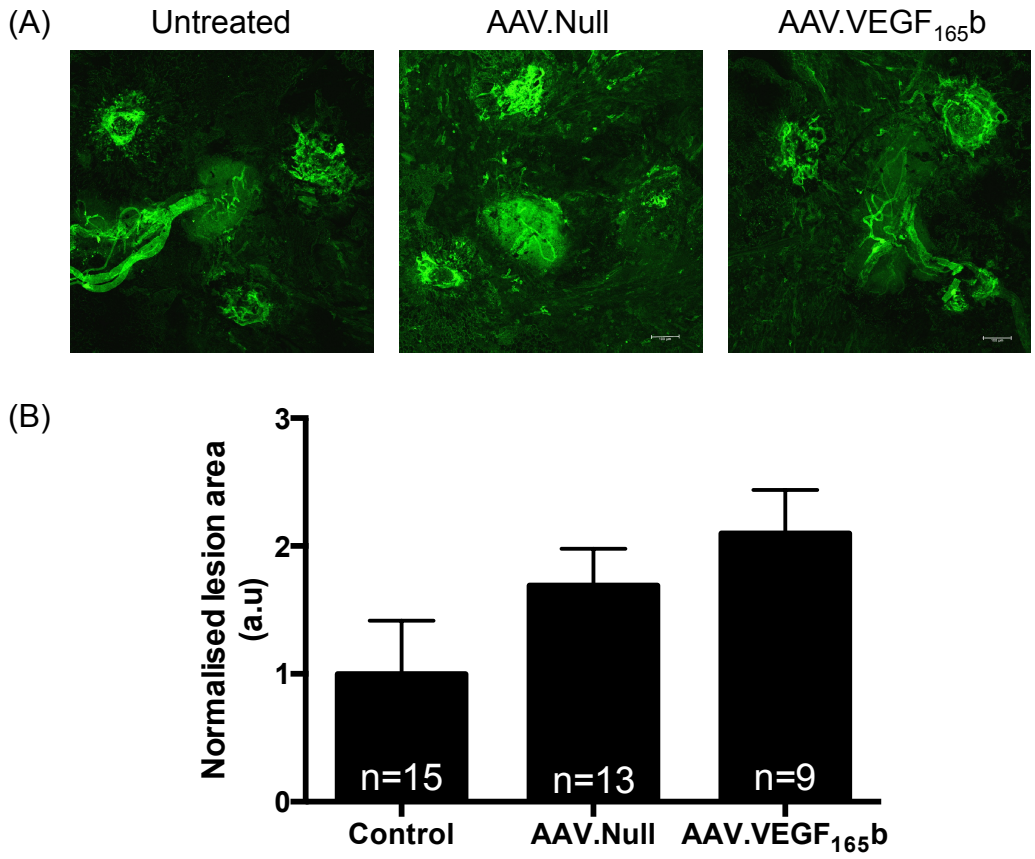

Figure 5.17. AAV.VEGF$_{165}$b is not anti-angiogenic in mice with laser-induced CNV. Female C57bl6j mice (n=14) were injected subretinally with 2x2µl AAV.VEGF$_{165}$b or AAV.Null (1x10^{12} vp/ml) or were left untreated. Two weeks post-injection, mice were subject to 3 laser burns using a 680nm laser to breach Bruch's membrane. Mice were culled 2-weeks post laser and choroids were dissected and stained for IB4 (A). Relative

lesion size was calculated using Image J (B) and showed that there was no significant difference in lesion size between treatment groups (1-way ANOVA with Tukey's post-test).

Figures 5.15, 5.16 and 5.17 all show that in alternative models of eye disease, AAV.VEGF$_{165}$b does not improve visual function nor does it prevent CNV.

5.4. Discussion

5.4.1. STZ-induced diabetes in Lewis rats is a poor model of diabetic retinopathy

Despite being hyperglycaemic, diabetic Lewis rats showed no significant difference in A- and B-wave amplitude at 4-months post-induction of diabetes, relative to control rats (figure 5.3). There does appear to be a slight reduction in scotopic B-wave amplitude in the diabetic animals, however this is not significant (figure 5.3D). When these data are further dissected into A- and B-wave responses evoked from the minimum and maximum intensities tested over the 4-month period (figure 5.4), again there is no significant difference across photopic and scotopic intensities at any time point, indicating that there is no dysfunction at the level of photoreceptors, RPE, Muller glia and ON-bipolar cells. However these data did not tell us the state of the RGC layer. Unfortunately, I was unable to stain these sections with NeuN, as I did in flat-mounts in chapter 4, and therefore counted DAPI-positive cells in the RGC layer as way of assessing RGC layer dysfunction (figure 5.5). Despite this not being the preferred method of quantification, I observed that there was no decrease in RGC layer thickness in diabetic retinae, indicating that a hallmark of diabetic retinopathy is not present in this model. Overall, these data indicate that the model did not sufficiently produce any kind of retinal neurodegeneration induced by diabetes.

The Kern group have written many reviews and have published data that this Lewis rats with STZ-induced diabetes do show differences in ERG amplitude as early as 3 months post onset of hyperglycaemic (Engerman & Kern 1995; Kern et al. 2010; Robinson et al. 2012b). As a result, this aspect of my project was based upon the Kern groups' findings. Despite keeping my protocol as identical to the Kern groups' as possible, there was one difference – the Kern group administer subcutaneous insulin 2-3 times per week upon onset of weight loss (*Tim Kern, personal communication*), whereas I implanted a subcutaneous insulin pellet on the same day as diabetes induction. I could not adhere to this method due to regulations set in place by the UCL BSU and ethics committee. This subtle difference in protocols is potentially why I observed no difference in ERG amplitude. Furthermore, STZ-diabetic rats that are treated with insulin show a reduction in the rate of IPL and GCL loss, compared to non-insulin treated diabetic rats, again confirming the hypothesis that poor glycaemic control attributes to

neurodegeneration in the retina (Barber et al., 1998). Interestingly in a review co-authored by Prof Kern (Kern & Barber 2008), it states that insulin is protective against RGC loss in animals (Barber et al. 1998; Barber et al. 2001). Insulin is also protective against diabetic retinopathy-induced RGC loss in humans (van Dijk et al. 2009). Insulin appears to be protective against apoptosis in culture by activating the PI3 kinase and Akt pathway and preventing activation of caspase 3 (Barber et al. 2001). It is possible that the glycaemic control of my animals was not "poor enough", and as a result I saw no pathology. This may be why the Kern group only administer insulin when needed as opposed to constant slow release. The constant exposure to insulin may have prevented any neurodegeneration in the retina in my study, however this was agreed upon method with the UCL ethics committee.

I may have seen a difference in ERG amplitude had I used a different model of diabetes, for example it has been shown that Sprague-Dawleys with STZ-induced diabetes show RGC loss after 7.5 months of diabetes (Kern et al. 2000). However the PPL I was working under was only licenced for 4 months diabetes therefore I would not have been able to pursue this model. The $Ins2^{Akita}$ mouse spontaneously develops type 1 diabetes, and histological analysis of the RGCs within 3 months of diabetes shows structural alterations such as axonal swelling and associated constriction. Also visible was enlarged cell bodies and increased dendritic branching and terminals in both medium ON-RGCs and large ON-RGCs. Further histological analysis of the retinae of the $Ins2^{Akita}$ Thy1-YFP mice showed that within the first three months of diabetes, the peripheral retina loses RGCs first and the surviving RGCs (particularly ON-RGCs) are undergo dendritic remodelling and changes in axonal properties, before they too eventually die (Gastinger et al. 2008). However, to maintain consistency throughout this project, I used the STZ-model of type 1 diabetes.

5.4.2. $VEGF_{165}b$ gene therapy exacerbated retinal neurodegeneration

This study has shown that the $AAVVEGF_{165}b$ virus I generated is not only ineffective in treating but worsens retinal neurovascular disease (figure 5.11), retinal neurodegeneration (figure 5.15) and choroidal neovascularisation (figure 5.16 and 5.17), areas where the recombinant protein has previously shown much potential. $AAV.VEGF_{165}b$ elicited detrimental effects to the neural retina, regardless of onset of

diabetes, as shown by figures 5.8-5.10. AAV.VEGF$_{165}$b-injected eyes consistently had the lowest ERG amplitudes compared to any treatment group (figure 5.11). Furthermore, AAV.VEGF$_{165}$b causes formation of vascularised internal structures (figure 5.14), which may attribute to the increase in atrophy and inability to image when assaying by SLO (figure 5.12). This may be due to AAV.VEGF$_{165}$b eyes being hypoxic, resulting in increased HIF-mediated vessel growth across the retina. There was a moderate increase in CD45 expression in the AAV.VEGF$_{165}$b injected eyes (figure 5.13) relative to control and null eyes and an increase in GFAP expression. This indicates that there is inflammation occurring in the AAV.VEGF$_{165}$b-injected retinae, however a different inflammatory marker would need to be used to confirm this such as TNFα. There is also an apparent disorganisation of the structure of these retinae, however this may be a result of processing due to the eyes being in such bad condition upon excision. Together, these data suggest that injection of this AAV.VEGF$_{165}$b virus may have triggered a response that results in increased infiltrating cells in the retinae, likely to be macrophages that accumulate and cause structural and functional damage to the eye. From personal observation, AAV.VEGF$_{165}$b injected eyes were much bigger in size than contralateral untreated eyes and greater than AAV.Null eyes, again indicating possible ocular inflammation.

In the CNV+AAV.VEGF$_{165}$b eyes, there is clear progressive worsening of SLO images, where only one eye could be images by 2 weeks (figure 5.16). However, the choroids appeared normal, despite the lesions, (figure 5.17). It is possible, that like I observed in the Lewis rats, there are many infiltrating cells in the retina and potential in the vitreous and this could be why imaging by SLO became progressively harder. Interestingly, the rate of onset of poor SLO imaging was much faster in the CNV mice (approximately 1 week, figure 5.16) than in the Lewis rats (approximately 3 months, figure 5.12). CNV does cause an increase in CD45 +ve cell infiltration in the burned regions (Blackey and Ved et al., unpublished results), and therefore it is possible that CNV increased the rate of macrophage production already triggered by pre-injection of this AAV.VEGF$_{165}$b virus.

AAVs are known for their low inflammatory profile (Vandendriessche et al. 2007), which make them the preferential virus for use in patients. AAVs themselves do not cause synthesis of viral proteins but rather are reliant on the helper plasmid it's packaged with. However the recombinant capsid is very similar to true viral capsids, and therefore any immune response to the vector is dependent on previous exposure to AAVs

and is likely to be directed towards the capsid (Vandendriessche et al. 2007). In humans, exposure to AAVs usually occurs at around 2-3 years of age (Mingozzi & High 2013), however as I have no knowledge to the exposure of rats to AAVs, if they have had a relative high exposure where they were bred, it may have triggered an immune response to my AAVs resulting in degeneration. I used an AAV2 capsid, one of the most prevalent serotypes, which has shown to evoke a T-cell response in muscle gene therapy (Brantly et al. 2009) and would in theory have the most anti-bodies produced against it, however in clinical trial data shows that AAV2 plasmids are well-tolerated in the eye with a minimal immune response (Bainbridge et al. 2008), likely due to the eye's limited regenerative capacity.

AAVs have shown to interact with toll-like receptor 9 *in vitro* and in mice, therefore interacting with the innate immune system and triggering a CD8+T cell response (Zhu et al. 2009). AAVs have also shown to trigger release of NFKB in the mouse liver (Jayandharan et al. 2011) which would cause the release of pro-inflammatory cytokines and chemokines potentially resulting in the dysfunction seen. Typically, activation of these immune pathways typically coincides with lack of transgene expression (Vandenberghe & Auricchio 2012) however I observed over expression of $VEGF_{165}b$ 2-weeks after AAV.$VEGF_{165}b$ injection (figure 5.2). It therefore seems likely that if it is an immune response, it is not directed at the AAV as there is not as diminished an ERG response in the AAV.Null eyes (Figure 5.11), nor was the SLO imaging as poor (figure 5.12) and there were less CD45+ cells and decreased GFAP (figure 5.13) relative to AAV.$VEGF_{165}b$ eyes. As immune-privileged regions such the eye and brain have relatively low neutralising antibodies to AAVs (Amado et al. 2010), its unlikely to be an adaptive immunity B-cell response that is driving the dysfunction. Again, if it were a response targeting the AAV, transgene expression would be supressed within hours (Mingozzi & High 2013), however there is still $VEGF_{165}b$ overexpression two-weeks post-injection.

It is possible that the dysfunction observed is indeed an immune response, but not to the viruses themselves but to contaminants in the vehicle that the viruses are made in. Endotoxin contamination of viruses may cause inflammation in the eye upon injection. Endotoxin-induced uveitis, a model of ocular inflammation (Csukas et al. 1990), uses endotoxin to induce ocular pathology. In Lewis rats, when injected at 100µg, there is macrophage recruitment in the eye (Rosenbaum et al. 1980). Any virus or plasmid with

an endotoxin concentration below 2.5EU/ml was deemed endotoxin negative. Whilst samples are rigorously endotoxin tested throughout the virus-making process, it is possible that samples were given a false negative after virus purification. It is also possible that a 10µl volume of virus that has ≤2.5EU/ml endotoxin could cause retinal degeneration. Endotoxin contamination is a highly likely candidate as similar degenerative and inflammatory effects have been observed in similar studies (*Prof. Andrew Dick, personal communication*).

The dysfunction may not be solely an immune response to what has been injected, but to the injection itself. Sub-retinal injections are designed to cause a temporary detachment of the retina, however there are occasions where the retina may not reattach quickly if at all. In such occasions, there has been increased photoreceptor apoptosis and increased TUNEL+ retinal neurones (Cook et al. 1995). There is also evidence of Muller cell remodelling, outer segment loss, reshaping of rod bipolar dendritic trees and changes in horizontal cell morphology, amongst other changes upon experimental subretinal detachment (Fisher & Lewis 2003). Upon reattachment, there is thinning of the retina and disorganisation of the retinal layers and where neurones innervate (Cook et al. 1995; Fisher & Lewis 2003). It is possible that the volume injected subretinally may have been too much, and as a result there was a disorganisation in the otherwise highly organised neural retina. This disorganisation showed a reduction in ERG amplitude that progressed over time that was worsened by an apoptosis-induced immune response that could not be overcome by the anti-inflammatory and neuroprotectivity of $VEGF_{165}b$.

Interestingly, AAV.$VEGF_{165}b$ groups consistently appear to the most damaged eyes in all assays, relative to control and AAV.Null eyes. If the above hypotheses were true, then both AAV.$VEGF_{165}b$ and AAV.Null eyes should be affected equally, indicating that it may be a $VEGF_{165}b$-mediated degeneration. At the time of writing this thesis, there was no literature published to suggest that overexpression of $VEGF_{165}b$ is deleterious, most papers show the contrary that either it is beneficial to the disease model used or that it has no effect. It could be that there is so much overexpression of $VEGF_{165}b$ that is causing geographic atrophy (GA) in the retina, as observed in many AMD patients treated with anti-VEGF therapy (Simo et al. 2014). RPE secreted VEGF is necessary for choriocapillaris maintenance (Saint-Geniez et al. 2009b), and mice incapable of producing $VEGF_{120}$ and $VEGF_{164}$ showed photoreceptor apoptosis, reduced ERG amplitude and loss of RPE. This was characterised as geographic atrophy (Saint-Geniez et al. 2009b) and highlighted the importance of the predominant pro-angiogenic isoforms.

It may be that the eyes' transcriptional ability was at maximum capacity upon AAV.VEGF$_{165}$b administration, and as a result failed to produce adequate amounts of VEGF$_{164}$ and VEGF$_{120}$ culminating in GA of the retina. This fits with SLO data in figure 5.12, as the time progresses, the eyes become more autofluorescent, usually indicative of RPE loss. However, I was unable to obtain OCT images of AAV.VEGF$_{165}$b eyes, especially at 4-months and OCT has been previously used to monitor GA (Fleckenstein et al. 2008), indicating much of the visual dysfunction may not be exclusively limited to the retina, but may also involve the anterior regions of the eye.

There are many different hypotheses to suggest why AAV.VEGF$_{165}$b showed such dramatic worsening of the eye. It is likely to be a combination of these events. I hypothesise that upon subretinal injection, any endotoxin present elicited an inflammatory response in tandem with the subretinal detachment unable to correct itself appropriately. This was further exacerbated by over-production of AAV.VEGF$_{165}$b, leaving little transcriptional capacity for other products that are essential for normal maintenance of the eye. Over time, the eye was unable to correct itself, and therefore worsened, resulting in a diminished A- and B-wave response and inability to image the eye *in vivo*. To test these hypotheses and improve upon this study, less volume of vector should be injected but at the same concentration, this would reduce the retinal detachment and therefore complications associated with it. Similarly, a parallel study would involve injecting a lower titre or a combination of both experiments and monitor over time how well these differing combinations are tolerated. This would give an indication of the ideal titre and ideal volume to inject in a study with a more appropriate model. It is possible that the subretinal injection itself is causing the greatest damage in the first instance; to remove this possibility a different promoter could be used. ShH10, a novel AAV similar to AAV6, targets Muller glia and can be injected intravitreally (Klimczak et al. 2009), thus removing the need for a subretinal injection. Considering Muller glia have been hypothesised to overproduce VEGF in models of diabetes (Wang et al. 2010), it may be also be a novel therapeutic target.

Another possible experiment would be to repeat this study and compare it to eyes intravitreally injected with rhVEGF$_{165}$b. Although this may increase the risk of endophthalmitis, this would give an indication of how well tolerated long term VEGF$_{165}$b expression is in the eye. This would illuminate whether the dysfunction is virus-mediated, route of injection mediated (subretinal vs. intravitreal) or VEGF$_{165}$b mediated.

Throughout this study, there was always a difference in degeneration between AAV.VEGF$_{165}$b and AAV.Null. Whilst AAV.Null was designed to express nothing, perhaps a better negative control would be something that has transgene expression. This way one could adequately compare side effects more appropriately. AAV.hrGFP was discounted as a potential negative control due to its apparent atrophy (Appendix 4), however this may have been an adequate negative control, as it would help to differentiate between overexpression of VEGF$_{165}$b-mediated dysfunction or general transgene induced dysfunction, if run in parallel with AAV.Null eyes.

This study can also be improved upon in future by using a much more rigorous endotoxin testing method, perhaps setting the upper limit lower than 2.5EU/ml. Using a different negative control in future would also help further studies. Unfortunately, do to lack of time and lack of resources; these ideas could not be further explored.

5.5. Concluding Remarks

Retinal gene therapy to treat blindness is a highly attractive concept considering the eye's immune privilege and potential to reduce injection-induced adverse events. There is little published evidence of anti-angiogenic gene therapy being unsuccessful. However, considering the limited successes in this field, it is likely that there have been unsuccessful studies. One study showed that using AAV mediated delivery of cilliary neurotrophic factor (CNTF), previously shown to prevent retinal and photoreceptor degeneration, was in fact damaging to the eye and reduced B-wave amplitude (Schlichtenbrede et al. 2003). Whilst a different type of growth factor, it is still reporting abnormalities similar to those observed in this study, albeit to not as great an extent. It is likely that other groups have had similar ideas and have had limited success with anti-angiogenic gene therapy for diabetic retinopathy, possibly due to a lack of an appropriate model or they observe a degenerative effect like this current study. This illustrates that although well researched, gene therapy to treat non-genetic retinal dysfunction is still in its infancy. AAV.VEGF$_{165}$b was detrimental to the eye due to many different possibilities; however with some more refinement and a working model, this field study could show success in the future.

Chapter 6: Discussion

This study aimed to look at how the hallmark pathologies associated with diabetic retinopathy, pathological neovascularisation, oedema and retinal neurodegeneration, could be ameliorated by targeting the outer BRB with $VEGF_{165}b$. This was investigated *in vitro* and *in vivo* using $rhVEGF_{165}b$ and $AAV.VEGF_{165}b$, and has contributed to some of the hypotheses shown in figure 6.1

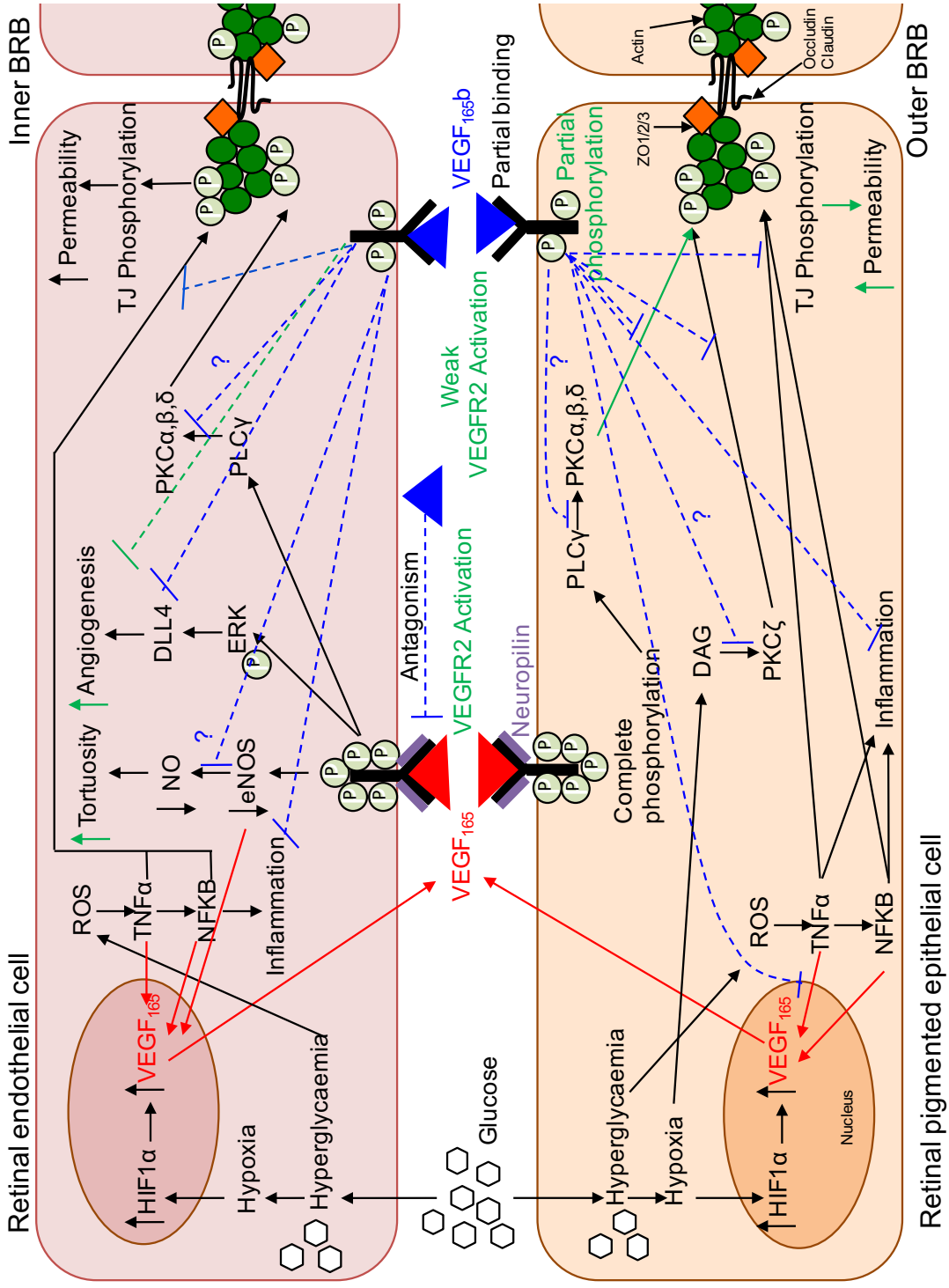

Figure 6.1. Proposed mechanisms involved in diabetic retinopathy in the inner and outer BRB.

Increased glucose results in hypoxia in and around both RECs and RPE; as a result there is greater HIF1α transcription, resulting in greater $VEGF_{165}$ transcription and translation. Hyperglycaemia also stimulates the production of ROS and as a result and increase in TNFα and NFKB, both of which also increase $VEGF_{165}$ production and activation of the inflammatory pathway. $VEGF_{165}$ binds to VEGFR2 and induces VEGFR2 dimerization and neuropilin stabilisation resulting in complete VEGFR2 phosphorylation. Phosphorylation results in activation of PLCγ and subsequent activation of typical PKC isoforms such as PKCα, β and δ. These PKC isoforms in turn phosphorylate tight junctions at the serine/threonine residue, resulting in their internalisation and degradation and subsequent increase in paracellular solute flux. In RPE, hypoxia stimulates *de novo* synthesis of DAG, resulting in atypical PKC activation resulting in further activation of TNFα and tight junction phosphorylation. In RECs it is likely that VEGFR2 phosphorylation also results in transient changes in eNOS and NO resulting in vessel tortuosity. VEGFR2 phosphorylation also results in ERK phosphorylation and subsequent DLL4 activation, resulting in sprouting angiogenesis. $VEGF_{165}$b, a competitive VEGFR2 antagonist, binds to VEGFR2 and causes its dimerization without neuropilin involvement, resulting in partial, transient VEGFR2 phosphorylation. $VEGF_{165}$b has been shown to prevent PKCε activation (*S.Bestall, personal communication*) and may also prevent activation of typical and atypical PKC isoforms, thus preventing tight junction phosphorylation. $VEGF_{165}$b may prevent DLL4 activation in RECs and therefore potentially preventing $VEGF_{165}$-induced angiogenesis. $VEGF_{165}$b has been shown to prevent TNFα-mediated $VEGF_{165}$ expression in RPE (Thichanpiang et al. 2014), therefore likely to prevent inflammation in RPE and potentially RECs. $VEGF_{165}$b may prevent transient changes in NO expression or prevent its detection, resulting in reduced vascular tortuosity via an unknown mechanism. Red arrows = actions caused by $VEGF_{165.}$ Blue inhibition arrows = actions caused by $VEGF_{165}$b. Green arrows = contributions from this thesis.

6.1. Permeability and the outer BRB

Breakdown of the BRB is responsible for fluid accumulation in the macula and exudate formation in the retina (A. J. Barber 2003). It is generally accepted that the BRB usually describes the tight junction complex formed between RECs, also known as the inner BRB, often leaving the outer BRB, formed by the RPE, overlooked. This is reflected in the literature with many papers using RECs when referring to the BRB *in vitro*. Of the groups that do use RPE, few of them use them intentionally as a model of the outer BRB, but rather the BRB in general. Many groups also use ARPE19 cells, an immortalised RPE line, likely due to their unlimited passage life and how easy they are to culture. However ARPE19s give an even less accurate representation of the BRB than

other primary RPE cells. I showed in chapter 3 that RPE extraction is a simple and reproducible protocol and moreover it can be used in a variety of assays.

Whilst the notion that $VEGF_{165}$ can induce BRB dysfunction and increase paracellular flux *in vitro* is not novel, there is limited published data in cultured 1˚hRPE. I have confirmed that $VEGF_{165}$ can induce TJ dysfunction in RPE cells that can be verified by a variety of techniques *in vitro* (chapter 3). A previous study looking at TER in foetal RPE showed that $VEGF_{165}$ treatment has no significant difference on TJ expression when using concentrations ranging from 50ng/ml to 300ng/ml (approximate 1nM to 7.5nM) (Peng et al. 2010). They also observe no change in TJ expression at these concentrations. Whilst these data appear to directly contradict what I have observed in chapter 2, they are using hfRPE, which may be more resistant and more resilient against a $VEGF_{165}$ challenge. Also, hfRPE are at a different developmental stage to 1˚RPE and therefore may display different characteristics in response to VEGF stimulation.

I have also shown novel data that $VEGF_{165}$-induced permeability can be reversed by an isoform of VEGF, as shown by figure 6.1. These changes are consistent with published data looking at immortalised bovine RECs as a measure of inner BRB dysfunction (Deissler et al. 2012). Deissler and colleagues used the same concentration of $VEGF_{165}$ (100ng/ml or 2.5nM) and observed in decrease in TER. TER was then increased with co-treatment with either bevacizumab or ranibizumab, with ranibizumab giving the greatest TER restoration, however to not as great an extent as I showed upon co-treatment with $VEGF_{165}$b. Whilst there is the caveat of different cell lines (iBREC vs. RPE), different BRBs (inner vs. outer) and different assays (TER vs. TEER), this does support my hypothesis that the outer BRB is likely to be involved in DME.

The literature concerning *in vitro* models of DME are in poor agreement. Experiments vary in length starting from 24 hours post glucose treatment (Pavan et al. 2014) to days post glucose treatment (Chronopoulos et al. 2011), with varying notions of "low glucose" and "high glucose". The majority of the literature suggests that 5mM glucose is sufficient to replicate normoglycaemia, whereas there is more disagreement surrounding what would truly represent hyperglycaemia, varying between 25mM glucose (Pavan et al. 2014; Qin et al. 2013) and 45mM glucose (Naggar et al. 2002) treatment. Based on these data I used 35mM glucose for 24 hours and showed novel data that acute high glucose treatment can indeed cause TJ loss and an increase in paracellular flux. Although I was unable to fully restore barrier properties using $VEGF_{165}$b, this again supports my hypothesis that hyperglycaemia can induce outer BRB breakdown. I also

showed that there is increased VEGF expression in the conditioned media from these RPE, which is likely to be exacerbating PKC-mediated TJ loss. Published data has shown that 25mM glucose alone had no effect on different PKC isoform expression, however when co-treated with VEGF there was a significant increase in expression of different PKC isoforms, including atypical isoforms such as PKCζ (Young et al. 2005). This is of particular interest as I hypothesise that $VEGF_{165}b$ is acting to prevent hypoxia and hyperglycaemia induced TJ dysfunction either by preventing activation of atypical PKCs, such as PKCζ. Inhibition of PKCζ prevented glucose-induced VEGF secretion in RPE cells (Young et al. 2005). It is possible that 35mM glucose is sufficient to increase VEGF expression, PKC activation and subsequent TJ breakdown as opposed to the lack of change observed with 25mM glucose alone used by Young and colleagues (Young et al. 2005).

It is harder to distinguish between changes in inner and outer BRB *in vivo* particularly when assaying changes in permeability. Techniques such as the Evans' blue dye perfusion technique limits how tissue can be used in ways other than measuring dye absorption. Xu and Le showed that by embedding eyes immediately after perfusion with FITC-dextran, it was possible to map out regions of dye leakage (Xu & Le 2011). They concluded that there was significant leakage from the RPE layer in models of diabetes, EIU and ischaemia-induced retinopathy relative to leakage from the inner BRB. Whilst I cannot definitively say that results from chapter 4 are indicative of outer BRB breakdown, results from Xu and Le's paper support my hypothesis in that there is outer BRB involvement *in vivo.* Furthermore, they used FITC-dextran (10 kDa) whereas I used Evans' blue (961 Da). Considering that Evans' blue has a much lower MW than FITC-dextran, its likely to leak from much smaller pores than FITC-dextran and is therefore more likely to give a better representation of BRB dysfunction. Therefore if significant dye leakage is shown from the RPE layer using FITC-dextran, the same is likely to be true of Evans' blue.

Many other groups have used the Evans' blue dye perfusion technique to assay BRB dysfunction (Xu et al. 2001; Qaum et al. 2001; Abcouwer et al. 2010) however results from these experiments usually conclude in inner BRB dysfunction. Studies have shown that bevacizumab (Abcouwer et al. 2010) and atypical PKC inhibitors (Titchenell et al. 2012) reduce Evans' blue leakage in the retina, however none to the same extent as I have shown using $VEGF_{165}b$. Titchenell and colleagues targeted the inner BRB using atypical PKC inhibitors (Titchenell et al. 2012), however only saw a partial reduction in

Evans' blue leakage. It has been shown that typical and atypical PKC isoforms are upregulated in hyperglycaemia (Young et al. 2005), and therefore targeting just one family may not be successful. As mentioned previously, $VEGF_{165}b$ could be acting as a VEGFR2 antagonist as well as a typical and atypical PKC inhibitor, thus preventing VEGF-induced TJ breakdown as shown by figure 6.1.

Considering the RPE layer has TJs, like RECs, it is likely that in diabetic eyes both barriers will suffer similar levels of ischaemic insult. The RPE protects the rest of the inner retina from the choroidal circulation, which is greater than the retinal circulation. Disruption of the outer BRB may include choroidal vascular leakage into the retina, which could be more deleterious than leakage of the retinal circulation from the inner BRB. Therefore more research should be focused towards prevention of outer BRB and inner BRB dysfunction rather than just inner BRB dysfunction.

6.2. Vascular remodelling and the outer BRB

Although I have hypothesised that RPE / the outer BRB has a significantly greater involvement in DME than is acknowledged, I believe that the vascular remodelling I observed *in vivo* is a result of REC activation. However this does not mean that RPE are not involved. The RPE layer secretes VEGF (Saint-Geniez et al. 2009b), and it is possible that the RPE secretes even more VEGF in the hyperglycaemic eye, as shown in chapter 3 *in vitro*, by many possible mechanisms induced by hypoxia (figure 6.1). As well outer BRB TJ breakdown, VEGF secreted by RPE could induce angiogenesis in neighbouring RECs that form microvessels, which may be in close proximity (figure 6.1). This may contribute to localised VEGFR2 activation and subsequent activation of DLL4, resulting in angiogenesis (figure 6.1). ARPE19s with a VEGF knock-down were co-cultured with normal RECs and showed that there was a reduction in REC proliferation relative to control groups (Ma et al. 2011). This indicates that VEGF secreted from the RPE layer may contribute to VEGF secreted by RECs and therefore may exacerbate the angiogenesis characteristic of PDR.

AMD, another form of blindness induced by pathological angiogenesis and TJ breakdown, has been linked to loss of RPE function (Bird et al. 1995), it is possible that the same may be true of PDR and that the loss of RPE contributes to macular dysfunction and angiogenesis. $VEGF_{165}b$ has been shown to reduce CNV (Hua et al. 2010) and reduce

OIR-induced neovascularization (Magnussen et al. 2010) and now I have shown that it prevents STZ-induced vascular remodelling, likely due to preventing DLL4 activation and PKC activation, as well as other mechanisms shown by figure 6.1 and described previously. I am cautious to interpret $VEGF_{165}b$ preventing angiogenesis in the 8-weeks STZ model, as we have not proved that it is angiogenesis that was observed. However, as $VEGF_{165}b$ has prevented angiogenesis in many other models of retinopathy and CNV, it is likely that it is also anti-angiogenic in STZ-induced diabetic retinopathy. Until further studies are done, I cannot fully conclude that $VEGF_{165}b$ is anti-angiogenic in this particular model. I can however conclude that there was indeed vascular remodelling induced by the model that presented as increased vascular density and that $VEGF_{165}b$ successfully prevented this remodelling.

Studies using small molecular inhibitors such as SRPIN340, an inhibitor of serine-rich protein kinase 1 (SRPK1) a regulator of pro-angiogenic splicing, facilitates splicing in favour of anti-angiogenic isoforms of VEGF have shown a reduction in neovascular area in CNV when applied topically (M. V Gammons et al. 2013). Based on the data presented in this thesis, $VEGF_{165}b$ is a good candidate therapeutic, however its half-life is significantly shorter than the gold standard drugs. By promoting splicing in favour of $VEGF_{165}b$, this small molecular inhibitor eye drop may be able to prevent or reduce the proliferative stage of PDR and may even prevent TJ breakdown, without the use of invasive intravitreal injections. Furthermore, SRPIN340 has also prevented the onset of peripheral neuropathy in the 8-week STZ rat model by promoting downregulation of pro-angiogenic VEGF isoforms (Hulse et al. 2014b), illustrating that it could be a successful future area to investigate as a potential therapeutic for diabetic retinopathy.

6.3. Eight weeks STZ-induced diabetes: a new model of diabetic retinopathy?

Throughout this thesis I have shown that 8 weeks STZ-induced diabetes with insulin supplementation presents some of the key features of diabetic retinopathy. I observed an increase in Evans' blue leakage, indicative of increased vascular permeability. I also saw an increased vessel density, indicative of vascular remodelling and potential angiogenesis. Whilst this model may appear to recapitulate the vascular complications associated with DR, I cannot confirm neuronal complications with DR. Although I observed RGC shrinkage in this model, I did not see RGC loss. It is possible

that the shrinkage is preceding apoptosis and that insulin is eliciting an unwanted neuroprotective effect, which is why there was no RGC loss after two months. Barber and colleagues used the same model of diabetes and insulin supplementation and showed there was no difference in TUNEL staining between diabetes + insulin and control retinae (Barber et al. 1998). They also showed that diabetic rats without insulin supplementation showed increased TUNEL staining at month 1 relative to control and diabetes + insulin, and that these results were mirrored in human studies whereby patients on insulin had significantly less TUNEL staining relative to diabetic patients that were not insulin-treated (Barber et al. 1998). Despite positive results shown in the absence of insulin supplementation I would not be able to repeat such an experiment as it would not be approved by most BSUs nor was it on the PPL.

Many other models of diabetic retinopathy are models of angiogenesis unrelated to diabetes such as OIR and CNV, however they present with clear neovascular areas. This thesis is one of the few studies that show vascular remodelling in response to hyperglycaemia in the retina. Again with further experiments such as confirmation of angiogenesis using Ki67 staining, this could potentially be a model for PDR. As most groups administer insulin *ad hoc* according to weight loss, usually many weeks after STZ has already been delivered, they may not see proliferation. Furthermore, most groups that use STZ do not use it as a model of PDR but rather a model of BRB breakdown and retinal neuronal dysfunction. As a result, potential changes in proliferation may be missed, as they are not being looked for, particularly when there are other models of vascular proliferation that may be faster and more definitive such as OIR.

STZ has been used in models of DME extensively (Xu et al. 2001; A. J. Barber 2003; Robinson et al. 2012b) and I have confirmed that it is a reproducible model at both 1 and 8 weeks post induction of diabetes. As rats do not have a macula, we cannot mimic DME completely, however this does induce TJ loss and shows an increase in solute flux and therefore I believe it is as representative a model as possible. Perhaps future investigation into this model would involve regular FFA imaging on non-albino rats to monitor existence and progression of microaneurysms. This would then provide further confirmation that the model recapitulates DME.

Unfortunately, I saw no difference in OCT thickness in diabetic Lewis rats indicating that either Lewis rats are not suitable for measuring changes in retinal thickness or that the changes in thickness are so small that they are not observed by OCT and thus unable to provide data on GCL thinning and thickening of the rest of the retina

from vessel leakage. A further study could involve repeating the 8-week STZ study and doing, for example, weekly OCT measurements in rats. OCT uses near-infra red light to penetrate the eye and if rats are injected with a dye with an near-infra red emission wavelength, such as Cy5, theoretically one could measure where there is dye leakage and compare within the different layers of the retina. This may result in a more definitive answer as to how involved the outer BRB is in the progression of DME.

There are many caveats to the 8-week STZ-induced diabetes model of diabetic retinopathy, as previously described. However future studies into this model such as increasing the duration of diabetes to observe RGC loss and measuring visual dysfunction using ERG and perhaps a visual test such as the water maze test, would confirm loss of retinal neuronal function. Validation of the vascular changes would involve confirmation of angiogenesis using Ki67. Further, more long-term studies would involve measuring the progression of the disease by staining retinae for example every week and staining for: pericyte dropout using NG2, sprouting angiogenesis using a DLL4 antibody, a combination of IB4 and staining for collagen IV to measure area of non-perfusion. To confirm the permeability observed, further studies would involve FFA on pigmented rats to observe microaneurysms and staining of leaked red blood cells using a Ter119 antibody.

Although there are many necessary experiments needed to confirm that this is indeed a good model of DR, I have confidence in it as a successful model of DME. Considering the concurrent dysfunction I observed in the peripheral nervous system and the increased sensitivity to pain at this time point, it is evident that these rats were also experiencing peripheral diabetic neuropathy. As diabetic retinopathy and diabetic neuropathy in patients is often linked (Dyck et al. 1993; Dyck et al. 1999), we can infer that as the rats had neuropathy, any changes I observed in the eyes are likely to be a model of DR. Few other models present with neuropathy simultaneously with retinopathy, again further supporting that this may be a good model. Nevertheless, further tests are required to fully confirm this model as a reliable and reproducible model of DR.

6.4. Gene therapy and diabetic retinopathy

Anti-angiogenic gene therapy in the eye has been investigated by targeting many areas such as: endostatin (Balaggan et al. 2006), PEDF (Campochiaro et al. 2006), sFlt1 (Bainbridge et al. 2002), erythropoietin (Xu et al. 2014) and many others, and have shown varying degrees of success. This was the first study that attempted RPE-targeted $VEGF_{165}b$ gene therapy to treat diabetic retinopathy and did not show a prevention of angiogenesis or increased neurone survival as I hypothesised. I observed a high level of inflammation in AAV.$VEGF_{165}b$-injected eyes, which was unexpected. I am hesitant to believe that this is novel data. I believe that this is likely to have occurred to many other groups experimenting with similar constructs and their negative data has not been published.

Vectors targeting sFlt1 appear to be the most successful anti-VEGF gene therapy in both targeting CNV (Bainbridge et al. 2002; Lai et al. 2009) and corneal neovascularisation (*Dr. M. Basche, manuscript in preparation*). A recent study in the brain shows that AAV.sFlt1 inhibits brain angiogenesis (Shen et al. 2015), however there have been few recent published studies on the use of AAV.sFlt1 in the eye.

It is unfortunate that my endeavour with gene therapy was unsuccessful, however it did reveal potential pitfalls and areas that should be revisited for further studies, as mentioned previously, such as more rigorous endotoxin testing especially when working with upregulating cytokines. Also more dose-adjustment studies of AAV.$VEGF_{165}b$ are required if this study is to repeated again in future.

6.5. Summary

Anti-angiogenic gene therapy to treat diabetic retinopathy has been the most successful form of treatment over the last decade. This thesis has shown that rh$VEGF_{165}b$, when injected as a recombinant protein, is a suitable candidate for further drug development as it prevents vascular dysfunction in two the ways relevant to sufferers of DR: prevention of TJ breakdown and prevention of vascular remodelling. As an injectable recombinant protein, it falls short relative to aflibercept, bevacizumab and ranibizumab when comparing half-life and frequency of injection. $VEGF_{165}b$ would need to be injected far more frequently than the current gold standard drugs, and therefore is

not a suitable alternative. Despite this, I still believe that $VEGF_{165}b$ is a suitable candidate to be further investigated in treating DR as it aims to upregulate already existing isoforms as opposed to targeting whole genes and it appears to also be neuroprotective in the eye.

This thesis has also demonstrated that the outer BRB may have a greater involvement in diabetic retinopathy than is acknowledged. Although RPE seem to react to $VEGF_{165}$ and glucose *in vitro* similarly to RECs, further studies are required to confirm my hypothesis of their greater involvement. Nevertheless, I believe that the RPE layer should be considered as a new target for future therapeutic intervention in treating diabetic retinopathy.

References

Abcouwer, S.F. et al., 2010. Effects of ischemic preconditioning and bevacizumab on apoptosis and vascular permeability following retinal ischemia-reperfusion injury. *Investigative ophthalmology & visual science*, 51(11), pp.5920–33. Available at: http://www.ncbi.nlm.nih.gov/pubmed/20554620 [Accessed December 9, 2014].

Ablonczy, Z. et al., 2009. Pigment epithelium-derived factor maintains retinal pigment epithelium function by inhibiting vascular endothelial growth factor-R2 signaling through gamma-secretase. *The Journal of biological chemistry*, 284(44), pp.30177–86. Available at: http://www.jbc.org/content/284/44/30177.full [Accessed July 21, 2015].

Acland, G.M. et al., 2001. Gene therapy restores vision in a canine model of childhood blindness. *Nature genetics*, 28(1), pp.92–5. Available at: http://www.ncbi.nlm.nih.gov/pubmed/11326284.

Adamis, A.P. et al., 1993. Synthesis and Secretion of Vascular Permeability Factor/Vascular Endothelial Growth Factor by Human Retinal Pigment Epithelial Cells. *Biochemical and Biophysical Research Communications*, 193(2), pp.631–638. Available at: http://www.sciencedirect.com/science/article/pii/S0006291X83716712 [Accessed June 9, 2015].

Ahrén, B., 2003. Gut peptides and type 2 diabetes mellitus treatment. *Current diabetes reports*, 3(5), pp.365–72. Available at: http://www.ncbi.nlm.nih.gov/pubmed/12975025 [Accessed August 10, 2015].

Aiello, L.P., 1995. Suppression of Retinal Neovascularization in vivo by Inhibition of Vascular Endothelial Growth Factor (VEGF) Using Soluble VEGF-Receptor Chimeric Proteins. *Proceedings of the National Academy of Sciences*, 92(23), pp.10457–10461. Available at: http://www.pnas.org/content/92/23/10457.short [Accessed October 31, 2012].

Aiello, L.P., 2002. The Potential Role of PKC β in Diabetic Retinopathy and Macular Edema. *Survey of Ophthalmology*, 47(null), pp.S263–S269. Available at: http://dx.doi.org/10.1016/S0039-6257(02)00391-0 [Accessed September 13, 2013].

Aiello, L.P., 1994. Vascular endothelial growth factor in ocular fluid of patients with diabetic retinopathy and other retinal disorders.

Aizu, Y. et al., 2002. Degeneration of retinal neuronal processes and pigment epithelium in the early stage of the streptozotocin-diabetic rats. *Neuropathology*, 22(3), pp.161–170. Available at: http://doi.wiley.com/10.1046/j.1440-1789.2002.00439.x [Accessed March 17, 2015].

Al-Shabrawey, M. et al., 2008. Role of NADPH oxidase in retinal vascular inflammation. *Investigative ophthalmology & visual science*, 49(7), pp.3239–44. Available at: http://www.iovs.org/content/49/7/3239.full [Accessed October 31, 2013].

Ali, R.R. et al., 2000. Restoration of photoreceptor ultrastructure and function in retinal degeneration slow mice by gene therapy. *Nature genetics*, 25(3), pp.306–10. Available at: http://www.nature.com/ng/journal/v25/n3/full/ng0700_306.html#B1 [Accessed July 2, 2015].

Amado, D. et al., 2010. Safety and efficacy of subretinal readministration of a viral vector in large animals to treat congenital blindness. *Science translational medicine*, 2(21), p.21ra16. Available at: http://stm.sciencemag.org/content/2/21/21ra16?ijkey=89f4d70ac91db127058d196913fb6017758afe54&keytype2=tf_ipsecsha [Accessed June 8, 2015].

Anand, V. et al., 2002. A deviant immune response to viral proteins and transgene product is generated on subretinal administration of adenovirus and adeno-associated virus. *Molecular therapy : the journal of the American Society of Gene Therapy*, 5(2), pp.125–32. Available at: http://dx.doi.org/10.1006/mthe.2002.0525 [Accessed July 3, 2015].

Anderson, R.E., Rapp, L.M. & Wiegand, R.D., 1984. Lipid peroxidation and retinal degeneration. *Current eye research*, 3(1), pp.223–7. Available at: http://www.ncbi.nlm.nih.gov/pubmed/6606531 [Accessed August 20, 2015].

Anon, Key findings 2014 | International Diabetes Federation. Available at: http://www.idf.org/diabetesatlas/update-2014 [Accessed August 10, 2015].

Anon, 1993. The effect of intensive treatment of diabetes on the development and progression of long-term complications in insulin-dependent diabetes mellitus. The Diabetes Control and Complications Trial Research Group. *The New England journal of medicine*, 329(14), pp.977–86. Available at: http://www.ncbi.nlm.nih.gov/pubmed/8366922 [Accessed July 22, 2014].

Antonetti, D. a, Klein, R. & Gardner, T.W., 2012. Diabetic retinopathy. *The New England journal of medicine*, 366(13), pp.1227–39. Available at: http://www.ncbi.nlm.nih.gov/pubmed/22455417 [Accessed March 10, 2013].

Antonetti, D.A., 1999a. Vascular Endothelial Growth Factor Induces Rapid Phosphorylation of Tight Junction Proteins Occludin and Zonula Occluden 1. A POTENTIAL MECHANISM FOR VASCULAR PERMEABILITY IN DIABETIC RETINOPATHY AND TUMORS. *Journal of Biological Chemistry*, 274(33),

pp.23463–23467. Available at: http://www.jbc.org/content/274/33/23463.short [Accessed October 31, 2012].

Antonetti, D.A., 1999b. Vascular Endothelial Growth Factor Induces Rapid Phosphorylation of Tight Junction Proteins Occludin and Zonula Occluden 1. A POTENTIAL MECHANISM FOR VASCULAR PERMEABILITY IN DIABETIC RETINOPATHY AND TUMORS. *Journal of Biological Chemistry*, 274(33), pp.23463–23467. Available at: http://www.jbc.org/content/274/33/23463.full [Accessed October 31, 2013].

Atkinson, M.A., Eisenbarth, G.S. & Michels, A.W., 2014. Type 1 diabetes. *Lancet*, 383(9911), pp.69–82. Available at: http://www.sciencedirect.com/science/article/pii/S0140673613605917 [Accessed October 22, 2014].

Auricchio, A. et al., 2002. Inhibition of retinal neovascularization by intraocular viral-mediated delivery of anti-angiogenic agents. *Molecular therapy : the journal of the American Society of Gene Therapy*, 6(4), pp.490–4. Available at: http://www.ncbi.nlm.nih.gov/pubmed/12377190 [Accessed July 3, 2015].

Avery, R.L. et al., 2006. Intravitreal bevacizumab (Avastin) in the treatment of proliferative diabetic retinopathy. *Ophthalmology*, 113(10), pp.1695.e1–15. Available at: http://dx.doi.org/10.1016/j.ophtha.2006.05.064 [Accessed August 14, 2013].

Baba, T. et al., 2012. VEGF 165 b in the developing vasculatures of the fetal human eye. *Developmental dynamics : an official publication of the American Association of Anatomists*, 241(3), pp.595–607. Available at: http://europepmc.org/abstract/med/22275161 [Accessed August 19, 2015].

Baggio, L.L. & Drucker, D.J., 2007. Biology of incretins: GLP-1 and GIP. *Gastroenterology*, 132(6), pp.2131–57. Available at: http://www.ncbi.nlm.nih.gov/pubmed/17498508 [Accessed July 15, 2014].

Bainbridge, J.W.B. et al., 2008. Effect of gene therapy on visual function in Leber's congenital amaurosis. *The New England journal of medicine*, 358(21), pp.2231–9. Available at: http://www.ncbi.nlm.nih.gov/pubmed/18441371 [Accessed July 5, 2015].

Bainbridge, J.W.B. et al., 2002. Inhibition of retinal neovascularisation by gene transfer of soluble VEGF receptor sFlt-1. *Gene therapy*, 9(5), pp.320–6. Available at: http://www.ncbi.nlm.nih.gov/pubmed/11938451 [Accessed May 8, 2014].

Bainbridge, J.W.B. et al., 2015. Long-term effect of gene therapy on Leber's congenital amaurosis. *The New England journal of medicine*, 372(20), pp.1887–97. Available at: http://www.ncbi.nlm.nih.gov/pubmed/25938638 [Accessed July 2, 2015].

Balaggan, K.S. et al., 2006. EIAV vector-mediated delivery of endostatin or angiostatin inhibits angiogenesis and vascular hyperpermeability in experimental CNV. *Gene therapy*, 13(15), pp.1153–65. Available at: http://dx.doi.org/10.1038/sj.gt.3302769 [Accessed April 8, 2015].

Barber, A.J., 2003. A new view of diabetic retinopathy: a neurodegenerative disease of the eye. *Progress in Neuro-Psychopharmacology and Biological Psychiatry*, 27(2), pp.283–290. Available at: http://www.sciencedirect.com/science/article/pii/S027858460300023X [Accessed October 26, 2013].

Barber, A.J. et al., 2001. Insulin rescues retinal neurons from apoptosis by a phosphatidylinositol 3-kinase/Akt-mediated mechanism that reduces the activation of caspase-3. *The Journal of biological chemistry*, 276(35), pp.32814–21. Available at: http://www.jbc.org/content/276/35/32814.full [Accessed June 30, 2015].

Barber, A.J., 2003. Mapping the Blood Vessels with Paracellular Permeability in the Retinas of Diabetic Rats. *Investigative Ophthalmology & Visual Science*, 44(12), pp.5410–5416. Available at: http://www.iovs.org/content/44/12/5410.abstract?ijkey=2e5b316d99c5022e9aa0fa5251c1d0d0d58e0d3c&keytype2=tf_ipsecsha [Accessed June 23, 2014].

Barber, A.J. et al., 1998. Neural apoptosis in the retina during experimental and human diabetes. Early onset and effect of insulin. *The Journal of clinical investigation*, 102(4), pp.783–91. Available at: http://www.pubmedcentral.nih.gov/articlerender.fcgi?artid=508941&tool=pmcentrez&rendertype=abstract [Accessed February 14, 2015].

Bates, D.O. et al., 2002a. VEGF165b, an Inhibitory Splice Variant of Vascular Endothelial Growth Factor, Is Down-Regulated in Renal Cell Carcinoma. *Cancer Res.*, 62(14), pp.4123–4131. Available at: http://cancerres.aacrjournals.org/content/62/14/4123.full [Accessed March 9, 2015].

Bates, D.O. et al., 2002b. VEGF165b, an Inhibitory Splice Variant of Vascular Endothelial Growth Factor, Is Down-Regulated in Renal Cell Carcinoma. *Cancer Res.*, 62(14), pp.4123–4131. Available at: http://cancerres.aacrjournals.org/content/62/14/4123.short [Accessed October 31,

2012].

Baumgartner, W.A., 2000. Etiology, pathogenesis, and experimental treatment of retinitis pigmentosa. *Medical hypotheses*, 54(5), pp.814–24. Available at: http://www.ncbi.nlm.nih.gov/pubmed/10859693 [Accessed October 26, 2013].

Beazley-Long, N. et al., 2013. VEGF-A165b Is an Endogenous Neuroprotective Splice Isoform of Vascular Endothelial Growth Factor A in Vivo and in Vitro. *The American Journal of Pathology*, 183(3), pp.918–929. Available at: http://www.sciencedirect.com/science/article/pii/S0002944013004252 [Accessed December 11, 2013].

Bergers, G. & Song, S., 2005. The role of pericytes in blood-vessel formation and maintenance. *Neuro-oncology*, 7(4), pp.452–64. Available at: http://www.pubmedcentral.nih.gov/articlerender.fcgi?artid=1871727&tool=pmcentrez&rendertype=abstract [Accessed September 5, 2014].

Bevan, H.S. et al., 2008. The alternatively spliced anti-angiogenic family of VEGF isoforms VEGFxxxb in human kidney development. *Nephron. Physiology*, 110(4), pp.p57–67. Available at: http://www.karger.com/Article/FullText/177614 [Accessed August 19, 2015].

Bhagat, N. et al., 2009. Diabetic macular edema: pathogenesis and treatment. *Survey of ophthalmology*, 54(1), pp.1–32. Available at: http://www.sciencedirect.com/science/article/pii/S0039625708001811 [Accessed August 18, 2015].

Bird, A.C. et al., 1995. An international classification and grading system for age-related maculopathy and age-related macular degeneration. *Survey of Ophthalmology*, 39(5), pp.367–374. Available at: http://www.surveyophthalmol.com/article/S003962570580092X/fulltext [Accessed August 2, 2015].

Birnbach, C.D. et al., 1994. Histopathology and Immunocytochemistry of the Neurosensory Retina in Fundus Flavimaculatus. *Ophthalmology*, 101(7), pp.1211–1219. Available at: http://www.sciencedirect.com/science/article/pii/S0161642013317254 [Accessed June 22, 2015].

Bloomgarden, Z.T., 2005. Diabetic Retinopathy and Neuropathy. *Diabetes Care*, 28(4), pp.963–970. Available at: http://care.diabetesjournals.org/content/28/4/963.full [Accessed March 24, 2015].

Brantly, M.L. et al., 2009. Sustained transgene expression despite T lymphocyte responses in a clinical trial of rAAV1-AAT gene therapy. *Proceedings of the National Academy of Sciences*, 106(38), pp.16363–16368. Available at: http://www.pnas.org/content/106/38/16363?ijkey=888a6f814b608279fdc07961337ce5df509e2a34&keytype2=tf_ipsecsha [Accessed July 5, 2015].

Brownlee, M., 2001. Biochemistry and molecular cell biology of diabetic complications. *Nature*, 414(6865), pp.813–20. Available at: http://dx.doi.org/10.1038/414813a [Accessed April 10, 2013].

Buch, P.K., Bainbridge, J.W. & Ali, R.R., 2008. AAV-mediated gene therapy for retinal disorders: from mouse to man. *Gene therapy*, 15(11), pp.849–57. Available at: http://www.ncbi.nlm.nih.gov/pubmed/18418417 [Accessed July 3, 2015].

Bursell, S.E. et al., 1996. Retinal blood flow changes in patients with insulin-dependent diabetes mellitus and no diabetic retinopathy. *Investigative Ophthalmology & Visual Science*, 37(5), pp.886–897. Available at: http://iovs.arvojournals.org/article.aspx?articleid=2180512 [Accessed January 10, 2016].

Cai, J. & Boulton, M., 2002. The pathogenesis of diabetic retinopathy: old concepts and new questions. *Eye*, 16(3), pp.242–260. Available at: http://dx.doi.org/10.1038/sj.eye.6700133 [Accessed September 13, 2013].

Campochiaro, P.A. et al., 2006. Adenoviral vector-delivered pigment epithelium-derived factor for neovascular age-related macular degeneration: results of a phase I clinical trial. *Human gene therapy*, 17(2), pp.167–76. Available at: http://online.liebertpub.com/doi/abs/10.1089/hum.2006.17.167 [Accessed July 3, 2015].

Carmeliet, P. et al., 1996. Abnormal blood vessel development and lethality in embryos lacking a single VEGF allele. *Nature*, 380(6573), pp.435–9. Available at: http://www.ncbi.nlm.nih.gov/pubmed/8602241 [Accessed July 21, 2015].

Chang, G.Q., Hao, Y. & Wong, F., 1993. Apoptosis: final common pathway of photoreceptor death in rd, rds, and rhodopsin mutant mice. *Neuron*, 11(4), pp.595–605. Available at: http://www.ncbi.nlm.nih.gov/pubmed/8398150 [Accessed April 25, 2015].

Chantelau, E. & Kohner, E.M., 1997. Why some cases of retinopathy worsen when diabetic control improves. *BMJ*, 315(7116), pp.1105–1106. Available at: http://www.bmj.com/content/315/7116/1105.short [Accessed April 12, 2015].

Chen, M., Forrester, J. V & Xu, H., 2011. Dysregulation in retinal para-inflammation and age-related retinal degeneration in CCL2 or CCR2 deficient mice. *PloS one*, 6(8), p.e22818. Available at: http://journals.plos.org/plosone/article?id=10.1371/journal.pone.0022818 [Accessed June 6, 2015].

Cheung, N., Mitchell, P. & Wong, T.Y., 2010. Diabetic retinopathy. *Lancet*, 376(9735), pp.124–36. Available at: http://www.sciencedirect.com/science/article/pii/S0140673609621243 [Accessed September 26, 2014].

Chronopoulos, A. et al., 2011. High glucose-induced altered basement membrane composition and structure increases trans-endothelial permeability: implications for diabetic retinopathy. *Current eye research*, 36(8), pp.747–53. Available at: http://informahealthcare.com/doi/abs/10.3109/02713683.2011.585735 [Accessed July 21, 2015].

Ciulla, T.A., Amador, A.G. & Zinman, B., 2003. Diabetic Retinopathy and Diabetic Macular Edema: Pathophysiology, screening, and novel therapies. *Diabetes Care*, 26(9), pp.2653–2664. Available at: http://care.diabetesjournals.org/content/26/9/2653.full [Accessed April 29, 2015].

Cook, B. et al., 1995. Apoptotic photoreceptor degeneration in experimental retinal detachment. *Investigative ophthalmology & visual science*, 36(6), pp.990–6. Available at: http://www.ncbi.nlm.nih.gov/pubmed/7730033 [Accessed July 4, 2015].

Cordeiro, M.F. et al., 2004. Real-time imaging of single nerve cell apoptosis in retinal neurodegeneration. *Proceedings of the National Academy of Sciences of the United States of America*, 101(36), pp.13352–6. Available at: http://www.pnas.org/content/101/36/13352.short [Accessed October 26, 2013].

da Cruz, L., 2008. New developments in age-related macular degeneration. *Community eye health / International Centre for Eye Health*, 21(67), p.50. Available at: http://www.pubmedcentral.nih.gov/articlerender.fcgi?artid=2580067&tool=pmcentrez&rendertype=abstract [Accessed February 17, 2014].

Csukas, S. et al., 1990. Time course of rabbit ocular inflammatory response and mediator release after intravitreal endotoxin. *Investigative Ophthalmology & Visual Science*, 31(2), pp.382–387. Available at: http://iovs.arvojournals.org/article.aspx?articleid=2199562&resultClick=1

[Accessed July 4, 2015].

Cunha-Vaz, J.G., 1976. The blood-retinal barriers. *Documenta ophthalmologica. Advances in ophthalmology*, 41(2), pp.287–327. Available at: http://www.ncbi.nlm.nih.gov/pubmed/1009819 [Accessed August 26, 2015].

Dahl-Jorgensen, K. et al., 1985. Rapid tightening of blood glucose control leads to transient deterioration of retinopathy in insulin dependent diabetes mellitus: the Oslo study. *BMJ*, 290(6471), pp.811–815. Available at: http://www.bmj.com/content/290/6471/811.short [Accessed April 12, 2015].

Dardano, A. et al., 2014. Optimal therapy of type 2 diabetes: a controversial challenge. *Aging*, 6(3), pp.187–206. Available at: http://www.pubmedcentral.nih.gov/articlerender.fcgi?artid=4012936&tool=pmcentrez&rendertype=abstract [Accessed July 12, 2015].

Dawson, D.W., 1999. Pigment Epithelium-Derived Factor: A Potent Inhibitor of Angiogenesis. *Science*, 285(5425), pp.245–248. Available at: http://www.sciencemag.org/content/285/5425/245 [Accessed June 9, 2015].

Dawson, D.W. et al., 1999. Pigment epithelium-derived factor: a potent inhibitor of angiogenesis. *Science (New York, N.Y.)*, 285(5425), pp.245–8. Available at: http://www.ncbi.nlm.nih.gov/pubmed/10398599 [Accessed July 3, 2015].

Decanini, A. et al., 2008. Human retinal pigment epithelium proteome changes in early diabetes. *Diabetologia*, 51(6), pp.1051–1061. Available at: http://link.springer.com/10.1007/s00125-008-0991-2 [Accessed March 17, 2015].

Deissler, H.L., Deissler, H. & Lang, G.E., 2012. Actions of bevacizumab and ranibizumab on microvascular retinal endothelial cells: similarities and differences. *The British journal of ophthalmology*, 96(7), pp.1023–8. Available at: http://bjo.bmj.com/content/96/7/1023.full [Accessed July 21, 2015].

Devendra, D., Liu, E. & Eisenbarth, G.S., 2004. Type 1 diabetes: recent developments. *BMJ (Clinical research ed.)*, 328(7442), pp.750–4. Available at: http://www.bmj.com/content/328/7442/750 [Accessed July 22, 2015].

van Dijk, H.W. et al., 2009. Selective loss of inner retinal layer thickness in type 1 diabetic patients with minimal diabetic retinopathy. *Investigative ophthalmology & visual science*, 50(7), pp.3404–9. Available at: http://www.iovs.org/content/50/7/3404.full [Accessed December 6, 2013].

Dobretsov, M., Romanovsky, D. & Stimers, J.R., 2007. Early diabetic neuropathy: triggers and mechanisms. *World journal of gastroenterology : WJG*, 13(2), pp.175–

91. Available at: http://www.pubmedcentral.nih.gov/articlerender.fcgi?artid=1829411&tool=pmcentrez&rendertype=abstract [Accessed August 11, 2015].

Donath, M.Y. & Shoelson, S.E., 2011. Type 2 diabetes as an inflammatory disease. *Nature reviews. Immunology*, 11(2), pp.98–107. Available at: http://dx.doi.org/10.1038/nri2925 [Accessed February 4, 2015].

Dong, X. et al., 2011. Influence of Dll4 via HIF-1α-VEGF signaling on the angiogenesis of choroidal neovascularization under hypoxic conditions. *PloS one*, 6(4), p.e18481. Available at: http://journals.plos.org/plosone/article?id=10.1371/journal.pone.0018481 [Accessed April 10, 2015].

Donnelly, R., Idris, I. & Forrester, J. V, 2004. Protein kinase C inhibition and diabetic retinopathy: a shot in the dark at translational research. *The British journal of ophthalmology*, 88(1), pp.145–51. Available at: http://www.pubmedcentral.nih.gov/articlerender.fcgi?artid=1771919&tool=pmcentrez&rendertype=abstract [Accessed August 21, 2015].

Dröge, W., 2002. Free radicals in the physiological control of cell function. *Physiological reviews*, 82(1), pp.47–95. Available at: http://www.ncbi.nlm.nih.gov/pubmed/11773609 [Accessed June 13, 2015].

Dyck, P.J. et al., 1999. Risk factors for severity of diabetic polyneuropathy: intensive longitudinal assessment of the Rochester Diabetic Neuropathy Study cohort. *Diabetes Care*, 22(9), pp.1479–1486. Available at: http://care.diabetesjournals.org/content/22/9/1479.abstract?ijkey=5c819ffe9a164d0ad7109beba88d1190f1a6fcd8&keytype2=tf_ipsecsha [Accessed August 2, 2015].

Dyck, P.J. et al., 1993. The prevalence by staged severity of various types of diabetic neuropathy, retinopathy, and nephropathy in a population-based cohort: The Rochester Diabetic Neuropathy Study. *Neurology*, 43(4), pp.817–817. Available at: http://www.neurology.org/content/43/4/817.short [Accessed September 14, 2013].

Early Treatment Diabetic Retinopathy Research Group, 1985. Photocoagulation for Diabetic Macular Edema. *Archives of Ophthalmology*, 103(12), p.1796. Available at: http://archopht.jamanetwork.com/article.aspx?articleid=635820 [Accessed August 18, 2015].

Engerman, R.L. & Kern, T.S., 1995. Retinopathy in animal models of diabetes. *Diabetes / Metabolism Reviews*, 11(2), pp.109–120. Available at:

http://doi.wiley.com/10.1002/dmr.5610110203 [Accessed June 23, 2014].

Estrach, S. et al., 2011. Laminin-binding integrins induce Dll4 expression and Notch signaling in endothelial cells. *Circulation research*, 109(2), pp.172–82. Available at: http://circres.ahajournals.org/content/109/2/172.short [Accessed April 10, 2015].

Falavarjani, K.G. & Nguyen, Q.D., 2013. Adverse events and complications associated with intravitreal injection of anti-VEGF agents: a review of literature. *Eye (London, England)*, 27(7), pp.787–94. Available at: http://dx.doi.org/10.1038/eye.2013.107 [Accessed July 21, 2015].

Ferrara, N. et al., 2006. Development of ranibizumab, an anti-vascular endothelial growth factor antigen binding fragment, as therapy for neovascular age-related macular degeneration. *Retina (Philadelphia, Pa.)*, 26(8), pp.859–70. Available at: http://www.ncbi.nlm.nih.gov/pubmed/17031284 [Accessed February 17, 2014].

Ferrara, N. et al., 2004. Discovery and development of bevacizumab, an anti-VEGF antibody for treating cancer. *Nature reviews. Drug discovery*, 3(5), pp.391–400. Available at: http://dx.doi.org/10.1038/nrd1381 [Accessed December 9, 2014].

Ferrara, N. et al., 1998. Vascular endothelial growth factor is essential for corpus luteum angiogenesis. *Nature Medicine*, 4(3), pp.336–340. Available at: http://dx.doi.org/10.1038/nm0398-336 [Accessed August 26, 2015].

Ferrara, N., 2004. Vascular endothelial growth factor: basic science and clinical progress. *Endocrine reviews*, 25(4), pp.581–611. Available at: http://www.ncbi.nlm.nih.gov/pubmed/15294883 [Accessed July 13, 2015].

Fioretto, P. & Mauer, M., 2007. Histopathology of diabetic nephropathy. *Seminars in nephrology*, 27(2), pp.195–207. Available at: http://www.sciencedirect.com/science/article/pii/S0270929507000149 [Accessed August 11, 2015].

Fisher, S.K. & Lewis, G.P., 2003. Müller cell and neuronal remodeling in retinal detachment and reattachment and their potential consequences for visual recovery: a review and reconsideration of recent data. *Vision Research*, 43(8), pp.887–897. Available at: http://www.sciencedirect.com/science/article/pii/S0042698902006806 [Accessed July 4, 2015].

Fleckenstein, M. et al., 2008. High-resolution spectral domain-OCT imaging in geographic atrophy associated with age-related macular degeneration. *Investigative ophthalmology & visual science*, 49(9), pp.4137–44. Available at: http://iovs.arvojournals.org/Article.aspx?articleid=2164702 [Accessed June 5,

2015].

Flynn, H.W. et al., 1992. Pars Plana Vitrectomy in the Early Treatment Diabetic Retinopathy Study. *Ophthalmology*, 99(9), pp.1351–1357. Available at: http://www.sciencedirect.com/science/article/pii/S0161642092317798 [Accessed August 17, 2015].

Fowler, M.J., 2008. Microvascular and Macrovascular Complications of Diabetes. *Clinical Diabetes*, 26(2), pp.77–82. Available at: http://clinical.diabetesjournals.org/content/26/2/77.short [Accessed November 30, 2014].

Foxton, R.H. et al., 2013. VEGF-A Is Necessary and Sufficient for Retinal Neuroprotection in Models of Experimental Glaucoma. *The American Journal of Pathology*, 182(4), pp.1379–1390. Available at: http://www.sciencedirect.com/science/article/pii/S000294401300045X [Accessed November 4, 2013].

Frank, R.N., 2004. Diabetic retinopathy. *The New England journal of medicine*, 350(1), pp.48–58. Available at: http://www.ncbi.nlm.nih.gov/pubmed/14702427.

FROST-LARSEN, K., LARSEN, H.-W. & SIMONSEN, S.E., 2009. OSCILLATORY POTENTIAL AND NYCTOMETRY IN INSULIN-DEPENDENT DIABETICS. *Acta Ophthalmologica*, 58(6), pp.879–888. Available at: http://doi.wiley.com/10.1111/j.1755-3768.1980.tb08313.x [Accessed October 26, 2013].

Gammons, M. V et al., 2013. Topical antiangiogenic SRPK1 inhibitors reduce choroidal neovascularization in rodent models of exudative AMD. *Investigative ophthalmology & visual science*, 54(9), pp.6052–62. Available at: http://www.pubmedcentral.nih.gov/articlerender.fcgi?artid=3771558&tool=pmcentrez&rendertype=abstract [Accessed August 3, 2015].

Gammons, M.V.R. et al., 2013. SRPK1 inhibition modulates VEGF splicing to reduce pathological neovascularization in a rat model of retinopathy of prematurity. *Investigative ophthalmology & visual science*, 54(8), pp.5797–806. Available at: http://www.iovs.org/content/54/8/5797.full [Accessed February 24, 2014].

Gardner, T.W. et al., 2002. Diabetic retinopathy: more than meets the eye. *Survey of ophthalmology*, 47 Suppl 2(December), pp.S253–62. Available at: http://www.ncbi.nlm.nih.gov/pubmed/12507627.

Gastinger, M.J. et al., 2008. Dendrite remodeling and other abnormalities in the retinal

ganglion cells of Ins2 Akita diabetic mice. *Investigative ophthalmology & visual science*, 49(6), pp.2635–42. Available at: http://www.iovs.org/content/49/6/2635.abstract?ijkey=412af2c578a2f5b2052880205456fa9adc022465&keytype2=tf_ipsecsha [Accessed November 2, 2013].

Geraldes, P. et al., 2009. Activation of PKC-delta and SHP-1 by hyperglycemia causes vascular cell apoptosis and diabetic retinopathy. *Nature medicine*, 15(11), pp.1298–306. Available at: http://dx.doi.org/10.1038/nm.2052 [Accessed October 27, 2013].

Gillies, M. et al., 1997. Effect of high glucose on permeability of retinal capillary endothelium in vitro. *Invest. Ophthalmol. Vis. Sci.*, 38(3), pp.635–642. Available at: http://www.iovs.org/content/38/3/635.short [Accessed March 17, 2015].

Gillies, M.C., 2006. What We Don't Know About Avastin Might Hurt Us. *Archives of Ophthalmology*, 124(10), p.1478. Available at: http://archopht.jamanetwork.com/article.aspx?articleid=418659#ref-eed60008-11 [Accessed November 13, 2013].

Giugliano, D., Ceriello, A. & Paolisso, G., 1996. Oxidative stress and diabetic vascular complications. *Diabetes care*, 19(3), pp.257–67. Available at: http://www.ncbi.nlm.nih.gov/pubmed/8742574 [Accessed May 9, 2014].

Greenberg, D.A. & Jin, K., 2005. From angiogenesis to neuropathology. *Nature*, 438(7070), pp.954–9. Available at: http://dx.doi.org/10.1038/nature04481 [Accessed November 11, 2013].

Gross, J.L. et al., 2004. Diabetic Nephropathy: Diagnosis, Prevention, and Treatment. *Diabetes Care*, 28(1), pp.164–176. Available at: http://care.diabetesjournals.org/content/28/1/164.short [Accessed January 20, 2015].

Grunwald, J.E. et al., 1986. Effect of Panretinal Photocoagulation on Retinal Blood Flow in Proliferative Diabetic Retinopathy. *Ophthalmology*, 93(5), pp.590–595. Available at: http://www.sciencedirect.com/science/article/pii/S0161642086336911 [Accessed February 20, 2015].

Guo, L. et al., 2010. Tracking longitudinal retinal changes in experimental ocular hypertension using the cSLO and spectral domain-OCT. *Investigative ophthalmology & visual science*, 51(12), pp.6504–13. Available at: http://www.iovs.org/content/51/12/6504.full [Accessed April 8, 2015].

Hammes, H.-P. et al., 2004. Angiopoietin-2 Causes Pericyte Dropout in the Normal Retina: Evidence for Involvement in Diabetic Retinopathy. *Diabetes*, 53(4), pp.1104–1110. Available at:

http://diabetes.diabetesjournals.org/content/53/4/1104.long [Accessed August 17, 2015].

Hammes, H.-P., 2013. Optimal treatment of diabetic retinopathy. *Therapeutic advances in endocrinology and metabolism*, 4(2), pp.61–71. Available at: http://tae.sagepub.com/content/early/2013/02/26/2042018813477886.abstract [Accessed March 18, 2015].

Hammes, H.-P. et al., 2002. Pericytes and the Pathogenesis of Diabetic Retinopathy. *Diabetes*, 51(10), pp.3107–3112. Available at: http://diabetes.diabetesjournals.org/content/51/10/3107.long [Accessed August 17, 2015].

Hammes, H.-P., 2005. Pericytes and the pathogenesis of diabetic retinopathy. *Hormone and metabolic research = Hormon- und Stoffwechselforschung = Hormones et métabolisme*, 37 Suppl 1, pp.39–43. Available at: http://europepmc.org/abstract/med/15918109 [Accessed August 13, 2015].

Hammes, H.P. et al., 1999. Differential accumulation of advanced glycation end products in the course of diabetic retinopathy. *Diabetologia*, 42(6), pp.728–36. Available at: http://www.ncbi.nlm.nih.gov/pubmed/10382593 [Accessed August 20, 2015].

Hammes, H.P., Federoff, H.J. & Brownlee, M., 1995. Nerve growth factor prevents both neuroretinal programmed cell death and capillary pathology in experimental diabetes. *Molecular medicine (Cambridge, Mass.)*, 1(5), pp.527–34. Available at: http://www.pubmedcentral.nih.gov/articlerender.fcgi?artid=2229962&tool=pmcentrez&rendertype=abstract [Accessed October 28, 2013].

Harhaj, N.S. et al., 2006. VEGF activation of protein kinase C stimulates occludin phosphorylation and contributes to endothelial permeability. *Investigative ophthalmology & visual science*, 47(11), pp.5106–15. Available at: http://www.iovs.org/content/47/11/5106.full [Accessed October 31, 2013].

Harhaj, N.S. & Antonetti, D.A., 2004. Regulation of tight junctions and loss of barrier function in pathophysiology. *The international journal of biochemistry & cell biology*, 36(7), pp.1206–37. Available at: http://www.sciencedirect.com/science/article/pii/S1357272503002978 [Accessed March 11, 2015].

Harper, S.J. & Bates, D.O., 2008. VEGF-A splicing: the key to anti-angiogenic therapeutics? *Nature reviews. Cancer*, 8(11Harper, S. J., & Bates, D. O. (2008). VEGF-A splicing: the key to anti-angiogenic therapeutics? Nature reviews. Cancer,

8(11), 880–7. doi:10.1038/nrc2505), pp.880–7. Available at: http://dx.doi.org/10.1038/nrc2505 [Accessed April 8, 2013].

HART, W. et al., 1999. Measurement and classification of retinal vascular tortuosity. *International Journal of Medical Informatics*, 53(2-3), pp.239–252. Available at: http://www.sciencedirect.com/science/article/pii/S1386505698001634 [Accessed March 21, 2015].

Heier, J.S. et al., 2012. Intravitreal aflibercept (VEGF trap-eye) in wet age-related macular degeneration. *Ophthalmology*, 119(12), pp.2537–48. Available at: http://www.sciencedirect.com/science/article/pii/S0161642012008652 [Accessed January 23, 2014].

Hellström, M. et al., 2007. Dll4 signalling through Notch1 regulates formation of tip cells during angiogenesis. *Nature*, 445(7129), pp.776–80. Available at: http://www.ncbi.nlm.nih.gov/pubmed/17259973 [Accessed September 4, 2014].

Hirschi, K.K. & D'Amore, P.A., 1996. Pericytes in the microvasculature. *Cardiovascular Research*, 32(4), pp.687–698. Available at: http://cardiovascres.oxfordjournals.org/content/32/4/687.long [Accessed August 17, 2015].

Ho, J.J.D., Man, H.S.J. & Marsden, P.A., 2012. Nitric oxide signaling in hypoxia. *Journal of molecular medicine (Berlin, Germany)*, 90(3), pp.217–31. Available at: http://www.ncbi.nlm.nih.gov/pubmed/22349396 [Accessed March 18, 2015].

Hoeben, A. et al., 2004. Vascular endothelial growth factor and angiogenesis. *Pharmacological reviews*, 56(4), pp.549–80. Available at: http://pharmrev.aspetjournals.org/content/56/4/549.full [Accessed January 26, 2015].

Holash, J. et al., 2002. VEGF-Trap: a VEGF blocker with potent antitumor effects. *Proceedings of the National Academy of Sciences of the United States of America*, 99(17), pp.11393–8. Available at: http://www.pnas.org/content/99/17/11393 [Accessed July 5, 2015].

Holz, F.G. et al., 2001. Fundus autofluorescence and development of geographic atrophy in age-related macular degeneration. *Investigative ophthalmology & visual science*, 42(5), pp.1051–6. Available at: http://europepmc.org/abstract/med/11274085 [Accessed June 17, 2015].

Hua, J. et al., 2010. Recombinant human VEGF165b inhibits experimental choroidal neovascularization. *Investigative ophthalmology & visual science*, 51(8), pp.4282–8. Available at:

http://www.iovs.org/content/51/8/4282.abstract?ijkey=c1ba62477969580df28ee14091a8e4f026c10408&keytype2=tf_ipsecsha [Accessed February 24, 2014].

Hulse, R.P. et al., 2014a. Regulation of alternative VEGF-A mRNA splicing is a therapeutic target for analgesia. *Neurobiology of disease*, 71, pp.245–59. Available at: http://www.pubmedcentral.nih.gov/articlerender.fcgi?artid=4194316&tool=pmcentrez&rendertype=abstract [Accessed August 3, 2015].

Hulse, R.P. et al., 2014b. Regulation of alternative VEGF-A mRNA splicing is a therapeutic target for analgesia. *Neurobiology of disease*, 71, pp.245–59. Available at: http://www.researchgate.net/publication/264986492_Regulation_of_alternative_VEGF-A_mRNA_splicing_is_a_therapeutic_target_for_analgesia [Accessed April 12, 2015].

Hulse, R.P. et al., 2015. Vascular endothelial growth factor-A165b prevents diabetic neuropathic pain and sensory neuronal degeneration. *Clinical science (London, England : 1979)*, 129(8), pp.741–56. Available at: http://europepmc.org/abstract/med/26201024 [Accessed August 4, 2015].

Inoguchi, T. et al., 2000. High glucose level and free fatty acid stimulate reactive oxygen species production through protein kinase C--dependent activation of NAD(P)H oxidase in cultured vascular cells. *Diabetes*, 49(11), pp.1939–1945. Available at: http://diabetes.diabetesjournals.org/content/49/11/1939.short [Accessed July 29, 2015].

Ishida, S., 2003. VEGF164 Is Proinflammatory in the Diabetic Retina. *Investigative Ophthalmology & Visual Science*, 44(5), pp.2155–2162. Available at: http://www.iovs.org/content/44/5/2155.full [Accessed October 31, 2013].

Javey, G., Schwartz, S.G. & Flynn, H.W., 2012. Emerging pharmacotherapies for diabetic macular edema. *Experimental Diabetes Research*, 2012.

Jayandharan, G.R. et al., 2011. Activation of the NF-kappaB pathway by adeno-associated virus (AAV) vectors and its implications in immune response and gene therapy. *Proceedings of the National Academy of Sciences of the United States of America*, 108(9), pp.3743–8. Available at: http://www.pnas.org/content/108/9/3743?ijkey=ff01212f3f61e425e58fec8fcf6af3195bbedbde&keytype2=tf_ipsecsha [Accessed July 5, 2015].

Jeansson, M. & Haraldsson, B., 2006. Morphological and functional evidence for an

important role of the endothelial cell glycocalyx in the glomerular barrier. *American journal of physiology. Renal physiology*, 290(1), pp.F111–6. Available at: http://ajprenal.physiology.org/content/290/1/F111 [Accessed August 11, 2015].

Jin, K. et al., 2002. Vascular endothelial growth factor (VEGF) stimulates neurogenesis in vitro and in vivo. *Proceedings of the National Academy of Sciences of the United States of America*, 99(18), pp.11946–50. Available at: http://www.pnas.org/content/99/18/11946.long [Accessed November 13, 2013].

Jin, K.L., Mao, X.O. & Greenberg, D.A., 2000. Vascular endothelial growth factor: Direct neuroprotective effect in in vitro ischemia. *Proceedings of the National Academy of Sciences*, 97(18), pp.10242–10247. Available at: http://www.pnas.org/content/97/18/10242 [Accessed October 26, 2013].

Joussen, A.M. et al., 2004. A central role for inflammation in the pathogenesis of diabetic retinopathy. *FASEB journal : official publication of the Federation of American Societies for Experimental Biology*, 18(12), pp.1450–2. Available at: http://www.fasebj.org/content/18/12/1450.short [Accessed October 27, 2013].

Juen, S., 1990. Electrophysiological Changes in Juvenile Diabetics Without Retinopathy. *Archives of Ophthalmology*, 108(3), p.372. Available at: http://archopht.jamanetwork.com/article.aspx?articleid=638321 [Accessed October 26, 2013].

Kaiser, N. et al., 1993. Differential Regulation of Glucose Transport and Transporters by Glucose in Vascular Endothelial and Smooth Muscle Cells. *Diabetes*, 42(1), pp.80–89. Available at: http://diabetes.diabetesjournals.org/content/42/1/80.short [Accessed August 20, 2015].

Kaur, C., Foulds, W.S. & Ling, E.A., 2008. Blood-retinal barrier in hypoxic ischaemic conditions: basic concepts, clinical features and management. *Progress in retinal and eye research*, 27(6), pp.622–47. Available at: http://www.sciencedirect.com/science/article/pii/S1350946208000554 [Accessed August 27, 2015].

Kawamura, H. et al., 2008. Vascular endothelial growth factor (VEGF)-A165b is a weak in vitro agonist for VEGF receptor-2 due to lack of coreceptor binding and deficient regulation of kinase activity. *Cancer research*, 68(12), pp.4683–92. Available at: http://cancerres.aacrjournals.org/content/68/12/4683.short [Accessed August 24, 2015].

Kern, T.S. et al., 2010. Comparison of three strains of diabetic rats with respect to the rate

at which retinopathy and tactile allodynia develop. *Molecular vision*, 16, pp.1629–39. Available at: http://www.pubmedcentral.nih.gov/articlerender.fcgi?artid=2927372&tool=pmcentrez&rendertype=abstract [Accessed October 31, 2013].

Kern, T.S. et al., 2000. Response of Capillary Cell Death to Aminoguanidine Predicts the Development of Retinopathy: Comparison of Diabetes and Galactosemia. *Invest. Ophthalmol. Vis. Sci.*, 41(12), pp.3972–3978. Available at: http://www.iovs.org/content/41/12/3972.abstract?ijkey=eb74fd660c8ea4fd36484d5074373792d946a7cf&keytype2=tf_ipsecsha [Accessed June 23, 2014].

Kern, T.S. & Barber, A.J., 2008. Retinal ganglion cells in diabetes. *The Journal of physiology*, 586(Pt 18), pp.4401–8. Available at: http://jp.physoc.org/content/586/18/4401.full [Accessed October 19, 2013].

Kerrigan, L.A., 1997. TUNEL-Positive Ganglion Cells in Human Primary Open-angle Glaucoma. *Archives of Ophthalmology*, 115(8), p.1031. Available at: http://archopht.jamanetwork.com/article.aspx?articleid=642246 [Accessed October 26, 2013].

Kim, I. et al., 1999. Constitutive Expression of VEGF, VEGFR-1, and VEGFR-2 in Normal Eyes. *Invest. Ophthalmol. Vis. Sci.*, 40(9), pp.2115–2121. Available at: http://www.iovs.org/content/40/9/2115.short [Accessed November 16, 2013].

Kim, I. et al., 1999. Constitutive expression of VEGF, VEGFR-1, and VEGFR-2 in normal eyes. *Investigative ophthalmology & visual science*, 40(9), pp.2115–21. Available at: http://europepmc.org/abstract/med/10440268 [Accessed May 18, 2015].

Klein, R., 1984. The Wisconsin Epidemiologic Study of Diabetic Retinopathy. *Archives of Ophthalmology*, 102(4), p.520. Available at: http://archopht.jamanetwork.com/article.aspx?articleid=635006 [Accessed October 26, 2013].

Kletzky, D.L., Tung, W.H. & Chylack, L.T., 1986. The protective effect of glucose on soluble rat lens hexokinase in the presence of oxidative stress. *Current eye research*, 5(6), pp.433–9. Available at: http://www.ncbi.nlm.nih.gov/pubmed/3015494 [Accessed March 17, 2015].

Klimczak, R.R. et al., 2009. A novel adeno-associated viral variant for efficient and selective intravitreal transduction of rat Müller cells. *PloS one*, 4(10), p.e7467. Available at:

http://journals.plos.org/plosone/article?id=10.1371/journal.pone.0007467 [Accessed July 5, 2015].

Koblizek, T.I. et al., 1998. Angiopoietin-1 induces sprouting angiogenesis in vitro. *Current Biology*, 8(9), pp.529–532. Available at: http://www.sciencedirect.com/science/article/pii/S0960982298702052 [Accessed August 13, 2015].

Kohner, E.M. & Henkind, P., 1970. Correlation of fluorescein angiogram and retinal digest in diabetic retinopathy. *American journal of ophthalmology*, 69(3), pp.403–14. Available at: http://www.ncbi.nlm.nih.gov/pubmed/4907465 [Accessed August 17, 2015].

Konopatskaya, O. et al., 2006. VEGF165b, an endogenous C-terminal splice variant of VEGF, inhibits retinal neovascularization in mice. *Molecular vision*, 12, pp.626–32. Available at: http://www.ncbi.nlm.nih.gov/pubmed/16735996 [Accessed December 11, 2013].

Kowluru, R.A. & Chan, P.-S., 2007. Oxidative stress and diabetic retinopathy. *Experimental diabetes research*, 2007, p.43603. Available at: http://www.pubmedcentral.nih.gov/articlerender.fcgi?artid=1880867&tool=pmcentrez&rendertype=abstract [Accessed August 20, 2015].

Koya, D. & King, G.L., 1998. Protein kinase C activation and the development of diabetic complications. *Diabetes*, 47(6), pp.859–866. Available at: http://diabetes.diabetesjournals.org/content/47/6/859.short [Accessed April 2, 2015].

Kusaka, M., Kishi, K. & Sokabe, H., 1987. Does so-called streptozocin hypertension exist in rats? *Hypertension*, 10(5), pp.517–521. Available at: http://hyper.ahajournals.org/content/10/5/517.short [Accessed August 5, 2015].

Lai, C.-M. et al., 2005. Long-term evaluation of AAV-mediated sFlt-1 gene therapy for ocular neovascularization in mice and monkeys. *Molecular therapy : the journal of the American Society of Gene Therapy*, 12(4), pp.659–68. Available at: http://dx.doi.org/10.1016/j.ymthe.2005.04.022 [Accessed July 2, 2015].

Lai, C.-M. et al., 2009. rAAV.sFlt-1 Gene Therapy Achieves Lasting Reversal of Retinal Neovascularization in the Absence of a Strong Immune Response to the Viral Vector. *Investigative Opthalmology & Visual Science*, 50(9), p.4279. Available at: http://www.ncbi.nlm.nih.gov/pubmed/19357358 [Accessed August 3, 2015].

Lenzen, S., 2008. The mechanisms of alloxan- and streptozotocin-induced diabetes. *Diabetologia*, 51(2), pp.216–26. Available at:

http://www.ncbi.nlm.nih.gov/pubmed/18087688 [Accessed March 9, 2015].

Leung, D. et al., 1989. Vascular endothelial growth factor is a secreted angiogenic mitogen. *Science*, 246(4935), pp.1306–1309. Available at: http://www.sciencemag.org/content/246/4935/1306.short [Accessed June 9, 2015].

Levick, J.R. & Michel, C.C., 1973. THE PERMEABILITY OF INDIVIDUALLY PERFUSED FROG MESENTERIC CAPILLARIES TO T1824 AND T1824-ALBUMIN AS EVIDENCE FOR A LARGE PORE SYSTEM. *Quarterly Journal of Experimental Physiology and Cognate Medical Sciences*, 58(1), pp.67–85. Available at: http://doi.wiley.com/10.1113/expphysiol.1973.sp002192 [Accessed August 4, 2015].

Lieth, E. et al., 2000. Retinal neurodegeneration: early pathology in diabetes. *Clinical and Experimental Ophthalmology*, 28(1), pp.3–8. Available at: http://doi.wiley.com/10.1046/j.1442-9071.2000.00222.x [Accessed December 17, 2012].

Ma, J. et al., 2011. The effect of siRNA-VEGF on the growth of REC in retinal pigment epithelial cell and retinal endothelial cell co-culture system. *Eye science*, 26(2), pp.75–9. Available at: http://europepmc.org/abstract/med/21692203 [Accessed August 2, 2015].

Maglione, D. et al., 1993. Two alternative mRNAs coding for the angiogenic factor, placenta growth factor (PlGF), are transcribed from a single gene of chromosome 14. *Oncogene*, 8(4), pp.925–31. Available at: http://www.ncbi.nlm.nih.gov/pubmed/7681160 [Accessed August 26, 2015].

Magnussen, A.L. et al., 2010. VEGF-A165b is cytoprotective and antiangiogenic in the retina. *Investigative ophthalmology & visual science*, 51(8), pp.4273–81. Available at: http://www.pubmedcentral.nih.gov/articlerender.fcgi?artid=2910648&tool=pmcentrez&rendertype=abstract [Accessed July 2, 2015].

Manetti, M. et al., 2011. Overexpression of VEGF165b, an inhibitory splice variant of vascular endothelial growth factor, leads to insufficient angiogenesis in patients with systemic sclerosis. *Circulation research*, 109(3), pp.e14–26. Available at: http://circres.ahajournals.org/content/109/3/e14.full [Accessed August 24, 2015].

Mauer, S.M. et al., 1984. Structural-functional relationships in diabetic nephropathy. *The Journal of clinical investigation*, 74(4), pp.1143–55. Available at: http://www.pubmedcentral.nih.gov/articlerender.fcgi?artid=425280&tool=pmcentrez

&rendertype=abstract [Accessed August 11, 2015].

McGahon, M.K. et al., 2007. Diabetes downregulates large-conductance Ca2+-activated potassium beta 1 channel subunit in retinal arteriolar smooth muscle. *Circulation research*, 100(5), pp.703–11. Available at: http://circres.ahajournals.org/content/100/5/703.short [Accessed August 28, 2015].

Miller, J.W. et al., 2013. Vascular endothelial growth factor a in intraocular vascular disease. *Ophthalmology*, 120(1), pp.106–14. Available at: http://www.aaojournal.org/article/S0161-6420(12)00673-2/abstract [Accessed March 11, 2013].

Mingozzi, F. & High, K.A., 2013. Immune responses to AAV vectors: overcoming barriers to successful gene therapy. *Blood*, 122(1), pp.23–36. Available at: http://www.pubmedcentral.nih.gov/articlerender.fcgi?artid=3701904&tool=pmcentrez&rendertype=abstract [Accessed March 25, 2015].

La Morgia, C. et al., 2010. Melanopsin retinal ganglion cells are resistant to neurodegeneration in mitochondrial optic neuropathies. *Brain : a journal of neurology*, 133(Pt 8), pp.2426–38. Available at: http://brain.oxfordjournals.org/content/133/8/2426.full [Accessed October 26, 2013].

Murakami, T., Felinski, E.A. & Antonetti, D.A., 2009. Occludin phosphorylation and ubiquitination regulate tight junction trafficking and vascular endothelial growth factor-induced permeability. *The Journal of biological chemistry*, 284(31), pp.21036–46. Available at: http://www.jbc.org/content/284/31/21036.full [Accessed October 31, 2013].

Naggar, H. et al., 2002. Downregulation of Reduced-Folate Transporter by Glucose in Cultured RPE Cells and in RPE of Diabetic Mice. *Invest. Ophthalmol. Vis. Sci.*, 43(2), pp.556–563. Available at: http://www.iovs.org/content/43/2/556.full [Accessed March 16, 2015].

National Diabetes Data Group, 1979. Classification and Diagnosis of Diabetes Mellitus and Other Categories of Glucose Intolerance. *Diabetes*, 28(12), pp.1039–1057. Available at: http://diabetes.diabetesjournals.org/content/28/12/1039.short [Accessed February 12, 2015].

Nentwich, M.M. & Ulbig, M.W., 2015. Diabetic retinopathy - ocular complications of diabetes mellitus. *World journal of diabetes*, 6(3), pp.489–99. Available at: http://www.pubmedcentral.nih.gov/articlerender.fcgi?artid=4398904&tool=pmcentrez&rendertype=abstract [Accessed April 30, 2015].

Nguyen, Q.D. et al., 2010. Two-year outcomes of the ranibizumab for edema of the mAcula in diabetes (READ-2) study. *Ophthalmology*, 117(11), pp.2146–51. Available at: http://www.ncbi.nlm.nih.gov/pubmed/20855114 [Accessed July 20, 2015].

Nieuwdorp, M. et al., 2006. Endothelial glycocalyx damage coincides with microalbuminuria in type 1 diabetes. *Diabetes*, 55(4), pp.1127–32. Available at: http://www.ncbi.nlm.nih.gov/pubmed/16567538 [Accessed August 11, 2015].

Nissen, N.N. et al., 1998. Vascular endothelial growth factor mediates angiogenic activity during the proliferative phase of wound healing. *The American journal of pathology*, 152(6), pp.1445–52. Available at: http://www.pubmedcentral.nih.gov/articlerender.fcgi?artid=1858442&tool=pmcentrez&rendertype=abstract [Accessed July 17, 2015].

Oishi, A. et al., 2013. Long-term effect of intravitreal injection of anti-VEGF agent for visual acuity and chorioretinal atrophy progression in myopic choroidal neovascularization. *Graefe's archive for clinical and experimental ophthalmology = Albrecht von Graefes Archiv für klinische und experimentelle Ophthalmologie*, 251(1), pp.1–7. Available at: http://www.ncbi.nlm.nih.gov/pubmed/22527326 [Accessed November 13, 2013].

Omri, S. et al., 2011. Microglia/macrophages migrate through retinal epithelium barrier by a transcellular route in diabetic retinopathy: role of PKCζ in the Goto Kakizaki rat model. *The American journal of pathology*, 179(2), pp.942–53. Available at: http://www.sciencedirect.com/science/article/pii/S000294401100424X [Accessed February 25, 2015].

Oshitari, T. et al., 2008. Mitochondria- and caspase-dependent cell death pathway involved in neuronal degeneration in diabetic retinopathy. *The British journal of ophthalmology*, 92(4), pp.552–6. Available at: http://bjo.bmj.com/content/92/4/552.abstract?ijkey=140ae48cd121848e60ce869148def1fef25d343b&keytype2=tf_ipsecsha [Accessed November 1, 2013].

Pang, J.-J. et al., 2010. Achromatopsia as a potential candidate for gene therapy. *Advances in experimental medicine and biology*, 664, pp.639–46. Available at: http://www.pubmedcentral.nih.gov/articlerender.fcgi?artid=3608407&tool=pmcentrez&rendertype=abstract [Accessed August 27, 2015].

Papadopoulos, N. et al., 2012. Binding and neutralization of vascular endothelial growth factor (VEGF) and related ligands by VEGF Trap, ranibizumab and bevacizumab.

Angiogenesis, 15(2), pp.171–85. Available at: http://www.pubmedcentral.nih.gov/articlerender.fcgi?artid=3338918&tool=pmcentrez&rendertype=abstract [Accessed February 17, 2014].

Parekh, D.B., Ziegler, W. & Parker, P.J., 2000. Multiple pathways control protein kinase C phosphorylation. *The EMBO journal*, 19(4), pp.496–503. Available at: http://embojnl.embopress.org/content/19/4/496.abstract [Accessed August 20, 2015].

Pautler, E. & Ennis, S., 1980. The effect of induced diabetes on the electroretinogram components of the pigmented rat. *Invest. Ophthalmol. Vis. Sci.*, 19(6), pp.702–705. Available at: http://www.iovs.org/content/19/6/702.abstract?ijkey=7602f5321fdaef33b9defb331543ebdb664520c3&keytype2=tf_ipsecsha [Accessed March 17, 2015].

Pavan, B., Capuzzo, A. & Forlani, G., 2014. High glucose-induced barrier impairment of human retinal pigment epithelium is ameliorated by treatment with Goji berry extracts through modulation of cAMP levels. *Experimental eye research*, 120, pp.50–4. Available at: http://www.sciencedirect.com/science/article/pii/S0014483513003503 [Accessed January 28, 2015].

Pe'er, J. et al., 1995. Hypoxia-induced expression of vascular endothelial growth factor by retinal cells is a common factor in neovascularizing ocular diseases. *Laboratory investigation; a journal of technical methods and pathology*, 72(6), pp.638–45. Available at: http://europepmc.org/abstract/med/7540233 [Accessed August 4, 2015].

Peng, S., Adelman, R.A. & Rizzolo, L.J., 2010. Minimal effects of VEGF and anti-VEGF drugs on the permeability or selectivity of RPE tight junctions. *Investigative ophthalmology & visual science*, 51(6), pp.3216–25. Available at: http://iovs.arvojournals.org/article.aspx?articleid=2186450 [Accessed July 21, 2015].

Perrin, R.M. et al., 2005. Diabetic retinopathy is associated with a switch in splicing from anti- to pro-angiogenic isoforms of vascular endothelial growth factor. *Diabetologia*, 48(11), pp.2422–7. Available at: http://www.ncbi.nlm.nih.gov/pubmed/16193288 [Accessed December 11, 2013].

Pomero, F. et al., 2003. Effects of protein kinase C inhibition and activation on proliferation and apoptosis of bovine retinal pericytes. *Diabetologia*, 46(3), pp.416–9. Available at: http://www.ncbi.nlm.nih.gov/pubmed/12687341 [Accessed August

21, 2015].

Poulaki, V. et al., 2002. Acute intensive insulin therapy exacerbates diabetic blood-retinal barrier breakdown via hypoxia-inducible factor-1alpha and VEGF. *The Journal of clinical investigation*, 109(6), pp.805–15. Available at: http://www.pubmedcentral.nih.gov/articlerender.fcgi?artid=150907&tool=pmcentrez&rendertype=abstract [Accessed December 10, 2012].

Qaum, T. et al., 2001. VEGF-initiated blood-retinal barrier breakdown in early diabetes. *Investigative ophthalmology & visual science*, 42(10), pp.2408–13. Available at: http://www.iovs.org/content/42/10/2408.abstract [Accessed March 25, 2015].

Qin, D., Zheng, X. & Jiang, Y., 2013. Apelin-13 induces proliferation, migration, and collagen I mRNA expression in human RPE cells via PI3K/Akt and MEK/Erk signaling pathways. *Molecular vision*, 19, pp.2227–36. Available at: http://www.pubmedcentral.nih.gov/articlerender.fcgi?artid=3820432&tool=pmcentrez&rendertype=abstract [Accessed March 17, 2015].

Rennel, E.S. et al., 2008. Recombinant human VEGF165b protein is an effective anti-cancer agent in mice. *European journal of cancer (Oxford, England : 1990)*, 44(13), pp.1883–94. Available at: http://www.pubmedcentral.nih.gov/articlerender.fcgi?artid=2565644&tool=pmcentrez&rendertype=abstract [Accessed March 25, 2015].

Robinson, R. et al., 2012a. Update on animal models of diabetic retinopathy: from molecular approaches to mice and higher mammals. *Disease models & mechanisms*, 5(4), pp.444–56. Available at: http://dmm.biologists.org/content/5/4/444.full [Accessed December 20, 2012].

Robinson, R. et al., 2012b. Update on animal models of diabetic retinopathy: from molecular approaches to mice and higher mammals. *Disease models & mechanisms*, 5(4), pp.444–56. Available at: http://www.pubmedcentral.nih.gov/articlerender.fcgi?artid=3380708&tool=pmcentrez&rendertype=abstract [Accessed January 7, 2015].

Rosenbaum, J.T. et al., 1980. Endotoxin-induced uveitis in rats as a model for human disease. *Nature*, 286(5773), pp.611–613. Available at: http://www.nature.com/nature/journal/v286/n5773/pdf/286611a0.pdf [Accessed July 5, 2015].

Rucker, H.K., Wynder, H.J. & Thomas, W.E., 2000. Cellular mechanisms of CNS pericytes. *Brain Research Bulletin*, 51(5), pp.363–369. Available at:

http://www.sciencedirect.com/science/article/pii/S0361923099002609 [Accessed August 17, 2015].

Rydén, L. et al., 2007. Guidelines on diabetes, pre-diabetes, and cardiovascular diseases: executive summary. The Task Force on Diabetes and Cardiovascular Diseases of the European Society of Cardiology (ESC) and of the European Association for the Study of Diabetes (EASD). *European heart journal*, 28(1), pp.88–136. Available at: http://eurheartj.oxfordjournals.org/content/28/1/88.short#sec-3 [Accessed August 10, 2015].

Saint-Geniez, M. et al., 2009a. An essential role for RPE-derived soluble VEGF in the maintenance of the choriocapillaris. *Proceedings of the National Academy of Sciences of the United States of America*, 106(44), pp.18751–6. Available at: http://www.pubmedcentral.nih.gov/articlerender.fcgi?artid=2774033&tool=pmcentrez&rendertype=abstract [Accessed February 10, 2015].

Saint-Geniez, M. et al., 2009b. An essential role for RPE-derived soluble VEGF in the maintenance of the choriocapillaris. *Proceedings of the National Academy of Sciences of the United States of America*, 106(44), pp.18751–6. Available at: http://www.pnas.org/content/106/44/18751.short [Accessed February 10, 2015].

Schlamp, C.L. et al., 2013. Evaluation of the percentage of ganglion cells in the ganglion cell layer of the rodent retina. *Molecular vision*, 19, pp.1387–96. Available at: http://www.pubmedcentral.nih.gov/articlerender.fcgi?artid=3695759&tool=pmcentrez&rendertype=abstract [Accessed March 22, 2015].

Schlichtenbrede, F.C. et al., 2003. Intraocular gene delivery of ciliary neurotrophic factor results in significant loss of retinal function in normal mice and in the Prph2Rd2/Rd2 model of retinal degeneration. *Gene therapy*, 10(6), pp.523–7. Available at: http://dx.doi.org/10.1038/sj.gt.3301929 [Accessed July 5, 2015].

Segawa, M. et al., 1988. The development of electroretinogram abnormalities and the possible role of polyol pathway activity in diabetic hyperglycemia and galactosemia. *Metabolism*, 37(5), pp.454–460. Available at: http://www.metabolismjournal.com/article/0026049588900467/fulltext [Accessed September 28, 2014].

Shakib, M. & Cunha-Vaz, J.G., 1966. Studies on the permeability of the blood-retinal barrier. *Experimental Eye Research*, 5(3), pp.229–IN16. Available at: http://www.sciencedirect.com/science/article/pii/S0014483566800118 [Accessed August 26, 2015].

Shen, F. et al., 2015. Inhibition of pathological brain angiogenesis through systemic delivery of AAV vector expressing soluble FLT1. *Gene therapy*. Available at: http://dx.doi.org/10.1038/gt.2015.57 [Accessed August 3, 2015].

Shibuya, M., Ito, N. & Claesson-Welsh, L., 1999. Structure and Function of Vascular Endothelial Growth Factor Receptor-1 and -2. In L. Claesson-Welsh, ed. *Vascular Growth Factors and Angiogenesis SE - 4*. Current Topics in Microbiology and Immunology. Springer Berlin Heidelberg, pp. 59–83. Available at: http://dx.doi.org/10.1007/978-3-642-59953-8_4.

Shima, D. et al., 1996. Cloning and mRNA expression of vascular endothelial growth factor in ischemic retinas of Macaca fascicularis. *Invest. Ophthalmol. Vis. Sci.*, 37(7), pp.1334–1340. Available at: http://www.iovs.org/content/37/7/1334.short [Accessed April 9, 2015].

Shima, D.T. et al., 1995. Hypoxic induction of endothelial cell growth factors in retinal cells: identification and characterization of vascular endothelial growth factor (VEGF) as the mitogen. *Molecular medicine (Cambridge, Mass.)*, 1(2), pp.182–93. Available at: http://www.pubmedcentral.nih.gov/articlerender.fcgi?artid=2229943&tool=pmcentrez&rendertype=abstract [Accessed November 16, 2013].

Shima, D.T. et al., 2004. VEGF-mediated neuroprotection in ischemic retina. *ARVO Meeting Abstracts*, 45(5), p.3270. Available at: http://abstracts.iovs.org/cgi/content/abstract/45/5/3270 [Accessed November 4, 2013].

Simó, R. et al., 2010. The retinal pigment epithelium: something more than a constituent of the blood-retinal barrier--implications for the pathogenesis of diabetic retinopathy. *Journal of biomedicine & biotechnology*, 2010, p.190724. Available at: http://www.pubmedcentral.nih.gov/articlerender.fcgi?artid=2825554&tool=pmcentrez&rendertype=abstract [Accessed March 17, 2015].

Simó, R. & Hernández, C., 2008. Intravitreous anti-VEGF for diabetic retinopathy: hopes and fears for a new therapeutic strategy. *Diabetologia*, 51(9), pp.1574–80. Available at: http://www.ncbi.nlm.nih.gov/pubmed/18404258 [Accessed April 13, 2015].

Simo, R., Sundstrom, J.M. & Antonetti, D.A., 2014. Ocular Anti-VEGF Therapy for Diabetic Retinopathy: The Role of VEGF in the Pathogenesis of Diabetic Retinopathy. *Diabetes Care*, 37(4), pp.893–899. Available at: http://care.diabetesjournals.org/content/37/4/893.full [Accessed July 5, 2015].

Singh, R. et al., 2001. Advanced glycation end-products: a review. *Diabetologia*, 44(2), pp.129–46. Available at: http://www.ncbi.nlm.nih.gov/pubmed/11270668 [Accessed July 16, 2015].

Soker, S. et al., 1998. Neuropilin-1 is expressed by endothelial and tumor cells as an isoform-specific receptor for vascular endothelial growth factor. *Cell*, 92(6), pp.735–745.

Steinberg, R.H., Wood, I. & Hogan, M.J., 1977. Pigment epithelial ensheathment and phagocytosis of extrafoveal cones in human retina. *Philosophical transactions of the Royal Society of London. Series B: Biological sciences*, 277(958), pp.459–474. Available at: http://www.scopus.com/inward/record.url?eid=2-s2.0-0017784901&partnerID=tZOtx3y1.

Stewart, M.W., 2014. Pharmacokinetics, pharmacodynamics and pre-clinical characteristics of ophthalmic drugs that bind VEGF. *Expert review of clinical pharmacology*, 7(2), pp.167–80. Available at: http://informahealthcare.com/doi/full/10.1586/17512433.2014.884458 [Accessed February 17, 2014].

Stitt, A.W. et al., 1997. Advanced glycation end products (AGEs) co-localize with AGE receptors in the retinal vasculature of diabetic and of AGE-infused rats. *The American journal of pathology*, 150(2), pp.523–31. Available at: http://www.pubmedcentral.nih.gov/articlerender.fcgi?artid=1858286&tool=pmcentrez&rendertype=abstract [Accessed August 17, 2015].

Stitt, A.W. et al., 2000. Advanced glycation end products induce blood-retinal barrier dysfunction in normoglycemic rats. *Molecular cell biology research communications : MCBRC*, 3(6), pp.380–8. Available at: http://www.ncbi.nlm.nih.gov/pubmed/11032761 [Accessed July 7, 2015].

Stitt, A.W. et al., 2015. The progress in understanding and treatment of diabetic retinopathy. *Progress in retinal and eye research*, 51, pp.156–186. Available at: http://www.sciencedirect.com/science/article/pii/S135094621500066X [Accessed January 20, 2016].

Stratton, I.M., 2000. Association of glycaemia with macrovascular and microvascular complications of type 2 diabetes (UKPDS 35): prospective observational study. *BMJ*, 321(7258), pp.405–412. Available at: http://www.bmj.com/content/321/7258/405?linkType=FULL&ck=nck&resid=321/7258/405&journalCode=bmj [Accessed March 10, 2015].

Suchting, S. et al., 2007. The Notch ligand Delta-like 4 negatively regulates endothelial tip cell formation and vessel branching. *Proceedings of the National Academy of Sciences*, 104(9), pp.3225–3230. Available at: http://www.pubmedcentral.nih.gov/articlerender.fcgi?artid=1805603&tool=pmcentrez&rendertype=abstract [Accessed April 10, 2015].

Szkudelski, T., 2001. The mechanism of alloxan and streptozotocin action in B cells of the rat pancreas. *Physiological research / Academia Scientiarum Bohemoslovaca*, 50(6), pp.537–46. Available at: http://europepmc.org/abstract/med/11829314 [Accessed April 13, 2015].

Takahashi, H. et al., 2006. Diabetes-associated Retinal Nerve Fiber Damage Evaluated With Scanning Laser Polarimetry. *American Journal of Ophthalmology*, 142(1), pp.88–94. Available at: http://www.sciencedirect.com/science/article/pii/S0002939406002595 [Accessed November 1, 2013].

Takahashi, K. et al., 2003. Intraocular expression of endostatin reduces VEGF-induced retinal vascular permeability, neovascularization, and retinal detachment. *FASEB journal : official publication of the Federation of American Societies for Experimental Biology*, 17(8), pp.896–8. Available at: http://www.fasebj.org/content/17/8/896.short [Accessed July 3, 2015].

Takata, K., 1996. Glucose Transporters in the Transepithelial Transport of Glucose. *Journal of Electron Microscopy*, 45(4), pp.275–284. Available at: http://jmicro.oxfordjournals.org/content/45/4/275.abstract [Accessed June 9, 2015].

Tang, J. & Kern, T.S., 2011. Inflammation in diabetic retinopathy. *Progress in retinal and eye research*, 30(5), pp.343–58. Available at: http://dx.doi.org/10.1016/j.preteyeres.2011.05.002 [Accessed December 17, 2012].

The Diabetic Retinopathy Research Group, 1981. Photocoagulation Treatment of Proliferative Diabetic Retinopathy. *Ophthalmology*, 88(7), pp.583–600. Available at: http://www.sciencedirect.com/science/article/pii/S0161642081349781 [Accessed August 17, 2015].

The National High Blood Pressure Education Program Working Group, 1994. National High Blood Pressure Education Program Working Group report on hypertension in diabetes. *Hypertension*, 23(2), pp.145–158. Available at: http://hyper.ahajournals.org/content/23/2/145.abstract?ijkey=5e1f4ce4a0a666cd3fbec72f305fd36fefaf4862&keytype2=tf_ipsecsha [Accessed June 12, 2015].

Thichanpiang, P. et al., 2014. TNF-α-induced ICAM-1 expression and monocyte adhesion in human RPE cells is mediated in part through autocrine VEGF stimulation. *Molecular vision*, 20, pp.781–9. Available at: http://www.pubmedcentral.nih.gov/articlerender.fcgi?artid=4057247&tool=pmcentrez&rendertype=abstract [Accessed April 12, 2015].

Titchenell, P.M. et al., 2012. Novel atypical PKC inhibitors prevent vascular endothelial growth factor-induced blood-retinal barrier dysfunction. *The Biochemical journal*, 446(3), pp.455–67. Available at: http://www.biochemj.org/bj/446/bj4460455.htm [Accessed January 18, 2013].

Tomlinson, D.R. & Gardiner, N.J., 2008a. Diabetic neuropathies: components of etiology. *Journal of the peripheral nervous system : JPNS*, 13(2), pp.112–21. Available at: http://www.ncbi.nlm.nih.gov/pubmed/18601656 [Accessed August 11, 2015].

Tomlinson, D.R. & Gardiner, N.J., 2008b. Glucose neurotoxicity. *Nature reviews. Neuroscience*, 9(1), pp.36–45. Available at: http://dx.doi.org/10.1038/nrn2294 [Accessed July 1, 2015].

Vandenberghe, L.H. & Auricchio, A., 2012. Novel adeno-associated viral vectors for retinal gene therapy. *Gene therapy*, 19(2), pp.162–8. Available at: http://dx.doi.org/10.1038/gt.2011.151 [Accessed July 3, 2015].

Vandendriessche, T. et al., 2007. Efficacy and safety of adeno-associated viral vectors based on serotype 8 and 9 vs. lentiviral vectors for hemophilia B gene therapy. *Journal of thrombosis and haemostasis : JTH*, 5(1), pp.16–24. Available at: http://www.ncbi.nlm.nih.gov/pubmed/17002653 [Accessed July 3, 2015].

Villarroel, M. et al., 2009. Effects of high glucose concentration on the barrier function and the expression of tight junction proteins in human retinal pigment epithelial cells. *Experimental eye research*, 89(6), pp.913–20. Available at: http://www.sciencedirect.com/science/article/pii/S0014483509002280 [Accessed March 17, 2015].

Wallow, I.H.L. & Engerman, R.L., 1977. Permeability and patency of retinal blood vessels in experimental diabetes. *INVEST.OPHTHAL.VISUAL SCI.*, 16(5), pp.447–461. Available at: http://www.scopus.com/inward/record.url?eid=2-s2.0-0017376347&partnerID=tZOtx3y1.

Wang, J. et al., 2010. Müller cell-derived VEGF is essential for diabetes-induced retinal inflammation and vascular leakage. *Diabetes*, 59(9), pp.2297–305. Available at: http://diabetes.diabetesjournals.org/content/59/9/2297.full [Accessed October 31,

2013].

Wang, W., Dentler, W.L. & Borchardt, R.T., 2001. VEGF increases BMEC monolayer permeability by affecting occludin expression and tight junction assembly. *Am J Physiol Heart Circ Physiol*, 280(1), pp.H434–440. Available at: http://ajpheart.physiology.org/content/280/1/H434.short [Accessed March 11, 2015].

Wang, Y.L. et al., 2007. Strengthening tight junctions of retinal microvascular endothelial cells by pericytes under normoxia and hypoxia involving angiopoietin-1 signal way. *Eye (London, England)*, 21(12), pp.1501–10. Available at: http://dx.doi.org/10.1038/sj.eye.6702716 [Accessed August 27, 2015].

Wautier, J.L. et al., 1996. Receptor-mediated endothelial cell dysfunction in diabetic vasculopathy. Soluble receptor for advanced glycation end products blocks hyperpermeability in diabetic rats. *The Journal of clinical investigation*, 97(1), pp.238–43. Available at: http://www.pubmedcentral.nih.gov/articlerender.fcgi?artid=507085&tool=pmcentrez&rendertype=abstract [Accessed July 8, 2015].

Weinberger, D. et al., 1995. Non-retinovascular leakage in diabetic maculopathy. *British Journal of Ophthalmology*, 79(8), pp.728–731. Available at: http://bjo.bmj.com/content/79/8/728.short [Accessed March 17, 2015].

Wells, J.A. et al., 2015. Aflibercept, bevacizumab, or ranibizumab for diabetic macular edema. *The New England journal of medicine*, 372(13), pp.1193–203. Available at: http://www.ncbi.nlm.nih.gov/pubmed/25692915 [Accessed May 4, 2015].

Whittles, C.E. et al., 2002. ZM323881, a novel inhibitor of vascular endothelial growth factor-receptor-2 tyrosine kinase activity. *Microcirculation (New York, N.Y. : 1994)*, 9(6), pp.513–22. Available at: http://www.ncbi.nlm.nih.gov/pubmed/12483548 [Accessed June 17, 2015].

Wilkinson, C.P. et al., 2003. Proposed international clinical diabetic retinopathy and diabetic macular edema disease severity scales. *Ophthalmology*, 110(9), pp.1677–82. Available at: http://dx.doi.org/10.1016/S0161-6420(03)00475-5 [Accessed September 13, 2013].

Wolbarsht, M.L. & Landers, M.B., 1980. The rationale of photocoagulation therapy for proliferative diabetic retinopathy: a review and a model. *Ophthalmic surgery*, 11(4), pp.235–45. Available at: http://europepmc.org/abstract/med/6155650 [Accessed August 4, 2015].

Woolard, J. et al., 2004. VEGF165b, an inhibitory vascular endothelial growth factor

splice variant: mechanism of action, in vivo effect on angiogenesis and endogenous protein expression. *Cancer research*, 64(21), pp.7822–35. Available at: http://www.ncbi.nlm.nih.gov/pubmed/15520188 [Accessed November 28, 2014].

Wu, Y., Tang, L. & Chen, B., 2014. Oxidative Stress : Implications for the Development of Diabetic Retinopathy and Antioxidant Therapeutic Perspectives. , 2014.

Xia, P. et al., 1996. Characterization of vascular endothelial growth factor's effect on the activation of protein kinase C, its isoforms, and endothelial cell growth. *The Journal of clinical investigation*, 98(9), pp.2018–26. Available at: http://www.pubmedcentral.nih.gov/articlerender.fcgi?artid=507645&tool=pmcentrez&rendertype=abstract [Accessed August 21, 2015].

Xu, H. et al., 2014. Subretinal Delivery of AAV2-Mediated Human Erythropoietin Gene Is Protective and Safe in Experimental Diabetic Retinopathy. *Investigative Opthalmology & Visual Science*, 55(3), p.1519. Available at: http://iovs.arvojournals.org/article.aspx?articleid=2190043 [Accessed July 2, 2015].

Xu, H.-Z. et al., 2011. RPE barrier breakdown in diabetic retinopathy: seeing is believing. *Journal of ocular biology, diseases, and informatics*, 4(1-2), pp.83–92. Available at: http://www.pubmedcentral.nih.gov/articlerender.fcgi?artid=3342408&tool=pmcentrez&rendertype=abstract [Accessed January 9, 2015].

Xu, H.-Z. & Le, Y.-Z., 2011. Significance of outer blood-retina barrier breakdown in diabetes and ischemia. *Investigative ophthalmology & visual science*, 52(5), pp.2160–4. Available at: http://www.pubmedcentral.nih.gov/articlerender.fcgi?artid=3080181&tool=pmcentrez&rendertype=abstract [Accessed March 16, 2015].

Xu, Q., Qaum, T. & Adamis, A.P., 2001. Sensitive blood-retinal barrier breakdown quantitation using Evans blue. *Investigative ophthalmology & visual science*, 42(3), pp.789–94. Available at: http://www.ncbi.nlm.nih.gov/pubmed/11222542 [Accessed March 25, 2015].

Yafai, Y. et al., 2004. Retinal endothelial angiogenic activity: effects of hypoxia and glial (Müller) cells. *Microcirculation (New York, N.Y. : 1994)*, 11(7), pp.577–86. Available at: http://doi.wiley.com/10.1080/10739680490503375 [Accessed August 27, 2015].

Yki-Järvinen, H., 2004. Thiazolidinediones. *The New England journal of medicine*, 351(11), pp.1106–18. Available at: http://www.ncbi.nlm.nih.gov/pubmed/15356308 [Accessed June 22, 2015].

Young, T.A. et al., 2005. Vascular endothelial growth factor expression and secretion by retinal pigment epithelial cells in high glucose and hypoxia is protein kinase C-dependent. *Experimental eye research*, 80(5), pp.651–62. Available at: http://www.sciencedirect.com/science/article/pii/S0014483504003471 [Accessed July 21, 2015].

Zhou, G. et al., 2001. Role of AMP-activated protein kinase in mechanism of metformin action. *The Journal of clinical investigation*, 108(8), pp.1167–74. Available at: http://www.pubmedcentral.nih.gov/articlerender.fcgi?artid=209533&tool=pmcentrez&rendertype=abstract [Accessed January 26, 2015].

Zhu, J., Huang, X. & Yang, Y., 2009. The TLR9-MyD88 pathway is critical for adaptive immune responses to adeno-associated virus gene therapy vectors in mice. *The Journal of clinical investigation*, 119(8), pp.2388–98. Available at: http://www.jci.org/articles/view/37607 [Accessed July 5, 2015].

List of Abbreviations

AAV – Adeno-associated virus

AGE - Advanced glycation end product

ANOVA – Analysis of variance

Akt – Serine/Threonine specific protein kinase (otherwise known as protein kinase-B (PKB))

AMD – Age-related macular degeneration

ARVO – Association for research in vision and ophthalmology

ASU – Animal services unit

BBB – Blood–brain barrier

BEH – Bristol Eye Hospital

BP – Base pairs

BSA – Bovine serum albumin

BRB – Blood-retina barrier

BRU – Biological resources unit

BSU – Biological services unit

Ca^{2+}- Calcium ions

cDNA – Complementary DNA

CMV - Cytomegalovirus

CNS – Central nervous system

CNV – Choroidal neovascularisation

CSME – Clinically significant macular oedema

Da – Daltons

DAG - Diacylglycerol

DLL4 – Delta–like ligand 4

DR – Diabetic retinopathy

DRG – Dorsal route ganglia

DME – Diabetic macular oedema

DMSO – Dimethyl sulphoxide

DSS – Distal splice site

EB – Evans' blue

ECL – Enhanced chemiluminesence

ECIS – Electric cell-substrate impedance sensing

ELISA – Enzyme-linked immunosorbent assay

eNOS – Endothelial nitric oxide synthase

ERG – Electroretinogram

ERK – Extracellular signal regulated kinases

FCS – Foetal calf serum

FFA – Fundus fluorescein angiography

FDA – Food and Drug Administration

FPLC – Fast protein liquid chromatography

GFP – Green fluorescent protein

GTP – Guanosine triphosphate

HEK – Human embryonic kidney

HBSS – Hank's balanced salt solution

HRP – Horseradish peroxidase

IB4 – Isolectin B4

ICAM – Intracellular adhesion molecule

INL – Inner nuclear layer

IO – Intraocular

IOP – Intraocular pressure

IP - intraperitoneal

IPL – Inner plexiform layer

ITR – Inverted terminal repeat

IVNV – Intravitreal neovascularization

IVT – Intravitreal

kDa – Kilodalton

MW – Molecular weight

NFKB - Nuclear factor kappa B

NV – Neovascularisation

NO – Nitric oxide

OIR – Oxygen induced retinopathy

ONL – Outer nuclear layer

OPL – Outer plexiform layer

PA – Permeability–Surface area product

PAGE – Polyacrylamide gel electrophoresis

PBS – Phosphate buffered saline

PCR – Polymerase chain reaction

PDGF – Pigment derived growth factor

PEI – Polyethylenimine

pERK – Phosphorylated ERK

PFA – Paraformaldehyde

PI3K – Phosphoinositide 3-kinase

PRNV – Pre-retinal neovascularisation

PRP – Pan-retinal laser photocoagulation

pVEGFR2 – Phosphorylated VEGF receptor 2

PSS – Proximal splice site

PVDF – Polyvinylidene fluoride

Q-PCR – Quantitative PCR

RDS – Retina degeneration slow

REC – Retinal endothelial cells

RGC – Retinal ganglion cell

rh – Recombinant human

RIPA – Radioimmunoprecipitation

RK – Rhodopsin kinase

ROP – Retinopathy of prematurity

ROS – Reactive oxygen species

RPE – Retinal pigment epithelium

RPGR – Retinitis pigmentosa GTPase regulator

SD – Sprague-Dawley

SDS – Sodium-dodecyl sulphate

SEM – Standard error of the mean

S-Flt1 – Soluble VEGFR1

SFM – Serum free media

SRPIN340 - SR phosphorylation inhibitor 340

STZ – Streptozotocin

TER – Trans-endothelial resistance

TEER – Trans-epithelial electrode resistance

TD – Tagmentation DNA

TH – Tyrosine hydroxylase

TJ – Tight junction

TNF-α – Tumour Necrosis Factor alpha

TUNEL - Transferase-mediated dUTP nick-end labelling

VSMC – Vascular Smooth Muscle Cells

VEGF – Vascular endothelial growth factor

VEGFR – Vascular endothelial growth factor receptor

VP – Capsid protein

YFP – Yellow fluorescent protein

ZO1 – Zonula Occludens 1

Chapter 7: Appendices

Appendix 1. Evans' blue calculations

a) Evans blue (EB) absorbance in wet weight (µg/g):

$$\frac{EB\ conc\ \left(\frac{\mu g}{ml}\right) X\ formimide\ vol\ (ml)}{Retina\ wet\ weight\ (g)}$$

EB absorbance in dry weight (µg/g): same as (a), substituting wet weight for dry weight

b) EB accumulation in tissue fluid (µg/ml):

$$\frac{EB\ conc\ \left(\frac{\mu g}{ml}\right) x\ formamide\ vol(ml)}{Retina\ wet\ weight\ (g) - dry\ weight\ (g)}$$

c) EB wet weight solute flux (µg/min/g):

$$\frac{EB\ wet\ weight\ absorbance\ (\frac{\mu g}{g})}{Time\ (\text{min})}$$

d) EB dry weight permeability-surface area product (ml/min/g):

$$\frac{EB\ dry\ weight\ solute\ flux\ (\frac{\frac{\mu g}{min}}{g})}{Time\ averaged\ Plasma\ EB\ conc\ \left(\frac{\mu g}{ml}\right) x\ total\ time\ (hr)}$$

Appendix 2. Plasmid Maps

All plasmid maps were generated using Serial Cloner - 5 freeware.

Humanised Renilla reniformis GFP (hrGFP) plasmid under the CMV promoter. Used to generate all AAVs named "AAV.GFP" with AAV2/2 ITRs.

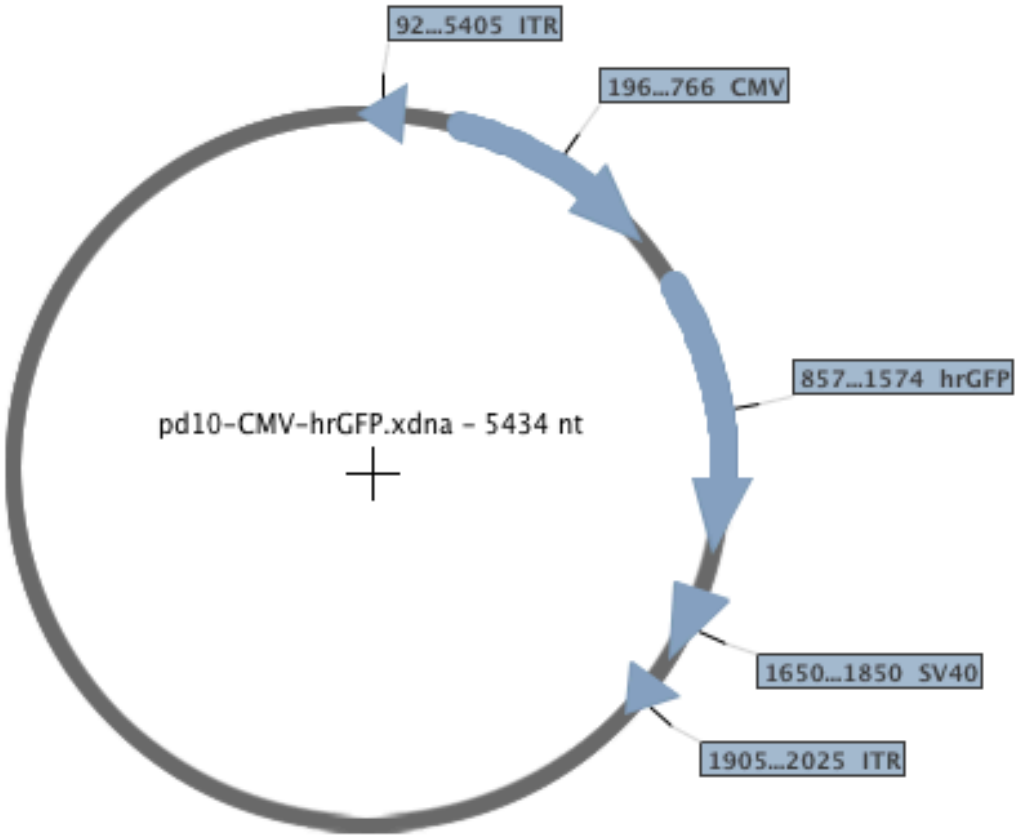

Figure. 7.1. pd10.CMV.hrGFP plasmid map.

Human $VEGF_{165}b$ gene under the CMV promoter. Used to generate all AAVs named "$AAV.VEGF_{165}b$" with AAV2/2 ITRs.

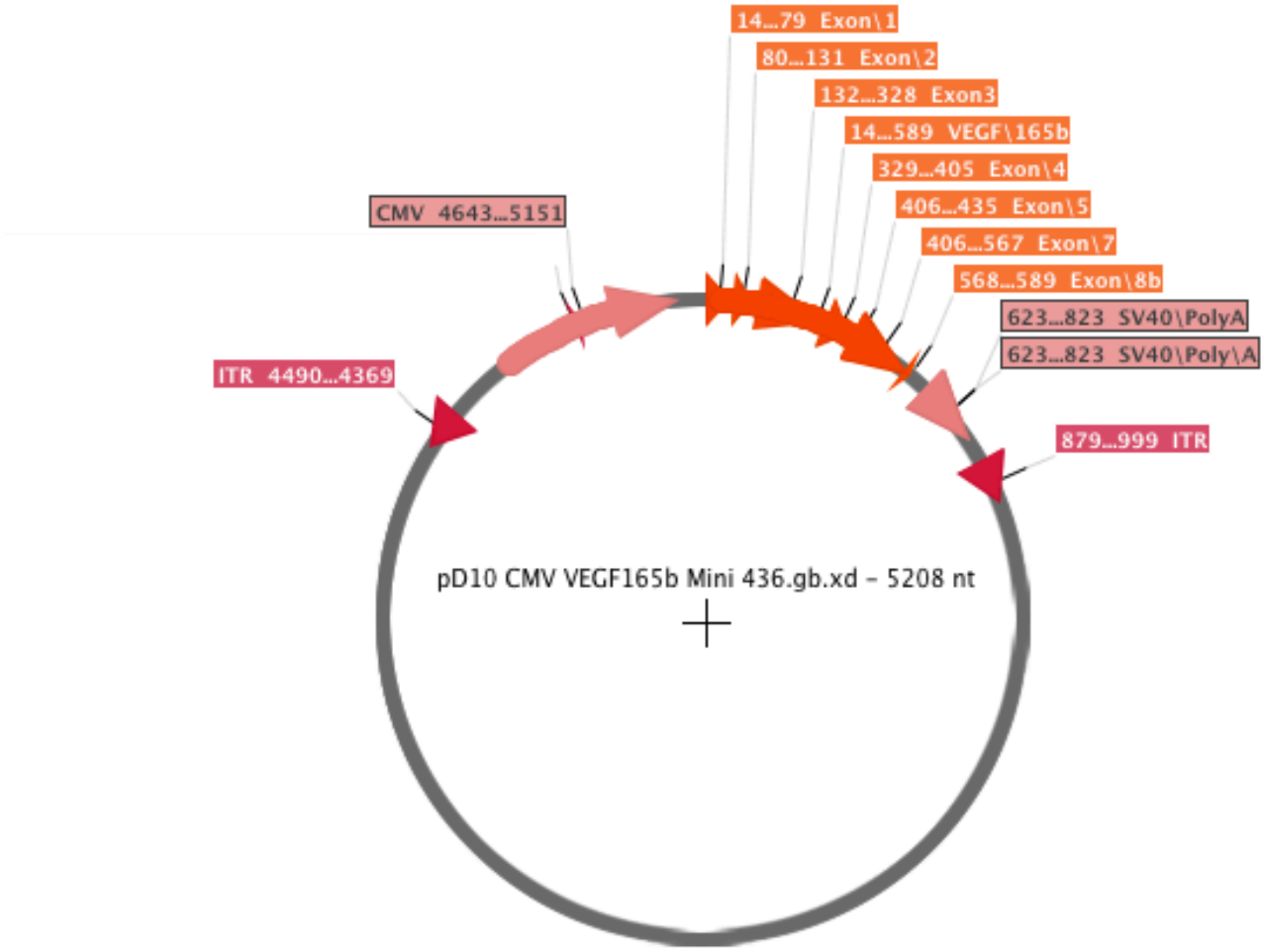

Figure. 7.2. pd10.CMV.$VEGF_{165}b$ plasmid map

Plasmid is a modified version of the pd10.RK.RPGR plasmid, but with no promoter. The RPGR gene is truncated and has no start codon. The AAV genomic construct is based on AAV2/2 ITRs. This plasmid generated all AAVs named "AAV.Null".

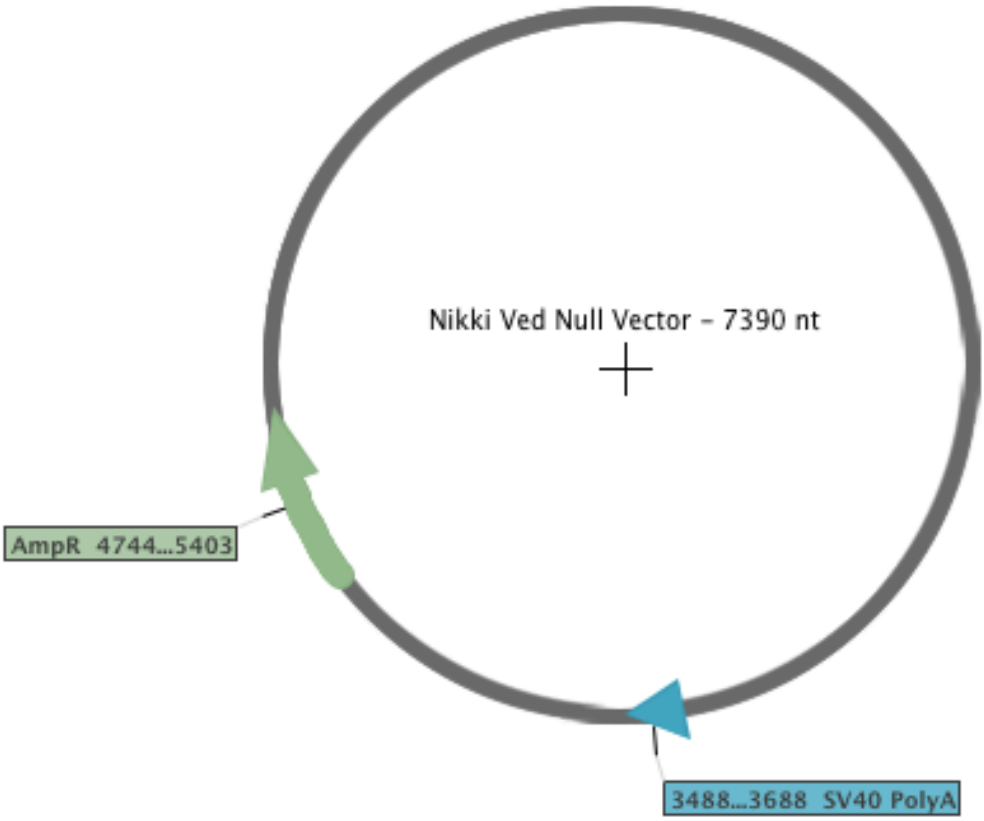

Figure. 7.3. pd10.Null plasmid map

Appendix 3. Plasmid and virus validation

7.3.1.AAV.VEGF$_{165}$b

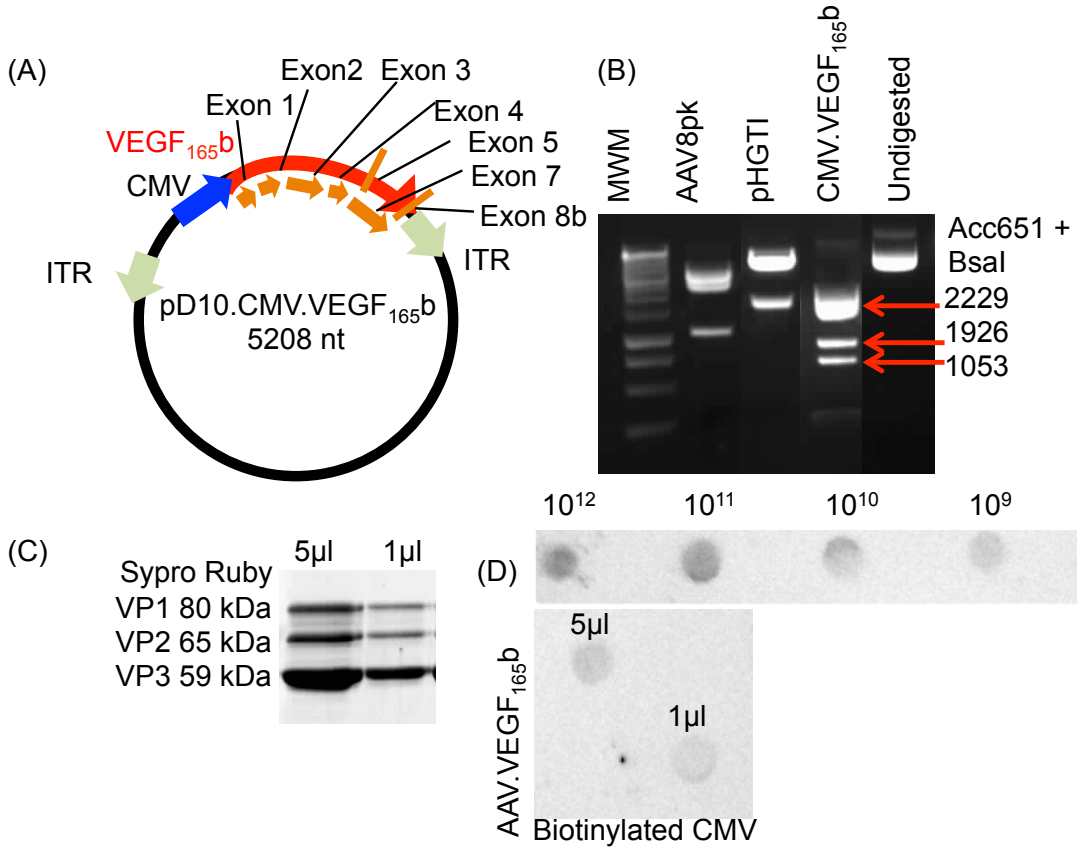

Figure. 7.4. Verification and validation of AAV.VEGF$_{165}$b

VEGF$_{165}$b plasmids (A) were first verified by plasmid digest (B). Following virus purification, the virus was validated by Sypro ruby SDS-PAGE (C) to assess the capsid (expected bands at 80, 65 and 59 kDa. Viruses were quantified using "dot blot" hybridisation, assaying against the CMV promoter.

7.3.2. AAV.Null

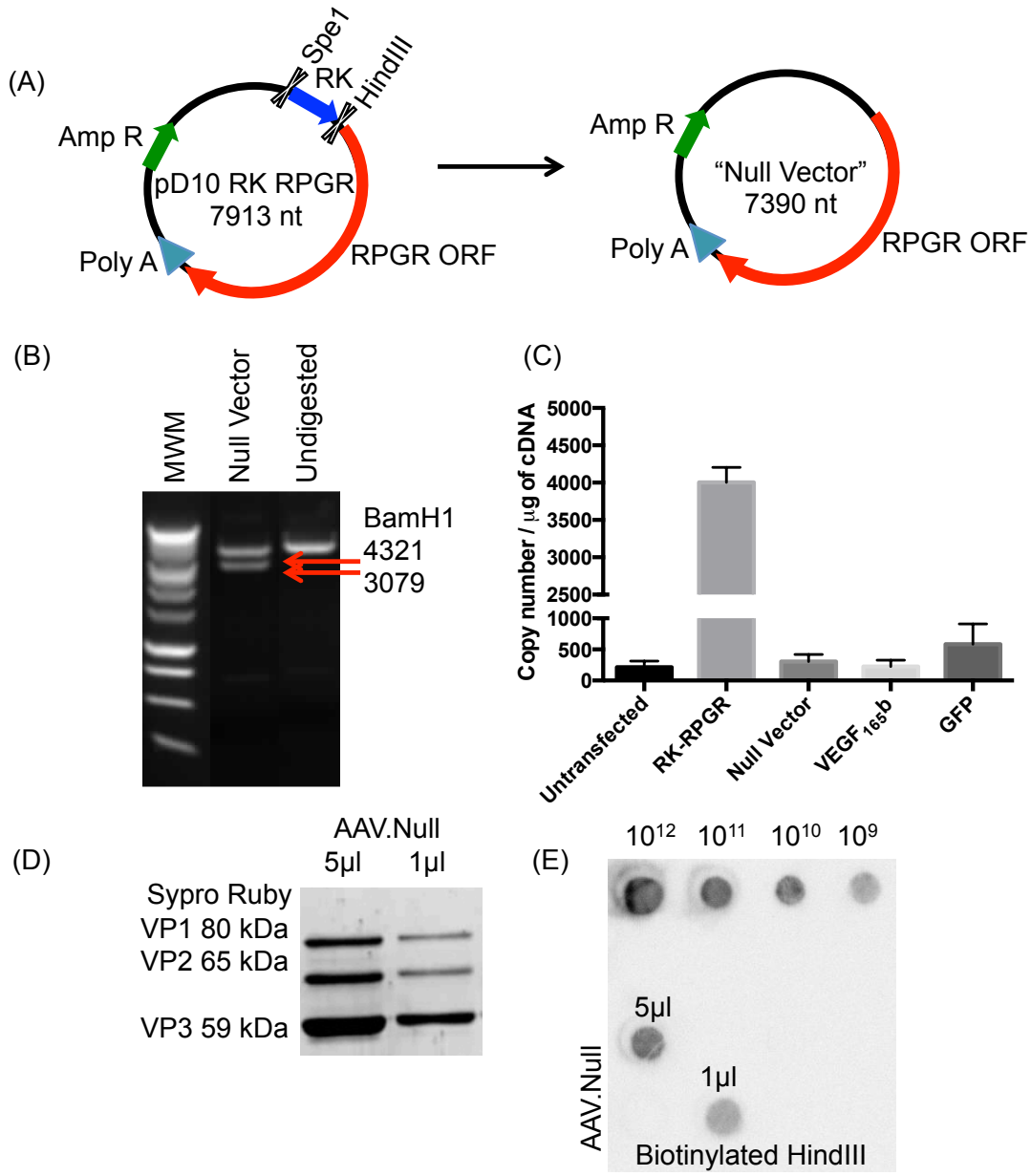

Figure. 7.5. Production and validation of AAV.Null

The RKRPGR plasmid (A) underwent promoter excision, as described in chapter 2: "Materials and Methods". Plasmids were then verified using the BamH1 endonuclease (B). Upon satisfactory results, HEK293Ts were transfected with an RK-RPGR plasmid, Null vector plasmid, $VEGF_{165}b$ plasmid and a GFP plasmid and were assayed to quantify the absolute expression of RK RPGR of each plasmid. The Null vector showed an almost negligible expression of RK RPGR relative to RK RPGR transfected wells, indicating that the Null vector is no longer causing expression of RK RPGR. That same plasmid was used to produce AAV.Null, which underwent the Sypro ruby capsid verification (D). Following validation, viruses were quantified using a custom-made biotinylated HindIII probe (E).

7.3.3.AAV.hrGFP

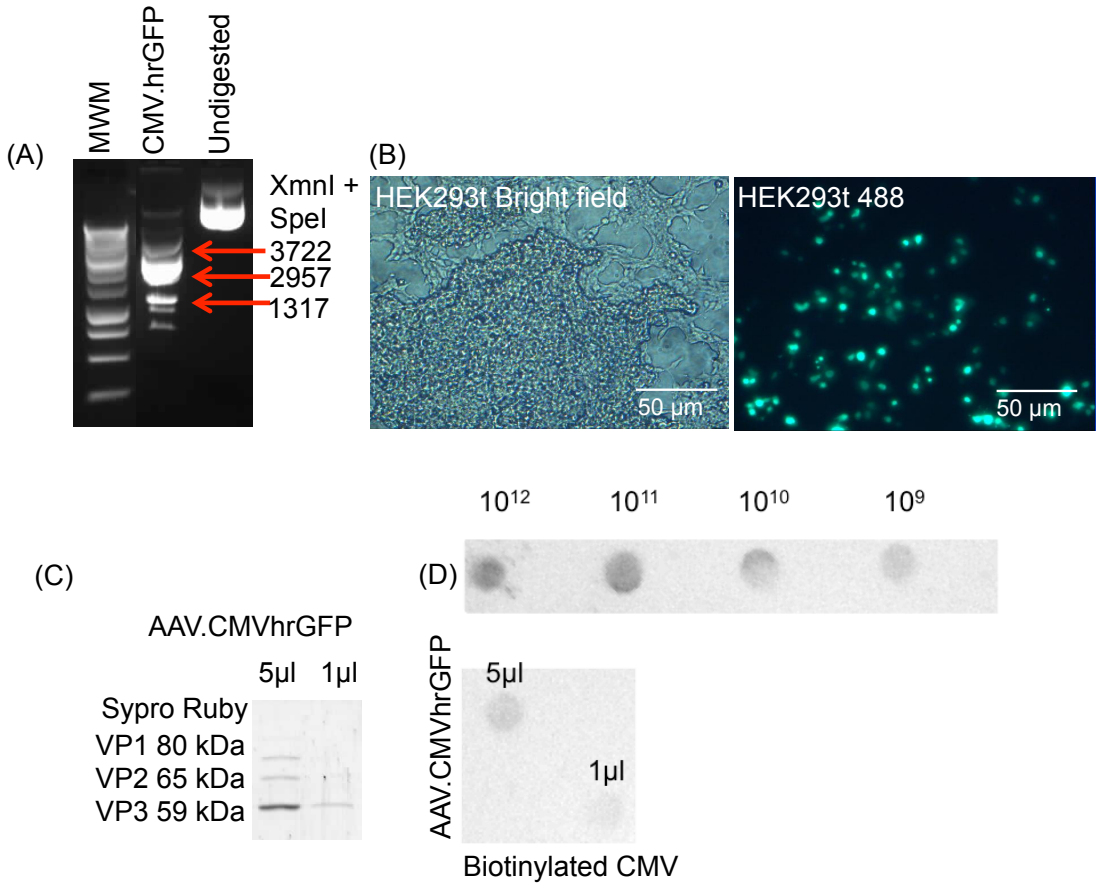

Figure. 7.6. Production of AAV.hrGFP

The GFP plasmid was verified by plasmid digest (A) and transfection of HEK293t cells (B). Cells were transfected for two days and imaged under bright field and under the 488 channel. Plasmids were deemed satisfactory of a high population of cells were green. Following virus purification, capsid integrity (C) and viral copy number (D) was assayed using the Sypro ruby assay and the dot blot hybridisation assay respectively.

Appendix 4. Optimisation of vector volume using AAV.hrGFP.

To assess the correct volume of vector to inject in Lewis rats, 3 volumes were tested for optimum transduction: 2 x 4µl (8µl), 2 x 5µl (10µl) and 2 x 6µl injections (12µl). Lewis rats (n=2 per group) were injected subretinally with AAV.hrGFP (1 x 10^{12} vp/ml), for further details refer to chapter 2 "Materials and Methods". Two weeks post injection, eyes were imaged using an HRA2 Spectralis (Heidelberg Engineering) and infrared and SLO images were taken to assess eye health and fluorescence respectively. Eyes injected with 2 x 4µl AAV.hrGFP showed poor transduction and eyes injected with 2 x 6 µl AAV.hrGFP also showed poor transduction as well as retinal atrophy. Injections of 2 x 5µl AAV.hrGFP showed little retinal atrophy in infrared images and showed the best transduction out of all the volumes assayed, and was therefore the chosen volume for all vector dosing in rats.

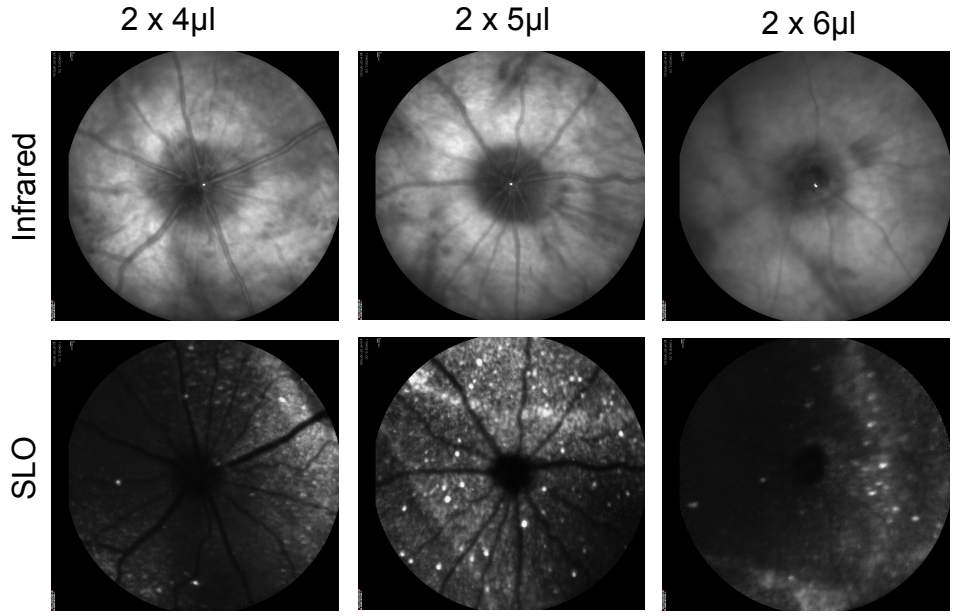

Figure. 7.7. Lewis rats injected with 12µl AAV.hrGFP show the greatest GFP expression and the lowest retinal atrophy.

Lewis rats (n=6) were injected with either 2 x 4µl, 2 x 5µl or 2 x 6µl AAV.hrGFP subretinally (1 x 10^{12} vp/ml) and were imaged for retinal atrophy and GFP transduction using infrared and SLO imaging. Those injected with 2 x 4µl and 2 x 6µl showed poor GFP expression and retinal atrophy, therefore 2 x 5µl was chosen as the optimum volume for vector administration in rats.